Synthesis and Reactivity of the Smallest Diboraheterocycles and Diboratabutadienes

Dissertation

Zur Erlangung des Grades des Doktors der Naturwissenschaften der Naturwissenschaftlich-Technischen Fakultät der Universität des Saarlandes

von

M. Sc. Philipp Grewelinger

Saarbrücken

2025

Tag des Kolloquiums:	05.09.2025
Dekan:	Prof. Dr.-Ing. Dirk Bähre
Berichterstatter:	Prof. Dr. David Scheschkewitz
	Prof. Dr. Dominik Munz
	Prof. Dr. Lutz Greb
Akad. Mitglied:	PD Dr. André Schäfer
Vorsitz:	Prof. Dr. Andreas Speicher

This dissertation was prepared in the time between February 2022 and September 2025 at the Institute for General and Inorganic Chemistry of the Faculty of Natural Science and Engineering at the Saarland University under the supervision of Prof. Dr. David Scheschkewitz.

Die vorliegende Dissertation wurde in der Zeit zwischen Februar 2022 und September 2025 am Institut für Allgemeine und Anorganische Chemie der Naturwissenschaftlich-Technischen Fakultät an der Universität des Saarlandes unter der Aufsicht von Prof. Dr. David Scheschkewitz erstellt.

Zusammenfassung

Die einzigartigen Eigenschaften von Borverbindungen machen sie für chemische Reaktionen und Anwendungen äußerst wertvoll und vielseitig. Während verschiedene zyklische und azyklische Organoborverbindungen ausgiebig untersucht wurden, sind die kleinsten neutralen oder geladenen diborhaltigen Heterozyklen noch nicht ausreichend erforscht, was wahrscheinlich auf ihre begrenzte Zugänglichkeit zurückzuführen ist. Um Untersuchungen an B_2C-Heterozyklen zu erleichtern, befasst sich die vorliegende Arbeit mit einem geradlinigen Zugang zu nicht-klassischen Diboriranen und Diboriraniden durch Funktionalisierung einfacher Diborane(4). Während die erhaltenen Diboriranide als σ-donierende Liganden gegenüber verschiedenen Metallen fungieren, führen nicht-klassische Diborirane zu Übergangsmetall π-Komplexen. Darüber hinaus wurde gezeigt, dass die erhaltenen Komplexe, die von nicht-klassischen Diboriranen abgeleitet sind, CO in Ringerweiterungsreaktionen in Abhängigkeit von der Art der verbrückenden Einheit BRB side-on oder end-on einbauen können.

Wie schon bei den kleinsten B-B-haltigen Heterozyklen haben kleine geladene azyklische Diborverbindungen im Vergleich zum schnell wachsenden Bereich der neutralen Diboran-Anwendungen wenig Aufmerksamkeit erhalten. Obwohl das Motiv eines 2,3-Diboratabutadiens seit Jahrzehnten bekannt ist, hat die Wahl ungeeigneter Substituenten vermutlich die Bildung von Butadien Metallkomplexen mit interner B-B-Bindung verhindert. In dieser Arbeit wurde gezeigt, dass ein neuartiges tetraaryliertes 2,3-Diboratabutadien ein geeigneter Ligand für Metallocene der Gruppe 4 ist.

Abstract

The unique properties of boron compounds make them extremely valuable and versatile in chemical reactions and applications. While various acyclic and cyclic organoboron compounds have been extensively studied, the smallest neutral and charged diboron-containing heterocycles remain underexplored, likely due to their limited accessibility. To facilitate investigations on B_2C-heterocycles, this thesis deals with the straightforward access to non-classical diboriranes and diboriranides through functionalization of simple diboranes(4). While the obtained diboriranides act as σ-donating ligands towards different metals, non-classical diboriranes give rise to transition metal π-complexes. Furthermore, the obtained complexes derived from non-classical diboriranes were shown to incorporate carbon monoxide in ring expansion reactions in side-on or end-on fashion depending on the nature of the bridging moiety BRB.

As for the smallest B-B containing heterocycles, small charged acyclic diboron compounds have received little attention compared to the rapidly growing field of neutral diborane applications. Although the structural motif of a 2,3-diboratabutadiene has been known for decades, the choice of unsuitable substituents presumably precluded the formation of butadiene metal complexes with internal B-B bond. In this thesis a novel tetraarylated 2,3-diboratabutadiene was shown to be a suitable ligand for Group 4 metallocenes.

Publications

This thesis has been published in parts in:

- P. Grewelinger, T. Wiesmeier, C. Präsang, B. Morgenstern, D. Scheschkewitz: ”Diboriranide σ-Complexes of d- and p-Block Metals” *Angew. Chem. Int. Ed.* **2023**, *62*, e202308678. https://doi.org/10.1002/anie.202308678; *Angew. Chem.* **2023**, *135*, e202308678. https://doi.org/10.1002/ange.202308678.

- P. Grewelinger, C. Präsang, M. Zimmer, B. Morgenstern, D. Scheschkewitz: “π-Complexes Derived from Non-classical Diboriranes: Side-on vs. End-on Carbonylative Ring Expansion*”* *Angew. Chem. Int. Ed.* **2024**, *63*, e202415378. https://doi.org/10.1002/anie.202415378; *Angew. Chem.* **2024**, *136*, e202415378. https://doi.org/10.1002/ange.202415378.

- P. Grewelinger, C. Präsang, B. Morgenstern, D. Scheschkewitz: “2,3-Diboratabutadiene Complexes of Group 4 Metals and their Donor-Induced Oxidative Cleavage to Methyleneboranes*”* *ChemistryEurope* **2025**, *00*, e202500153. https://doi.org/10.1002/ceur.202500153.

Danksagung

Ich möchte mich bei **Prof. Dr. David Scheschkewitz** dafür bedanken, dass er mir die Möglichkeit gegeben hat meine Doktorarbeit in seinem Arbeitskreis anzufertigen. Darüber hinaus danke ich für die Unterstützung beim Verfassen von Manuskripten sowie der Ermöglichung zahlreicher Konferenzbesuche während meiner Zeit im Arbeitskreis. Vielen Dank für das entgegengebrachte Vertrauen in meine Arbeit, die gewährten Freiheiten und die ständige Verfügbarkeit für Fragen und Diskussionen. Danke auch für alle Informationen, Wissensvermittlungen, Hilfestellungen und Gespräche, egal ob sie wissenschaftlicher oder anderer Natur waren.

Weiterhin bedanke ich mich bei **Prof. Dr. Dominik Munz**, der sich gerne als Zweitgutachter für diese Arbeit bereit erklärt hat. Als mein wissenschaftlicher Begleiter war er stets in mein Thema involviert und hat mir mit wertvollen Diskussionen und Ratschlägen dabei geholfen, die Arbeit voranzutreiben.

Einen großen Dank an **Dr. Carsten Präsang** der insbesondere zu Beginn der Promotion eine große Hilfe war und bedeutenden Anteil an dem Erfolg meiner Doktorarbeit hat. Sein großer Erfahrungsschatz an theoretischem und praktischem Wissen hat wesentlich zu meiner Entwicklung als Chemiker beigetragen.

Auch danke an **Dr. Diego Andrada** und seine Gruppe, die mir unter anderem bei Fragen bezüglich quantenchemischer Rechnungen stets behilflich waren.

Dr. Bernd Morgenstern danke ich sowohl für die Kristallmessungen und Strukturverfeinerungen. Danke für den enormen Aufwand und die großen Bemühungen, auch in aussichtslosen Situationen eine Lösung bereitzuhaben.

Dr. Michael Zimmer danke ich für die Messung der VT- und Festkörper NMR Spektren, sowie für den Betrieb und die Wartung der NMR-Geräte. **Susanne Harling** danke ich für die Messung der CHN-Analysen und **Britta Schreiber** danke ich für das Anfertigen und Reparieren von Glasgeräten.

Dem Arbeitskreis: **Dr. Nasrina Parvin**, **Henrike Waller**, **Anna-Lena Thömmes**, **Luisa Giarrana**, **Daniel Mühlhausen**, **Peter Spies**, **Ankur Urpils**, **Liane Müller**, **Tim Wiesmeier** und **Michel Böhmert** danke ich für die gute Zusammenarbeit. Ein Arbeitskreis gefüllt mit Freunden, sodass jeder Labortag mit Vorfreude auf den nächsten beendet werden konnte. Unzählige Gespräche, Sprüche, Witze und vieles mehr – insbesondere mit meinem Abzugspartner – haben dafür gesorgt, dass sich kein Tag wie Arbeit angefühlt hat. Und auch wenn manche Situationen hin und wieder herausfordernd waren, werde ich den AK mit mindestens einem weinenden Auge verlassen.

Ein spezieller Dank geht an die Studenten, die ich in meiner Zeit als Doktorand betreuen durfte, um somit wertvolle Erfahrung zu sammeln: **Tim Wiesmeier**, **Liane Müller**, **Simon Muhm** und **Nelson Kapidani**.

Danke an weitere aktuelle und ehemalige Mitarbeiter des Arbeitskreises: **Dr. Andreas Rammo**, **Andreas Adolf**, **Bianca Iannuzzi, Dominika Posse**, **Emily Klein**, **Dr. Paresh Kumar Majhi**, **Dr. Nadine Poitiers**, **Dr. Yvonne Kaiser**, **Dr. Taiki Imagawa, Dr. Marc Hunsicker, Thomas Büttner** und **Eveline Altmeyer**.

Von Herzen danke ich meiner Partnerin **Luisa Giarrana** für ihre stetige Unterstützung, Aufmerksamkeit und Liebe. Danke für den großen Rückhalt innerhalb und außerhalb der Universität.

Ich danke allen meinen Freunden, die mich in meiner Zeit während der Promotion begleitet haben.

Zuletzt gilt auch meiner Familie ein großes Danke: **Guido**, **Marion** und **Steffen Grewelinger** sowie **Marie-Luise Dûchene**.

Table of Contents

Abbreviations

^{t}BuLi	*tert*-butyl lithium
Cy	cyclo-hexyl
Dur	duryl = 2,3,5,6-tetramethylphenyl
Eq	equiv = equivalents
Et	ethyl
exc.	excess
h	hour
HOMO	highest occupied molecular orbital
LUMO	lowest unoccupied molecular orbital
IMe	1,3,4,5-tetramethylimidazol-2-ylidene
Me	methyl
Mes	mesityl = 2,4,6-trimethylphenyl
NHC	*N*-heterocyclic carbene
NMR	nuclear magnetic resonance
Ph	phenyl
^{i}Pr	*iso*-propyl
thf	tetrahydrofuran
TMP	tetramethylpiperidine
UV	ultraviolet
Vis	visible

Preface

Despite its early position in the Periodic Table (atomic number = 5), boron is not a product of stellar nuclear fusion, but is formed exclusively through fission of heavier nuclei by cosmic radiation,[1] and therefore constitutes only about 17 ppm by weight of the Earth's crust.[2] In nature, boron only occurs in bonded form in one of its many minerals such as colemanite, kernite, ulexite, or tincal. Almost the entire known deposits of these minerals, which are classified as strategic resources by the EU, are found in western hemisphere.[3] The isolation of elemental boron was first achieved in 1808 by Gay-Lussac and Thenard through the heating of boron-containing minerals with potassium[4] and only nine days later by Davy through electrolysis,[5] although neither of them obtained the element in high purity.[6] The production of boron is, however, unnecessary for most applications, as the element is rarely used in elemental form, p-type doping of semiconductors being the best-known exception.[7] In contrast, the application of boron compounds is wide-spread, for instance as materials: boron oxide is added during glass fibre production to improve processing and a variety of properties.[8] In borosilicate glass, B_2O_3 reduces thermal expansion thus improving thermal resistance.[9] Metal borates have found applications as fire retardants[10] while metal borides are employed due to their extreme hardness.[11] Similarly, boron carbide and boron nitride are the hardest known materials next to diamond and accordingly are widely used as ceramics.[12] In addition, borax (sodium tetraborate) is popular as a detergent in households while perborates show good properties as a bleaching agent.[13] Along with the use as fertilizers,[14] these applications constitute about three quarters of the worldwide borate consumption.

Due to their high specific energy of combustion compared to hydrocarbons, boranes were potentially attractive as jet and rocket fuels, which led to exponentially increasing research in molecular boron chemistry starting in the 1950s. Although the major breakthrough in the use of boranes as a fuel has not materialized as hoped for,[15] it has paved the way for numerous potential applications in various fields. In comparison to its heavier Group 13 homologues, boron shows more similarity to carbon and silicon and thus a pronounced tendency to form covalent bonds allowing for a rich molecular chemistry. For example, the hydroboration of olefins and the palladium-catalysed cross-coupling of boronic esters are crucial cornerstones of modern organic chemistry.

Both syntheses earned their discoverers H.C Brown and A. Suzuki the Nobel Prize in Chemistry,[16,17] underscoring their enormous importance.[18] Research in the field of dodecahedral carboranes has led to applications in the field of neutron capture therapy to combat certain types of cancer.[19] In addition, several boron-based drugs have recently been approved for clinical use due to their unique binding properties to biological targets, while numerous more are currently in clinical trials.[20] The inherent electron deficiency of boron is responsible for a high Lewis acidity, which results in an effective orbital interaction with π-systems. With the formally vacant p_z orbital at the boron center, and its sp^2-hybridization, boranes inherently feature a trigonal-planar coordination geometry around the boron atom, predestining them for application in 2D molecules e.g. *via* BN isosters of arenes.[21] Incorporation of boron into carbon-based π-systems leads to interaction between the vacant p_z orbital and the π-symmetric molecular orbitals of the conjugated system. This interaction drastically lowers the LUMO energies and thus improves the electron-acceptor properties.[22] As a result, numerous boron compounds have found applications in energy-related processes.[23] Because of their electronic structure, boron species (in particular low-valent) can exhibit properties usually associated with transition metals, while at the same time being less toxic, inexpensive, abundant and overall more environmentally benign.[24] These metallomimetic compounds have proven useful as catalysts[25] or for the activation of small molecules.[26] In addition, boron containing heterocycles can be used as ligands for transition metals.[27]

Last but not least, the unique electronic structure of many boron species has been pivotal in the development of chemical bonding theories. The structure of diborane(6),[28] B_2H_6, remained a conundrum of valence bond theory: Linus Pauling upheld his conviction of an ethane-like connectivity for a long time.[29] The electronic structure of diborane(6) with its two bridging hydrogen atoms was correctly proposed by Longuet-Higgins and Bell at the beginning of the 20th century.[30] The thorough theoretical understanding of bonding in boranes earned William Lipscomb the Nobel Prize in Chemistry in 1976.[31] Almost half a century later, considerable theoretical and experimental efforts in molecular boron chemistry continue to be driven by academic curiosity, ultimately providing the fundamental base for the remarkable broadening of the application prospects of boron-containing molecules.

1 Introduction

The propensity of boron containing compounds to form delocalized multicenter bonds results in boranes predominantly adopting deltahedral cluster structures. Consequently, electron-precise interactions in boron chains or cycles are energetically disfavoured, accounting for their lower incidence.[32] Recent decades, however, have seen great effort to compensate this shortfall. Diboranes(4), containing a classical two-electron two center (2e2c) bond, are key to a rapidly evolving field in organic syntheses with vast application. For details, the interested reader is referred to pertinent review articles.[33] Promoting the structural diversity in the simplest boron chains (only one B-B bond) is of high academic interest. Despite several investigations addressing the B-B bond, in particular charged derivatives have received rather sporadic attention.
Due to their versatile electronic properties, boron-containing carbocycles have found substantial interest.[34] For instance, the use of tricoordinated boron in fused polycyclic aromatics is of particular interest with regards to the application in organic optoelectronic materials.[35] The potential of such systems to mimic transition metals has been demonstrated by several examples of small molecule activation. Furthermore, boron-containing heterocycles find more and more use as pharmaceutical reagents[36] and are particularly suitable as ligands for different metals.[37] In comparison to their all-carbon analogues, smaller boron-containing carbocycles (3-, 4-, and 5-membered) exhibit a higher propensity for strain-releasing ring-expansions. This is facilitated by substrates inserting into relatively weak endocyclic bonds, particularly in systems featuring homoatomic diboron bonds, where this tendency is further amplified. In comparison to the tremendous increase of research in boracycles in general, studies dealing with B-B bonded systems are scarce.

The following literature review accordingly refers to recent areas of molecular boron research: Firstly, recent developments concerning the electron precise homoatomic diboron bond are addressed. Subsequently, previously reported smaller (three- to five-membered) heterocycles containing a B-B bond and, if known, their reactivity will be discussed.

1.1 Acyclic diboron compounds

1.1.1 Diboranes, Diborenes and Diborynes

While the parent borane BH_3 dimerises to diborane(6) *via* two three-center two-electron (3c2e) BHB bonds, diboranes(4) contain an electron-precise B-B bond. Boron's homonuclear σ-bond dissociation enthalpy is in between that of carbon and silicon, both elements that are well known to form homoatomic bonds. The B-B bond is thus thermodynamically stable, albeit less so than many heteroatom-boron bonds (B–O, B–N or B–C).[38] Due to their vacant p-orbitals, diboranes(4) are susceptible to be attacked by nucleophiles, which can, however, be mitigated thermodynamically by π-donating substituents and/or kinetically by bulky groups. The first diborane(4), tetrachlorodiborane(4), was obtained as early as 1925 by A. Stock *et al.* under quite harsh conditions but was of limited use for synthetic chemistry due to its low stability.[39] Decades later, Brotherton *et al.* reported a synthetic pathway to the remarkable stable tetraaminodiborane(4) **2** (Scheme 1) tamed by the +M effect of the nitrogen atoms and its moderate steric bulk, giving access to diboranes(4) in large scale for the first time.[40] Bis(dimethylamino)chloroborane **1** gives tetrakis(dimethylamino)diborane(4) **2** in a Wurtz-like coupling using a suspension of molten sodium. Although it has so far not been unambiguously elucidated, the most likely mechanistic scenarios are either the combination of two boryl radicals or the nucleophilic attack of a boryl anion to chloroborane **1**. These transient low-valent species can cause side reactions resulting in reduced yields and by-products. Despite considerable efforts to identify alternative access routes, this method remains the most common for the synthesis of diboranes(4) to date.[41]

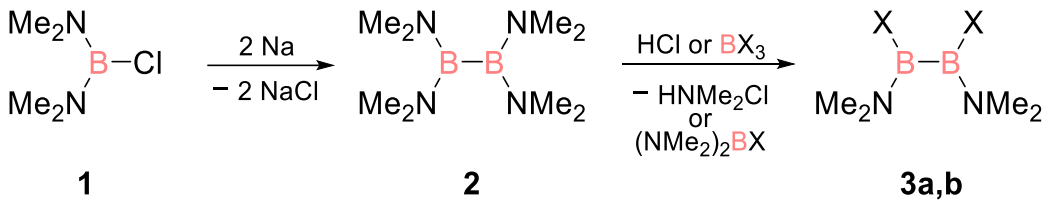

1 **2** **3a,b**

Scheme 1. Wurtz-like coupling of diaminochloroborane **1** to tetraaminodiborane(4) **2** and consecutive conversion to 1,2-dihalo-1,2-diaminodiboranes(4) **3** using HCl or BX_3 (**a**: X = Cl; **b**: X = Br).

Since amino-substituted diboranes(4) are stabilized by considerable π backdonation from nitrogen to boron, the Lewis acidity is largely quenched. To address this issue, two amino groups of diborane(4) **2** can be converted to halo substituents with better leaving group characteristics using hydrochloric acid[42] or BX_3 (X = Cl, Br)[43,44] to give 1,2-halo-1,2-diaminodiborane(4) **3** (Scheme 1). In straightforward nucleophilic substitution reactions with RM (R = aryl, alkyl, allyl; M = Li, Na, MgCl) under salt elimination bis(dimethylamino)diboranes(4) **4** are obtained (Scheme 2).[42,44-53] Furthermore, diboranes(4) **4** can either be halogenated directly with BX_3 (X = Cl, Br) to give dihalodiboranes(4) **6**[46] or transformed into the alkoxy functionalized derivatives **5**.[54]

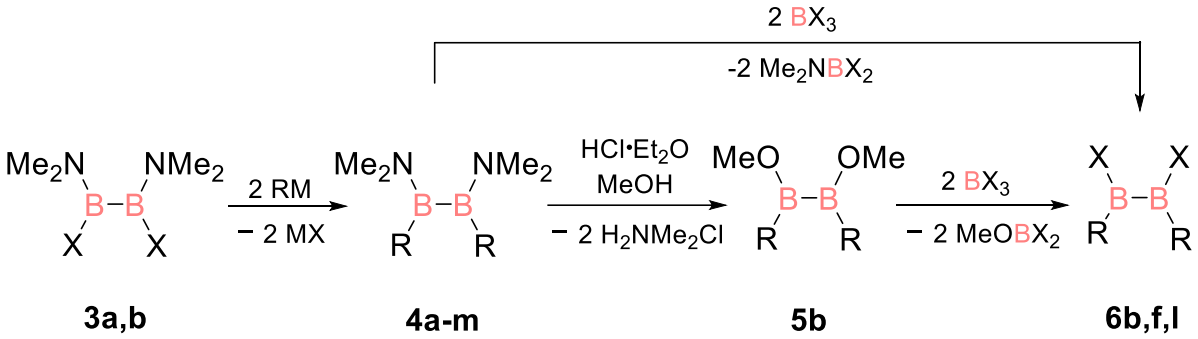

Scheme 2. Addition of organometallic reagents RM (M = Li, Na, MgCl) to 1,2-dihalodiboranes(4) **3a,b** to give diboranes(4) **4** (**a**: R = Bu;[42] **b**: = Mes;[44] **c**: R = Ph;[44] **d**: R = Flu = fluorenyl;[45] **e**: R = CCPh;[45] **f**: R = ^{t}Bu;[46] **g**: R = indenyl;[47] **h**: R = ferrocene;[48] **i**: R = difluorenylmetallocene;[49] **j**: R = Tip = triisopropylphenyl;[50] **k**: R = Ant = anthracene[51]; **l**: R = allyl[52]; **m**: R = Cp = cyclopentadienyl[53]). Dihalodiborane(4) **6** (**b**: R = Mes, X = Cl; **f**: R = ^{t}Bu, X = Cl; **l**: R = Mes, X = Br) is either obtained by addition of BX_3[46] or *via* 1,2-dimethoxydiborane(4) **5** (**b**: R = Mes).[54]

Starting from 1,2-bis(aryl)-1,2-dichlorodiborane(4) **6**, straightforward incorporation of the B-B moiety with retained vacant p-orbitals into more complex, otherwise elusive, systems is possible. Through these vacant p-orbitals the LUMO in diboranes(4), formally representing a bonding π-orbital, is readily accessible. In 1981, Berndt and coworkers reported on the first one-electron-reduction of a neopentyldiborane(4) to a radical anion with formal π-bond order of 0.5, verified by EPR spectroscopy.[55] The first dianionic B=B double bond was then reported a decade later by Power and coworkers.[56] B_2Mes_3Ph **7** was reduced using an excess of lithium powder in diethyl ether to obtain dianion $\mathbf{7}^{2-}$ (formal π-bond order of 1) that crystallises as a contact ion pair in diethyl ether (Scheme 3a). Formal addition of two electrons to diboranes(4)

accordingly renders them isoelectronic and isostructural to alkenes, fulfilling the favourable octet rule. The molecular structure of a diborane(4) radical monoanion in the solid state was reported by P. Power years after its first observation. Dimethoxydiborane(4) **8** shows a slight B-B bond contraction upon reduction to radical monoanion $\mathbf{8}^{\bullet-}$ (Scheme 3b).[57] Due to increased Coulomb repulsion of the negative charges in diborataethene $\mathbf{7}^{2-}$ the bond length ($\mathbf{7}^{2-}$**:** 1.636 Å) is virtually the same as in $\mathbf{8}^{\bullet-}$ (1.636 Å) but shorter than the neutral diboranes(4) (**7**: 1.706 Å **8** 1.724 Å). A significantly decreased B-B bond length (~1.55 Å) in dianionic diboranes(4) was reported by Nöth *et al.* shortly after the seminal discoveries by Berndt and Power. In a tetra(amino)diborane(4), the π-electrons are strongly localized at the B-B bond, induced by the planarity of the B_2N_4 unit with pyramidalized nitrogen atoms precluding delocalization.[58]

Recently, Wagner and Yamashita independently reported on the reactivity of diborataethenes as masked boryl anions[59] related to the Wanzlick equilibrium known between carbenes and alkenes.[60] These examples comprise one of the few reactivity reports for dianionic diboranes(4).

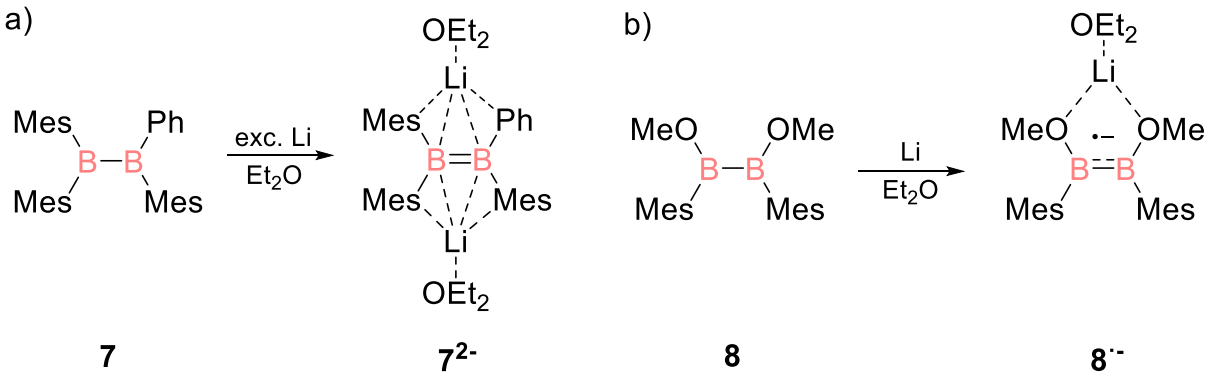

7 $\mathbf{7}^{2-}$ **8** $\mathbf{8}^{\bullet-}$

Scheme 3. a) Two electron reduction of diborane(4) **7** to dianionic diborataethene $\mathbf{7}^{2-}$ and b) single electron reduction of dimethoxydiborane(4) **8** to radical anion $\mathbf{8}^{\bullet-}$.

Neutral compounds with homoatomic boron bonds of bond order higher than one have first been isolated by Robinson *et al.* in 2007.[61] Reduction of NHC stabilized tribromoborane **9** with potassium graphite resulted in the formation of diborene **10** (Scheme 4a). The synthesis of the presumable intended species with B-B triple bond was not achieved *via* this pathway since hydride abstraction of the solvent prevented full reductive dehalogenation as seen by the formation of hydrides in diborene **10** and side product **11**. Several years later, Braunschweig *et al*. succeeded in the isolation of

the first room temperature-stable diboryne **14** starting from NHC stabilized tetrabromodiborane(4) **12** (Scheme 4b) with a pre-established B-B bond.[62] Addition of four equivalents of sodium/naphthalene results in the formation of the neutral triple bond in **14**, while addition of two equivalents gives diborene **13**. The addition of diborane **12** to diboryne prompts a comproportionation to diborene **13** which in turn is transformed into the diboryne after adding two equivalents of sodium/naphthalene. The isolation of such a species was a long-awaited goal, preceded by several theoretical studies[63] and matrix isolated transient intermediates.[64] The small *trans*-bent angle of diboryne **14** compared to its heavier dianionic homologues (Al≡Al, Ga≡Ga), reported decades earlier,[65] supports the presence of a genuine triple bond rather than a significant triplet character.[66]

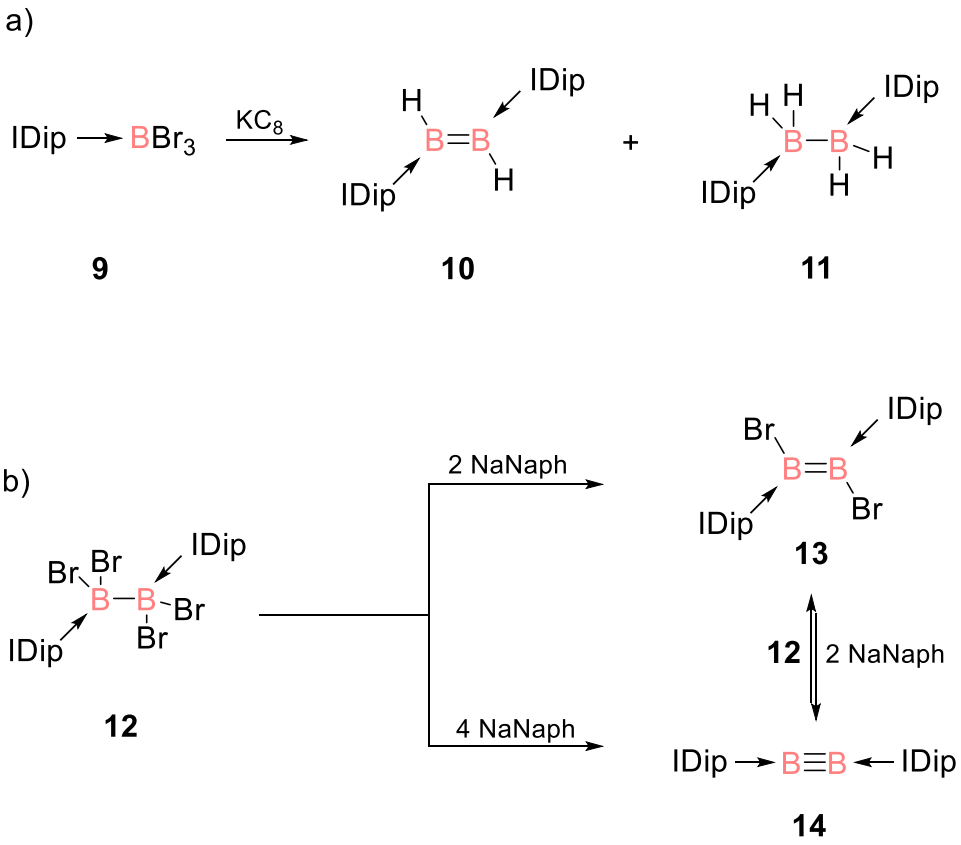

Scheme 4. a) Reduction of IDip stabilized tribromoborane **9** to diborene **10** and diborane(4) **11**. b) First reported preparation of room temperature-stable diboryne **14** starting from IDip stabilized tetrabromodiborane(4) **12**. Addition of two equivalents NaNaph to **12** gives diborene **13** (IDip = 1,3-bis-(2,6-diiso-propylphenyl)imidazol-2-ylidene).

The ligand choice for diborynes is crucial since a more π-acidic donor results in the formation of a cumulene like structure instead of the diboryne as reported by the same

group in subsequent works.[67] Neutral B-B multiple bonds have mainly found application in the activation of small molecules[24,68] and as ligands for transition metals.[69] A diborene platinum complex also reported by Braunschweig *et al.* in 2012 marks the first complex in which the π-backbonding from a transition metal to the B=B moiety actually strengthens the bond and is thus of particular interest.[70] Additionally, this complex constitutes the only fully characterised donor-free diborene to date.

1.1.2 Diboratabutadienes

Multiple bonds between boron and carbon atoms have been published decades earlier than their homonuclear diboron counterparts. In 1967, Arzoumanian reported on the first borataalkene with its anionic B=C double bond, isoelectronic to alkenes.[71] The first examples of so-called methyleneboranes with neutral B=C double bonds, isoelectronic to vinyl cations, followed shortly thereafter in a report by Berndt and coworkers.[72,73] While anionic borataalkynes with a certain triple bond character are known for decades[74] the according neutral boryne had only been reported very recently.[75]

The preparation of anionic C=B double bonds is usually performed by deprotonation of α-boryl carbon atoms, which are relatively acidic due to the stabilization of the lone pair of electrons of the corresponding base by the adjacent vacant p-orbital of boron.[73,76] In such polarized double bonds, the 2p-orbital of the more electronegative carbon has a higher contribution to the occupied molecular orbitals while boron's corresponding orbital shows a higher contribution to the unoccupied molecular orbitals (Scheme 5a). Thus, a carbanionic ylide/ylene resonance structure (**15/15'** in Scheme 5b) can be assumed, which is supported by applications in bora-Wittig reactions.[77] The same property allows the application of borataalkenes as versatile ligands for transition metals providing an attractive alternative to the ubiquitous isoelectronic alkene complexes with their industrial relevance in catalysis.[78] As in case of the latter, the bonding situation in borataalkenes complexes can be rationalized with the Dewar-Chatt-Duncanson model and its π-complex/metallocyclopropane dichotomy.[79] While alkenes usually bind to metals in η^2- fashion, borataalkenes can also bind in η^1-B or η^1-C coordination modes depending on the nature of the transition metal.[80] This

flexibility in the coordination mode has led to the increased utilization of borataalkenes as ligands in recent years.[80]

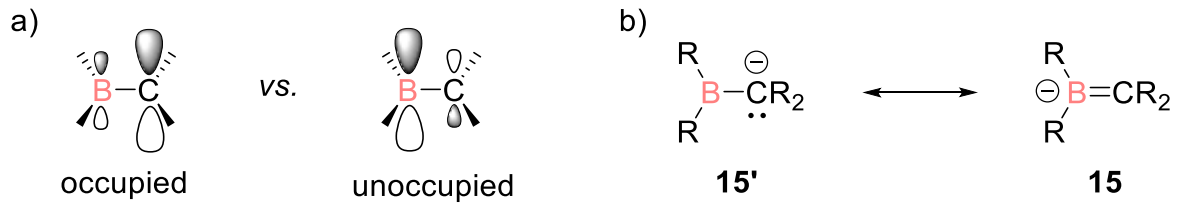

Scheme 5. a) Contribution of boron and carbon to occupied and unoccupied orbitals. b) Mesomeric structures of α-borylanion **15'** (bora-ylide) and borataalkene **15** (bora-ylene).

Butadienes as the simplest conjugated systems are of particular interest due to their versatile ligand properties as well as their relevance for catalysis.[81] The first dianionic butadiene with a central B-B bond was reported as early as 1990.[82] Methyleneborane **16** is reduced with lithium powder in toluene, presumably *via* a single electron transfer (SET) mechanism, resulting in the formation of an intermediate mono-radical anion **17**$^{\bullet-}$ (Scheme 6). Subsequent symmetrical radical dimerization yields 2,3-diboratabutadiene **18a**. The choice of substituents in this reaction proved crucial as, for instance, the use of duryl substituents results in dimerization under C-C bond formation at the sterically unprotected *para*-position of the aryl ring. Due to Coulomb repulsion of the anionic charges in diboratabutadiene **18a**, the B-B bond is significantly stretched compared to neutral diboranes(4). The steric demand of the four silyl groups apparently prevented reactivity studies so far.

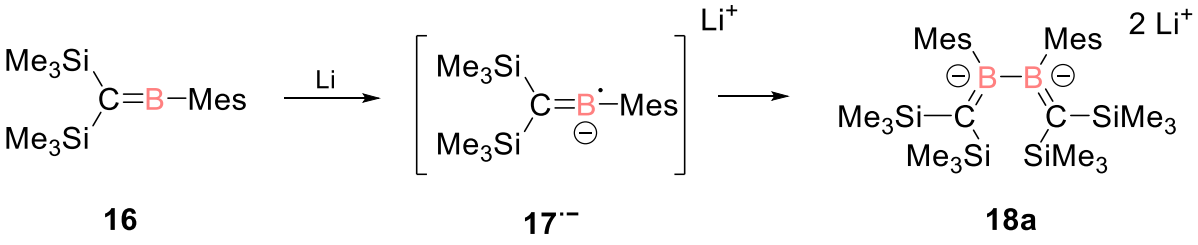

Scheme 6. Synthesis of the first 2,3-diboratabutadiene **18a** by Berndt and coworkers.

A few years later, investigations by Nöth and coworkers showed that starting from a diborane(4), the diboratabutadiene is accessible in a more straightforward fashion due to an already established B-B bond.[83]

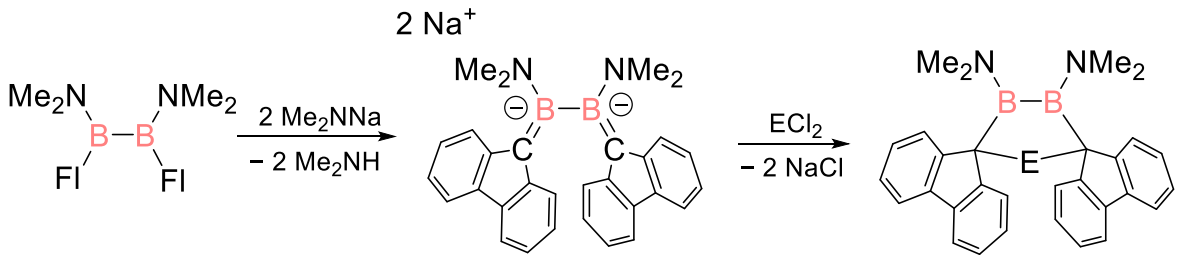

4d **18b** **19a-c**

Scheme 7. Synthesis of dianionic diboratabutadiene **18b** *via* deprotonation of diborane(4) **4d** with $NaNMe_2$ (Fl = Fluorenyl). Addition of main group halides (**a**: E = AsCl, **b**: E = $PbMe_2$, **c**: E = $SnMe_2$) results in the formation of five membered heterocycles **19**.

The addition of fluorenyllithium to readily available 1,2-bis(dimethylamino)-1,2-dichlorodiborane(4) results in the incorporation of α-boryl carbon centers with residual acidic hydrogen atoms to give 1,2-bis(fluorenyl)-1,2-bis(dimethylamino)diborane(4) **4d** (Scheme 7). Subsequent double deprotonation with sodium dimethylamide yields dianionic 2,3-diboratabutadiene **18b**. In the same study, the first five-membered cyclic diboranes(4) **19** with main group motifs (AsCl, $SnMe_2$ and $PbMe_2$, Scheme 7) were obtained by treatment of **18b** with the corresponding electrophiles. The $2e^-$-oxidation of diboratabutadiene **18b** was shown to yield 1,2-diboretanes (*vide infra*). Diboratabutadiene **18c** was synthesized in adaptation of Nöth's protocol by Berndt and coworkers later on (Scheme 8).[84] The consecutive addition of $B(OMe)_3$ and BCl_3 to diboratabutadiene **18c** resulted in triboracyclopentane **20** (Scheme 8). Reduction of this compound provided access to an anionic bishomo-derivative of a lithium triboriranide **21** with strong 3c2e bonds.[84]

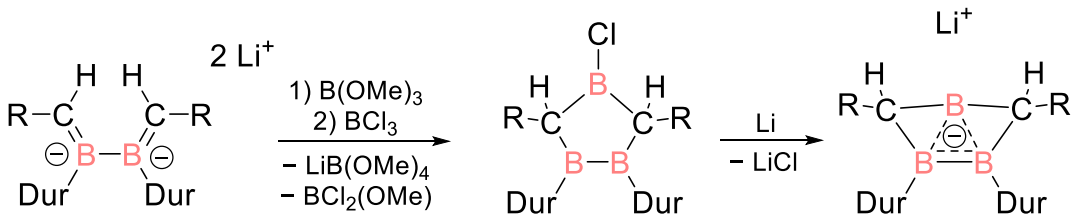

18c **20** **21**

Scheme 8. Synthesis of anionic bishomo triboriranide **21** *via* triboracyclopentane **20** starting from diboratabutadiene **18c** (R = $SiMe_3$).

Similar results were obtained with a Group 14 electrophile: The addition of dichloromethylsilane results in the formation of the five-membered heterocycle **22** under elimination of lithium chloride (Scheme 9).[85] The Si-H functionality is converted to Si-Cl using BCl_3, which upon reduction with lithium powder in diethyl ether results in the formation of anionic system **23** containing strong homoaromatic interactions. Furthermore, hydrogen migration from the silicon atom in **22** to the B-B bond to give the neutral heterocycle **24**, again with homoaromatic interaction, is induced by addition of tetrahydrofuran (Scheme 9).[86]

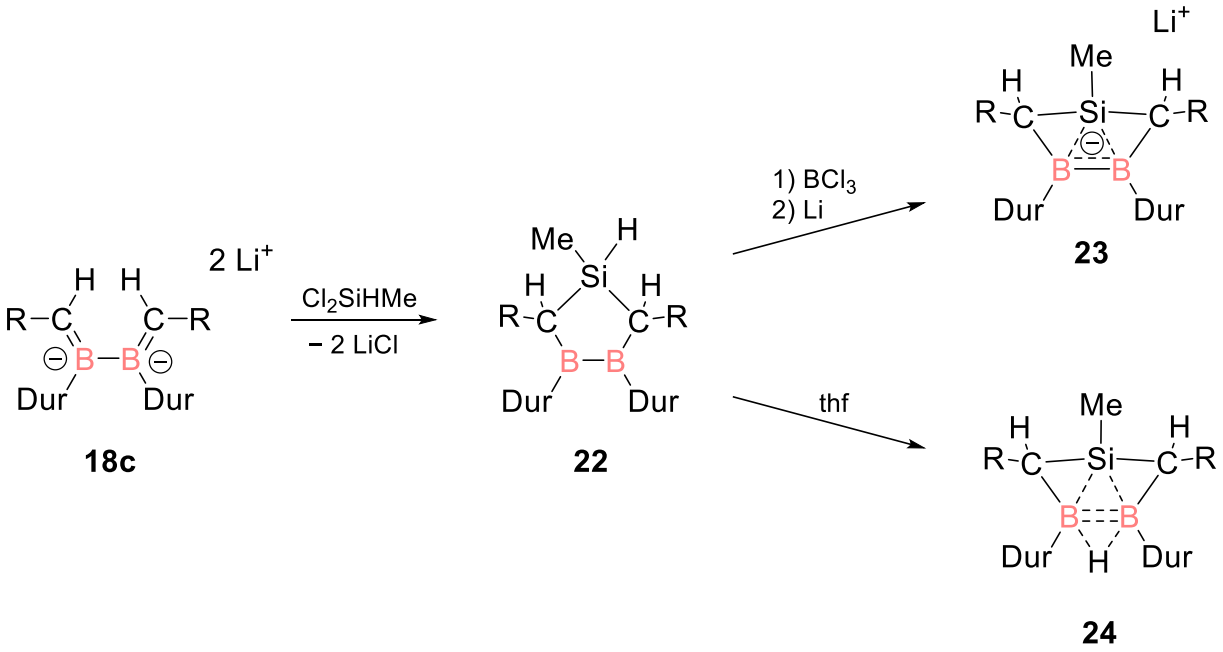

Scheme 9. Synthesis of siladiboracyclopentane **22** from diboratabutadiene **18c**. Consecutive chlorination and reduction yields anionic homoaromatic derivative **23** while addition of tetrahydrofuran (thf) results in irreversible H-migration into the BHB bridging position in neutral homoaromatic heterocycle **24**.

Transition metal borabutadiene complexes are so far only known without internal B-B bond.[87] Although 2,3-diboratabutadienes have been known for decades, reactivity studies are limited to main group electrophiles.

1.2 Boron-containing heterocycles

1.2.1 Five- and four-membered rings containing a B-B bond

Five-membered rings with endocyclic B-B bond are relatively rare and can be grouped in three classes according to the presence or absence of further heteroatoms: (1) without additional endocyclic heteroatoms, (2) with s- and p-block heteroatoms, and (3) with endocyclic transition metal centers. In the following, selected examples for each class will be provided:

(1) The class of 1,2-diborolanes (1,2-diboracyclopentanes) has been introduced in 1990 by Herberich.[88] Diborolane **25a** (Scheme 10) was prepared by reductive cyclization of an open-chained 1,3-bis(chloroboryl)propane. The Berndt group employed a different approach starting from a 1-allyl-2-chlorodiborane(4): Reduction of an allyldiborane(4) with lithium powder in thf affords 1,2-diborolanide **26** (Scheme 10).[89] The Braunschweig group recently synthesized 1,2-diborolane **27** by thermally induced intramolecular C-H activation of a 1,2-(dianthracene)diborene.[90]

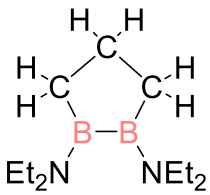

25a

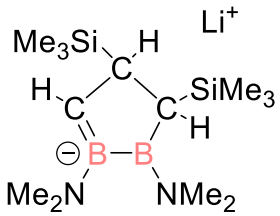

26

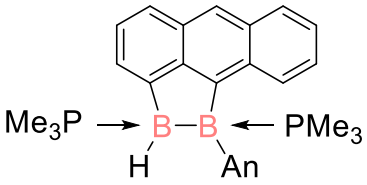

27

Scheme 10. Recently reported 1,2-diborolane species by Herberich **25a**, Berndt **26** and Braunschweig **27** (An = Anthracene).

1,2-Diborolanes mostly react *via* insertion of small molecules or nucleophiles in the B-B bond. For instance, Siebert reported on the carbon monoxide and isonitrile insertion into the B-B bond of 1,2-diborolanes (Scheme 11).[91] The addition of xylyl isonitrile to 1,2-diborolane **28** results in the formation of 1,3-diboracyclohexene **29**. The addition of water induces a rearrangement to five-membered boryl-boracyclopentene **30**. Similarly, the addition of carbon monoxide to 1,2-diborolane **28** was speculated to result in the formation of the albeit undetected insertion product **31**. Dimerization of the

proposed transient diboracyclohexene **31** was invoked to explain the formation of spirocyclic boracyclopentene dimer **32**.

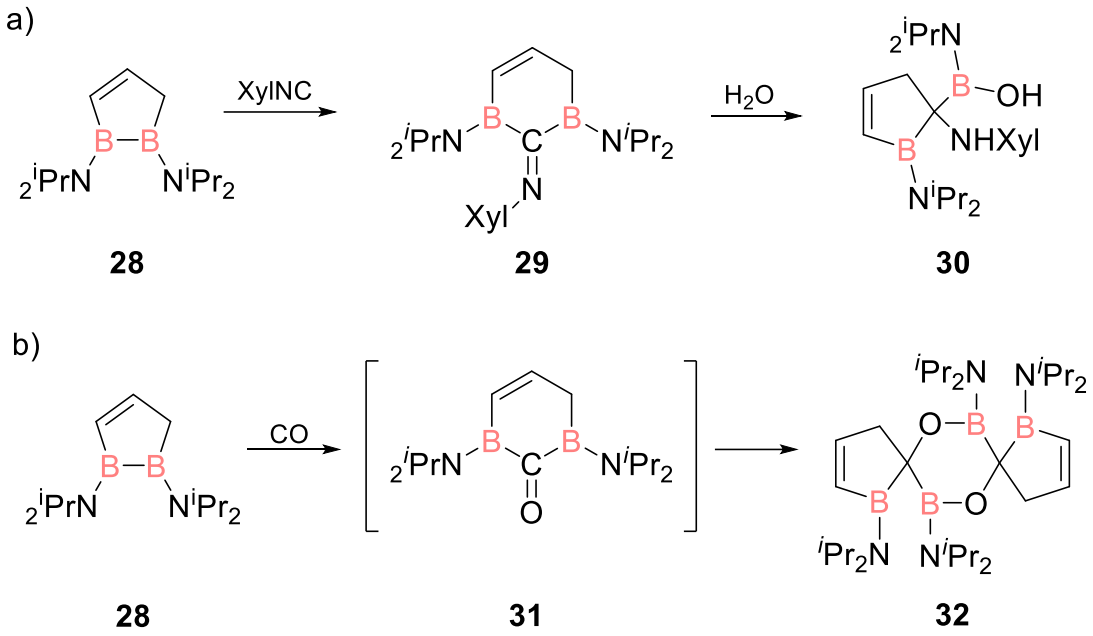

Scheme 11. a) Addition of XylNC to diborolane **28** to give six-membered **29**. Addition of water results in boryl-boracyclopentene **30**. b) Treatment of diborolane **28** with CO results in the insertion into the B-B bond to presumably give transient **31** and subsequent dimerization product **32**.

Berndt *et al*. employed the reductive dimerization of a 1,2- diborolane for the formation of a central four-membered aromatic ring with planar-tetracoordinate boron atoms and very short B-B distances.[92] Further synthetic applications have been reported by the Berndt[93] and Braunschweig group.[90] Recently, 1,2-diborolanes attracted renewed interest as pharmacologically active ingredients.[94]

(2) Five-membered 1,2-diboraheterocycles with p-block elements exist in several combinations, but N-heterocycles are the most prevalent. For instance, 1,4-diaza-2,3-diboroles are isoelectronic to cyclopentadienide: two C-C double bonds are formally replaced by BN units. Kong *et al*. recently reported on the synthesis of the five-membered heterocycle **33** by addition of dicyclohexylcarbodiimide to a 1,2-dichlorodiborane(4) followed by reduction.[95] In the same work diazadiborole **33** was used as a synthon for different boracycles (Scheme 12). With the same B_2N_2C scaffold, Braunschweig reported on several isolable cyclic radicals **34**$^{\cdot}$ in 2018.[96] Already a decade earlier, Roesler reported stable crystalline N-heterocyclic carbene **35** with a B-

B bond in the backbone showing better σ-donating abilities than Arduengo-type carbenes.[97]

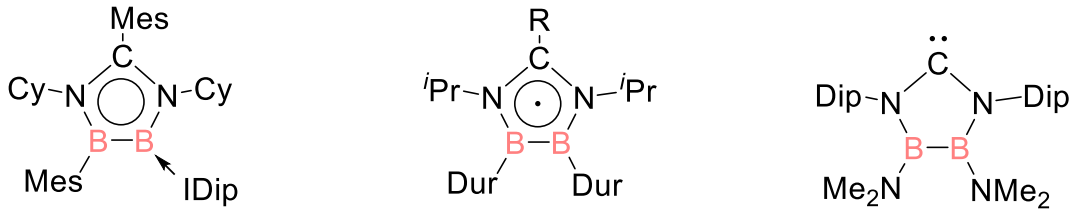

33 **34˙a,b** **35**

Scheme 12. Selected examples of 1,4-diaza-2,3-diborolane species by Kong **33**, Braunschweig **34˙** (**a**: R = Ph; **b**: R = N^{i}Pr$_2$) and Roesler **35** (Cy = cyclohexyl, Mes = Mesityl, IDip = 1,3-diisopropyl-4,5-dimethylimidazol-2-ylidene, Dip = Diisopropylphenyl).

The corresponding phosphorus analogue, a 1,4-diphospha-2,3-diborolane was reported by Braunschweig as a cyclic diborene stabilized by coordination of bis(diphenylphosphino)methane.[98] Moreover, several 1,2-diborolane motifs bearing three Group 15 heteroatoms have been reported in recent years.[99]

1,2,3-Triborolanes had only been known as metallocarborane derivatives[100] until Meller and coworkers reported a genuine example in the early 1990s using π-donating amino substituents as a stabilizing factor.[101] Since small molecules with several neighbouring boron atoms tend to form polyhedral clusters rather than electron precise molecules, the triborolane motif without donating ligands was only applied in the coordination sphere of transition metals.[102] Their reactivity behaviour remains mostly undiscovered. In contrast, the 1,2,4-triborolanes, synthesized by Berndt *et al*. were used to generate bishomoaromatic species (see Chapter 1.1.2).[84,103] 1,2,4,-triborolanes containing additional endocyclic heteroatoms have been reported by several groups.[104] While five-membered rings containing four or five boron atoms are predominantly known as submotifs of carborane clusters, an exception was reported by Braunschweig and co-workers very recently.[105]

Further examples with different heteroelements of the s- and p-block of the periodic table include Li, Na, K, Cs, Mg, Ca, Ba,[106] O[107], S[108], As[83], Si[85,86], Sn[83], Pb[83] as ring members.

(3) Diboracycles with endocyclically incorporated transition metals often include additional Group 15 or 16 elements as ligation sites: Metalloheterocycles of type **36** were prepared by the addition of a 1,2-diamide-1,2-diborane(4) to Group 4 metal

halides (Scheme 13).[109] An example with oxygen as heteroelement donor was recently reported by Mashima and Tsurugi.[110] They made use of the lone pairs of electrons in bis(neopentylglycolato)diborane(4) as a bidentate ligand **37** for several transition metal halides. The heavier homologue, with sulfur had already been established decades earlier by the Nöth group using $Li_2S_2Fe_2(CO)_6$ as a precursor:[111] Addition of the metallodisulfide to 1,2-bis(dimethylamino)-1,2-dichlorodiborane(4) results in diborairon-biscyclopentane **38** (Scheme 13).

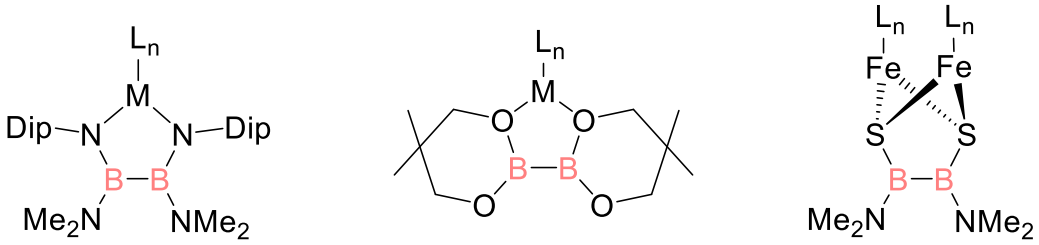

36a-c **37a-e** **38**

Scheme 13. Selected examples of metal-containing 1,2-diboracyclopentanes **36** (**a**: M = Ti, L = Cl, n =2; **b**: M = Ti, L = Me, n = 2; **c**: M = Zr, L = benzyl, n = 2; Dip = diisopropylphenyl), **37** (**a**: M = Nb; **b**: M = Mo; **c**: M = Zr; **d**: M = Ta; **e**: M = Ti, L = Cl, n = 4) and **38** (L = CO, n = 3).

Five-membered, transition metal containing diboracycles without additional heteroelements are not known as of today.

The four-membered rings containing a B-B bond can similarly be grouped in two different classes depending on the presence of further heteroatoms: (1) without additional heteroatoms or (2) with additional p-block heteroelements.

(1) Fully saturated four-membered heterocycles including a B-B bond are known since the early 1990s.[112] An unsaturated derivative, however, had already been reported in 1981 by van der Kerk *et al.*, namely a dihydrodiborete, which constitutes a formally 2π-aromatic non-Kékulé species:[113] Reduction of a 1,2-bis(bromoboryl)ethylene plausibly resulted in the formation of a transient 1,2-dihydro-1,2-diborete that rapidly rearranges to the puckered, thermodynamically favoured 1,3-isomer. The findings were confirmed shortly afterwards in related work by the Siebert group.[114] One year later, they even reported on the first isolation of a room temperature stable 1,2-dihydro-1,2-diborete using bulky diisopropylamino substituents at the boron centers for kinetic and electronic stabilization.[115] While this persistent 1,2-dihydrodiborete still rearranges at

elevated temperatures, Kaufmann disclosed the first thermally stable derivative by preventing the isomerization through annulation with a benzene ring in the backbone.[116] The addition of sodium/potassium alloy to *ortho*-bis(bromoboryl)benzene **39** gave stable 1,2-dihydro-1,2-diborete **40** (Scheme 14a). Attempts towards a 1,2-diborete, a formally 4π-antiaromatic cycle, were also preceded by reports on the rearrangement to the energetically favoured 1,3-isomer[117, 68b] until the Braunschweig group prepared a cAAC-stabilized derivative with a similar benzannulated structure: Reduction of *ortho*-bis(dibromoboryl)naphthalene **41** with lithium powder in diethyl ether gave 1,2-diborete **42** (Scheme 14b).[118] The cAAC ligands' strong σ-donating and π-accepting properties play a crucial role in stabilizing the inherently 4π-antiaromatic C_2B_2 ring by delocalizing electron density towards the periphery in the biradicaloid structure of **42**.

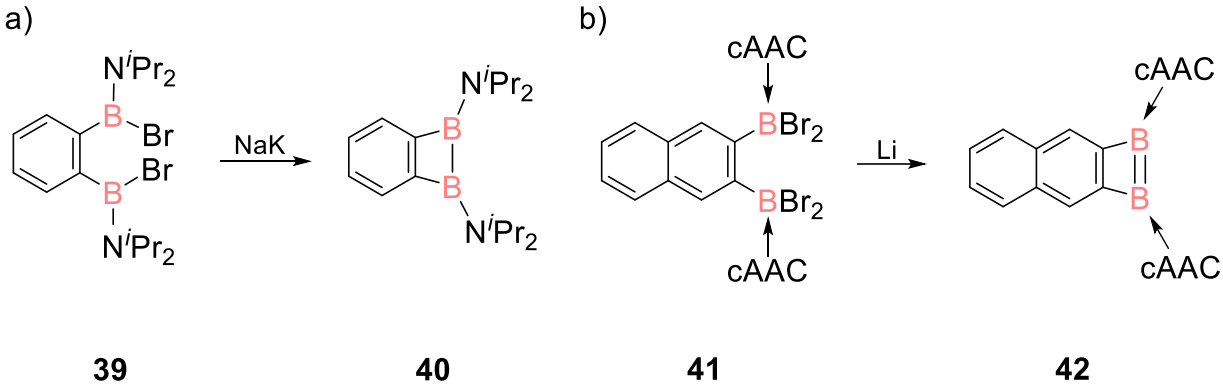

39 **40** **41** **42**

Scheme 14. a) Synthesis of benzannulated 1,2-dihydro-1,2-diborete **40** starting from *ortho*-bis(bromoboryl)benzene **39** using sodium/potassium alloy. b) Reduction of *ortho*-bis(dibromoboryl)naphthalene **41** with lithium powder results in cAAC-stabilized 1,2-diborete **42** (cAAC = 1-(2,6-diisopropylphenyl)-3,3,5,5-tetramethylpyrrolidin-2-ylidene).

The 1,2-dihydro-1,2-diborete, for instance, reacts with iron pentacarbonyl under photolytically induced B-B bond cleavage to a 1,4-diborabutadiene complex in the coordination sphere of a $Fe(CO)_3$ piano stool fragment.[87e] The 1,2-diborete can mimic a bis(borylene) to form adducts with CO making use of the reactive B-B bond.[118] Additionally, carbon monoxide can be inserted end-on into the B-B bond to generate a bisborylketone as very recently elaborated by Braunschweig and coworkers.[119]

(2) Only a few examples of 1,2-diboretes with endocyclic heteroatoms other than boron exist. A 1,2-diborete containing just one additional heteroatom was recently reported

by Braunschweig: The addition of dilithio diazabutadiene to a 1,2-dichlorodiborane results in the formation of azadiboretidine **43** (Scheme 15).[120] The structural motif had already been proposed three decades earlier by Meller *et al*. although without unambiguous evidence.[121] In 2001, the Nöth group reported the formation of an azatriborete **44** by adding Me_3SnLi to a 1,3-dibromo-triborane(5), a rare example of an electron-precise four-membered ring with three boron atoms and a heteroatom.[122] In 1992, Paetzold introduced the 1,2-diaza-3,4-diboretidine **45**, isoelectronic to cyclobutadiene and 1,2-diborete.[123] Two years later, Nöth reported on the first example of the heavier homologue **46**, a 1,2-diphospha-3,4-diboretane (Scheme 15).[104]

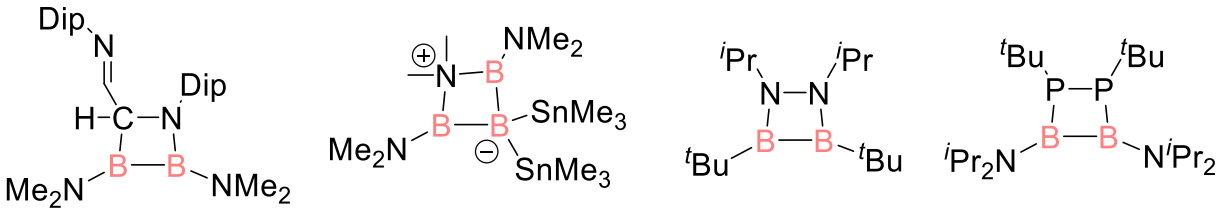

43 **44** **45** **46**

Scheme 15. Selected four-membered diboraheterocycles: azadiboretidine **43**, azatriborete **44**, 1,2-diaza-3,4-diazadiboretidine **45** and its heavier homologue 1,2-diphospha-3,4-diazadiboretidine **46**.

Four-membered heterocycles with at least three boron ring members exhibit a pronounced tendency to engage in non-classical bonding as elaborated in a recent review by Himmel.[124]

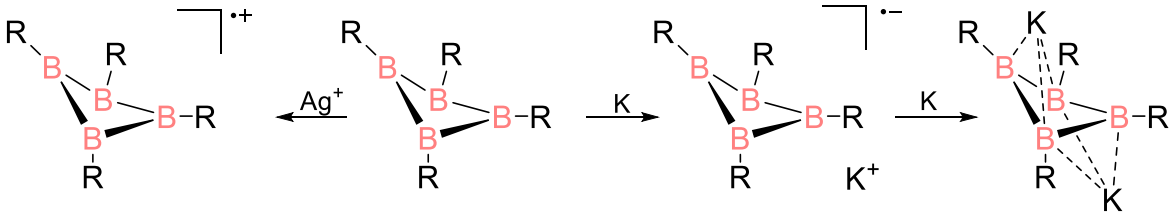

50$^{\bullet+}$ **47** **48**$^{\bullet-}$ **49**$^{2-}$

Scheme 16. Four different charged tetraborane rings. Neutral **47**, monoradical anion **48**$^{\bullet-}$, dianion **49**$^{2-}$ and monoradical cation **50**$^{\bullet+}$ (R = NCy_2, Cy = cyclohexyl).

A rare exception was reported by Braunschweig with a tetraborane ring[125] that can exist in four different charge states.[126] Addition of one or two equivalents of potassium

to tetraborane **47** results in monoradical anionic species **48**$^{\cdot-}$ or the dianionic ring **49**$^{2-}$. The one electron oxidation with a silver salt furnishes the monoradical cationic tetraborane **50**$^{\cdot+}$ (Scheme 16).

1.2.2 Three-membered rings containing a B-B bond

Borirenes have recently experienced a resurgence through the facile access by [1+2] cycloaddition of borylenes to alkynes.[127] They have thus been the subject of several reactivity studies in recent years,[127] including some investigations on their coordination behaviour towards transition metals.[128] In contrast, three-membered ring systems with endocyclic B-B bonds have received much less attention.

1.2.2.1 Diboriranes

While an undistorted sp^3 hybridized carbon center shows a tetrahedral coordination environment with bond angles of about 109.5°, three-membered rings allow for a maximum sum of inner angles of 180°. On average, inner angles are therefore considerably more acute leading to the well-known “banana” bonds with pronounced p-orbital contributions as well as considerable ring strain.[129] This effect is even more severe in case of donor-free bora substitution because of the sp^2-hybridization at boron with its 120° bond angles. In addition to its Lewis acidity, this deviation is a key factor contributing to the intrinsic instability of classical diboriranes.

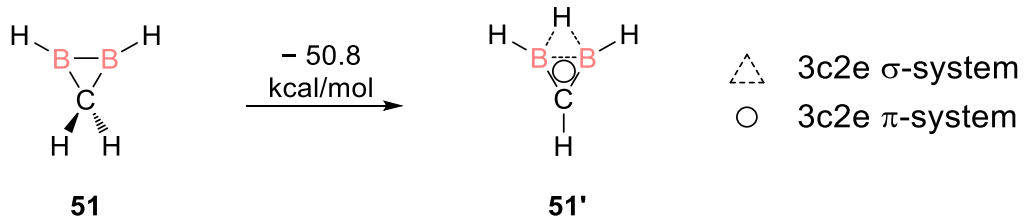

51 **51'**

Scheme 17. Classical diborirane **51** and global minimum: non-classical diborirane **51’**.

The electronically unfavourable arrangement is thus settled by the formation of a BHB bridge (3c2e bond) and a cyclic 2π electron system resulting in non-classical structure **51’**. The BHB bridge and the ring carbon in **51’** arrange in one plane, so the geometry contradicts the van´t Hoff/Le Bel rule (tetracoordinated main group atoms reside in

tetrahedral geometry).[130] Quantum chemical calculations by Jemmis *et al.* suggest that the parent non-classical diborirane **51'** is 50.8 kcal mol^{-1} lower in energy than its classical counterpart **51** (Scheme 17).[131] Accordingly, to date only Liu's donor-stabilized diborirane **52**[132] and Wagner's dianionic diborirane "ate" complex **53**[133] are known as examples approximating classical diboriranes (Scheme 18). The B-B bond in **53** is generated by adding electrons in between two three-coordinated boron atoms in neutral bis(boryl) precursor.

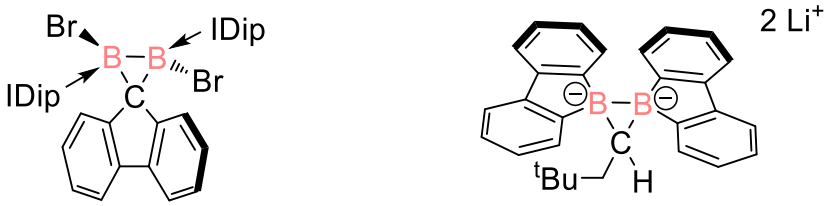

52 **53**

Scheme 18. Previously reported NHC stabilized diborirane **52** and dianionic diborirane **53** (IDip = 1,3-diisopropyl-4,5-dimethylimidazol-2-ylidene).

The few synthetic pathways towards non-classical diboriranes have been developed by the Berndt group. They suffer, however, from low selectivity, moderate yields and/or scope. The first access towards a non-classical diborirane was reported in 1985: The 1,1-diboration of bis(trimethylsilyl)acetylene with diborane(4) **6f** gives bis(boryl)alkene **54a** with ^{t}Bu-groups at the boron atoms which serves as direct precursor for reductive ring closure (Scheme 19).[134]

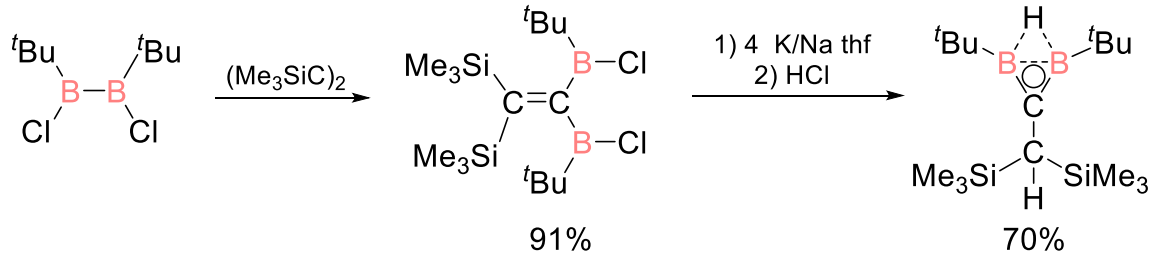

6f **54a** **55a**

Scheme 19. Synthesis of non-classical diborirane **55a** from reduction of 1,1-bis(chloroboryl)alkene **54a** by four equivalents of K/Na alloy, starting from 1,2-dichlorodiborane(4) **6f**.

After reduction with sodium/potassium alloy in tetrahydrofuran and consecutive protonation with hydrochloric acid, the non-classical diborirane **55a** was indeed

obtained.[135] One problem that arises is the apparently limited scope of the reaction since the choice of other substituents and/or reducing agents leads to other products, as was shown several years later by Berndt and coworkers.

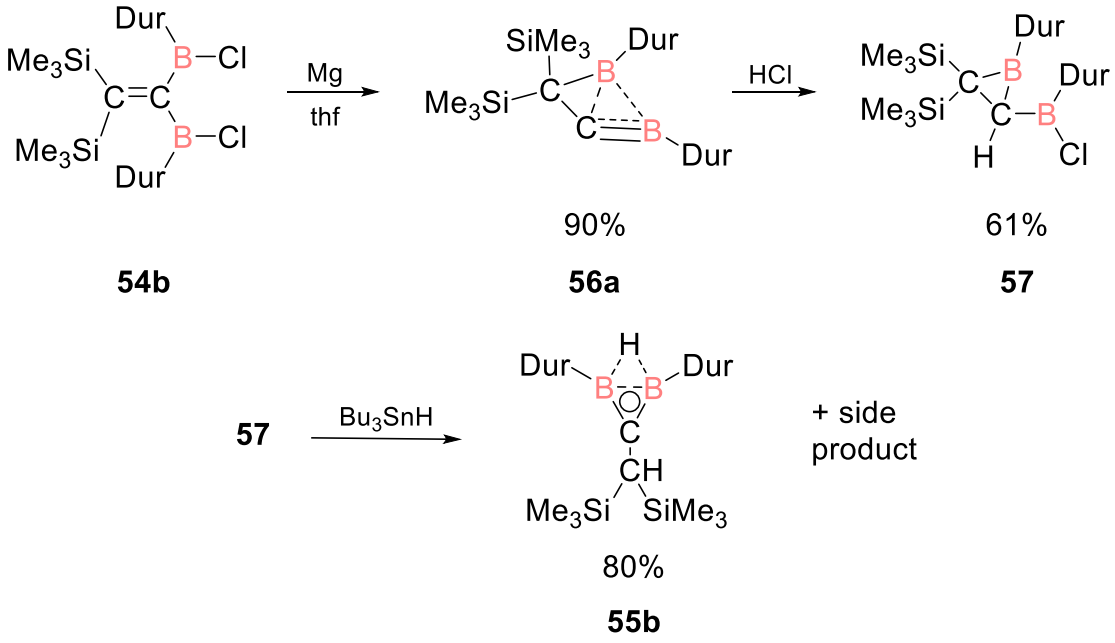

Scheme 20. Synthesis of non-classical diborirane **55b** by reaction of borylborirane **57** with Bu_3SnH and a subsequent rearrangement. Borirane **57** was obtained *via* protonation of boranediylborirane **56a** starting from reduction of bis(boryl)alkene **54b** with magnesium (Dur = 2,3,5,6-tetramethylphenyl).

For instance, reduction of bis(boryl)alkene **54b** with duryl groups at the boron center with magnesium results in boranediylborirane **56a** containing a 3c2e bond, which can be regarded as a homo-bridged diborirane (Scheme 20).[136]

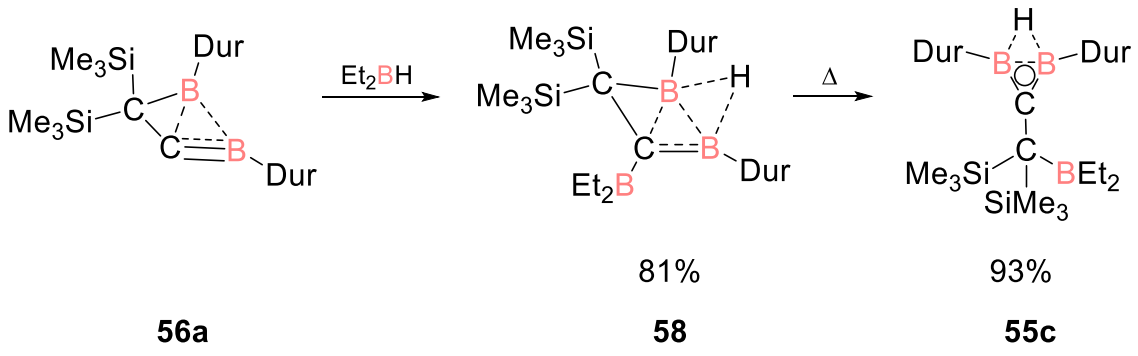

Scheme 21. Synthesis of non-classical diborirane **55c** by thermal conversion of non-classical diboretane **58** starting from boranediylborirane **56a** (Dur = 2,3,5,6-tetramethylphenyl).

In order to still address a non-classical diborirane, Berndt and co-workers resorted to further manipulations: The addition of hydrochloric acid to **56a** gives borylborirane **57**[137] (Scheme 20) which is subsequently converted to non-classical diborirane **55b** by Cl-H exchange through addition of Bu_3SnH.[138]

In addition to the lengthy synthetic pathway and the poor overall yields, a non-classical 1,2-diboretane is obtained as side product. Boranediylborirane **56a** is systematically converted to non-classical 1,2-diboretane **58** using diethylborane. Thermal conversion results in non-classical diborirane **55c** with pending boryl group (Scheme 21).[139] Unlike the magnesium reduction, treatment of duryl-substituted bis(boryl)alkene **54b** with an excess of lithium powder in diethyl ether and consecutive protonation with hydrochloric acid gives borylborataalkyne **59** (Scheme 22).[73,74b] Dimethylchlorosilane is nucleophilically attacked by the anionic carbon center of borylborataalkyne **59** under LiCl elimination. The Si-bonded hydrogen initially migrates to a boron center while one of the duryl groups migrates in turn to silicon yielding non-classical diborirane **55d**.[139]

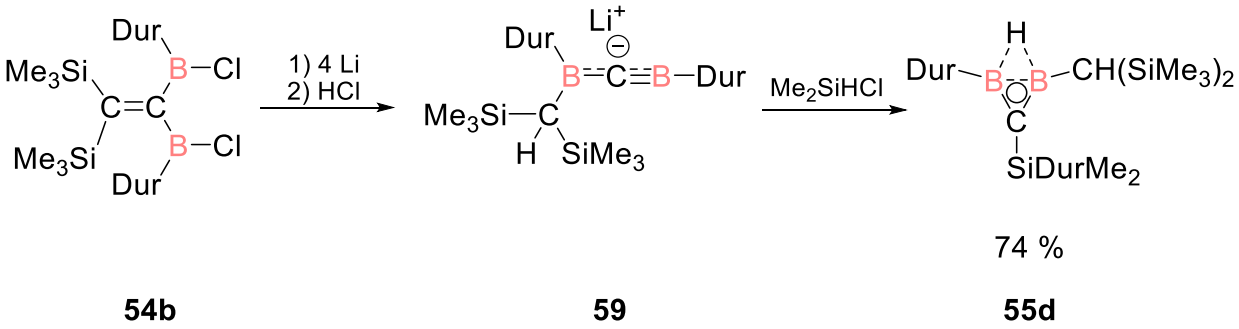

Scheme 22. Synthesis of non-classical diborirane **55d** *via* the addition of dimethylchlorosilane to borylborataalkyne **59**, starting from reduction and subsequent protonation of 1,1-bis(chloroboryl)alkene **54b** (Dur = 2,3,5,6-tetramethylphenyl).

In more recent work, Berndt and coworkers serendipitously isolated non-classical diborirane **55e** from the product mixture of thermal decomposition of diboracyclopentane **25b** (see Chapter 1.2).[93] Starting from a diborane(4), however, it takes six steps to obtain the diborirane **55e** in poor yields (Scheme 23).

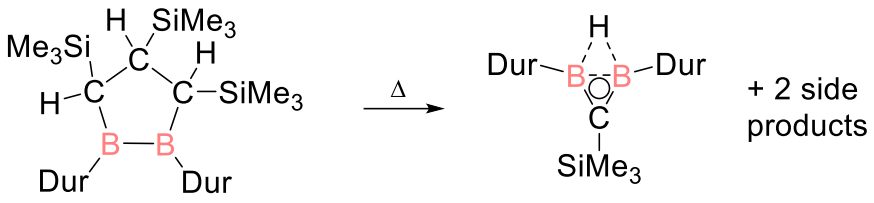

25b **55e**

Scheme 23. Thermal decomposition of diboracyclopentane **25b** to give non-classical diborirane **55e** amongst other products (R = $SiMe_3$, R' = Dur = 2,3,5,6-tetramethylphenyl).

One reported example of non-classical diborirane reactivity is the addition of elemental iodine to diborirane **55b**, which leads to a ring opening reaction to afford bis(iodoboryl)ethane **60** (Scheme 24).[136] Notably, **55b** is regenerated by reduction of **60** with sodium/potassium alloy.

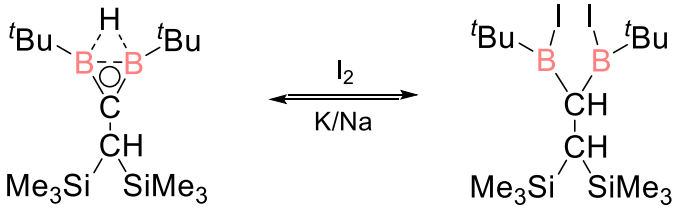

55b **60**

Scheme 24. Synthesis of bis(iodo)borane **60** by addition of elemental iodine to non-classical diborirane **55b**. Reduction of **60** with K/Na again gives non-classical diborirane **55b**.

Otherwise, the reactivity on non-classical diboriranes remains unexplored, e.g. the reactivity behaviour of the BHB bridge, the complexation of the π-system or the reactivity towards main group nucleophiles.

1.2.2.2 Diboriranides

Aromaticity is one of the most fundamental concepts in organic and inorganic chemistry. In 1865, Kekulé proposed the nowadays well-known structure of benzene,[140] while decades later, Hückel and Pauling shed light on the phenomenon from a theoretical perspective introducing the 4n+2 counting rule and resonance stabilization respectively.[141]

The formal substitution of ring carbon atoms by heteroelements has been extensively studied and continues to tremendously increase the structural diversity of aromatic systems. Incorporation of boron is of particular interest due to the interaction of the π-system with the vacant p-orbital at boron leading to a significant decrease of the LUMO energies and thus the electron accepting properties.[23] Cyclopropenium cation **61** is the smallest hydrocarbon that complies with Hückel's rules for aromaticity. Due to its ring strain and the delocalized π-system, the molecule has been exploited as a C_3 building block and as a ligand for transition metals in several coordination modes.[142]

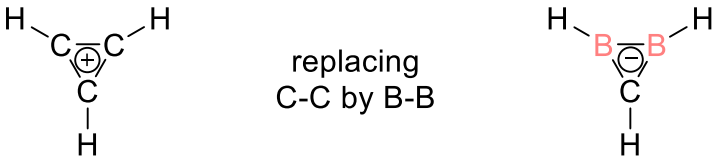

61 **62**

Scheme 25. Cyclopropenium cation **61** and isoelectronic diboriranide **62**.

Anionic diboriranides **62** are isoelectronic to cyclopropenium cations **61**, formally replacing a C-C bond with a B-B bond and adding two electrons (Scheme 25) and therefore comprise the lightest conceivable monoanionic aromatic system. As with non-classical diboriranes, only little is known about the reactivity of diboriranides **62**, in stark contrast to their all-carbon congener **61**. A few synthetic pathways towards diboriranides have been developed by the group of Berndt decades ago.[135,136,143]

The first synthesis was reported in 1985 starting from 1,1-bis(chloroboryl)alkene **54a**. Addition of four equivalents of sodium/potassium alloy in thf gives diboriranide dianion **63** (Scheme 26). Single protonation with tert-butyl-trimethylsilylamine as weak Brønstedt acid results in monoanionic diboriranide **64a**. As discussed in Section 1.2.2.1, further protonation of this diboriranide does not result in the formation of a

classical diborirane but yields the energetically more favourable non-classical diborirane **55a** (Scheme 19).[134] An alternative route with improved yield was developed some years later: Starting once more from bis(chloroboryl)alkene **54a**, the boranediylborirane **56b** is obtained by addition of one equivalent of magnesium turnings in thf under sonication.

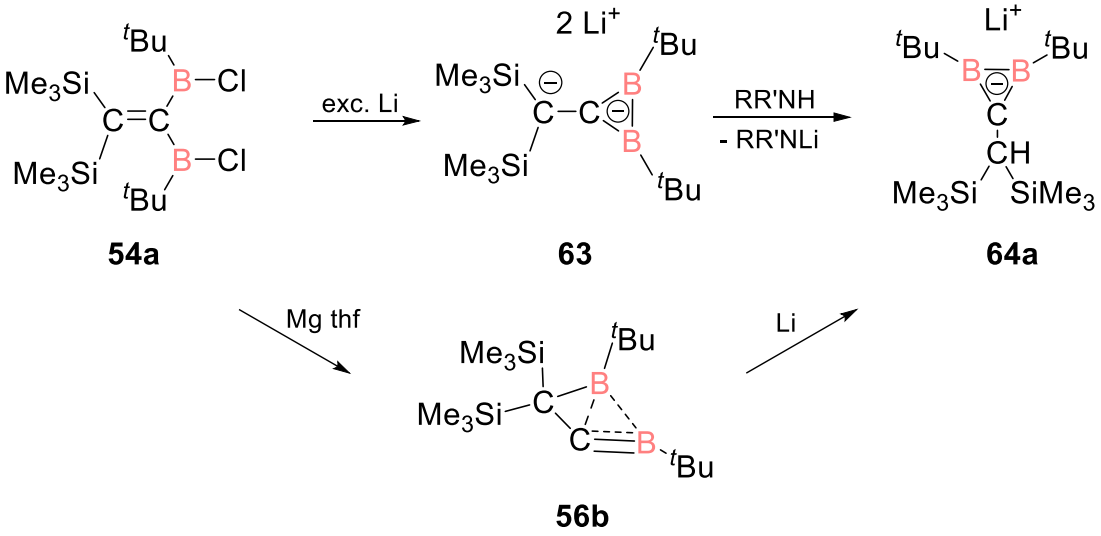

Scheme 26. Synthesis of diboriranide **64a** *via* two different reduction pathways starting from bis(chloroboryl)alkene **54a**. Excess of lithium powder in Et_2O gives dianionic **63** while an equimolar amount of magnesium in thf results in boranediylborirane **56b** (R = $SiMe_3$, R' = ^{t}Bu = *tert*-butyl).

Diboriranide **64a** is obtained after reduction of boranediylborirane **56b** with lithium powder in diethyl ether in 90% yield (Scheme 26). Further work by Berndt shows that the diboriranide **64b** can also be obtained from non-classical diborirane **55d** by reduction with excess lithium powder in diethyl ether under liberation of lithium hydride (Scheme 27).[143] The same reactivity was reported earlier for a homoaromatic derivative of a non-classical diborirane.[144]

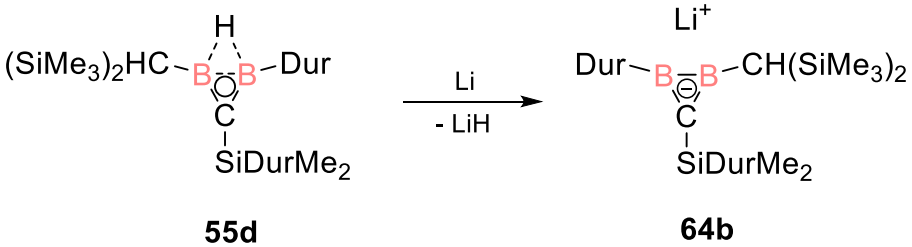

Scheme 27. Synthesis of 1,2-diboriranide **64b** by reacting non-classical diborirane **55d** with lithium under elimination of LiH.

As stated above, the general reactivity of diboriranides is severely underexplored being limited to protonation and the reactions with a few main group electrophiles.

For example, diboriranide **64b** reacts with Et_2AlCl at −60°C in hexane to the diethylaluminium-bridged diborirane **65a** (Scheme 28). The aluminium atoms reside in the ring plane while some degree of BCB 3c2e bonding is retained. A similar result has been observed for $PhBF_2$ according to multinuclear NMR spectroscopy, in the absence of a single crystal x-ray diffraction study.[143] Addition of $PhBF_2$ to diboriranide **64c** also results in boryl bridged diborirane **65b**.

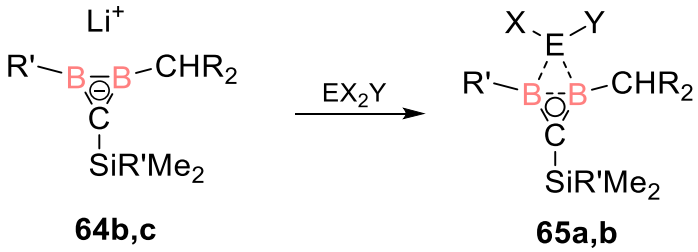

64b,c **65a,b**

Scheme 28. Synthesis of E bridged diborirane **65a,b** (**a**: R' = Dur = 2,3,5,6-tetramethylphenyl, R = $SiMe_3$, E = Al, X = Et, Y = Cl; **b**: R' = Mes = 2,4,6-trimethylphenyl, R = $SiMe_3$, E = B, X = F, Y = 3,5-di-*tert*-butylphenyl) from diboriranide **64b,c** (**b**: R' = Dur, R = $SiMe_3$; **c**: R' = Mes, R = $SiMe_3$).

In contrast, addition of dichlorophenylborane to diboriranide **64b** does not appear to react *via* the B-B σ-bridge but *via* the formal anionic ring carbon. Formation of transient classical boryldiborirane **66** was speculated, which presumably rearranges to the energetically more favourable 1,3-diboraindane **67** under migration of the chloro substituent from boron to silicon (Scheme 29).[143]

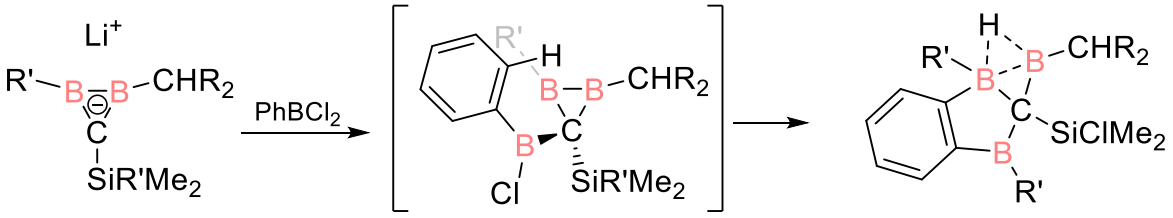

64b **66** **67**

Scheme 29. Synthesis of 1,3-diboraindane **67** *via* transient classical boryl-diborirane **66** starting from diboriranide **64b** by adding $PhBCl_2$ (R' = Mes = 2,4,6-trimethylphenyl, R = $SiMe_3$).

Ten years later, Siebert and Berndt *et al.* isolated the first examples of Group 15 element-bridged diboriranes.[145] Addition of Ph_2ECl (E = P, As) gives mesoionic phosphoniumdiboretanide **68a** and arsoniumdiboretanide **68b** (Scheme 30).

Consecutive reduction of phosphoniumdiboretanide **68a** with lithium in diethyl ether yields phosphadiboretanide **69** under liberation of phenyllithium.

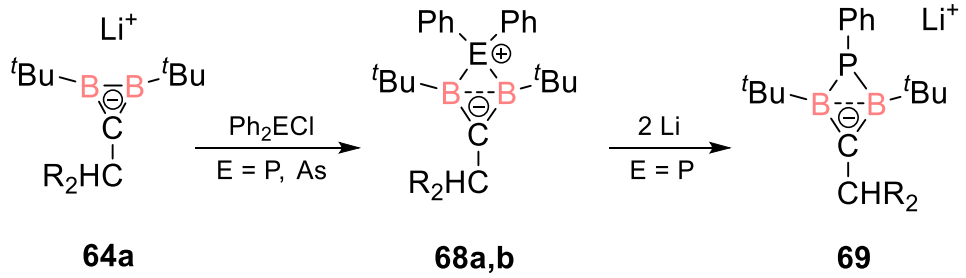

64a **68a,b** **69**

Scheme 30. Synthesis of phosphoniumdiboretanide **68a** and arsoniumdiboretanide **68b** from diboriranide **64a** after addition of Ph_2ECl (**a**: E= P; **b**: E = As) and consecutive reduction of **68a** to phosphadiboretanide **69** (R = $SiMe_3$).

The discussed reactivity of diboriranides indicates the tendency to react as a nucleophile *via* its B-B σ-bridge (despite one counterexample), while a certain π-interaction is retained in the BCB backbone.

1.2.2.3 Triboriranes

Three membered triboracycles had only been known as homoderivatives[146] for a long time until Braunschweig *et al.* reported the lithium salt of a triborirandiide **70** in 2015.[147] A neutral B_3 ring **71** was reported some years later by Yamamoto albeit with only weak π-interactions between two of the boron atoms.[148]

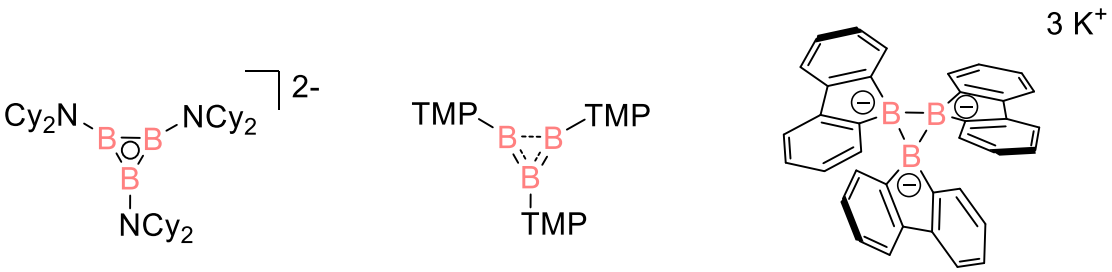

70 **71** **72**

Scheme 31. Recently reported three membered triboracycles: triborirandiide **70**, neutral triboracyclopropane **71** and trianionic **72**.

A cyclic triborane only comprised of σ-bonds **72**, which exclusively reacts under B-B bond cleavage, was recently reported by Kinjo and coworkers (Scheme 31).[149]

1.2.2.4 Heteroatom derivatives of three-membered 1,2-diboracycles

Three membered rings with B-B bond and a third endocyclic atom besides boron or carbon are also known. While heavier Group 13 atoms in an electron-precise B_2X cyclic scaffold are not known, a B_2Si ring was recently reported by Mo as silylene stabilized siladiborirene **73** (Scheme 32).[150] Azadiboriridines **74**, isoelectronic to diboriranides, are known since several decades. Accordingly, several derivatives and reactivity studies have been reported over the years.[151] Expectedly, B_2N heterocycle mostly react under ring-strain releasing B-B bond cleavage.[152] In contrast, the B_2P rings have only recently been reported.[153] Similarly, while diboroxiranes **75a** have been described in 1992 by Paetzold,[154] their heavier homologues **75b-d** have only been obtained recently by Braunschweig by addition of the element to B-B multiple bonds.[155] Finally, Braunschweig reported on halogen-bridged diboranes(4) **76a-c**.[156]

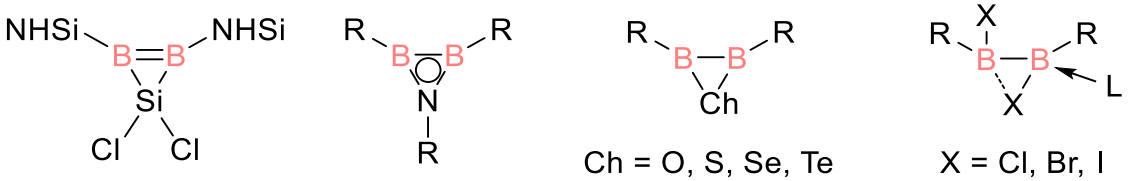

73 **74** **75a-d** **76a-c**

Scheme 32. Siladiborirene **73**, azadiboriridines **74**, chalcogen containing three membered rings B_2Ch **75** (**a**: Ch = O; **b**: Ch = S; **c**: Ch = Se; **d**: Ch = Te) and halide bridged diborane(4) **76** (**a**: X = Cl; **b**: X = Br; **c:** X = I; L = PMe_3).

2 Aims and Scope

Despite the huge variety of potential functionalities (Scheme 33), investigations on the reactivity of the smallest diboracycles are scarce. Since organometallic transition metal complexes are of immense interest for organic and inorganic synthesis, for instance as homogenous catalysts, the implementation of such heterocycles as ligands *via* the available π-system would be desirable. Intriguing reactivities can be expected from other functional groups in the system: While the borane in resonance structure **I'** may allow for hydroboration of various double and triple bonds, the Lewis acidic methyleneborane could be susceptible either to nucleophilic attack or to cycloadditions (Scheme 33). In addition, diboriranide **II,** that should be accessible from the non-classical diborirane **I** by reductive hydride elimination, could also act as a versatile ligand for transition metals either by coordination of the σ-bridge or by its π-system. In combination with the inherent ring strain of these systems, a versatile reactivity is to be expected.

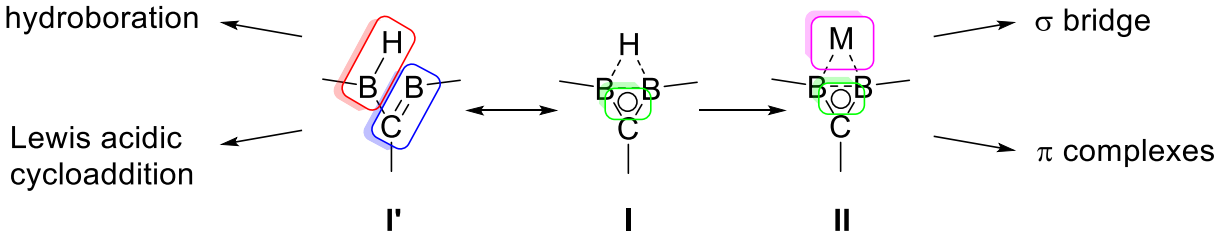

Scheme 33. Synthesis of diboriranide **II** from non-classical diborirane **I** (resonance structure **I'**) with both heterocycles comprising several potential functionalities.

The paucity of research on these systems is likely due to two key challenges: the complex substitution patterns found in all known examples and the difficulty of accessing them, which typically involves multi-step processes with low yields and limited general applicability. For example, the absence of aromatic substituents at the ring carbon atom restricts the exploration of the unique electronic properties in expanded conjugated systems. Accordingly, the central focus of this thesis is to develop a straightforward synthesis of perarylated non-classical diboriranes and anionic diboriranides and the examination of their reactivity towards small molecules

and transition metals, following recent investigations in the Scheschkewitz group (Scheme 34).

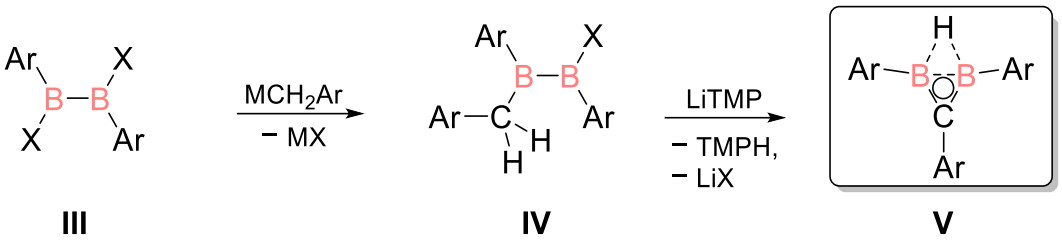

Scheme 34. Synthesis of non-classical diborirane **V** from diborane(4) **III** *via* deprotonation of asymmetric diborane(4) **IV** (Ar = Aryl, X = halide, M = Group 1 or 2 metal).

The initial sequence consists of three steps starting from a 1,2-dihalodiborane(4) **III** to result in an asymmetric diborane(4) **IV** with α-boryl C-Hs at one boron and a suitable leaving group at the pending boron atom. Deprotonation of the α-boryl carbon atom should result in the formation of non-classical diborirane **V**. The synthesis may depend on the choice of suitable reagents. A high-yielding protocol would facilitate investigations of the diborirane and the corresponding diboriranide – by extension based on the synthesis reported by the Berndt group.[144]

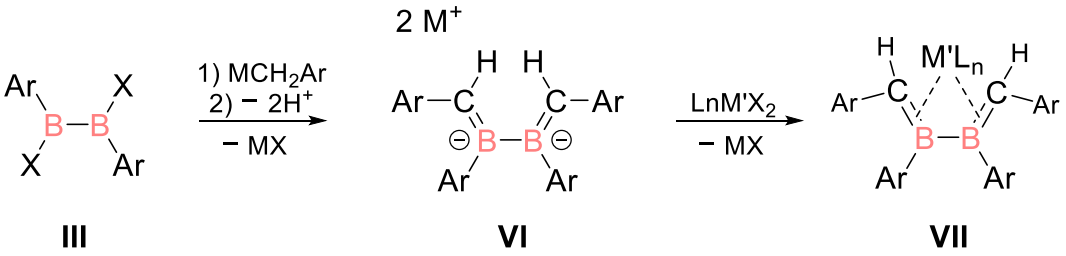

Scheme 35. Synthesis of diboratabutadiene **VI** from 1,2-dihalodiborane(4) **III** and consecutive formation of metal complexes **VII** (Ar = Aryl, X = halide, M = Group 1 or 2 metal, M' = transition metals).

Olefin metal complexes have been a cornerstone of organometallic chemistry research for nearly two centuries, with butadienes being of particular interest as the simplest conjugated π-ligands, featuring two C=C double bonds. Recently, bora-substituted neutral and anionic alkene homologues have emerged as a promising alternative class of ligands with distinct applications.[80] Although dianionic 2,3-diboratabutadienes with central B-B bonds have been reported decades ago, transition metal complexes of bora-substituted butadienes have so far only been explored with terminal boron centers (see Chapter 1.1.2).[87] The potential for a residual internal B-B bond to unlock new synthetic pathways makes the concept of a 2,3-diboratabutadiene transition metal

complex highly appealing. Previous attempts to synthesize such a complex may have failed due to unsuitable choices of substituent, as the steric bulk of $SiMe_3$ groups at the anionic carbon centers in **18c** (Scheme 8, Section 1.2.1) likely promoted electron and proton transfer over nucleophilic substitutions at bulky transition metal centers. We hypothesized that replacing silyl groups with less sterically demanding phenyl substituents, like the approach used for diborirane **V**, could overcome these challenges. Accordingly, the second focus of this work was the synthesis of the corresponding diboratabutadiene **VI** and the examination of its reactivity towards transition metals in anticipation of metal complexes **VII** (Scheme 35). Moreover, its reactivity, especially with respect to the retained B-B bond, was to be investigated.

3 Results

3.1 Diboriranide σ-Complexes of d- and p-Block Metals

P. Grewelinger, T. Wiesmeier, C. Präsang, B. Morgenstern, D. Scheschkewitz, *Angew. Chem. Int. Ed.* **2023**, *62*, e202308678. https://doi.org/10.1002/anie.202308678; *Angew. Chem.* **2023**, *135*, e202308678. https://doi.org/10.1002/ange.202308678

Author Contributions:

Philipp Frank Grewelinger (Conceptualization: Equal (DS); Data curation: Lead; Formal analysis: Lead; Investigation: Lead; Writing – original draft: Lead)

Tim Wiesmeier (Data curation: Supporting, Formal analysis: Supporting, Investigation: Supporting)

Carsten Präsang (Conceptualization: Supporting; Data curation: Supporting; Formal analysis: Supporting; Investigation: Supporting; Writing – original draft: Supporting)

Bernd Morgenstern (Data curation: Lead; Formal analysis: Supporting; Methodology: Supporting; Visualization: Supporting)

David Scheschkewitz (Conceptualization: Lead; Formal analysis: Supporting; Funding acquisition: Lead; Investigation: Supporting; Methodology: Supporting; Project administration: Lead; Resources: Lead; Supervision: Lead; Writing – review & editing: Lead)

How to cite: *Angew. Chem. Int. Ed.* **2023**, *62*, e202308678
doi.org/10.1002/anie.202308678

Main Group Chemistry

Diboriranide σ-Complexes of d- and p-Block Metals

*Philipp Grewelinger, Tim Wiesmeier, Carsten Präsang, Bernd Morgenstern, and David Scheschkewitz**

Abstract: Diboriranides are the smallest conceivable monoanionic aromatic cycles, yet only limited examples have been reported and their reactivity and complexation behavior remain completely unexplored. We report a straightforward synthesis of the first peraryl diboriranide c-$(DurB)_2CPh^-$ as its lithium salt in three steps via the corresponding non-classical diborirane from a readily available 1,2-dichlorodiborane(4) (Dur = 2,3,5,6-tetramethylphenyl). With the preparation and complete characterization of representative complexes with tin, copper, gold and zinc, we demonstrate the strong preference of the diboriranide for σ-type coordination modes towards main group and transition metal centers under unperturbed retention of the three-membered B_2C-ring's $2e^-$ π-system.

Introduction

The coordination chemistry of aromatic species such as benzene,[1] cyclopentadienide anions[2] and tropylium cations[3] is dominated by the dative bonding of the π-system to electron-deficient acceptors from the p- and the d-block of the periodic table. The isoelectronic replacement of carbon atoms of the ring systems by one or two boron atoms led to various examples of borole dianions,[4] boratabenzenes[5] and diboratabenzenes[6] as well as the seven-membered borepins.[7] While monoanionic boratabenzenes and neutral borepins are employed as conceptually obvious substitutes for cyclopentadienide ligands, the dianionic species allow for a straightforward access to various triple decker complexes.[8] In comparison, the coordination chemistry of three-membered aromatics is much less developed: Although the all-carbon cyclopropenium cations **I** (Scheme 1) have been employed as ligands, they predominantly react under reductive ring-opening, in other words oxidative addition of the σ-framework to the transition metal.[9] Borirenes **II**, formally derived by isoelectronic replacement of one carbon by a boron atom, have enjoyed particular attention due to the convenient access by borylene transfer to alkynes.[10] This methodology also provides facile access to borirenes in X-type coordination to transition metals,[11] but the coordination to transition metals as L-type ligands is rare and occurs exclusively in the η^3-mode through the π-system.[12]

While a few diboriranides **III** were described by Berndt et al.,[13] triborirandiides **IV** have only been known as homoaromatic derivatives[14] until Braunschweig et al. reported a monocyclic example in 2015.[15] Stable complexes with d- and p-block elements are unknown in both cases. In fact, even the general reactivity of diboriranides **III** is an almost unchartered terrain, presumably due to (a) the relatively bulky substitution patterns in all known examples and (b) the rather complicated access, typically in multi-step procedures and/or poor yields.

The first diboriranides reported by Berndt et al. in 1985 had been prepared by excessive reduction of 1,1-bis(chloroboryl)-2,2-bis(trimethylsilyl)alkene.[13a] In this reaction, the boryl-substituted end of the C=C bond becomes part of the anionic B_2C ring and the silyl-substituted end is transformed into an exocyclic methyl group with an additional anionic charge that can be selectively protonated to give **A** (Scheme 2). While the procedure requires only three

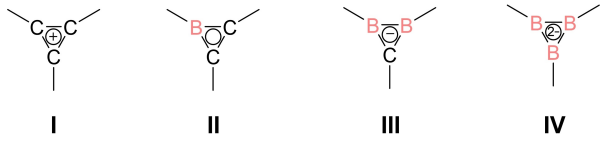

Scheme 1. Schematic representation of isoelectronic cyclopropenium analogues with boron atoms.

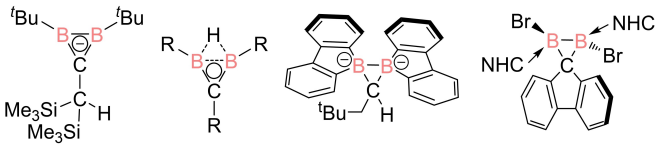

Scheme 2. Previously reported B_2C ring structures (NHC = 1,3-diisopropyl-4,5-dimethylimidazol-2-ylidene).

[*] M. Sc. P. Grewelinger, B. Sc. T. Wiesmeier, Dr. C. Präsang, Prof. Dr. D. Scheschkewitz
Krupp-Chair for General and Inorganic Chemistry, Saarland University
66123 Saarbrücken (Germany)
E-mail: scheschkewitz@mx.uni-saarland.de
Dr. B. Morgenstern
Service Center X-ray diffraction, Saarland University
66123 Saarbrücken (Germany)

steps from a 1,2-dichlorodiborane(4), it is inherently limited in scope. All other diboriranides reported after 1985 have been prepared from neutral diboriranes **B** by reductive cleavage of the B–B-bridging hydrogen atom, allegedly as hydride.[16]

The procedures, however, often involve more than six steps from 1,2-dichlorodiboranes(4), result in mediocre yields and lack general applicability.[13a,17] For example, aromatic substituents at the ring carbon atom remain inaccessible, thus precluding any extension of the conjugated system for the exploitation of the peculiar electronic properties in extended systems. The same limitation applies to the two classical diboriranes **C** and **D** reported by the groups of Wagner[18] and Liu,[19] which are inherently unsuitable as precursors for diboriranides anyway due to the tetracoordinate ring carbon atoms and the absence of a suitable leaving group in this position.

We now report the straightforward and high yielding synthesis of a simple diboriranide with a sterically innocent and potentially conjugated phenyl substituent at the ring carbon atom in three steps from a readily available 1,2-diaryl-1,2-dichlorodiborane(4). As we will show, the coordination of the thus obtained diboriranide to p- and d-block elements is dominated by the B–B σ-bond leaving the $2e^-$ π-system essentially unperturbed and resulting without exception in species with an anti-van't Hoff/Le Bel-geometry at the boron centers.

Results and Discussion

Synthesis of lithium diboriranide

Carbon atoms in α-position to an electron deficient boron center can readily be deprotonated to result in the corresponding methyleneborates with a B–C double bond.[20] We therefore anticipated that the restrictions mentioned above may be overcome by the deprotonation of a suitably substituted derivative of a 1-methyl-2-halodiborane(4) and subsequent ring closure to the corresponding diborirane under salt elimination. Instead of the parent methyl, we opted for a benzyl group to further facilitate deprotonation and provide minimal kinetic stabilization while still maintaining a relative steric innocence and - at the same time - extending the conjugated system of the diboriranide by a phenyl substituent.

The required 1-benzyl-2-chloro-1,2-diduryldiborane(4) **1** was prepared by the surprisingly selective reaction of 1,2-dichloro-1,2-diduryldiborane(4)[21] with one equivalent of benzyl magnesium chloride[22] at −78 °C in 97 % yield. It was characterized by multinuclear NMR spectroscopy and single crystal x-ray diffraction (see Supporting Info). The deprotonation of **1** in benzylic position is indeed possible using lithium tetramethylpiperidide (LiTMP) and results in instant ring closure to the non-classical diborirane **2** (Scheme 3), which was isolated from a concentrated toluene solution at −23 °C as colorless crystals in 85 % yield. The ^{11}B NMR chemical shift at δ = 25.7 ppm is very similar to those of the previously reported diboriranes with duryl substituents at the

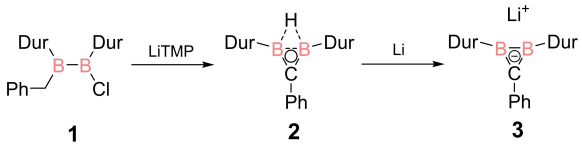

1 **2** **3**

Scheme 3. Synthesis of lithium diboriranide **3** from 1-benzyl-2-chlorodiborane(4) **1** via non-classical diborirane **2** (Dur = duryl = 2,3,5,6-tetramethylphenyl; TMP = 2,2,6,6-tetramethylpiperidide).

boron atoms (δ^{11}B = 24 to 29 ppm).[17] The ^{1}H NMR signal at δ = 7.3 ppm is attributed to the BHB bridge (BHB of preceding 1,2-diduryldiboriranes δ^1H = 7.36 to 7.83 ppm).[17] The substantial broadening caused by the coupling to the two quadrupolar boron nuclei confirms this assignment.

In adaption of the protocol by Berndt et al.,[16,23] the addition of an excess of lithium powder to a solution of **2** in diethylether leads to the formation of diboriranide **3** (Scheme 3), which was isolated as pale-yellow crystals in 60 % yield by crystallization from Et_2O/thf. The ^{11}B NMR spectrum in thf-d_8 shows one broad signal at δ = 44.2 ppm. The deshielding compared to diborirane **2** is probably due to the more pronounced Hückel aromaticity of the B_2C ring system. Accordingly, the ring carbon atom of **3** at δ^{13}C = 151.9 ppm is also deshielded compared to that of diborirane **2** (^{13}C = 135.7 ppm) and thus in range of cyclopropenium cations **I**,[12a] borirenes **II**[10] and other diboriranides.[13] The lithium counter cation in **3** is probably solvent-separated in thf-d_8 as concluded from the absence of significant broadening of the ^{7}Li NMR signal at the unremarkable chemical shift of δ = 0.4 ppm.

Syntheses of diboriranide metal complexes

In view of the 2e3c σ-BHB-bridges that allow for the retention of the $2e^-$ Hückel aromaticity of the three-membered ring of non-classical diboriranes, we envisaged the possibility of similar coordination modes for the metal complexes of diboriranides.

Under the conditions indicated in Table 1, the addition of the appropriate metal halides to lithium diboriranide **3** leads to near quantitative conversion (according to NMR-spectroscopy) to new metal-bridged diboriranides **4** to **7** (Scheme 4).

The reaction of one equivalent of Me_3SnCl with diboriranide **3** in hexane at room temperature affords the tin-bridged diborirane **8**, albeit with small traces (10 %) of

Table 1: Reaction conditions of the addition of reactants to diboriranide **3**. All reactions were carried out at room temperature.

Compound	reactant	Eq.	solvent	duration	yield
4	$AuCl(PPh_3)$	1	thf	15 min	47 %
5	CuCl or $CuI(PPh_3)_3$	0.5	thf	1 h	39 %
6	CuCl	1	thf	12 h	42 %
7	$ZnCl_2$	1	thf	15 min	96 %
8	Me_3SnCl	1	hexane	1 h	50 %

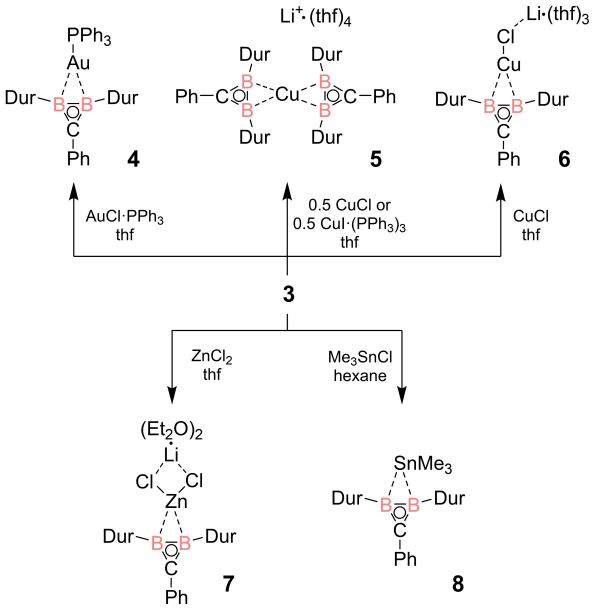

Scheme 4. Syntheses of metal complexes starting from diboriranide **3** (Dur = 2,3,5,6-tetramethylphenyl).

diborirane **2** as a side-product. In all cases, the ^{1}H NMR spectra in solution show only one singlet each for the *ortho*- and *meta*- methyl groups of the duryl substituents confirming their chemical equivalence and therefore symmetric structure of the products in solution on the NMR time scale. The ^{31}P NMR spectrum of the crude product of the addition of 0.5 equivalents of CuI[$(PPh_3)_3$] shows a single signal at $\delta = -4.9$ ppm, which was assigned to free PPh_3,[24] thus suggesting the dissociation of the phosphane-ligand and the formation of cuprate **5**. Indeed, the reaction of CuCl with two equivalents of **3** yields an identical product. In contrast, the ^{31}P NMR spectrum of gold complex **4** shows a downfield-shifted signal at $\delta = 52.2$ ppm, which confirms the retention of PPh_3 in the product. Similar ^{11}B NMR signals are observed in all five complexes (**4**: 37.9 ppm, **5**: 34.7 ppm, **6**: 34.4 ppm, **7**: 32.9 ppm, **8**: 34.0 ppm), somewhat upfield-shifted compared to the precursor, lithium diboriranide **3**.

The ^{119}Sn NMR spectrum of **8** shows a sharp singlet ($\nu_{1/2} = 13.2$ Hz) at $\delta = -38.0$ ppm, in stark contrast to the broad signals of reported stannyl-bridged borane clusters.[25] The absence of coupling of ^{119}Sn to the quadrupolar ^{11}B nuclei suggests a predominant p-character of the 3c2e BSnB bond. The ^{13}C NMR chemical shifts of the ring carbon atoms are all closer to that of diboriranide **3** than to that of diborirane **2** (**4**: 147.8 ppm, **5**: 153.9 ppm, **6**: 151.1 ppm, **7**: 144.0 ppm, **8**: 144.5 ppm, determined at −40 °C to −70 °C, see SI), which indicates a similarly ionic character of the interaction between the B_2C ring and the metal center.

X-Ray diffraction studies

Single crystals of the non-classical diborirane **2** and all diboriranide complexes **3** to **8** were obtained by crystallization from the appropriate solvents (see Supporting Information for conditions).[26] The x-ray diffraction studies confirm the presence of B_2C ring systems in which the B–B bonds are bridged by the hydrogen atom or the incorporated metal fragments, respectively (Figure 1). The cuprate **5** features two η^2-bonded diboriranides, both coordinating edge-on to the spirocyclic copper center with the B–B bonds. The angle between the two B_2C planes indicates almost perpendicularity (B1,B2,C1 and B3,B4,C28: 84.1(2)°). The solvent-separated lithium counter cation of **5** is coordinated by four thf molecules. The B_2C rings, the phenyl-*ipso*-carbon atoms and the B–B-bridging atoms approximately reside in one plane in all complexes **3** to **8**; the largest deviation with 0.23 Å occurs for Li1 of diboriranide **3** (Table 2). The coordination environments of the boron atoms thus approach tetragonal planarity and constitute further examples of violations of the van't Hoff/Le Bel-rule.[27,28] The B–B bond length of 1.769(2) Å in

Table 2: Crystallographic data of diborirane **2** and diboriranide s-, p- and d-block metal complexes **3** to **8**.[a] Duryl-*ipso*-carbon.[b] Angle between B_2C-ringplane and the phenyl-ring plane.[c] Composed of B1,B2,C1, the phenyl-*ipso*-carbon atom and the corresponding metal or hydrogen atom (X).[d] One selected molecule of two in the unit cell.

Compound	B–B [Å]	B–X [Å]	B-Cring [Å]	B-CDur [Å]	B–B-CDur [°][a]	B-Cring-B [°]	dihedral angle [°][b]	Out of plane deviation [Å][c]
2 (X=H)	1.769(2)	1.278(2)	1.442(2)	1.564(2)	155.4(1)	75.6(1)	1.2(1)	0.01 (H1)
		1.309(2)	1.442(2)	1.560(2)	157.2(1)			
3 (X=Li)	1.630(4)	2.402(6)	1.454(4)	1.570(3)	159.3(2)	68.2(2)	16.3(2)	0.23 (Li1)
		2.389(6)	1.455(4)	1.571(3)	159.4(2)			
4 (X=Au)	1.809(4)	2.142(2)	1.442(3)	1.577(3)	167.6(2)	77.8(2)	12.9(1)	0.06 (C1)
		2.242(2)	1.440(3)	1.588(3)	166.8(2)			
5 (X=Cu)	1.690(4)	2.150(3)	1.445(4)	1.577(4)	168.2(2)	71.5(1)	35.2(3)	0.16 (B2)
		2.140(3)	1.448(4)	1.567(4)	167.7(2)			
	1.702(4)	2.147(3)	1.448(4)	1.567(4)	169.5(2)	71.9(2)	1.5(2)	0.20 (B4)
		2.148(3)	1.449(4)	1.573(4)	165.2(2)			
6 (X=Cu)	1.728(5)	2.093(4)	1.450(5)	1.584(4)	165.0(3)	73.3(2)	13.2(2)	0.02 (C1)
		2.071(4)	1.444(5)	1.578(4)	166.1(3)			
7 (X=Zn)[d]	1.719(3)	2.186(2)	1.443(2)	1.577(2)	161.4(1)	73.2(1)	8.2(2)	0.10 (B1)
		2.199(2)	1.440(2)	1.581(2)	163.0(1)			
8 (X=Sn)	1.799(2)	2.462(2)	1.453(2)	1.568(2)	160.1(1)	77.5(1)	10.6(1)	0.08 (B1)
		2.636(2)	1.419(2)	1.559(2)	174.6(1)			

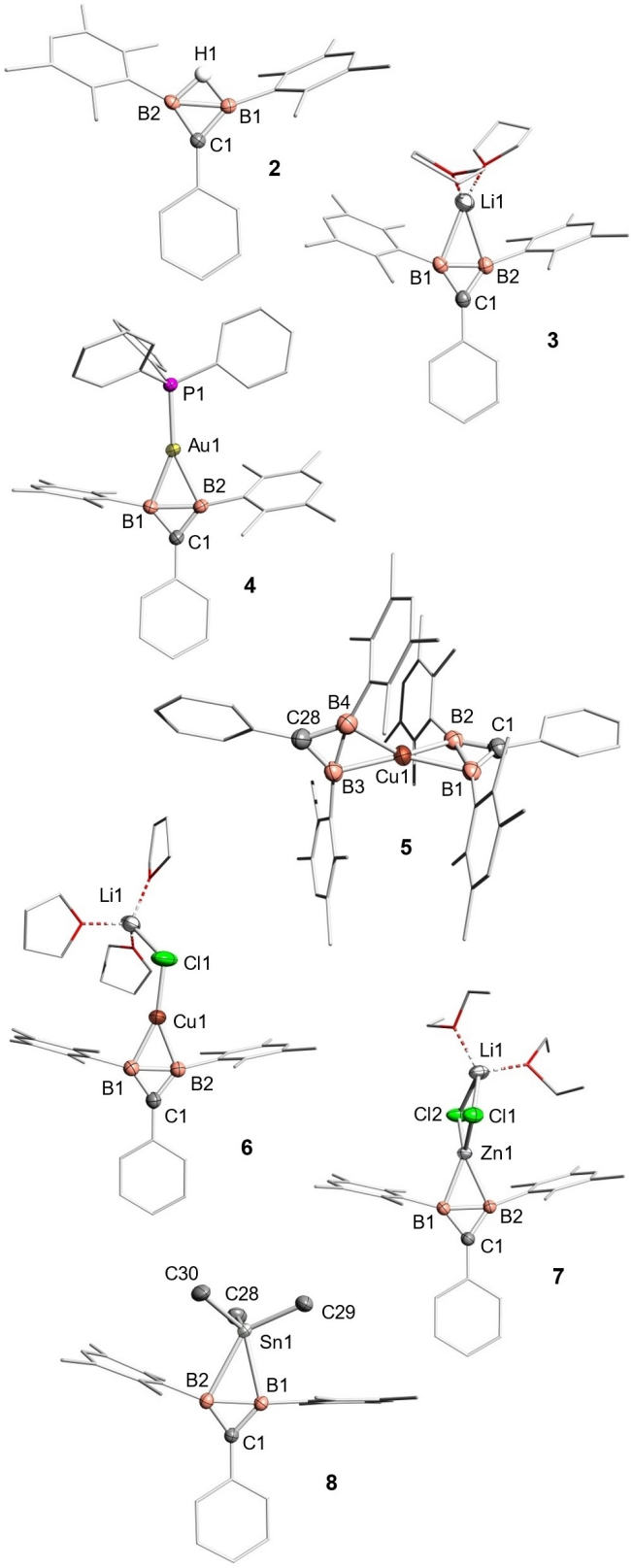

Figure 1. Molecular structures of diborirane **2** and diboriranide metal complexes **3** to **8** in the solid state: gold diboriranide **4**, bis(diboriranide) cuprate **5**, copper diboriranide **6**, zinc diboriranide complex **7**, trimethylstannyl-bridged diboriranide **8**. Most hydrogen atoms, solvent separated counter cation of **5**, and disordered solvent molecules omitted for clarity. Thermal ellipsoids at 50%.[26]

non-classical diborirane **2** is in the typical range of B–B bonds with one bridging hydrogen[17,29] and as such much longer than the one observed in lithium diboriranide **3** (1.630(4) Å).

The latter distance is only slightly longer than neutral B=B double bonds,[30] which is in line with cyclic delocalization of the π electrons, but shorter than most dianionic examples[31] reflecting the absence of Coulomb repulsion. The small dihedral angle (16.3(2)°) between the phenyl group and the diborirane plane in diboriranide **3** agrees with extended π-conjugation although this value is larger than the one in the non-classical diborirane **2** (1.2(1)°).

While the duryl groups at the boron atoms of diborirane **2** are only slightly distorted from the ideal arrangement in an isosceles triangle (Table 2; B1–B2–C_{Dur} 155.4(1)° and B2–B1–C_{Dur} 157.2(1)°), the distortion in diboriranide complexes **3** to **7** becomes progressively more pronounced (159.4(1)° to 169.5(2)°), even approaching linearity in the homoleptic cuprate **5**, which could be attributed to the increased electron density at the copper center.

The diboriranide gold complex **4** shows a nearly linear arrangement of the PPh_3 ligand and the η^2-bonded B–B unit (P1–Au1-centroid B1,B2 176.0(4)°). The B–B σ-bond (B1–B2 1.809(4) Å) is much longer than in lithium diboriranide **3** (B1–B2 1.630(4) Å), but noticeably shorter than in a related azadiboriridine gold complex (1.889 Å).[32] At the same time, the Au–B distances in **4** (B1–Au1 2.214(2) Å, B2–Au1 2.242(2) Å) are elongated compared to the said azadiboridine Au(I) complex (2.118 Å), quite possibly an effect of the electron-withdrawing chloro-ligand at the Au center of the latter. Indeed, the Au–B distances in **4** are comparable to those in boryl (2.21–2.30 Å)[33] and diborene complexes (2.21–2.22 Å),[34] both equally free of electronegative ligands at their Au centers. It should be noted that the azadiboriridine ligand is only of limited value for comparison anyway because of the less effective delocalization of the two π-electrons in the B_2N heterocycle due to the higher electronegativity of the nitrogen center.

Compared to gold complex **4**, the coordination to copper lengthens the B–B distances to a lesser extent: for the homoleptic cuprate **5** (B1–B2 1.690(4), B3–B4 1.702(4) Å) they are in the range of heteroleptic copper complexes of dianionic diboranes(4) (1.68–1.73 Å),[35] the only other example of a cuprate with at least one B–B ligand. The B–Cu distances in **5** (B1–Cu1 2.150(3) Å and B2–Cu1 2.140(3) Å, B3–Cu1 2.147(3) Å, B4–Cu1 2.148(3) Å) are similar to those of neutral (2.10–2.15 Å)[36] and dianionic (2.14–2.23 Å)[35] B=B double bond π-complexes.

The solid-state structure of the heteroleptic monocuprate **6**, which can alternatively be obtained by diboriranide transfer from **5** to a second equivalent of CuCl, revealed the completion of the coordination sphere at the copper center by the chloride ion of one equivalent of LiCl. The lithium cation is in turn coordinated by three thf molecules and the chloride. In line with the presence of the electronegative and thus weakly donating chloride ligand, the B–B bond in **6** is noticeably longer (B1–B2 1.728(5) Å) and the B–Cu bonds (B1–Cu1 2.093(4), B2–Cu1 2.071(4) Å) shorter than in **5**. This observation is confirmed by the molecular structure of the zinc complex **7** in the solid state, which just like **6** contains

one equivalent of LiCl to complete the coordination sphere of the metal center. The B–B bond of **7** (B1–B2 1.719(3) Å) is almost identical to that in **6**. The boron-zinc distances (B1–Zn1 2.186(2) Å, B2–Zn1 2.199(2) Å) in the zinc complex **7** are significantly shorter than in π-complexes of neutral diborenes with zinc dihalides (2.29–2.36 Å),[37] a manifestation of increased Coulomb attraction. The B–B bond lengthening seems to be a direct measure for the σ-donation to the d-block metal in complexes **4** to **7**. Although steric effects cannot be ruled out completely, the σ-donation by the diboriranide to Zn and Cu is approximately the same, but considerably smaller than to Au.

Surprisingly, the x-ray diffraction study on single crystals of tin-bridged diboriranide **8**, also reveals an edge-on coordination of the tin atom to the B–B moiety thus resulting in an expanded five-fold coordination at the Sn1 center as in reported Ph_3Sn-bridged pentaborane(9) clusters.[25a] The B–B bond (B1–B2 1.799(2) Å) is even slightly shorter than in the gold complex **4**. In contrast to the d-block diboriranide complexes, however, the tin atom is noticeably inclined towards one of the boron atoms: the B–Sn bond lengths strongly differ (B1–Sn1: 2.462(2); B2–Sn1 2.636(2) Å), all the while being both longer than the typical B–Sn single bonds of electron precise stannyl boranes (2.28–2.32 Å).[38] While the smaller B1–B2–C_{Dur} angle of 160.1(1)° is in range of the other diboriranide metal complexes **4** to **7**, the larger B2–B1–C_{Dur} angle is with 174.6(1)° remarkably close to linearity.

The structural parameters support a significant contribution by the methyleneborane resonance structure **8′** (Scheme 5). While there is no indication for such a lowering of the symmetry in solution, this may well be due to a fast exchange on the ^{1}H NMR time scale even at −40 °C.

DFT calculations

The electronic structure of the diborirane **2** and the diboriranide metal complexes **3**, **4**, **5**, **7** and **8** was investigated by DFT calculations at the B3LYP/def2tzvpp level of theory. The Kohn–Sham molecular orbitals (MOs) were calculated from structures that were optimized at the BP86/def2SVP level of theory. Whereas the optimized structures of **2**, **3**, **4**, **5**, **7** and **8** match the crystal structures reasonably well, the experimentally determined Cl–Cu–BB(centroid) angle in the mono(diboriranide)cuprate **6** was not reproduced by the computations, presumably due to packing effects in the solid state (see SI). Therefore, the MOs of **6** are derived from a single point calculation using the coordinates experimentally obtained from the solid state structure.

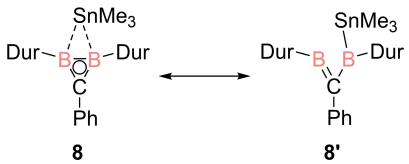

Scheme 5. Tin bridged diboriranide complex **8** and methyleneborane resonance structure **8′**.

Whereas the all-bonding combination of the π-orbitals of the B_2C ring represents the HOMO in case of the diborirane **2**, the σ-donation to the Li^+ counterion is raised to above the corresponding π-orbital in **3** (Figure 2 and SI). Natural bond orbital (NBO) analyses yields a 3c2e interaction of nearly perfect π-symmetry for both **2** and **3** (at least 99.7 % p-character for all involved atoms). In addition, the non-classical diborirane **2** features the expected BHB 3c2e σ-interaction which is approximately composed of sp^3-hybrids at the boron centers (see SI). The disappearance of the BHB 3c2e σ-bond in diboriranide **3** in favor of a classical 2e2c σ-bond is further confirmed by increasing Wiberg bond indexes of the B–B bond from diborirane **2** (0.53) to diboriranide **3** (1.06). Concomitantly, the positive charges at the boron atoms decrease according to natural population analysis (NPA; **2**: B1: +0.49, B2: +0.48; **3**: B1: +0.20, B2: +0.19), illustrating the higher electron density in the B_2C ring system in diboriranide **3** compared to diborirane **2**. As expected, the main negative charge is located at the carbon atom of the ring system (**2**: −0.62, **3**: −0.60).

The HOMO of the gold(I) complex **4** (Figure 3) is an antibonding combination of the σ-orbital of the B–B moiety and the d_{z^2} orbital of the metal center. The HOMO−1 corresponds to the all-bonding aromatic π-system delocalized across the B_2C ring with only very minor contributions by the Au center, which further supports the essentially σ-only coordination. The LUMO of **4** is mainly composed of an antibonding phosphorus-centered orbital of the PPh_3 ligand with stabilizing interactions to the π-system of one of the three phenyl groups at phosphorus.

In contrast to gold complex **4**, both the homoleptic and heteroleptic cuprates **5** and **6**, respectively, exhibit a LUMO resulting from the constructive interaction of the π*-system at the B_2C ring with the pending phenyl ring. The HOMO of both cuprate complexes **5** and **6** is similar to that of the gold complex **4** consisting of an antibonding combination of the σ-orbital of the B–B moiety and the d_{z^2} orbital of the metal center. Here as well, the HOMO−1 represents the all-bonding delocalized π-system of the B_2C ring with minor

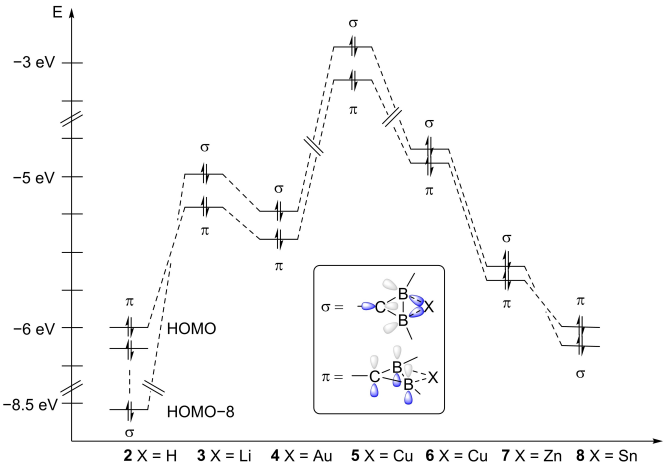

Figure 2. Relative energies of the HOMOs and HOMOs−1 of diborirane **2** and diboriranide derivatives **3** to **8**.

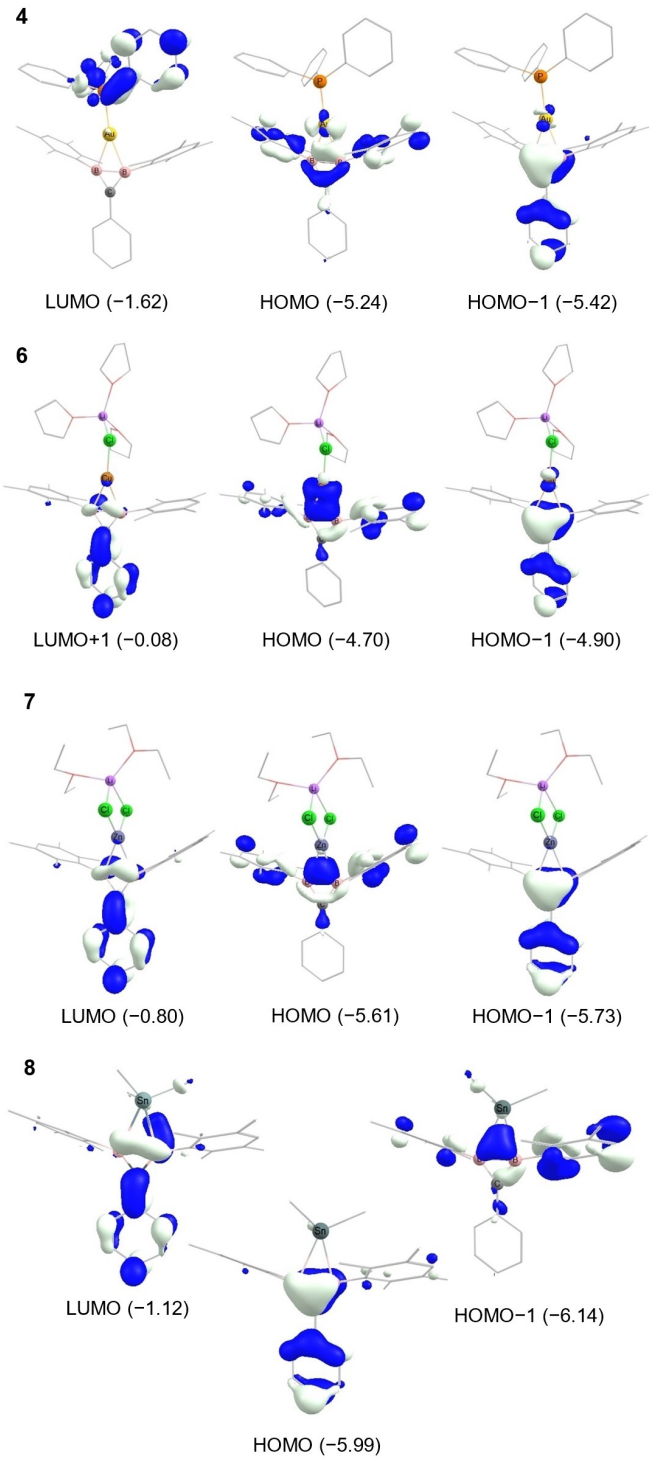

Figure 3. Selected frontier orbitals of diboriranide metal complexes **4** and **6** to **8** (energy in eV, contour value = 0.05).

contributions by the copper centers. While the LUMO of cuprate **6** is composed of σ*-orbitals at the solvent molecules (see SI), the LUMO + 1 of **6** corresponds to the LUMO of bis(diboriranide) **5** being mainly composed of the π*-system at the boron atoms and the phenyl ring.

The HOMO of zincate **7** represents the donation of σ-electrons from the boron atoms to the zinc atom. In contrast to the corresponding orbitals of the complexes discussed above, it does not show contributions of any zinc-centred orbital although the HOMO−1 once more represents the diboriranide π-system.

Most notably, the energetic order of occupied frontier orbitals is reversed in the Me_3Sn-bridged **8**: the HOMO represents the π-system and the HOMO−1 the σ-donation to the tin center (Figure 2). The LUMO of **8** represents the π*-system at the boron atoms and is of comparably low energy (−1.12 eV). The increased energy of the π-orbitals of **8** lends further support to the disturbance of cyclic delocalization by a significant contribution of resonance structure **8′** (Scheme 5).

For further confirmation of the aromaticity of diborirane **2** and diboriranide complexes **3** to **8**, nucleus independent chemical shifts (NICS) were calculated in the geometrical center of the B_2C moieties at the B3LYP/def2TZVP level of theory (Table 3). The obtained values for NICS(0) are similar to that of the cyclopropenium cation, which we calculated at the same level of theory for comparison (NICS(0) = −23.2).[39] In order to minimize the effect of localized ring currents as well as the shielding by the σ-framework, NICS were also calculated 1 Å above and below the B_2C ring plane.[40] All values for NICS(1/−1) in the range of −10.6 to −13.3 are only slightly lower than that of the cyclopropenium cation (NICS(1) = −14.9)[39] and thus confirm the 2π-aromaticity of the three membered ring systems in **2** to **8** and its essential independency from the nature of the coordinated metal. Notably, even the coordination of the Me_3Sn group in **8** does not seem to exert an adverse effect on the magnetically induced ring current.

Conclusion

We have disclosed a straightforward synthetic strategy to access diboriranes in two steps from a readily available 1,2-dichlorodiborane(4). Unlike in previously reported diboriranes, a phenyl group is attached to the ring carbon atom; its coplanarity allows for π-conjugation with the B_2C ring plane for the first time, thus offering new perspectives regarding the incorporation of non-classical diborirane motifs into extended π-systems. The nearly planar anti-van't Hoff/Le Bel-geometry at the boron centers is retained upon reduction to lithium diboriranide **3** and - more importantly - also upon complexation to various d-block elements, namely gold (**4**), copper (**5**, **6**), and zinc (**7**). The diboriranide binds to the p- and d-block metal complexes in this very same plane, essentially by σ-only coordination thus leaving the π-system mostly unperturbed. In case of the stannyl-bridged diboriranide **8**, however, crystallographic evidence suggests a weakening of the cyclic delocalization as one of the two Sn–B distances is substantially elongated to localize the bonding to some extent and hence lower the degree of hypercoordination at the tin-center, which is considered to be unfavorable in the absence of electronegative substituents.

Table 3: Different values for NICS (in ppm) of diborirane **2** and diboriranide derivatives **3** to **8**. Calculated from the geometric center of the B_2C plane (NICS(0)) and 1 Å above and below the B_2C ring plane (NICS(1/−1)).

Compound	NICS(0)	NICS(1/−1)
2	−25.3	−12.6/−12.8
3	−19.5	−12.1/−12.7
4	−19.9	−10.6/−11.7
5	−19.9	−12.4/−12.7
	−20.1	−12.9/−13.2
6	−20.4	−11.9/−12.5
7	−23.3	−12.2/−12.7
8	−22.8	−13.3/−10.7

The scope of the new method, in particular with regards to the tolerance of functional groups as well as to the further extension of the π-conjugated system is currently under investigation in our laboratory.

Acknowledgements

We gratefully acknowledge the funding by Saarland University. We thank Dr. Diego Andrada for assistance with computations, helpful discussions, and access to his computational cluster. We acknowledge the Service Center X-ray Diffraction established with financial support from Saarland University and the Deutsche Forschungsgemeinschaft (INST 256/506-1). Open Access funding enabled and organized by Projekt DEAL.

Conflict of Interest

The authors declare no conflict of interest.

Data Availability Statement

The data that support the findings of this study are available in the supplementary material of this article.

Keywords: Aromatics · Boron · Coordination Chemistry · Transition Metals

[1] a) H. Wadepohl, *Angew. Chem. Int. Ed. Engl.* **1992**, *31*, 247–262; b) D. Braga, P. J. Dyson, F. Grepioni, B. F. G. Johnson, *Chem. Rev.* **1994**, *94*, 1585–1620; c) K. M. Wedderburn, S. Bililign, M. Levy, R. Gdanitz, *Chem. Phys.* **2006**, *326*, 600–604.

[2] L. D. Field, C. M. Lindall, A. F. Masters, G. K. B. Clentsmith, *Coord. Chem. Rev.* **2011**, *255*, 1733–1790.

[3] P. L. Pauson, G. H. Smith, J. H. Valentine, *J. Chem. Soc. C* **1967**, 1061–1065.

[4] a) C.-W. So, D. Watanabe, A. Wakamiya, S. Yamaguchi, *Organometallics* **2008**, *27*, 3496–3501; b) G. E. Herberich, B. Buller, B. Heßner, W. Oschmann, *J. Organomet. Chem.* **1980**, *195*, 253–259; c) J. He, F. Rauch, M. Finze, T. B. Marder, *Chem. Sci.* **2021**, *12*, 128–147.

[5] For selected examples of bora and boratabenzenes see: a) G. E. Herberich, G. Greiss, H. F. Heil, *Angew. Chem. Int. Ed. Engl.* **1970**, *9*, 805–806; b) G. E. Herberich, H. Ohst, *Adv. Organomet. Chem.* **1986**, *25*, 199–236; c) A. J. Ashe III, P. Shu, *J. Am. Chem. Soc.* **1971**, *93*, 1804–1805; d) R. Boese, N. Finke, J. Henkelmann, G. Maier, P. Paetzold, H. P. Reisenauer, G. Schmid, *Chem. Ber.* **1985**, *118*, 1644–1654; e) G. C. Fu, *Adv. Organomet. Chem.* **2001**, *47*, 101–119.

[6] For selected examples of dibora- and diboratabenzenes see: a) G. E. Herberich, B. Heßner, M. Hostalek, *Angew. Chem. Int. Ed. Engl.* **1986**, *25*, 642–643; b) G. E. Herberich, B. Heßner, M. Hostalek, *J. Organomet. Chem.* **1988**, *355*, 473–484; c) W. Weinmann, H. Pritzkow, W. Siebert, *Chem. Ber.* **1994**, *127*, 611–613; d) C. Balzereit, H.-J. Winkler, W. Massa, A. Berndt, *Angew. Chem. Int. Ed. Engl.* **1994**, *33*, 2306–2308; e) G. E. Herberich, B. Heßner, *Chem. Ber.* **1982**, *115*, 3115–3127; f) J. W. Taylor, A. McSkimming, C. F. Guzman, W. H. Harman, *J. Am. Chem. Soc.* **2017**, *139*, 11032–11035; g) M. Arrowsmith, J. Böhnke, H. Braunschweig, M. A. Celik, C. Claes, W. C. Ewing, I. Krummenacher, K. Lubitz, C. Schneider, *Angew. Chem. Int. Ed.* **2016**, *55*, 11271–11275; h) Q. Sun, C. G. Daniliuc, C. Mück-Lichtenfeld, G. Kehr, G. Erker, *Angew. Chem. Int. Ed.* **2022**, *61*, e202205565.

[7] For selected examples of borepins see: a) A. J. Ashe III, F. J. Drone, C. M. Kausch, J. Kroker, S. M. Al-Taweel, *Pure Appl. Chem.* **1990**, *62*, 513–517; b) A. J. Ashe, III, W. Klein, R. Rousseau, *Organometallics* **1993**, *12*, 3225–3231; For selected examples of boron containing heterocycles see: c) C. W. Allen, D. E. Palmer, *J. Chem. Educ.* **1978**, *55*, 497–500; d) G. E. Herberich, *Comprehensive Organometallic Chemistry II*, *Vol. 1*, Elsevier, Amsterdam, **1995**, chap. 5, pp. 197–216; e) B. Su, R. Kinjo, *Synthesis* **2017**, *49*, 2985–3034; f) J. T. Goettel, H. Braunschweig, *Coord. Chem. Rev.* **2019**, *380*, 184–200; g) U. M. Dzhemilev, L. I. Khusainova, K. S. Ryazanov, L. O. Khafizova, *Russ. Chem. Bull. Int. Ed.* **2021**, *70*, 1851–1892.

[8] a) K.-F. Wörner, W. Siebert, *Z. Naturforsch. B* **1989**, *44*, 1211–1213; b) D. A. Loginov, D. V. Muratov, P. V. Petrovskii, Z. A. Starikova, M. Corsini, F. Laschi, F. D. B. Fabrizi, P. Zanello, A. R. Kudinov, *Eur. J. Inorg. Chem.* **2005**, 1737–1746; c) W. Siebert, A. R. Kudinov, P. Zanello, M. Y. Antipin, V. V. Scherban, A. S. Romanov, D. V. Muratov, Z. A. Starikova, M. Corsini, *Organometallics* **2009**, *28*, 2707–2715; d) D. A. Loginov, D. V. Muratov, Y. V. Nelyubina, J. Laskova, A. R. Kudinov, *J. Mol. Catal. A* **2017**, *426*, 393–397.

[9] a) P. D. Frisch, G. P. Khare, *J. Organomet. Chem.* **1977**, *142*, 61–64; b) A. Keasey, P. M. Maitlis, *J. Chem. Soc. Dalton Trans.* **1978**, 1830–1839; c) C. Mealli, S. Midollini, S. Moneti, L. Sacconi, *J. Organomet. Chem.* **1981**, *205*, 273–279; d) R. P. Hughes, D. S. Tucker, A. L. Rheingold, *Organometallics* **1994**, *13*, 4664–4666; e) M. S. Morton, J. P. Selegue, *J. Organomet. Chem.* **1999**, *578*, 133–143; f) K. Komatsu, T. Kitagawa, *Chem. Rev.* **2003**, *103*, 1371–1428; g) C. Jandl, K. Öfele, A. Pöthig, *Organometallics* **2017**, *36*, 4348–4350; h) D. N. Platonov, D. N. Kholodkov, I. K. Goncharova, M. A. Belaya, Y. V. Tkachev, P. V. Dorovatovskii, A. D. Volodin, A. A. Korlyukov, Y. V.

Tomilov, A. V. Arzumanyan, R. A. Novikov, *Organometallics* **2021**, *40*, 3876–3885.
[10] a) H. Braunschweig, T. Herbst, D. Rais, F. Seeler, *Angew. Chem. Int. Ed.* **2005**, *44*, 7461–7463; b) H. Braunschweig, T. Herbst, D. Rais, S. Ghosh, T. Kupfer, K. Radacki, A. G. Crawford, R. M. Ward, T. B. Marder, I. Fernández, G. Frenking, *J. Am. Chem. Soc.* **2009**, *131*, 8989–8999.
[11] a) H. Braunschweig, Q. Ye, K. Radacki, *Chem. Commun.* **2009**, 6979–6981; b) H. Braunschweig, Q. Ye, K. Radacki, P. Brenner, G. Frenking, S. De, *Inorg. Chem.* **2011**, *50*, 62–71; c) H. Braunschweig, Q. Ye, K. Radacki, T. Kupfer, *Dalton Trans.* **2011**, *40*, 3666–3670; d) H. Braunschweig, A. Damme, R. D. Dewhurst, S. Ghosh, T. Kramer, B. Pfaffinger, K. Radacki, A. Vargas, *J. Am. Chem. Soc.* **2013**, *135*, 1903–1911.
[12] a) X. Meng, T. P. Fehlner, A. L. Rheingold, *Organometallics* **1990**, *9*, 534–536; b) H. Braunschweig, R. D. Dewhurst, *Dalton Trans.* **2011**, *40*, 549–558; c) H. Braunschweig, R. D. Dewhurst, K. Radacki, C. W. Tate, A. Vargas, *Angew. Chem. Int. Ed.* **2014**, *53*, 6263–6266.
[13] a) R. Wehrmann, H. Meyer, A. Berndt, *Angew. Chem. Int. Ed. Engl.* **1985**, *24*, 788–790; b) H. Meyer, G. Schmidt-Lukasch, G. Baum, W. Massa, A. Berndt, *Z. Naturforsch. B* **1988**, *43*, 801–806.
[14] a) D. Scheschkewitz, A. Ghaffari, P. Amseis, M. Unverzagt, G. Subramanian, M. Hofmann, P. V. R. Schleyer, H. F. Schaefer, III, G. Geiseler, W. Massa, A. Berndt, *Angew. Chem. Int. Ed.* **2000**, *39*, 1272–1275; b) W. Lößlein, H. Pritzkow, P. V. R. Schleyer, L. R. Schmitz, W. Siebert, *Eur. J. Inorg. Chem.* **2001**, 1949–1956; c) N. Li, B. Wu, C. Yu, T. Li, W.-X. Zhang, Z. Xi, *Angew. Chem. Int. Ed.* **2020**, *59*, 8868–8872.
[15] T. Kupfer, H. Braunschweig, K. Radacki, *Angew. Chem. Int. Ed.* **2015**, *54*, 15084–15088.
[16] M. Unverzagt, PhD thesis, University of Marburg, **1997**.
[17] a) D. Steiner, C. Balzereit, H.-J. Winkler, N. Stamatis, W. Massa, A. Berndt, M. Hoffmann, P. V. R. Schleyer, *Angew. Chem. Int. Ed. Engl.* **1994**, *33*, 2303–2306; b) M. Menzel, D. Steiner, H.-J. Winkler, D. Schweikart, S. Mehle, S. Fau, G. Frenking, W. Massa, A. Berndt, *Angew. Chem. Int. Ed. Engl.* **1995**, *34*, 327–329; c) C. Präsang, Y. Sahin, M. Hofmann, G. Geiseler, W. Massa, A. Berndt, *Eur. J. Inorg. Chem.* **2008**, 5046–5055.
[18] A. Hübner, T. Kaese, M. Diefenbach, B. Endeward, M. Bolte, H.-W. Lerner, M. C. Holthausen, M. Wagner, *J. Am. Chem. Soc.* **2015**, *137*, 3705–3714.
[19] Y. Wang, X. Zhang, J. Han, Q. Li, R. Wei, D. A. Ruiz, L. L. Liu, C.-H. Tung, L. Kong, *Angew. Chem. Int. Ed.* **2022**, *61*, e202117053.
[20] A. Berndt, *Angew. Chem. Int. Ed. Engl.* **1993**, *32*, 985–1009.
[21] H. Hommer, H. Nöth, J. Knizek, W. Ponikwar, H. Schwenk-Kircher, *Eur. J. Inorg. Chem.* **1998**, 1519–1527.
[22] K. V. Baker, J. M. Brown, N. Hughes, A. J. Skarnulis, A. Sexton, *J. Org. Chem.* **1991**, *56*, 698–703.
[23] D. Steiner, H. J. Winkler, C. Balzereit, T. Happel, W. Massa, A. Berndt, M. Hofmann, G. Subramanian, P. V. R. Schleyer, *Angew. Chem. Int. Ed. Engl.* **1996**, *35*, 1990–1992.
[24] A. C. Vetter, K. Nikitin, D. G. Gilheany, *Chem. Commun.* **2018**, *54*, 5843–5846.
[25] a) D. K. Srivastava, N. P. Rath, L. Barton, *Organometallics* **1992**, *11*, 2263–2273; b) H. Fang, D. Zhao, L. Brammer, L. Barton, *J. Chem. Soc. Chem. Commun.* **1994**, 1531–1532; c) H. Fang, D. Zhao, N. P. Rath, L. Brammer, L. Barton, *Organometallics* **1995**, *14*, 1700–1711.
[26] Deposition numbers 2269482 (for **1**), 2269486 (for **2**), 2269489 (for **3**), 2269491 (for **4**), 2269493 (for **5**), 2269495 (for **6**), 2269501 (for **7**), 2269505 (for **8**). contain the supplementary crystallographic data for this paper. These data are provided free of charge by the joint Cambridge Crystallographic Data Centre and Fachinformationszentrum Karlsruhe Access Structures service.
[27] a) R. Hoffmann, R. W. Alder, C. F. Wilcox Jr., *J. Am. Chem. Soc.* **1970**, *92*, 4992–4993; b) R. Hoffmann, *Pure Appl. Chem.* **1971**, *28*, 181–194.
[28] For selected examples of anti-van't Hoff/Le Bel-geometry see: a) M. Driess, J. Aust, K. Merz, C. van Wüllen, *Angew. Chem. Int. Ed.* **1999**, *38*, 3677–3680; b) R. Keese, *Chem. Rev.* **2006**, *106*, 4787–4808; c) M. J. Cowley, V. Huch, D. Scheschkewitz, *Chem. Eur. J.* **2014**, *20*, 9221–9224; d) F. Ebner, L. Greb, *J. Am. Chem. Soc.* **2018**, *140*, 17409–17412; e) F. Ebner, H. Wadepohl, L. Greb, *J. Am. Chem. Soc.* **2019**, *141*, 18009–18012; f) F. Ebner, L. Greb, *Chem* **2021**, *7*, 2151–2159; g) P. Ghana, J. Rump, G. Schnakenburg, M. I. Arz, A. C. Filippou, *J. Am. Chem. Soc.* **2021**, *143*, 420–432; h) C. Shan, S. Dong, S. Yao, J. Zhu, M. Driess, *J. Am. Chem. Soc.* **2023**, *145*, 7084–7089.
[29] X. Mao, J. Zhang, Z. Lu, Z. Xie, *Chem. Sci.* **2022**, *13*, 3009–3013.
[30] For examples of neutral B=B double bonds see a) Y. Wang, B. Quillian, P. Wei, C. S. Wannere, Y. Xie, R. B. King, H. F. Schaefer III, P. V. R. Schleyer, G. H. Robinson, *J. Am. Chem. Soc.* **2007**, *129*, 12412–12413; b) Y. Wang, B. Quillian, P. Wei, Y. Xie, C. S. Wannere, R. B. King, H. F. Schaefer, III, P. V. R. Schleyer, G. H. Robinson, *J. Am. Chem. Soc.* **2008**, *130*, 3298–3299; c) H. Braunschweig, R. D. Dewhurst, K. Hammond, J. Mies, K. Radacki, A. Vargas, *Science* **2012**, *336*, 1420–1422; d) P. Bissinger, H. Braunschweig, A. Damme, T. Kupfer, A. Vargas, *Angew. Chem. Int. Ed.* **2012**, *51*, 9931–9934; e) W. Lu, Y. Li, R. Ganguly, R. Kinjo, *J. Am. Chem. Soc.* **2017**, *139*, 5047–5050.
[31] For examples of anionic B–B π-bonds see: a) H. Klusik, A. Berndt, *Angew. Chem. Int. Ed. Engl.* **1981**, *20*, 870–871; b) W. J. Grigsby, P. P. Power, *Chem. Eur. J.* **1997**, *3*, 368–375; c) A. Moezzi, R. A. Bartlett, P. P. Power, *Angew. Chem. Int. Ed. Engl.* **1992**, *31*, 1082–1083; d) A. Moezzi, M. Olmstead, P. P. Power, *J. Am. Chem. Soc.* **1992**, *114*, 2715–2717; e) P. P. Power, *Inorg. Chim. Acta* **1992**, *198–200*, 443–447; f) W. J. Grigsby, P. P. Power, *Chem. Commun.* **1996**, 2235–2236.
[32] R. Shang, S. Saito, J. O. C. Jimenez-Halla, Y. Yamamoto, *Dalton Trans.* **2018**, *47*, 5181–5188.
[33] H. Braunschweig, A. Damme, R. D. Dewhurst, T. Kramer, S. Östreicher, K. Radacki, A. Vargas, *J. Am. Chem. Soc.* **2013**, *135*, 2313–2320.
[34] W. Lu, R. Kinjo, *Chem. Eur. J.* **2018**, *24*, 15656–15662.
[35] S. Akiyama, S. Ikemoto, S. Muratsugu, M. Tada, M. Yamashita, *Organometallics* **2020**, *39*, 500–504.
[36] M. Dömling, T. E. Stennett, A. Belyaev, B. Hupp, C. Claes, S. Ullrich, S. Endres, E. Freytag, T. Kramer, T. Kupfer, F. Schorr, T. Thiess, M. Arrowsmith, A. Steffen, H. Braunschweig, *Inorg. Chem.* **2022**, *61*, 14058–14066.
[37] S. R. Wang, M. Arrowsmith, H. Braunschweig, R. Dewhurst, M. Dömling, J. D. Mattock, C. Pranckevicius, A. Vargas, *J. Am. Chem. Soc.* **2017**, *139*, 10661–10664.
[38] T. Habereder, H. Nöth, *Z. Anorg. Allg. Chem.* **2001**, *627*, 789–796.
[39] Previously a value of −23.5 ppm had been reported for NICS(0) of $C_3H_3^+$ at a slightly different level of theory: C. Foroutan-Nejad, S. Shabazian, P. Rashidi-Ranjbar, *Phys. Chem. Chem. Phys.* **2010**, *12*, 12630–12637.
[40] P. V. R. Schleyer, H. Jiao, N. J. R. V. E. Hommes, V. G. Malkin, O. L. Malkina, *J. Am. Chem. Soc.* **1997**, *119*, 12669–12670.

Manuscript received: June 20, 2023
Accepted manuscript online: July 31, 2023
Version of record online: August 28, 2023

3.2 π-Complexes Derived from Non-classical Diboriranes: Side-on vs. End-on Carbonylative Ring Expansion

P. Grewelinger, C. Präsang, M. Zimmer, B. Morgenstern, D. Scheschkewitz, *Angew. Chem. Int. Ed.* **2024**, *63*, e202415378. https://doi.org/10.1002/anie.202415378; *Angew. Chem.* **2024**, *136*, e202415378. https://doi.org/10.1002/ange.202415378.

Author Contributions:

Philipp Frank Grewelinger (Conceptualization: Equal (DS); Data curation: Lead; Formal analysis: Lead; Investigation: Lead; Writing – original draft: Lead)

Carsten Präsang (Conceptualization: Supporting; Data curation: Supporting; Formal analysis: Supporting; Investigation: Supporting; Writing – original draft: Supporting)

Michael Zimmer (Data curation: Supporting; Formal analysis: Supporting; Methodology: Supporting; Validation: Supporting)

Bernd Morgenstern (Data curation: Lead; Formal analysis: Supporting; Methodology: Supporting; Visualization: Supporting)

David Scheschkewitz (Conceptualization: Lead; Formal analysis: Supporting; Funding acquisition: Lead; Investigation: Supporting; Methodology: Supporting; Project administration: Lead; Resources: Lead; Supervision: Lead; Writing – review & editing: Lead)

How to cite: *Angew. Chem. Int. Ed.* **2024**, *63*, e202415378
doi.org/10.1002/anie.202415378

Diboriranes

π-Complexes Derived from Non-classical Diboriranes: Side-on vs. End-on Carbonylative Ring Expansion

*Philipp Grewelinger, Carsten Präsang, Michael Zimmer, Bernd Morgenstern, and David Scheschkewitz**

Abstract: Unlike cyclopropanes, the analogous B_2C species (diboriranes) tend to adopt non-classical Hückel-aromatic structures with bridging moieties R between the boron atoms. The coordination of the thus generated cyclic $2e^-$ π-system to transition metals is completely unexplored. We here report that complexation of non-classical diboriranes cyclo-μ-RB_2Dur_2CPh (R=H, $SnMe_3$; Dur=2,3,5,6-tetramethylphenyl) to $Fe(CO)_3$ fragments allows for the carbonylative ring expansion of the B_2C ring to either four- or five-membered rings depending on the nature of the BRB 3-center-2-electron bond (3c2e): The H-bridged diborirane (R=H) initially reacts with $Fe_2(CO)_9$ to the allylic π-complex with an agostic BH/Fe interaction. Subsequent formal hydroboration of CO from excess $Fe_2(CO)_9$ results in the side-on ring expansion under formation of a five-membered B_2C_2O ring, coordinated to the $Fe(CO)_3$ moiety. In contrast, in case of the stannyl-bridged diborirane (R=$SnMe_3$) under the same conditions, CO is added end-on to the B–B bond with the carbon terminus formally inserting into the B_2Sn 3c2e-bond. The two carbonylative ring expansion products can also be described as *nido* and *closo* clusters, respectively, according to the Wade-Mingos rules.

Introduction

Organometallic transition metal species are of tremendous importance in organic and inorganic chemistry, first and foremost as catalysts but also as structure-determining motifs[1] and functional groups[2,3] in materials. Aromatic π-coordinating ligands such as benzene, cyclopentadienide and related have been at the forefront of the field during the past 60 years. The coordination chemistry of boron containing aromatic heterocycles such as diboretes,[4] boroledііdes,[5] bora- and boratabenzenes[6] and borepins[7] is similarly dominated by the donation of the π-system toward the electron deficient metal center. In contrast, transition metal complexes of three-membered aromatic boracycles are even scarcer than those of the isoelectronic cyclopropenium cations.[8] For instance, the first and still only triborirandiide was obtained by Braunschweig et al. as a dimer with inverse double-sandwich structure involving four sodium counter cations,[9] but its ligand properties toward transition metals remain unexplored. Similarly, despite the straightforward access to borirenes by borylene transfer to alkynes,[10] only a few borirene metal complexes have been reported. Apart from a borirene σ-complex,[11] there is only one example of a η^3-bonded π-complex, recently reported by Braunschweig and co-workers: the chromium carbonyl complex **I** (Scheme 1) is obtained in low yield as a side-product during the photolytic transfer of a bulky borylene from $Cr(CO)_5$ to tolane, PhCCPh.[12] Recently, we disclosed the straightforward synthesis of a non-classical diborirane and the corresponding anionic diboriranides **II** as well as first investigations into the coordination behavior of the latter.[13] Complexes **II** with the cationic metal centers M, exclusively bonded in σ-fashion to the perimeter of the anionic B_2C ring, were readily obtained by salt metathesis with the lithium salt. Apart from the reduction to the diboriranide, the reactivity of the neutral diborirane – containing a "non-classical" 3c2e σ-bond (BHB) – is completely unknown. According to DFT calculations, the Hückel-aromatic $2e^-$ π-system of neutral non-classical diboriranes constitutes the

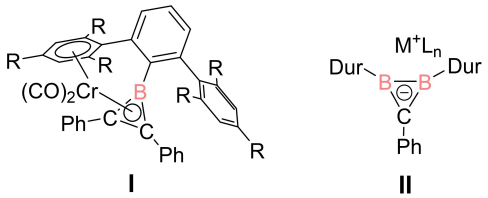

I II

Scheme 1. Selected metal complexes of three-membered aromatic boracycles (**I**: R=^{i}Pr; **II**: M^+L_n=Li(thf)$_2$, AuPPh$_3$, CuClLi(thf)$_3$, ZnCl$_2$Li-(OEt$_2$)$_2$, SnMe$_3$, Dur=2,3,5,6-Me$_4$C$_6$H).

[*] M. Sc. P. Grewelinger, Dr. C. Präsang, Dr. M. Zimmer, Prof. Dr. D. Scheschkewitz
Krupp-Chair for General and Inorganic Chemistry,
Saarland University
66123 Saarbrücken, Germany
E-mail: scheschkewitz@mx.uni.saarland.de

Dr. B. Morgenstern
Service Center X-ray diffraction
Saarland University
66123 Saarbrücken, Germany

highest occupied molecular orbital (HOMO) and should therefore be amenable to η^3-coordination.[13]

Here, we report the first π-complexes involving B_2C moieties that retain a certain – albeit weak – B–B interaction. The coordination to iron carbonyl fragments gives rise to subsequent carbonylative ring expansion. Depending on the nature of the B–B-bridge in the diborirane precursor this occurs either side-on or end-on to yield five- and four-membered ligand systems, respectively.

Results and Discussion

Synthesis of diborirane π-complexes

Quantum chemical calculations had shown that the HOMO of diborirane **1** is composed of the delocalized π-system of the B_2C ring.[13] We therefore anticipated it to be well suited as π-ligand for transition metals. In addition, the BHB bridge could support the coordination through its σ-electrons as BH bonds have been repeatedly employed as σ-donors to transition metal centers.[14] Inspired by the first diborane transition metal complexes as well as by Fehlner's borirene-containing Fe_3C_2B *closo* cluster,[15] we opted for an iron carbonyl as precursor.

The addition of 1.6 equivalents of $Fe_2(CO)_9$ to the non-classical diborirane **1** in benzene indeed results in a color change from colorless to red. After workup, the diborirane iron complex **2** is obtained as red crystals from hexane after 18 hours (Scheme 2). Upon heating the iron complex **2** to 150 °C for 1 h, the non-classical diborirane **1** is liberated as verified by multinuclear NMR spectroscopy (Scheme 2), which suggests that the diborirane coordination to the $Fe(CO)_3$ fragment is only moderately strong. For comparison, the addition of $Fe_2(CO)_9$ to the lithium salt of diboriranide **II** ($M^+Ln{=}Li(thf)_2$) does not lead to the uniform formation of a product, but only to an intractable product mixture underscoring the differences between the neutral diborirane **1** and the anionic diboriranide.

X-ray diffraction on a single crystal of **2** confirmed the coordination of the $Fe(CO)_3$ fragment above the B_2C moiety (Figure 1). The hydrogen atom has forfeited its bridging position between the two boron atoms and bridges B1 and Fe1 instead in an agostic interaction of the BH bond. Upon coordination to the iron center, the B1–B2 distance is widened significantly (**1**: 1.769 Å); **2**: 2.380(3) Å). The B–C–B angle (106.7(1)°), however, is more acute than in

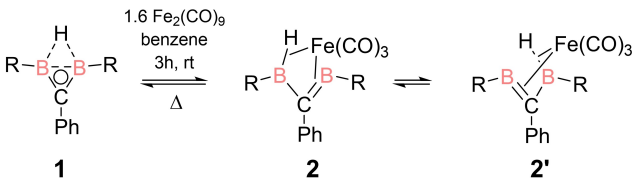

Scheme 2. Synthesis of diborirane iron carbonyl complex **2** starting from non-classical diborirane **1** and the degenerate equilibrium in solution between **2** and **2'** involving 1,3-hydride migration (R=Dur=2,3,5,6-Me_4C_6H).

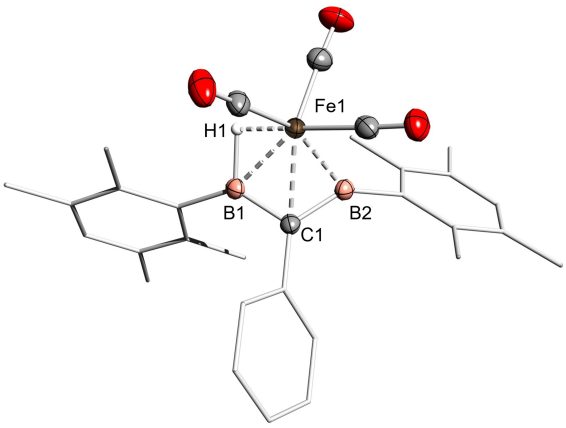

Figure 1. Molecular structure of diborirane iron complex **2** in the solid state. Thermal ellipsoids at 50% probability. Selected bond lengths [Å] and angles [°]: B1–B2 2.380(3), B1–C1 1.498(2), B2–C1 1.496(2), B1–H1 1.296(2), B1–Fe1 2.150(2), B2–Fe1 2.038(2), Fe1–H1 1.61(2), C1–Fe1 2.137(2); B1–C1–B2 106.7(1).[19]

Berndt's borylmethyleneborane suggesting some remaining bonding interaction between the boron atoms in **2**.[16] Homodiborirane complexes reported by Siebert and Berndt also show larger B–C–B angles (132.3 to 150.3°) and B–B bond lengths (2.573 to 2.896 Å) than **2**.[17]

The elongation of the $B–C_{ring}$ bonds upon coordination is significantly more pronounced for B1–C1 than for B2–C1 (**1**: B1–C1 1.442(2) Å; B2–C1 1.442(2) Å; **2**: B1–C1 1.498 (2) Å; B2–C1 1.469(2) Å), which is consistent with a certain B2–C1 double bond character (Scheme 2). In line with this assertion, the iron atom is located closer to B2 (B2–Fe1 2.038(2) Å) than to B1 (B1–Fe1 2.105(2) Å), presumably an effect of the stronger donation of the B=C π-bond compared to the BH σ-bond. The C1–Fe1 distance of 2.137(2) Å is similar to those in the aforementioned borirene-derived *closo* cluster[15] and in a methyleneborane iron complex reported by the Braunschweig group.[18] The BH distance in **2** (B1–H1 1.296(2) Å) remains almost unchanged from those of the bridging hydrogen of diborirane **1** (B1–H1 1.278(2) Å; B2–H1 1.309(2) Å) indicating a considerable agostic interaction with Fe1. Indeed, the Fe1–H1 bond of 1.61(2) Å is in the range of such bonds in reported borohydride iron complexes.[14h,i]

The ^1H NMR signal in the far high field at $\delta = -11.4$ ppm is attributed to the BH hydrogen. The broadening caused by the coupling to one quadrupolar boron nucleus confirms this assignment. Compared to non-classical diborirane **1**, the signal for the B-bonded hydrogen is exceptionally upfield shifted by $\Delta\delta = 18.7$ ppm, unambiguously proving its hydridic character due to agostic interactions with the iron fragment.[14c] The *ortho* and *meta* CH_3 groups of the duryl substituents each give rise to only one ^1H and ^{13}C NMR signal, which could either be due to a more symmetrical structure or rapid equilibration between the degenerate species **2** and **2'** in solution (Scheme 2). VT NMR did not help in discriminating between these two orthogonal explanations as even at −60 °C no splitting of the signals was observed.

Consistent with above, the ^{11}B NMR spectrum of the diborirane complex **2** shows only one signal at $\delta = 68.4$ ppm. In contrast, ^{11}B SPE/MAS NMR detects two distinct signals at $\delta = 85.1$ ppm and 50.6 ppm in line with the two chemically inequivalent boron atoms in the solid state. The average of these chemical shifts of 67.5 ppm, however, is very close to the observed solution signal and thus provides a first indication of fluxionality in solution. DFT calculations at the BP86/def2SVP level further strengthen this interpretation: attempts to optimize a symmetrical geometry analogous to BHB-bridged diborirane **1** unequivocally led to relaxation to unsymmetrical **2** (Scheme 2). The GIAO-computed ^{11}B NMR shifts at $\delta = 79.5$ and 44.5 ppm (B3LYP/def2tzvpp) are very close to the experimental signals in the solid state. While the boron atom associated to the downfield signal is slightly more shielded than in Braunschweig's methyleneborane iron complex,[18] the upfield shifted signal is in the range for σ-borane complexes.[14j] The alternative explanation of an inherently symmetrical structure in solution can be excluded as the signal for the ring carbon atom matches the one in the solid state ^{13}C CP/MAS spectrum. It is significantly upfield shifted compared to diborirane **1** ($\delta = 50.0$ for **2** vs. 136.4 ppm for **1**) indicating little if any cyclic delocalization of the π-electrons across the B_2C ring.

The solid state IR spectrum of **2** shows three clear signals at 1967, 1986 and 2045 cm^{-1} (see SI). DFT calculations at the BP86/def2SVP level of theory give vibrations at 2004, 2013 and 2059 cm^{-1}, only slightly blue shifted compared to the experimental data. In hexane solution, two bands at 1990 and 2049 cm^{-1} in an approximate 2:1 ratio are observed suggesting rapid turnstile-like exchange of the CO positions in solution.[20] DFT calculations indicate the B–H stretching frequency at 1782 cm^{-1}, which, however, cannot be assigned due to its occurrence in the fingerprint area (see SI).

The longest wavelength absorption in the experimental UV/Vis spectrum of **2** (see SI) is observed as a very broad band at an estimated λ_{max} of about 420 nm ($\varepsilon = 1445$ M^{-1} cm^{-1}) tailing to about 500 nm. A TD-DFT calculation at the B3LYP/def2tzvpp level of theory assigns the band to two weak transitions at 470 nm (HOMO→LUMO) and at 407 nm (HOMO−1→LUMO; see SI). The HOMO of complex **2** corresponds to the backdonation of an occupied d orbital at iron into the vacant σ-type p orbital at B2 of the B=C bond (Figure 2). The HOMO−1 reflects the bonding combination of the B_2C π-system (predominantly but not exclusively located at C1 and B2) and a vacant d orbital at the iron center. The LUMO is dominated by the vacant p orbital at hydrogen-bonded B1 with some minor contributions at the pending duryl groups and the iron center. The bonding interaction between the BH σ-bond and a d orbital at iron is identified at very low energy as HOMO−18 (see SI). Quantum theory of atoms in molecules (QTAIM, see SI) confirms the substantial weakening of the B–B interaction in **2** as no bond critical point is found between the boron atoms.

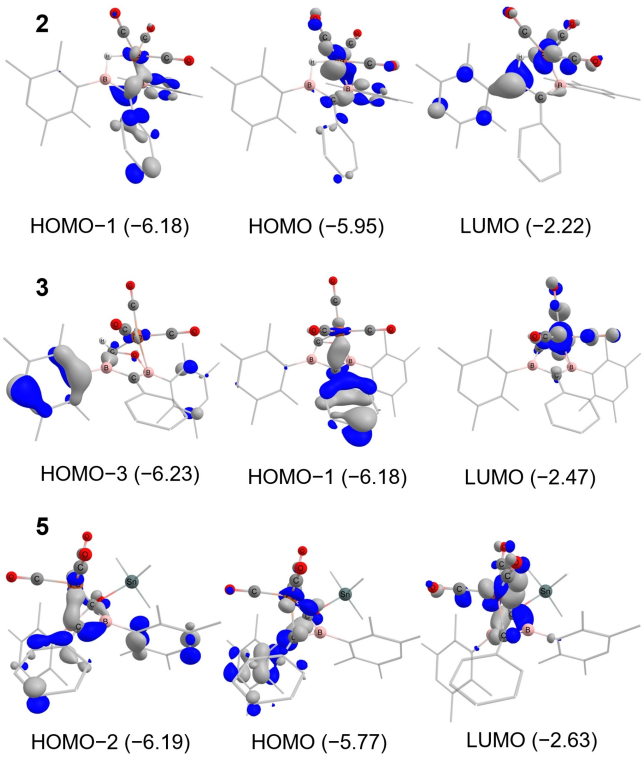

Figure 2. Selected frontier orbitals of iron complexes **2**, **3** and **5** (energy in eV, contour value = 0.06).

Carbonylative ring expansion

The interest in boron containing transition metal complexes is intimately related to their role in important catalytic processes[21] and hence to the activation of the C–B or BH bond for reactions with otherwise unreactive substrates. In view of the borylmethyleneborane nature of **2** with coordination of both the BH σ-bond and the B–C π-bond to the iron center, we envisaged the possibility of hydroboration of a small molecule such as carbon monoxide with iron complex **2**. While extended exposure of **2** to an excess of CO only results in the liberation of the free diborirane **1**, stirring of **2** with five equivalents $Fe_2(CO)_9$ in toluene for 72 h indeed leads to the formation of a new product as indicated by ^1H NMR monitoring.

Two singlets each for the *ortho* and *meta* CH_3 groups confirm the chemical inequivalence of the duryl substituents and hence a less symmetric structure. Consequently, the ^{11}B NMR spectrum also shows two signals for the boron atoms at $\delta = 26.2$ ppm and 34.5 ppm and thus upfield-shifted signals compared to that of iron complex **2**. The similarity of the chemical shifts to those of 1,3-diborole metal complexes[22] suggests the constitution of **3**, the formal hydroboration product of **2** and one molecule of CO and hence the expansion of the diborirane to a five-membered ring (Scheme 3). Carbonylative ring expansions by transition metal carbonyls have been reported for various strained heterocycles,[23] but not for boron containing systems.

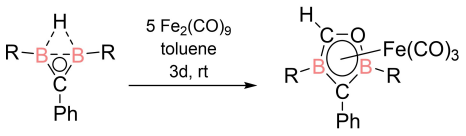

1 3

Scheme 3. Hydroboration of carbon monoxide with **1** to yield η^5-complex of five-membered diboracycle **3** (R=Dur=2,3,5,6-Me_4C_6H).

Due to the higher electronegativity of oxygen compared to carbon, the signal at $\delta = 34.5$ ppm is tentatively assigned to the oxygen-bonded boron atom. The ^{13}C NMR spectrum at 213 K shows two broad signals at $\delta = 109.0$ and 90.0 ppm which we attribute to the ring carbon atoms. The signal at $\delta = 109.0$ ppm, still in the aromatic region, is due to the B–C–B carbon atom. The significant downfield shift compared to the ring carbon in diborirane complex **2** ($\delta =$ 50.0 ppm) confirms a more pronounced cyclic delocalization of the π-electrons. This gains further support from the ^{13}C NMR signal of the other endocyclic carbon signal at $\delta =$ 90.0 ppm being substantially deshielded compared to Erker's saturated oxadiborolane NHC adduct **III** ($\delta = 77.4$ ppm, Scheme 4).[24]

The IR spectrum of the red solid shows two strong signals at 2000 cm^{-1} and 2059 cm^{-1} in the region for CO stretching modes. DFT calculations find CO vibrations at 2026, 2028 and 2079 cm^{-1} again slightly blue shifted compared to the experimental data. The significant blue-shift compared to diborirane complex **2** suggests weaker backbonding from the iron center to the CO π*-orbitals due to an increased charge transfer to the boron ligand. Incidentally, the CO stretching frequencies are very similar to those of Herberich's $Fe(CO)_3$-borole complex **IV** (Scheme 4).[25]

The η^5-complex **3** can also be obtained by adding 3.4 equivalents of $Fe_2(CO)_9$ to diborirane iron complex **2**, confirming its intermediacy. As the formal hydroboration product **3** cannot be obtained from isolated **2** by simple addition of 1 atm of CO gas, we assume an initial addition of an $Fe_x(CO)_y$ fragment of an unknown nature to **2** and subsequent transfer of a CO molecule. The spatially proximal B–H would then hydroborate a polarized CO bond. The liberated $Fe_x(CO)_y$ fragment could react with $Fe_2(CO)_9$ explaining that more than one equivalent of $Fe_2(CO)_9$ are required for full conversion. Free non-classical diborirane **1** does not react with CO either, which underscores the necessity of the presence of the unknown iron species.

Crystallization from a concentrated hexane solution yields dark-red single crystals suitable for x-ray diffraction (Figure 3). The structure was solved in the triclinic space group $P\bar{1}$ and confirms the constitution of **3** as an 4-oxa-1,3-diborole ligand η^5-coordinated to the $Fe(CO)_3$ fragment in a piano-stool fashion. In accordance with the Wade-Mingos counting rules (16 skeletal electrons for six centers), the compound can equally be described as six-vertex *nido* cluster with a pentagonal-pyramidal polyhedron. The donation of the π-electrons to the iron fragment in **3** is more pronounced than in **2**, which is expressed in longer B–C bonds (**2**: B1–C1 1.498(2) Å, B2–C1 1.496(2) Å; **3**: B1–C1 1.544(2) Å; B2–C1 1.559(2) Å), albeit still shorter than typical B–C single bonds. The B2–C2 bond of **3** of 1.501(2) Å is shorter than the other two B–C bonds, which is probably a consequence of the much lower steric congestion at C2.

The five-membered ring in **3** adopts an envelope conformation with the phenyl-substituted C1 bent toward Fe1 (folding angle B1–C1–B2/B1–O1–C2–B2 22.1(1)°). This folding minimizes the steric interactions between the phenyl and the duryl substituents although it is less pronounced than in an iron sandwich complex with an anionic η^5-1,3-diborole ligand reported by Siebert et al. (**V** in Scheme 4; folding angle 41.3°).[22a] In any case, the bent structure appears to maximize the overlap between the B_2C_2O π-electrons and the d_z^2 orbital at the iron center in sight of considerable steric strain. Compared to Siebert's 1,3-diborole complex **V**, the boron-iron distances in **3** (B1–Fe1 2.299(2) Å; B2–Fe1 2.315(2) Å) are only slightly larger (**V**: 2.248 Å), while the iron contact of the folded carbon (**3**: C1–Fe1 2.175(2) Å) is substantially elongated (**V**: 1.899 Å). In turn, the other carbon-iron distance in **3** (C2–Fe1 2.025(2) Å) is significantly shorter (**V**: 2.116 Å).

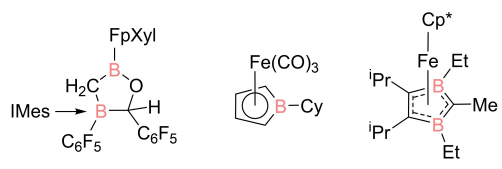

III IV V

Scheme 4. Reported five-membered diboracycle **III**[24] and complexes **IV**[25] and **V**[22a] (FpXyl=2,5-bis(trifluoromethyl)phenyl; IMes=N,N'-dimesitylimidazolylidene; Cp*=pentamethylcyclopentadienyl).

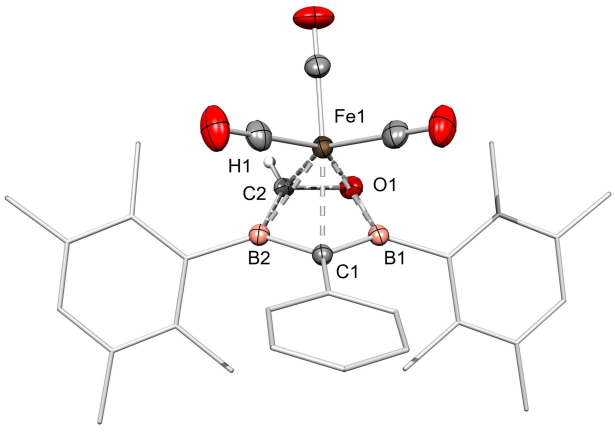

Figure 3. Molecular structure of formal hydroboration product **3** in the solid state. Thermal ellipsoids at 50% probability. Selected bond lengths [Å] and angles [°]: B1–C1 1.544(2), B2–C1 1.559(2), B1–O1 1.466(2), B2–C2 1.501(2), C2–O1 1.440(2), B1–Fe1 2.229(2), B2–Fe1 2.315(2), C1–Fe1 2.175(2), C2–Fe1 2.025(2); B1–C1–B2 106.3(1).

These observations can be rationalized with the canonical orbitals as calculated by DFT at the B3LYP/def2tzvpp level of theory (Figure 2) since the significant overlap of the rings π-system mainly located at C1 with the irons d orbital can be seen in the HOMO−1. The HOMO−3 is composed of the bonding combination of the lone pair at C2 and another d orbital of iron. The LUMO shows a vacant d orbital with antibonding combination of the COs π-system. The longest wavelength absorption in the experimental UV/Vis spectrum (see SI) at $\lambda_{max}=403$ nm ($\varepsilon=2450\ M^{-1}\ cm^{-1}$) tails to around 500 nm in a similar manner as diborirane complex **2**. A TD-DFT calculation at the B3LYP/def2tzvpp level of theory assigns the band to the HOMO→LUMO transition at 401 nm.

Although certainly nowhere near as well developed as hydroboration, borostannylation has been reported as an effective tool for the cyclization of α,ω-dienes.[26] We were thus interested in the behavior of Me_3Sn-bridged diborirane **4**[13] toward $Fe_2(CO)_9$. As in the case of the non-classical diborirane **1**, DFT calculations showed that the HOMO of diborirane derivative **4** is composed of the B_2C rings π-system.[13] Indeed, the addition of 1.2 equivalents of $Fe_2(CO)_9$ to the tin-bridged diborirane **4** in toluene leads to a color change of the reaction mixture from colorless to red-brown and the appearance of a uniform set of new signals in the ^{1}H NMR spectrum (Scheme 5). The product appears to be symmetrical in solution due to the presence of only one signal each for the *ortho* and *meta*-CH_3 groups of the duryl substituents. The single ^{11}B NMR signal at $\delta=-17.7$ ppm is considerably more shielded than in both **2** and **3**. While the ^{13}C NMR signal for the endocyclic Ph-substituted carbon atom ($\delta=111.2$ ppm) is similar to the one in the five-membered ligand of complex **3** ($\delta=109.0$ ppm), the oxygen-bonded ring carbon signal is dramatically downfield shifted to $\delta=257.7$ ppm.

This carbon atom is thus considerably more deshielded than the COs at the iron center ($\delta=211.6$ ppm). This is indicative of a small degree of backdonation from the iron center to the empty p orbital of the CO moiety. The ^{119}Sn NMR spectrum shows a signal at $\delta=191.3$ ppm, downfield-shifted by $\Delta\delta=230$ ppm compared to precursor **4** as expected for the reduction in coordination number at tin from five to four. The IR spectrum shows CO vibrations at similar wavenumbers as in diborirane complex **2** at 1966, 1983 and 2045 cm^{-1}. DFT calculated values at 1994, 2013 and 2059 cm^{-1} are once more slightly blue-shifted compared to the experimental data. Taken together, the analytical data is in line with the constitution of 1,3-dihydro-1,3-diborete complex **5**.

Dark red-brown crystals of **5** suitable for an x-ray diffraction analysis were obtained from a concentrated hexane solution at 0 °C (Figure 4). The crystal structure confirms the end-on insertion of one carbon monoxide ligand into the 3c2e BBSn bond to yield a four-membered 1,3-diborete ring system coordinated in η^4-fashion to the $Fe(CO)_3$ moiety. With a cluster electron count of 12, the compound can be described as a five-vertex *closo* cluster with an B_2C_2Fe scaffold and thus as a distorted trigonal bipyramid. As a consequence, the B_2C_2 moiety adopts a bicyclo(1.1.0)butane-like structure, which is, however, also familiar for free 1,3-diboretes.[27] The $Fe(CO)_3$ unit resides above this moiety, yet the boron atoms retain a considerable degree of mutual interaction as the B–B distance is elongated just moderately (B1–B2: 1.871(5) Å) compared to precursor **4** (B–B: 1.799 Å).[13] In Stone's ferracar-borates with $FeCB_7$ and Fe_2CB_7 scaffolds the distance between the two carbon-connected boron vertices are considerably expanded to 2.137 and 1.996 Å, respectively.[28] In fact, the B–B distance in **5** is significantly shorter than in a free 1,3-diborete (2.16 Å)[27] and slightly shorter than in 1,3-diborete nickel complex (1.890 Å), recently reported by Braunschweig and co-workers.[29]

The longest wavelength absorption in the experimental UV/Vis spectrum (see SI) is observed as a very broad band of low intensity at $\lambda_{max}=600$ nm ($\varepsilon=481\ M^{-1}\ cm^{-1}$) tailing to around 650 nm. The TD-DFT calculated $\lambda_{max}=620$ nm

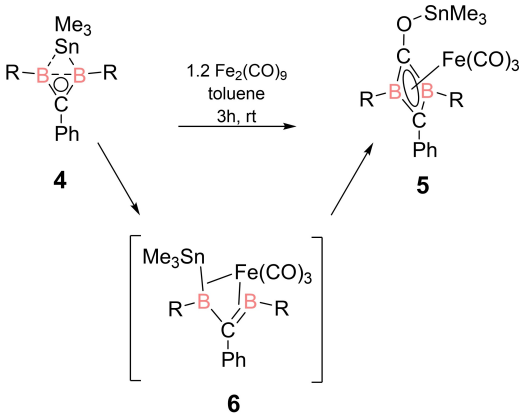

Scheme 5. Complexation of tin bridged diborirane **4** to the four-membered iron complex **5** (R=Dur=2,3,5,6-Me_4C_6H) and the presumed intermediate complex **6**.

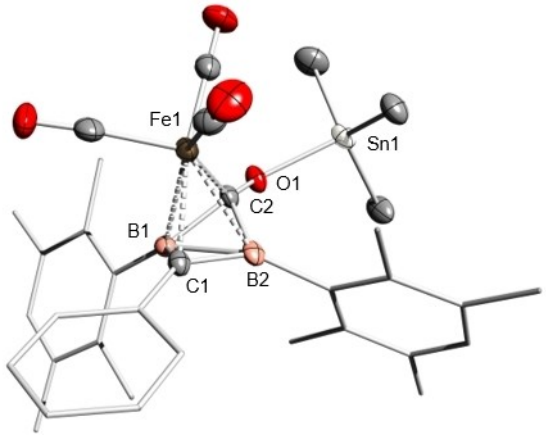

Figure 4. Molecular structure of 1,3-diborete iron complex **5** in the solid state. Thermal ellipsoids at 50% probability. Selected bond lengths [Å] and angles [°]: B1–B2 1.871(5), B1–C1 1.529(4), B2–C1 1.510(4), B1–C2 1.599(4), B2–C2 1.620(4), B1–Fe1 2.210(3), B2–Fe1 2.291(3), C1–Fe1 2.065(3), C2–Fe1 1.906(3) C2–O1 1.318(3); B1–C1–B2 76.0(2), B1–C2–B2 71.1(2).

matches the experimental value reasonably well. The calculated HOMO–LUMO gap is 1.96 eV and thus significantly smaller than for compound **2** and **3**. The computed UV/Vis spectrum consists of a large number of transitions which, taken together, agree well with the experimental spectrum (see SI). The electronic structure, investigated by DFT calculations at the B3LYP/def2tzvpp level of theory, shows the LUMO to be composed of ligand- and metal-centered orbitals (Figure 2).

HOMO and HOMO−2 each show significant overlap between π-electrons, each predominantly located at C1 and C2 and the d orbital at the $Fe(CO)_3$ fragment. HOMO−5 shows orbital overlap of the entire π-system delocalized over the B_2C_2 centers with the $Fe(CO)_3$ fragment, suggesting a donation in η^4-fashion.

We propose a similar mechanism for the formation of the four-membered ring **5** as for complex **3**. The first step could be the generation of the, albeit undetected, Sn-bridged diborirane complex **6**. The product of oxidative addition of a B–Sn bond to a palladium center was reported by Tanaka and co-workers.[26a] A reason for the instability of the putative intermediate might be the much weaker B–Sn bond, which would facilitate the insertion of either the Fe center or a carbonyl ligand ultimately leading to the 1,3-diborete complex **5**. The free energy of calculated intermediate **6** and free CO is $\Delta G = 21.9\ kcal\,mol^{-1}$ higher than that of product **5** (see SI). Alternatively, a π-complex of B=C bond and a $Fe(CO)_4$ fragment without agostic BSn interaction could be envisaged, which, however, is calculated to be $\Delta G = 7.1\ kcal\,mol^{-1}$ higher in free energy than compound **6** and free CO (see SI). We did not attempt to compute any of the involved transition states keeping in mind that the unclear nature of the involved $Fe_x(CO)_y$ fragments would make this a futile exercise. The preference of this system for the end-on insertion vs. the side-on insertion observed for **3** is ascribed to the pronounced oxophilicity of the $SnMe_3$ group. The apparent kinetic product **5** is calculated to be $\Delta G = 2.0\ kcal\,mol^{-1}$ higher in free energy than the hypothetical thermodynamic product, the Me_3Sn analogue of **3** (see SI). Heating of **5** above the melting point of 168 °C, however, leads to its decomposition.

As in case of H-bridged diborirane **1**, the uncomplexed Me_3Sn-derivative **4** does not react with CO in the absence of iron carbonyls, confirming the involvement of an unknown $Fe_x(CO)_y$ species. As a side remark, although numerous reactions of B–Sn reagents with C–C multiple bonds have been reported,[26] the formation of **5** appears to be the first formal borastannylation of a heteronuclear multiple bond.

Conclusion

We have prepared the first diborirane π-complex **2** derived from hydrogen-bridged diborirane **1** and $Fe_2(CO)_9$. The $Fe(CO)_3$ fragment is coordinated by the B_2C π-system as well as the BH σ-bond so that the non-classical diborirane acts as a $4e^-$ donor toward the iron center retaining only weak BB interaction. The formal hydroboration of carbon monoxide by non-classical diborirane **2** results in the ring expansion to an η^5-coordinated B_2C_2O ligand **3**, although only in the presence of $Fe_2(CO)_9$. The particularly strong backdonation from the iron center, which formally turns the 4π-system into a 6π-system, can be seen in the ^{13}C NMR signals of the ring carbon atom as well as in the IR stretching frequencies. In contrast, upon treatment with $Fe_2(CO)_9$, the Me_3Sn-bridged derivative of **1** is expanded by an end-on inserted CO molecule to yield the η^4-bonded 1,3-diborete complex **5**. The inherent Hückel aromaticity of the 1,3-diborete results in almost negligible backdonation from metal to ligand as the ^{13}C NMR signal is hardly affected by the coordination.

Supporting Information

Plots of NMR, UV and IR spectra as well as details of the single crystal x-ray diffractions studies and DFT-calculations are available in the Supporting Information of this article. Deposition numbers 2357653 (for **2**), 2357652 (for **3**), and 2357648 (for **5**) contain the supplementary crystallographic data for this paper. These data are provided free of charge by the joint Cambridge Crystallographic Data Centre and Fachinformations-zentrum Karlsruhe Access Structures service. The authors have cited additional references within the Supporting Information.[30–40]

Acknowledgements

We acknowledge the Service Center X-ray Diffraction established with financial support from Saarland University and the Deutsche Forschungsgemeinschaft (INST256/506-1). We thank Prof. Stella Stopkowicz and Dr. Diego Andrada for access to their computational clusters as well as helpful discussions. Open Access funding enabled and organized by Projekt DEAL.

Conflict of Interest

The authors declare no conflict of interest.

Data Availability Statement

The data that support the findings of this study are available in the supplementary material of this article.

Keywords: boron · aromatics · transition metal · coordination chemistry · ring expansion

[1] For selected reviews of metal–organic frameworks see: a) V. F. Yusuf, N. I. Malek, S. K. Kailasa, *ACS Omega* **2022**, *7*, 44507–44531; b) H.-C. Zhou, J. R. Long, O. M. Yaghi, *Chem. Rev.* **2012**, *112*, 673–674.

[2] For selected reviews of dye-sensitized solar cells see: a) A. B. Munoz-Garcia, I. Benesperi, G. Boschloo, J. J. Concepcion,

J. H. Delcamp, E. A. Gibson, G. J. Meyer, M. Pavone, H. Pettersson, A. Hagfeldt, M. Freitag, *Chem. Soc. Rev.* **2021**, *21*, 12450–12550; b) A. Hagfeldt, G. Boschloo, L. Sun, L. Kloo, H. Pettersson, *Chem. Rev.* **2010**, *110*, 6595–6663.

[3] For selected reviews of metallopolymers see: a) Y. Yan, J. Zhang, L. Ren, C. Tang, *Chem. Soc. Rev.* **2016**, *45*, 5232–5263; b) Y. Wang, D. Astruc, A. S. Abd-El-Aziz, *Chem. Soc. Rev.* **2019**, *48*, 558–636; c) R. Whitell, I. Manners, *Adv. Mater.* **2007**, *19*, 3439–3468.

[4] For selected examples of boron containing heterocycles see: a) B. Su, R. Kinjo, *Synthesis* **2017**, *49*, 2985–3034; b) U. M. Dzhemilev, L. I. Khusainova, K. S. Ryazanov, L. O. Khafizova, *Russ. Chem. Bull. Int. Ed.* **2021**, *70*, 1851–1892.

[5] a) C.-W. So, D. Watanabe, A. Wakamiya, S. Yamaguchi, *Organometallics* **2008**, *27*, 3496–3501; b) J. He, F. Rauch, M. Finze, T. B. Marder, *Chem. Sci.* **2021**, *12*, 128–147.

[6] For selected examples of bora and boratabenzenes see: a) G. E. Herberich, G. Greiss, H. F. Heil, *Angew. Chem. Int. Ed. Engl.* **1970**, *9*, 805–806; b) G. E. Herberich, H. Ohst, *Chem.* **1986**, *25*, 199–236; c) A. J. Ashe III, P. Shu, *J. Am. Chem. Soc.* **1971**, *93*, 1804–1805; d) G. C. Fu, *Adv. Organomet. Chem.* **2001**, *47*, 101–119.

[7] For selected examples of borepins see: a) A. J. Ashe III, F. J. Drone, C. M. Kausch, J. Kroker, S. M. Al-Taweel, *Pure Appl. Chem.* **1990**, *62*, 513–517; b) A. J. Ashe III, W. Klein, R. Rousseau, *Organometallics* **1993**, *12*, 3225–3231.

[8] H. Goodman, L. Mei, T. L. Gianetti, *Front. Chem.* **2019**, *7*, 1–19.

[9] T. Kupfer, H. Braunschweig, K. Radacki, *Angew. Chem. Int. Ed.* **2015**, *54*, 15084–1508.

[10] a) H. Braunschweig, T. Herbst, D. Rais, F. Seeler, *Angew. Chem. Int. Ed.* **2005**, *44*, 7461–7463; b) H. Braunschweig, T. Herbst, D. Rais, S. Ghosh, T. Kupfer, K. Radacki, A. G. Crawford, R. M. Ward, T. B. Marder, I. Fernández, G. Frenking, *J. Am. Chem. Soc.* **2009**, *131*, 8989–8999.

[11] H. Braunschweig, P. Brenner, R. D. Dewhurst, I. Krummenacher, B. Pfaffinger, A. Vargas, *Nat. Commun.* **2012**, *3*, 872.

[12] H. Braunschweig, R. D. Dewhurst, K. Radacki, C. W. Tate, A. Vargas, *Angew. Chem. Int. Ed.* **2014**, *53*, 6263–6266.

[13] P. Grewelinger, T. Wiesmeier, B. Morgenstern, C. Präsang, D. Scheschkewitz, *Angew. Chem. Int. Ed.* **2023**, *62*, e202308678.

[14] For selected examples see: a) D. Sharmila, B. Mondal, R. Ramalakshmi, S. Kundu, B. Varghese, S. Ghosh, *Chem. Eur. J.* **2015**, *21*, 5074–5083; b) R. Prakash, A. N. Pradhan, M. Jash, S. Kahlal, M. Cordier, T. Roisnel, J.-F. Halet, S. Ghosh, *Inorg. Chem.* **2020**, *59*, 1917–1927; c) A. Wagner, A. Kaifer, H.-J. Himmel, *Chem. Commun.* **2012**, *48*, 5277–5279; d) K. Saha, D. K. Roy, R. D. Dewhurst, S. Ghosh, H. Braunschweig, *Acc. Chem. Res.* **2021**, *54*, 1260–1273; e) Y. C. Tang, A. L. Thompson, S. Aldridge, *J. Am. Chem. Soc.* **2010**, *132*, 10578–10591; f) T. M. Douglas, A. B. Chaplin, A. S. Weller, X. Yang, M. B. Hall, *J. Am. Chem. Soc.* **2009**, *131*, 15440–15456; g) M. Shimoi, S. Nagai, M. Ichikawa, Y. Kawano, K. Katoh, M. Uruichi, H. Ogino, *J. Am. Chem. Soc.* **1999**, *121*, 11704–11712; h) M. P. Mehn, S. D. Brown, T. K. Paine, W. W. Brennessel, C. J. Cramer, J. C. Peters, L. Que Jr, *Dalton Trans.* **2006**, 1347–1351; i) M. Maekawa, C. G. Daniliuc, P. G. Jones, J. Hohenberg, J. Sutter, K. Meyer, M. D. Walter, *J. Inorg. Chem.* **2013**, 4097–4104; j) K. K. Pandey, *Coord. Chem. Rev.* **2009**, *253*, 37–55.

[15] X. Meng, T. P. Fehlner, A. L. Rheingold, *Organometallics* **1990**, *9*, 534–536.

[16] C. Präsang, Y. Sahin, M. Hofmann, G. Geiseler, W. Massa, A. Berndt, *Eur. J. Inorg. Chem.* **2008**, 5046–5055.

[17] A. Gunale, D. Steiner, D. Schweikart, H. Pritzkow, A. Berndt, W. Siebert, *Chem. Eur. J.* **1998**, *4*, 44–52.

[18] H. Braunschweig, Q. Ye, K. Radacki, A. Damme, *Angew. Chem. Int. Ed.* **2012**, *51*, 7839–7842.

[19] Deposition numbers 2357653 (for **2**), 2357652 (for **3**), and 2357648 (for **5**) contain the supplementary crystallographic data for this paper. These data are provided free of charge by the joint Cambridge Crystallographic Data Centre and Fachinformationszentrum Karlsruhe Access Structures service.

[20] J. J. Turner, M. Bühl, *J. Phys. Chem. A* **2018**, *122*, 3497–3505.

[21] For selected reviews on boron containing transition metal complexes see: a) G. J. Irvine, M. J. G. Lesley, T. B. Marder, N. C. Norman, C. R. Rice, E. G. Robins, W. R. Roper, G. R. Whittell, L. J. Wright, *Chem. Rev.* **1998**, *98*, 2685–2722; b) C. W. Allen, D. E. Palmer, *J. Chem. Educ.* **1978**, *55*, 497–500; c) J. T. Goettel, H. Braunschweig, *Coord. Chem. Rev.* **2019**, *380*, 184–200.

[22] a) R. Hettrich, M. Kaschke, H. Wadepohl, W. Weinmann, M. Stephan, H. Pritzkow, W. Siebert, I. Hyla-Kryspin, R. Gleiter, *Chem. Eur. J.* **1996**, *2*, 487–494; b) W. Siebert, M. Bochmann, *Angew. Chem. Int. Ed. Engl.* **1977**, *16*, 857–858; c) W. Siebert, D. Büchner, H. Pritzkow, H. Wadepohl, F.-W. Grevels, *Chem. Ber.* **1987**, *120*, 1511–1514.

[23] For selected examples see: a) K. Khumtaveeporn, H. Alper, *Acc. Chem. Res.* **1995**, *28*, 414–422; b) A. Brand, P. Wegener, A. Hepp, W. Uhl, *Organometallics* **2020**, *39*, 1384–1392; c) J.-B. Peng, F.-P. Wu, X.-F. Wu, *Chem. Rev.* **2019**, *119*, 2090–2127.

[24] K. Skoch, C. Chen, C. G. Daniliuc, G. Kehr, G. Erker, *Dalton Trans.* **2022**, *51*, 7695–7704.

[25] G. E. Herberich, W. Boveleth, B. Hessner, D. P. J. Köffer, M. Negele, R. Saive, *J. Organomet. Chem.* **1986**, *308*, 153–166.

[26] a) S. Onozawa, Y. Hatanaka, T. Sakakura, S. Shimada, M. Tanaka, *Organometallics* **1996**, *15*, 5450–5452; b) L. Weber, H. Wartig, H.-G. Stammler, A. Stammler, B. Neumann, *Organometallics* **2000**, *19*, 2891–2895; c) R. R. Singidi, A. M. Kutney, J. C. Gallucci, T. V. RajanBabu, *J. Am. Chem. Soc.* **2010**, *132*, 13078–13087.

[27] M. Hildenbrand, H. Pritzkow, U. Zenneck, W. Siebert, *Angew. Chem. Int. Ed. Engl.* **1984**, *23*, 371–372.

[28] A. Franken, T. D. McGrath, F. G. A. Stone, *Organometallics* **2005**, *24*, 5157–5166.

[29] A. Hermann, F. Fantuzzi, M. Arrowsmith, T. Zorn, I. Krummenacher B Ritschel, K. Radacki, B. Engels, H. Braunschweig, *Angew. Chem. Int. Ed.* **2020**, *59*, 15717–15725.

[30] G. R. Fulmer, A. J. M. Miller, N. H. Sherden, H. E. Gottlieb, A. Nudelman, B. M. Stoltz, J. E. Bercaw, K. I. Goldberg, *Organometallics* **2010**, *29*, 2176–2179.

[31] L. Benco, T. Demuth, J. Hafner, F. Hutschka, H. Toulhoat, *J. Catal.* **2002**, *205*, 147–156.

[32] G. M. Sheldrick, *Acta Crystallogr.* **2015**, *A71*, 3–8.

[33] G. M. Sheldrick, *Acta Crystallogr.* **2015**, *C71*, 3–8.

[34] C. B. Hübschle, G. M. Sheldrick, B. Dittrich, *J. Appl. Crystallogr.* **2011**, *44*, 28–28.

[35] Gaussian 09, Revision A.02, M. J. Frisch, G. W. Trucks, H. B. Schlegel, G. E. Scuseria, M. A. Robb, J. R. Cheeseman, G. Scalmani, V. Barone, G. A. Petersson, H. Nakatsuji, X. Li, M. Caricato, A. Marenich, J. Bloino, B. G. Janesko, R. Gomperts, B. Mennucci, H. P. Hratchian, J. V. Ortiz, A. F. Izmaylov, J. L. Sonnenberg, D. Williams-Young, F. Ding, F. Lipparini, F. Egidi, J. Goings, B. Peng, A. Petrone, T. Henderson, D. Ranasinghe, V. G. Zakrzewski, J. Gao, N. Rega, G. Zheng, W. Liang, M. Hada, M. Ehara, K. Toyota, R. Fukuda, J. Hasegawa, Ishida, M. T. Nakajima, Y. Honda, O. Kitao, H. Nakai, T. Vreven, K. Throssell, J. A. Montgomery Jr, J. E. Peralta, F. Ogliaro, M. Bearpark, J. J. Heyd, E. Brothers, K. N. Kudin, V. N. Staroverov, T. Keith, R. Kobayashi, J. Normand, K. Raghavachari, A. Rendell, J. C. Burant, S. S. Iyengar, J. Tomasi, M. Cossi, J. M. Millam, M. Klene, C. Adamo, R. Cammi, J. W. Ochterski, R. L. Martin, K. Morokuma, O. Farkas, J. B. Foresman, D. J. Fox, Gaussian, Inc., Wallingford CT, **2016**.

[36] a) J. P. Perdew, *Phys. Rev. B* **1986**, *33*, 8822–8824; b) A. D. Becke, *Phys. Rev. A* **1988**, *38*, 3098–3100.
[37] a) A. Schäfer, H. Horn, R. Ahlrichs, *J. Chem. Phys.* **1992**, *97*, 2571–2577; b) A. Schäfer, C. Huber, R. Ahlrichs, *J. Chem. Phys.* **1994**, *100*, 5829–5835; c) F. Weigend, R. Ahlrichs, *Phys. Chem. Chem. Phys.* **2005**, *7*, 3297–3305; d) F. Weigend, *Phys. Chem. Chem. Phys.* **2006**, *8*, 1057–1065.
[38] S. Grimme, J. Antony, S. Ehrlich, H. Krieg, *J. Chem. Phys.* **2010**, *132*, 154104.
[39] Chemcraft - graphical software for visualization of quantum chemistry computations. https://www.chemcraftprog.com.
[40] T. Lu, F. Chen, *J. Comput. Chem.* **2012**, *33*, 580–592.

Manuscript received: August 12, 2024
Accepted manuscript online: October 16, 2024
Version of record online: November 13, 2024

3.3 2,3-Diboratabutadiene Complexes of Group 4 Metals and their Donor-Induced Oxidative Cleavage to Methyleneboranes

P. Grewelinger, C. Präsang, B. Morgenstern, D. Scheschkewitz, *ChemisryEurope* **2025**, *00*, e202500153. https://doi.org/10.1002/ceur.202500153

The article is reproduced with permission of all authors. No modifications were made. The results are additionally concluded and put into context in Chapter 4.

Author Contributions:

Philipp Frank Grewelinger (Conceptualization: Equal (DS); Data curation: Lead; Formal analysis: Lead; Investigation: Lead; Writing – original draft: Lead)

Carsten Präsang (Conceptualization: Supporting; Data curation: Supporting; Investigation: Supporting; Writing – original draft: Supporting)

Bernd Morgenstern (Data curation: Lead; Formal analysis: Supporting; Methodology: Supporting)

David Scheschkewitz (Conceptualization: Lead; Formal analysis: Supporting; Funding acquisition: Lead; Investigation: Supporting; Methodology: Supporting; Project administration: Lead; Resources: Lead; Supervision: Lead; Writing – review & editing: Lead)

ChemistryEurope
Excellence in Chemistry Research Worldwide

Research Article
doi.org/10.1002/ceur.202500153

www.journal.chemistry-europe.org

2,3-Diboratabutadiene Complexes of Group 4 Metals and their Donor-Induced Oxidative Cleavage to Methyleneboranes

Philipp Grewelinger, Carsten Präsang, Bernd Morgenstern, and David Scheschkewitz*

Metal complexes of conjugated olefins have been known for a century. The formal heterosubstitution of carbon atoms in such ligands significantly alters their electronic properties. While several examples with terminal boron centers are known, butadiene transition metal complexes with internal B—B bonds and thus bora-substitution in 2,3-position remain elusive. Herein, the first peraryl 2,3-diboratabutadiene dianion is reported, prepared in two steps as its lithium salt from readily available 1,2-dichloro-1,2-diduryldiborane(4) (duryl = 2,3,5,6-tetramethylphenyl). The reactions with Cp_2MCl_2 (M = Zr, Hf) afford unprecedented 2,3-diboratabutadiene π-complexes with unique coordination modes in between the familiar s-*cis* and s-*trans* conformations of the corresponding all-carbon derivatives. Addition of the N-heterocyclic carbene 1,3,4,5-tetramethylimidazol-2-ylidene (IMe) to the complexes gives rise to the donor-induced oxidation of the B—B bond, resulting in two separate IMe-coordinated methyleneboranes with B=C double bonds and the liberation of transient metal(II) fragments "MCp_2". At longer reaction times, the methyleneboranes are hydrogenated by the active "MCp_2" species as evidenced by isolation of the corresponding saturated methyl borane adducts.

1. Introduction

Almost two centuries ago, the first transition metal alkene complex marked the dawn of organometallic chemistry, an ethylene complex of $[PtCl_3]^-$, now known as Zeise's salt.[1] Nowadays, alkenes are among the most common ligands of transition metals and have made their way into chemistry textbooks for their prototypical bonding situation according to the Dewar–Chatt–Duncanson model[2–4] as well as for their industrial relevance in catalysis.[5–8] Butadienes as the simplest conjugated systems comprising two C=C bonds are versatile precursors for transition metal-catalyzed transformations in organic chemistry[9–11] due to their different coordination modes, namely the η^2-coordination of either C=C bond as well as the competing s-*cis* and s-*trans* η^4-modes of the entire π-system.[12–14]

On grounds of the topologically similar, yet electronically very different structure, the bora-substituted neutral and anionic alkene homologues are emerging as an alternative class of ligands with unique applications.[15] Concerning the corresponding butadiene analogues, dianionic **Ia-c** with central B—B bonds were reported as early as 1990,[16–18] but their reactivity is limited to main group electrophiles.[19,20] Transition metal borabutadiene complexes are so far only known with one or two terminal boron centers: Siebert et al. described the synthesis of 1-borabutadiene complex **II** through ring-opening and isomerization of a diborolane by coordination to the CpCo fragment (**Scheme 1**).[21]

The related rhodium complex **III** was obtained in the Erker group by exchange of the ethylene ligands in $[Rh(C_2H_4)_2Cl]_2$ for an N-heterocyclic carbene (NHC)-stabilized borabutadiene (NHC = IMe = 1,3,4,5-tetramethylimidazol-2-ylidene).[22] Irradiation of a bis (borylene) iron complex in the presence of $Me_3SiC{\equiv}CSiMe_3$ yields the 1,4-diborabutadiene complex **IV** according to Braunschweig and coworkers.[23] The 1,2-divinyldiborene complex **V** reported by the same group is the only butadiene complex so far with an intact B—B bond.[24] Lindley et al. prepared complex **VI** by UV-promoted insertion of the $Fe(CO)_3$ fragment into the B–B bond of the corresponding 1,2-diborete precursor.[25] The availability of butadiene ligands with retained central B—B bonding can thus be expected to open up fundamentally new preparative avenues in this regard.

We now report the straightforward and high yielding synthesis of a 2,3-diboratabutadiene with a sterically innocent and conjugated phenyl substituent in two steps from a readily available 1,2-diaryl-1,2-dichlorodiborane (4). As we will show, the 2,3-diboratabutadiene coordinates to group 4 metallocene fragments in a manner right in between the well-known s-*cis* and s-*trans* coordination modes of all-carbon butadiene ligands. Addition of N-heterocyclic carbene allows for the oxidative cleavage of the B—B bond into two B=C-containing methyleneborane fragments.

P. Grewelinger, C. Präsang, D. Scheschkewitz
Krupp-Chair in General and Inorganic Chemistry
Saarland University
66123 Saarbrücken, Germany
E-mail: scheschkewitz@mx.uni.saarland.de

B. Morgenstern
Service Center X-Ray Diffraction
Saarland University
66123 Saarbrücken, Germany

Supporting information for this article is available on the WWW under https://doi.org/10.1002/ceur.202500153

Research Article
doi.org/10.1002/ceur.202500153

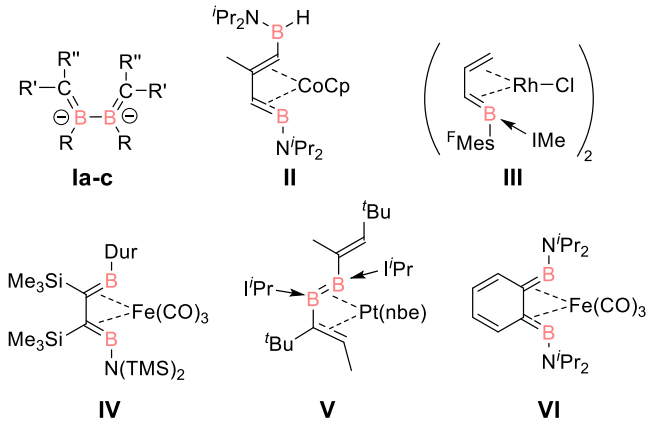

Scheme 1. Reported 2,3-diboratabutadienes **Ia-c** and boron-containing butadiene complexes **II** to **VI**.[21–25] (a: R = NMe_2, R′ + R″; = fluorenyl, b: R = Dur, R′ = R″; = $SiMe_3$, c: R = Dur, R′ $SiMe_3$, R″; = H, Dur = duryl = 2,3,5,6-tetramethylphenyl, ^{i}Pr = iso-propyl, IMe = 1,3,4,5-tetramethylimidazol-2-ylidene, ^{Id}Pr = 1,3-diisopropylimidazol-2-ylidene, nbe = norbornene).

2. Results and Discussion

Initially, we tested the reaction of the literature known 2,3-diboratabutadiene **Ic** with Cp_2ZrCl_2, which resulted in a mixture of products, presumably due to competing protonation and redox reactions. The steric constraints imposed by the $SiMe_3$ groups at the anionic carbon centers likely favor electron and proton transfer over attack by the bulky group 4 electrophile. We anticipated that these problems may be overcome by replacement of the silyl by sterically more innocuous phenyl substituents.

The required 1,2-dibenzyl-1,2-diduryldiborane (4) **1** was prepared by the selective reaction of 1,2-dichloro-1,2-diduryldiborane (4)[26] with two equivalents of benzyl magnesium chloride[27–31] at −78 °C in 97% yield and characterized by multinuclear NMR spectroscopy and single crystal X-ray diffraction (see Supporting Information). In adaptation of the procedure by Berndt et al. for a trimethylsilyl-substituted derivative,[17] double deprotonation with $LiNMe_2$ at the benzylic positions results in the essentially quantitative formation of 2,3-diboratabutadiene **2** (**Scheme 2**). The liberated Me_2NH initially coordinates to the lithium counter cations but is readily removed by repeated washing with Et_2O. The ^{11}B-NMR chemical shift at δ = 58.1 ppm is very close to those of previously reported diboratabutadienes.[16–18] The phenyl-substituted **2** is isolated from a concentrated Et_2O/toluene solution at −23 °C as yellow crystals in 79% yield. X-ray diffraction on a single crystal revealed the structure of **2** as a contact ion pair with the lithium counter cations canted away from above and below the planar CBBC motif to enable contacts to one B═C bond each (**Figure 1**). Li1 is thus coordinated by B1═C1 (C1-Li1 2.164(3), B1-Li1 2.438(3) Å) and Li2 by B2═C2 (C2-Li2 2.162(3), B2-Li2 2.432(3) Å). The coordination sphere of the lithium cations is completed by the respective distal boron atom and its pending duryl *ipso*-carbon as well as one equivalent of Et_2O each. While the B═C bond lengths are in the typical double bond range (B1-C1 1.476(2), B2-C2 1.479(2) Å), the B—B bond is slightly longer (B1-B2 1.749(2) Å) compared to a single bond, presumably due to Coulomb repulsion of the formally negatively charged boron atoms.[33]

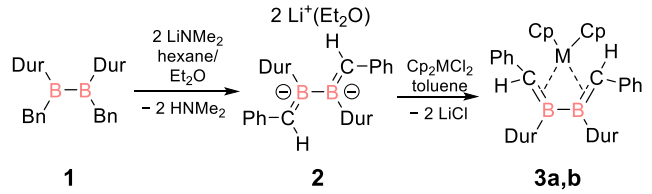

Scheme 2. Conversion of diborane (4) **1** via dilithium 2,3-diboratabutadiene **2** to the corresponding metal complexes **3a, b** (Dur = duryl = 2,3,5,6-tetramethylphenyl, Bn = benzyl; **3a**: M = Zr, **3b**: M = Hf).

In contrast to the *s-cis* geometry of the silyl-substituted diboratabutadiene reported by Berndt et al.,[17] the phenyl-derivative **2** adopts an *s-trans* geometry with both phenyl groups almost coplanar with the butadiene unit (dihedral angles Ph-*ortho*-C-*ipso*-C—C═B: 22.1°, 21.6°). The thus extended conjugation path exerts a considerable effect on the longest wavelength absorption in the UV/Vis spectrum of **2** at λ_{max} = 395 nm, red-shifted by $\Delta\lambda$ = 80 nm from that of non-arylated diboratabutadiene **Ic**[17] (recorded for comparison, see Figure S7, Supporting Information). The only reported examples of formal group 4 borataalkene complexes are based on cyclopentadienyl ligands with pending boryl groups, which reportedly do not show any interaction with the metal centers.[34–36] Therefore—although titanium, zirconium, and hafnium complexes with carbon-based olefins have long been used as catalysts for Ziegler–Natta polymerization[37–39]—"real" borataalkene coordination to Group 4 metals remains elusive (excepting boratabenzenes complexes with reduced B—C bond order).[40–42]

With the 2,3-diboratabutadiene **2** at hand, we became curious whether the proximity of the central B—B bond to the two anionic α-carbon atoms may allow for authentic butadiene-like coordination modes. Indeed, the addition of one equivalent of Cp_2ZrCl_2 to a solution of **2** in toluene results in a color change from yellow to red in the course of 18 h. After workup, the diboratabutadiene complex **3a** is obtained as red crystals in 64% yield (Scheme 2). The corresponding reaction of Cp_2HfCl_2 in thf/toluene solution requires 5 days for full conversion and the hafnocene complex **3b** is obtained as orange crystals from toluene in 57% yield (see SI). Reactions of **2** with Cp_2TiCl_2 under the same conditions seem to be adversely affected by competing redox reactions and did not result in analogous complexes.

The ^{11}B-NMR signals of both complexes (**3a**: 73.5 ppm, **3b**: 75.5 ppm) are shifted downfield compared to that of the precursor, 2,3-diboratabutadiene **2** (δ = 58.1 ppm), but upfield compared to donor-free diborane (4) **1** (δ = 100.0 ppm). This suggests the retention of considerable B═C double bond character, which is in line with the description of **3** as a π-complex with little backdonation from the Group 4 metals in contrast to a hypothetical diborametallacyclopentane[19,20] bonding situation that would require strong backdonation according to the Dewar–Chatt–Duncanson model, an unlikely yet not impossible situation for a formal d^0 transition metal center.[5–8] This interpretation is further supported by the ^{13}C-NMR signals of the formally anionic carbon centers (**3a**: 90.4 ppm **3b**: 89.7 ppm) in the typical range of borataalkenes, only slightly shielded compared to that of the lithium precursor **2** (δ = 95.4 ppm).

Research Article
doi.org/10.1002/ceur.202500153

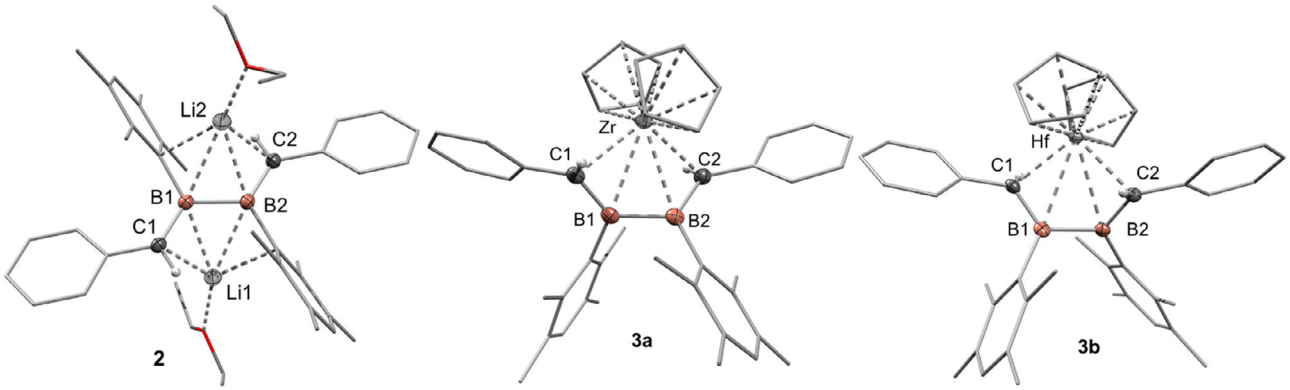

Figure 1. Molecular structure of dilithium 2,3-diboratabutadiene **2** and the corresponding group 4 complexes **3a** and **3b** in the solid state. Thermal ellipsoids at 50% probability. Selected bond lengths [Å] and angles [°]: **2**: B1-B2 1.749(2), B1-C1 1.476(2), B2-C2 1.479(2), C1-Li1 2.164(3), B1-Li1 2.438(3), B2-Li2 2.562(3), C2-Li2 2.162(3), B2-Li2 2.432(3); B2-Li1 2.543(3), Σ◁C1 359.4, Σ◁C2 359.4, C1-B1-B2-C2 177.4; **3a**: B1-B2 1.777(2), B1-C1 1.531(2), B2-C2 1.503(2), C1-Zr 2.354(3), C2-Zr 2.358(3) B1-Zr 2.728(3), B2-Zr 2.733(3), Σ◁C1 353.4, Σ◁C2 353.1, C1-B1-B2-C2 63.1; **3b**: B1-B2 1.750(2), B1-C1 1.523(2), B2-C2 1.535(2), C1-Hf 2.324(2), C2-Hf 2.340(2), B1-Hf 2.813(2), B2-Hf 2.800(3), Σ◁C1 348.0, Σ◁C2 351.0, C1-B1-B2-C2 61.3.[32]

The solid state structures of complexes **3a, b** determined by X-ray diffraction on single crystals confirm the description as butadiene-type ligand systems in both cases. The B—C bond lengths in the metallocene complexes are slightly longer than in precursor **2** (**3a**: B1-C1 1.531(2), B2-C2 1.503(2) Å; **3b**: B1-C1 1.523(2), B2-C2 1.535(2) Å; 2: B1-C1 1.476(2), B2-C2 1.479(2) Å) but still within the B═C double bond range. Notably, the B—B bond length (**3a**: B1-B2 1.777(2) Å; **3b**: B1-B2 1.750(2) Å) is slightly increased despite an anticipated lower charge density at the boron centers compared to **2** (B1-B2 1.749(2) Å) (vide infra). The C—M bonds (**3a**: C1-Zr 2.354(3), C2-Zr 2.358(3) Å; **3b**: C1-Hf 2.324(2), C2-Hf 2.340(2) Å) are significantly shorter than the B—M bonds (**3a**: B1-Zr 2.728(3), B2-Zr 2.733(3) Å; **3b**: B1-Hf 2.813(2), B2-Hf 2.800(3) Å) even when considering the larger van-der-Waals radius of boron.[43–45] Nonetheless, the B—Zr bond lengths are reminiscent of those of reported boratabenzene complexes.[40–42] Compared to the all-carbon zirconocene complexes the C—M bonds are shorter than in reported s-*trans* complex (2.45–2.50 Å)[46,47] and slightly longer than in an s–*cis* complex (2.300 Å) reported by Erker.[48] The sum of angles around the carbon centers (excluding the metal centers M) suggests an approximate sp^2-hybridization rather than sp^3 (**3a**: Σ◁C1 353.4, Σ◁C2 353.1°; **3b**: Σ◁C1 348.0, Σ◁C2 351.0°) underpinning the portrayal as π-complexes. The two B═C moieties in butadiene complex **3a** are twisted by 63.1° (**3b**: 61.3°), which—remarkably—is about equidistant from the values in known s-*trans* and s-*cis* configurations of all-carbon butadiene zirconocenes.[46–48] Complexes **3a** and **3b** are thus best described as s-*gauche* diboratabutadiene π-complexes. As in the reported butadiene s-*trans* complexes,[47,48] diboratabutadiene complexes **3a, b** feature a C_2 rotational axis, which is confirmed by the occurrence of single ^1H and ^{13}C NMR signals for the two Cp-moieties (see SI). A hypothetical s-*cis* coordination mode would result in lower symmetry and thus two signals each.

To rationalize the unprecedented intermediate bonding situation, we carried out DFT computations at the B3LYP/def2tzvpp level of theory. The second highest occupied molecular orbital (HOMO − 1) of the optimized structure $\mathbf{3a_{opt}}$ is composed of the B═C π-bond in noticeable bonding combination with a d-orbital at Zr. The strongest interaction between the ligand and the Zr center, however, is identified in the HOMO of $\mathbf{3a_{opt}}$, which reflects the donation by the BC π-system (predominantly but not exclusively located at C) and the vacant d_z^2-orbital at zirconium. The considerable antibonding character between the boron atoms caused by the twisting of the π-bonds is presumably responsible for the increased B—B bond length compared to **2**.

The lowest unoccupied molecular orbital (LUMO) is dominated by another mostly antibonding π^*-component at the B—B bond in destructive interference with a vacant d-orbital at Zr. The occupied frontier orbitals of the hafnocene complex $\mathbf{3b_{opt}}$ are very similar to those of $\mathbf{3a_{opt}}$ (**Figure 2**). The LUMO in this case, however, shows the bonding combination of the vacant p-orbitals at boron and a vacant d-orbital at zirconium while LUMO + 1 of $\mathbf{3b_{opt}}$ reflects an essentially identical orbital combination as the LUMO of $\mathbf{3a_{opt}}$ (see SI). The longest wavelength absorption in the experimental UV/Vis spectrum (see SI) for **3a** is observed as a very broad band of medium intensity at $\lambda_{max} = 460$ nm

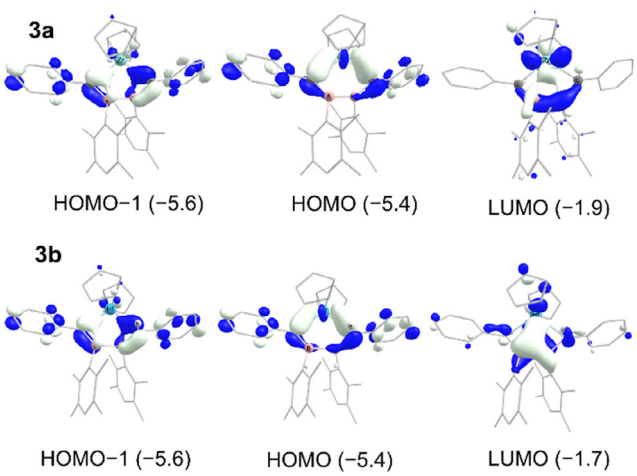

Figure 2. Selected frontier orbitals of diboratabutadiene complexes **3a** and **3b** (energy in eV, contour value = 0.05).

Research Article
doi.org/10.1002/ceur.202500153

($\varepsilon = 4255\ M^{-1}\ cm^{-1}$) tailing to around 550 nm. The TD-DFT calculated $\lambda_{max} = 443$ nm for the HOMO → LUMO transition matches the experimental value reasonably well. The calculated HOMO → LUMO gap for **3a$_{opt}$** is 2.80 eV and thus slightly smaller than for compound **3b$_{opt}$** (2.97 eV) due to the energetically lower LUMO of **3a$_{opt}$** (Figure 2). The longest wavelength absorption in the experimental UV/Vis spectrum for **3b** is observed at $\lambda_{max} = 415$ nm in excellent agreement with the calculated $\lambda_{max} = 417$ nm for the HOMO → LUMO transition (see SI).

2.1. Donor-Induced B—B Bond Cleavage

B—B bonds can be activated by the coordination of n-donors, which can cause the bond to be cleaved either homolytically or heterolytically yielding borates,[49] boryl radicals,[50] borane radical anions[51] or transient boryl anions,[52] and borylenes.[53] Prompted by the B—B antibonding nature of the LUMO of **3a**, we thus probed the behavior of **3a** toward an NHC.

The addition of two equivalents of 1,3,4,5-tetramethylimidazol-2-ylidene (IMe) to **3a** in thf (**Scheme 3**) resulted in the darkening of the red solution within 3 h and the formation of three new products according to ^{1}H and ^{11}B-NMR monitoring. In the crude mixture, three sets of two singlets each for the *ortho* and *meta*-CH_3 groups of the duryl substituent match the intensity of IMe methyl signals and thus confirm the presence of three distinct products. Interestingly, no signals in the ^{1}H-NMR spectrum could be assigned to the Cp hydrogen atoms of a necessarily formed zirconocene byproduct, which therefore might be paramagnetic in nature. The ^{11}B-NMR of the mixture shows one broad signal at $\delta = 26.3$ ppm and one doublet at $\delta = -16.5$ ($^{1}J_{BH} = 85$ Hz) ppm indicative of a directly B-bonded H atom. After workup (see SI) of the crude mixture colorless crystals were isolated from a thf/hexane mixture. X-ray diffraction on a single crystal confirms the formation of methyleneborane/IMe adduct *Z*-**4** (**Figure 3**) the formal product of the NHC-promoted B—B bond oxidation of the diboratabutadiene ligand.

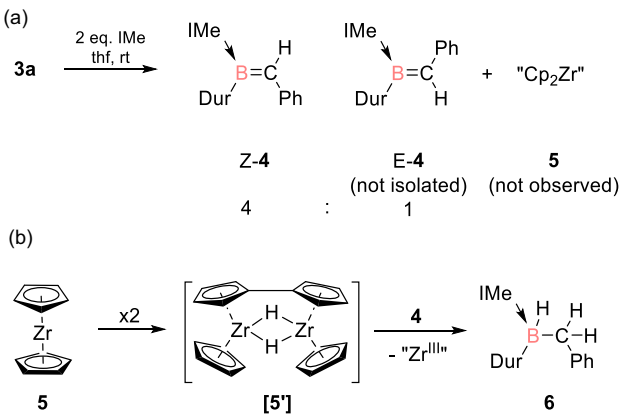

Scheme 3. a) Formation of methyleneboranes *Z*-**4** and *E*-**4** and zirconocene **5** from diboratabutadiene complex **3b** and NHC; b) hydrogenation of methyleneboranes **4** with "Cp_2Zr" **5** via dimeric [**5′**] to give benzylborane **6** (IMe = 1,3,4,5-tetramethylimidazol-2-ylidene; Dur = duryl = 2,3,5,6-tetramethylphenyl).

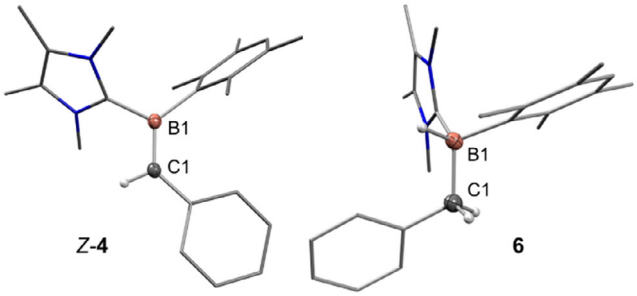

Figure 3. Molecular structure of methyleneborane/NHC adduct *Z*-**4** and borane/NHC adduct **6** in the solid state. Thermal ellipsoids at 50% probability. Selected bond lengths [Å]: *Z*-**4**: B1-C1 1.457(2), Σ◁C1 360.0, **6**: B1-C1 1.638(2).

The short B—C bond (B1-C1 1.457(2) Å) and the sum of angles around C1 of 360.0° confirm the presence of a B═C double bond. The ^{11}B-NMR chemical shift of *Z*-**4** at $\delta = 26.3$ ppm is in range for donor-stabilized methyleneboranes, albeit slightly shielded compared to recent examples.[52] After subsequent workup of the mother liquor (see SI), another fraction of colorless crystals is obtained. The crystal structure confirms the formation of the NHC adduct of saturated borane **6** and thus the hydrogenation product of methyleneboranes **4**. The ^{11}B-NMR shows the aforementioned doublet at $\delta = -16.5$ ($^{1}J_{BH} = 85$ Hz) ppm confirming the presence of a hydrogen atom at the boron center. The same coupling constant is also observed in ^{1}H-NMR as a very broad quartet (SI). The remaining set of signals in the ^{1}H-NMR of the crude mixture is tentatively assigned to *E*-**4** (Scheme 3), due to its similarity with the data of *Z*-**4** (Z:E ratio: 4:1). The ^{11}B-NMR signal of *E*-**4** can reasonably be expected to be very similar to that of *Z*-**4** and is therefore probably concealed in the ^{11}B-NMR spectrum of the crude. In contrast, the addition of 10 equivalents of IMe to diboratabutadiene **2** does only slightly change the multinuclear NMR data suggesting simple replacement of the coordinated Et_2O at the lithium counter cations of **2**.

The postulated systematic by-product of the B—B bond oxidation is the reduction product of the zirconium center of **3a** to result in the transient zirconocene 'Cp_2Zr' fragment **5**. Such unstable group 4 metallocenes are known to form a hydrogen-bridged dimer upon C—H activation of the Cp ring, capable of hydrogenating various multiple bonds.[54–60] It is therefore safe to assume that methyleneborane was hydrogenated by an undetected dimer of type [**5′**] (Scheme 3). The transition metal fragment itself is oxidized to an unknown species in the course of this hydrogenation, which is confirmed by the appearance of a sextet in the EPR spectrum, consistent with a paramagnetic Zr (III) species (see SI). The addition of two equivalents of IMe to the hafnium complex **3b** in thf resulted in the same product mixture as for **3a** according to ^{1}H and ^{11}B-NMR spectra.

3. Conclusion

In conclusion, we reported the straightforward synthesis of the first perarylated 2,3-diboratabutadiene dianion in two steps as

Research Article
doi.org/10.1002/ceur.202500153

its lithium salt from a readily available diborane (4) precursor. The limited steric strain not only allows for the coplanarity of the phenyl substituents and thus extended conjugation, it also provides access to the first transition metal complexes of 2,3-diboratabutadienes: the reactions with Cp_2MCl_2 (M = Zr, Hf) afford complexes of considerable π-character with unique coordination s-*gauche* modes in between the well-known s-*cis* and s-*trans* modes of the corresponding carbon-based butadienes. The B—B bond of the Zr complex is oxidatively cleaved by the addition of IMe under liberation of the transient '$ZrCp_2$' fragment, resulting in E/Z-isomers of the corresponding NHC-coordinated methyleneboranes. The transient '$ZrCp_2$' likely forms a hydride-bridged dimer that subsequently hydrogenates methyleneboranes to give the corresponding saturated borane and a paramagnetic Zr (III) species.

Acknowledgements

The authors thank Prof. Stella Stopkowicz for access to their computational clusters, Dr. Michael Zimmer for helping with VT-NMR measurements, and Susanne Harling for the elemental analysis. The authors acknowledge the Service Center X-ray Diffraction established with financial support from Saarland University and the Deutsche Forschungsgemeinschaft (INST256/506-1 and 256/582-1).

Conflict of Interest

The authors declare no conflict of interest.

Data Availability Statement

The data that support the findings of this study are available in the supplementary material of this article.

Keywords: boron · butadiene · coordination chemistry · N-heterocyclic carbenes · transition metal

[1] L. B. Hunt, *Platinum Met. Rev.* **1984**, *28*, 76.
[2] M. J. S. Dewar, *Bull. Soc. Chim. Fr.* **1951**, *48*, 112.
[3] J. Chatt, L. A. Duncanson, *J. Chem. Soc.* **1953**, 2939.
[4] J. Chatt, L. A. Duncanson, L. M. Venanzi, *J. Chem. Soc.* **1955**, 4456.
[5] C. Chen, *Nat. Rev. Chem.* **2018**, *2*, 6.
[6] S. Mecking, *Angew. Chem., Int. Ed.* **2001**, *40*, 534.
[7] H. H. Brintzinger, D. Fischer, R. Mülhaupt, B. Rieger, R. M. Waymouth, *Angew. Chem., Int. Ed., Engl.* **1995**, *34*, 1143.
[8] M. Stürzel, S. Mihan, R. Mülhaupt, *Chem. Rev.* **2016**, *116*, 1398.
[9] A. M. Canfield, D. Rodina, S. M. Paradine, *Angew. Chem., Int. Ed.* **2024**, *63*, e202401550.
[10] S. K.-H. Thiele, D. R. Wilson, *J. Macromol. Sci. Part C Polym. Rev.* **2003**, *43*, 581.
[11] G. Ricci, G. Leone, *Polyolefins J.* **2014**, *1*, 43.
[12] H. Reihlen, A. Gruhl, G. v Heßling, O. Pfrengle, *Justuts Liebigs An. Chem.* **1930**, *482*, 161.
[13] G. Erker, G. Kehr, R. Fröhlich, *J. Organomet. Chem.* **2004**, *689*, 4305.
[14] G. Erker, G. Kehr, R. Fröhlich, *J. Organomet. Chem.* **2005**, *690*, 6254.
[15] M. Eaton, Y. Zhang, S.-Y. Liu, *Chem. Soc. Rev.* **2024**, *53*, 1915.
[16] M. Pilz, J. Allwohn, P. Willershausen, W. Massa, A. Berndt, *Angew. Chem., Int. Ed., Engl.* **1990**, *29*, 1030.
[17] D. Scheschkewitz, A. Ghaffari, P. Amseis, M. Unverzagt, G. Subramanian, M. Hofmann, P. v. R. Schleyer, H. F. Schaefer III, G. Geiseler, W. Massa, A. Berndt, *Angew. Chem., Int. Ed.* **2000**, *39*, 1272.
[18] R. Littger, N. Metzler, H. Nöth, M. Wagner, *Chem. Ber.* **1994**, *127*, 1901.
[19] D. Scheschkewitz, M. Hofmann, A. Ghaffari, P. Amseis, C. Präsang, W. Mesbah, G. Geiseler, W. Massa, A. Berndt, *J. Organomet. Chem.* **2002**, *646*, 262.
[20] C. Präsang, P. Amseis, D. Scheschkewitz, G. Geiseler, W. Massa, M. Hofmann, A. Berndt, *Angew. Chem., Int. Ed.* **2006**, *45*, 6745.
[21] G. Gabbert, W. Weinmann, H. Pritzkow, W. Siebert, *Angew. Chem., Int. Ed., Engl.* **1992**, *31*, 1603.
[22] C. Chen, C. G. Daniliuc, G. Kehr, G. Erker, *J. Am. Chem. Soc.* **2021**, *143*, 21312.
[23] H. Braunschweig, Q. Ye, K. Radacki, A. Damme, *Angew. Chem., Int. Ed.* **2012**, *51*, 7839.
[24] A. Hermann, F. Fantuzzi, M. Arrowsmith, T. Zorn, I. Krummenacher, B. Ritschel, K. Radacki, B. Engels, H. Braunschweig, *Angew. Chem., Int. Ed.* **2020**, *59*, 15717.
[25] R. A. Thornton, B. M. Lindley, *Organometallics* **2023**, *42*, 1454.
[26] H. Hommer, H. Nöth, J. Knizek, W. Ponikwar, H. Schwenk-Kircher, *Eur. J. Inorg. Chem.* **1998**, *10*, 1519.
[27] P. Grewelinger, T. Wiesmeier, B. Morgenstern, C. Präsang, D. Scheschkewitz, *Angew. Chem., Int. Ed.* **2023**, *62*, e202308678.
[28] J. Möbus, G. Kehr, C. G. Daniliuc, R. Fröhlich, G. Erker, *Dalton Trans.* **2014**, *43*, 632.
[29] H. Klusik, A. Berndt, *Angew. Chem., Int. Ed., Engl.* **1983**, *22*, 877.
[30] A. B. Buenca, E. Fernandez, *Chem. Soc. Rev.* **2021**, *50*, 72.
[31] R. J. Maza, J. J. Carbo, E. Fernandez, *Adv. Synth. Catal.* **2021**, *363*, 2274.
[32] *Deposition numbers 2443028 (for 1), 2443035 (for 2), 2443036 (for 3a), 2443038 (for 3b) 2443039 (for Z-4) and 2443043 (for 6) contain the supplementary crystallographic data for this paper. These data are provided free of charge by the joint Cambridge Crystallographic Data Centre and Fachinformationszentrum Karlsruhe Access Structures service.*
[33] A. Berndt, *Angew. Chem., Int. Ed., Engl.* **1993**, *32*, 985.
[34] S. Kohrt, G. Kehr, G. C. Daniliuc, R. S. Rojas, B. Rieger, C. Troll, G. Erker, *Organometallics* **2016**, *35*, 2689.
[35] M. T. Reetz, H. Brümmer, M. Kessler, J. Kuhnigk, *Chimia*, **1995**, *49*, 501.
[36] S. Duchateau, S. J. Lancaster, M. Thornton-Pett, M. Bochmann, *Organometallics* **1997**, *16*, 4995.
[37] H. A. Alt, A. Köppl, *Chem. Rev.* **2000**, *100*, 1205.
[38] S. L. Buchwald, R. B. Nielsen, *Chem. Rev.* **1988**, *88*, 1047.
[39] P. C. Möhring, N. J. Coville, *J. Organomet. Chem.* **1994**, *479*, 1.
[40] A. J. Ashe III, S. Al-Ahmad, X. Fang, J. W. Kampf, *Organometallics* **2001**, *20*, 468.
[41] X. Wang, W. Peng, P. Cui, X. Leng, W. Xia, Y. Chen, *Organometallics* **2013**, *32*, 6166.
[42] A. Glöckner, P. Cui, Y. Chen, C. G. Daniliuc, P. G. Jones, M. Tamm, *New J. Chem.* **2012**, *36*, 1392.
[43] P. Pyykkö, S. Riedel, M. Patzschke, *Chem. Eur. J.* **2005**, *11*, 3511.
[44] P. Pyykkö, *J. Phys. Chem. A.* **2015**, *119*, 2326.
[45] P. Pyykkö, M. Atsumi, *Chem. Eur. J.* **2009**, *15*, 12770.
[46] M. Dahlmann, G. Erker, R. Fröhlich, O. Meyer, *Organometallics* **1999**, *18*, 4459.
[47] Y. Kai, N. Kanehisa, K. Miki, N. Kasai, K. Mashima, K. Nagasuna, H. Yasuda, A. Nakamura, *J. Chem. Soc., Chem. Commun.* **1982**, 191.
[48] G. Erker, J. Wicher, K. Engel, F. Rosenfeldt, W. Dietrich, C. Krüger, *J. Am. Chem. Soc.* **1980**, *102*, 6344.
[49] S. Bairagi, S. Giri, G. Joshi, E. D. Jemmis, S. Ghosh, *Angew. Chem., Int. Ed.* **2025**, *64*, e202417170.
[50] L. Kuehn, L. Zapf, L. Werner, M. Stang, S. Würtemberger-Pietsch, I. Krummenacher, H. Braunschweig, E. Lacote, T. B. Marder, U. Radius, *Chem. Sci.* **2022**, *13*, 8321.
[51] S. Li, F. Shiri, G. Xu, S.-M. Yiu, H. K. Lee, T. H. Ng, Z. Lin, Z. Lu, *J. Am. Chem. Soc.* **2024**, *146*, 17348.
[52] A. Bonet, C. Pubill-Ulldemolins, C. Bo, H. Gulyas, E. Fernandez, *Angew. Chem., Int. Ed.* **2011**, *50*, 7158.
[53] M. Shimoi, S. Ikubo, Y. Kawano, K. Katoh, H. Ogino, *J. Am. Chem. Soc.* **1998**, *120*, 4222.

Research Article
doi.org/10.1002/ceur.202500153

[54] X. Jie, C. Chen, C. G. Daniliuc, G. Kehr, G. Erker, *Angew. Chem., Int. Ed.* **2023**, *62*, e202214700.
[55] H. Brintzinger, J. E. Bercaw, *J. Am. Chem. Soc.* **1970**, *92*, 6182.
[56] B. N. Strunin, M. K. Minacheva, P. V. Petrovskii, V. B. Shur, *Russ. Chem. Bull.* **1996**, *45*, 2259.
[57] U. Rosenthal, A. Ohff, M. Michalik, H. Görls, V. V. Burlakov, V. B. Shur, *Angew. Chem., Int. Ed., Engl.* **1993**, *32*, 1193.
[58] S. Fortier, A. Gomez-Torres, *Chem. Commun.* **2021**, *57*, 10292.
[59] A. M. May, J. L. Dempsey, *Chem. Sci.* **2024**, *15*, 6661.
[60] H. C. London, T. J. Whittemore, A. G. Gale, C. D. McMillen, D. Y. Pritchett, A. R. Myers, H. D. Thomas, G. C. S. P. S. Wagenknecht, *Inorg. Chem.* **2021**, *60*, 14399.

Manuscript received: May 6, 2025
Revised manuscript received: June 13, 2025
Version of record online:

4 Summary, Outlook and Conclusion

Previously reported neutral and anionic three-membered B_2C rings suffered from either complicated access, low yields, or insufficient scope (see Chapter 1.2.2.1). The first part of this thesis therefore addressed the development of a straightforward and high-yielding route to non-classical diboriranes and diboriranides. Starting from a readily available 1,2-dichloro-1,2-diduryldiborane(4) (see Chapter 1.1.1), 1-benzyl-2-chloro-1,2-diduryldiborane(4) **77** was obtained in virtually quantitative yield by the addition of one equivalent of benzyl magnesium chloride and was fully characterized. With the bulky base lithium tetramethylpiperidide (LiTMP), deprotonation of **77** in benzylic position was achieved (Scheme 36). The plausibly generated, yet unobserved benzylic anion nucleophilically attacks the β-boron atom and results in rapid ring closure to give the first perarylated non-classical diborirane **55e** in 85% yield. According to x-ray diffraction on a single crystal, the phenyl group at the ring carbon atom is coplanar with the B_2C plane thus allowing for extended π-conjugation. In the future, the incorporation of non-classical diborirane motifs into extended π-systems could be made possible through the synthesis of *para*-functionalized derivatives.

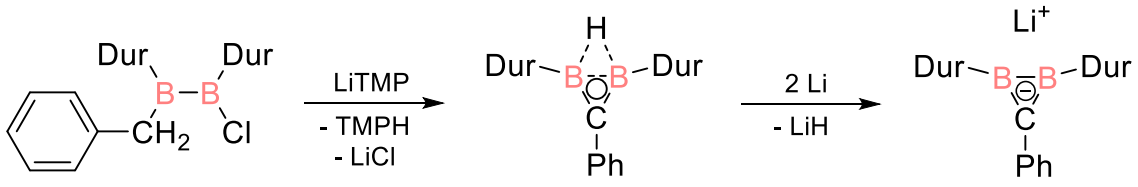

77 **55e** **64c**

Scheme 36. Synthesis of non-classical diborirane **55e** from 1-benzyl-2-chloro-1,2-diduryldiborane(4) **77** and consecutive reductive hydride elimination of **55e** to diboriranide **64c**.

In adaption of the protocol by Berndt and coworkers,[143] the addition of an excess of lithium powder to a solution of diborirane **55e** in diethyl ether leads to the formation of diboriranide **64c** (Scheme 36), which was isolated in 60% yield by crystallization. Single crystal x-ray diffraction revealed the side-on coordination of the lithium counter cation in the B_2C plane. DFT calculations at the B3LYP/def2tzvpp level of theory suggest that the σ-donation from the B_2C ligand to the lithium cation represents the

HOMO of diboriranide **64c**. In view of the in-plane σ-bridge, retaining 2e⁻ Hückel aromaticity in non-classical diboriranes, the possibility of similar coordination modes for different metal complexes of diboriranides was anticipated.

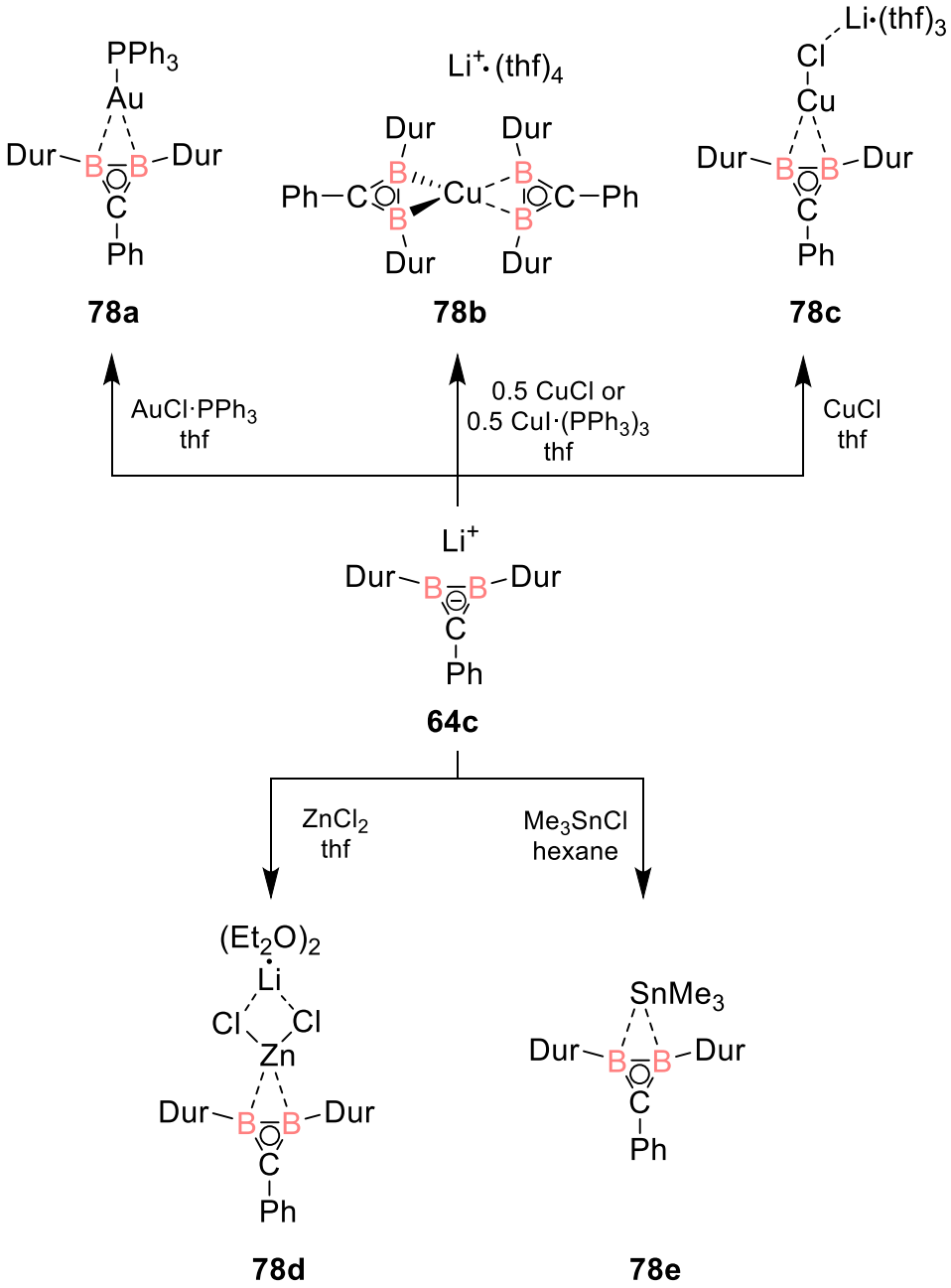

Scheme 37. Synthesis of diboriranide metal complexes **78a-e** from lithium diboriranide **64c**.

The addition of diboriranide **64c** to representative p- and d-block metal chlorides results in the formation of metal diboriranides **78a-e** (Scheme 37). X-ray diffraction studies revealed the presence of the B_2C ring structure with the metals indeed bonded in the same plane. In case of tin-bridged diborirane, the parameters obtained by the x-ray

diffraction indicate a contribution of methyleneborane resonance structure **78e'** presumably to avoid unfavourable penta-coordination of tin (Scheme 38). The difference in the B−B bond lengths in the reported metal complexes is apparently a measure for the σ-donation to the metal fragment. The B-B bond length of the gold complex **78a** (1.809(4) Å) is considerably longer than that for Cu and Zn complexes **78c** (1.728(4) Å) and **78d** (1.719(4) Å), possibly also due to steric effects.

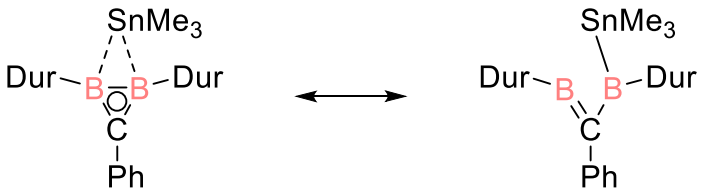

78e **78e'**

Scheme 38. Me_3Sn-bridged diborirane **78e** and boryl-methyleneborane resonance structure **78e'**.

DFT calculations at the B3LYP/def2tzvpp level of theory suggest that the diboriranide binds to the p- and d-block metals in σ-coordination leaving the π-system mostly unperturbed. NBO calculations only show minor contributions of π-backdonation from the B_2C ligand to the metal while NICS calculations reveal aromatic ring currents, in all cases of comparable magnitude as in the isoelectronic cyclopropenium cation. While in the case of d-block metal-bridged complexes **78a-d** the HOMO is composed of the σ-donation to the metal (as in lithium diboriranide **64c**), the HOMO of Me_3Sn-bridged diboriranide **78e** is composed of the B_2C delocalized π-system (as in H-bridged diborirane **55e**).

Based on these considerations, both **55e** and **78e** were expected to be suitable as π-ligand for transition metals. Additionally, given that BH bonds are well-known to engage in agostic interactions with transition metals, coordination was expected to be further supported through the σ-electrons of the BHB bridge in **55e**. The general lack of cyclic B_2C moieties as π-ligands inspired the second major task of this thesis. The addition of $Fe_2(CO)_9$ to non-classical diborirane **55e** indeed results in the formation of the first diborirane derived π-complex **79** showing the anticipated coordination modes (Scheme 39).

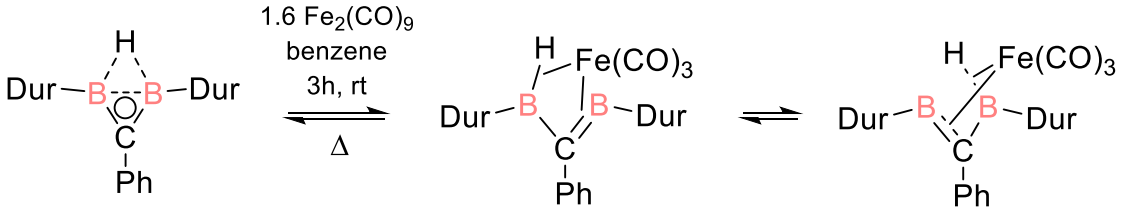

55e **79** **79'**

Scheme 39. Diborirane $Fe(CO)_3$ complex **79** derived from the addition of non-classical diborirane **55e** to 1.6 equivalents of $Fe_2(CO)_9$ in two allylic resonance structures **79** and **79'**.

X-ray diffraction on a single crystal shows that the $Fe(CO)_3$ coordination sphere is completed by the π-system of the B_2C moiety, while the BH bond donates σ-electrons to the iron center in an agostic interaction. Due to a comparatively small BCB angle (106.7(1)°), some residual, albeit weak, BB interaction was proposed for diborirane complex **79**. Multinuclear NMR spectra suggest a symmetric structure in solution. For example, the ^{11}B NMR spectrum of the diborirane complex **79** shows only one signal at δ = 68.4 ppm, whereas the ^{11}B SPE/MAS NMR detects two distinct signals (δ = 85.1 ppm and 50.6 ppm), as expected for two chemically different boron atoms in the solid state. Since the median of the two solid state shifts resembles the one observed in solution, fluxionality between resonance structures **79** and **79'** is the most plausible explanation for these findings.

In view of the boryl-methyleneborane nature of **55e** (see Chapter 2, Scheme 33), the ring expansion (hydroboration by B-H and attack of a Lewis basic center to B=C) with a small molecule such as carbon monoxide was tested. Coordination of the BH σ-bond as well as the B−C π-bond to iron in complex **79** could further facilitate the incorporation of small molecules.

In the presence of $Fe_2(CO)_9$, the formal hydroboration of carbon monoxide by non-classical diborirane **55e** indeed results in an η^5-coordinated five-membered B_2C_2O ligand **80**, coordinating $Fe(CO)_3$ (Scheme 40). Single crystal x-ray diffraction revealed an envelope conformation of the thus obtained five-membered cyclic ligand.

Due to the formally antiaromatic character of the ligand system, the backdonation from the iron center is particularly strong, formally turning the ligand into a 6π-system as can be seen e.g. in the IR stretching frequencies.

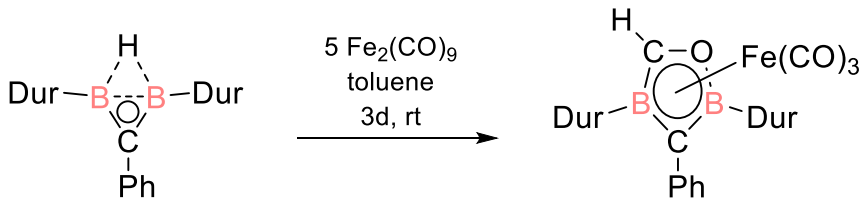

55e **80**

Scheme 40. Synthesis of five-membered $Fe(CO)_3$ complex **80** starting from non-classical diborirane **55e** after addition of five equivalents of $Fe_2(CO)_9$.

Treatment of $Fe_2(CO)_9$ with tin bridged diborirane **78e** results in the formal borastannylation of carbon monoxide in a ring expansion reaction to $Fe(CO)_3$ complexed diborete **81**. In contrast to the side-on insertion of CO into BHB diborirane **55e**, the carbonylative ring expansion of **78e** occurs in end-on fashion presumably as a result of the pronounced oxophilicity of tin. Due to the weaker B-Sn bond compared to B-H, no intermediate resembling complex **79** could be isolated. Nonetheless, the formation of diborete complex **81** could occur *via* an intermediate such as **82** (Scheme 41). The mechanistic considerations are supported by the optimization and energy comparison of potential alternative intermediates at the B3LYP/def2tzvpp level of theory.

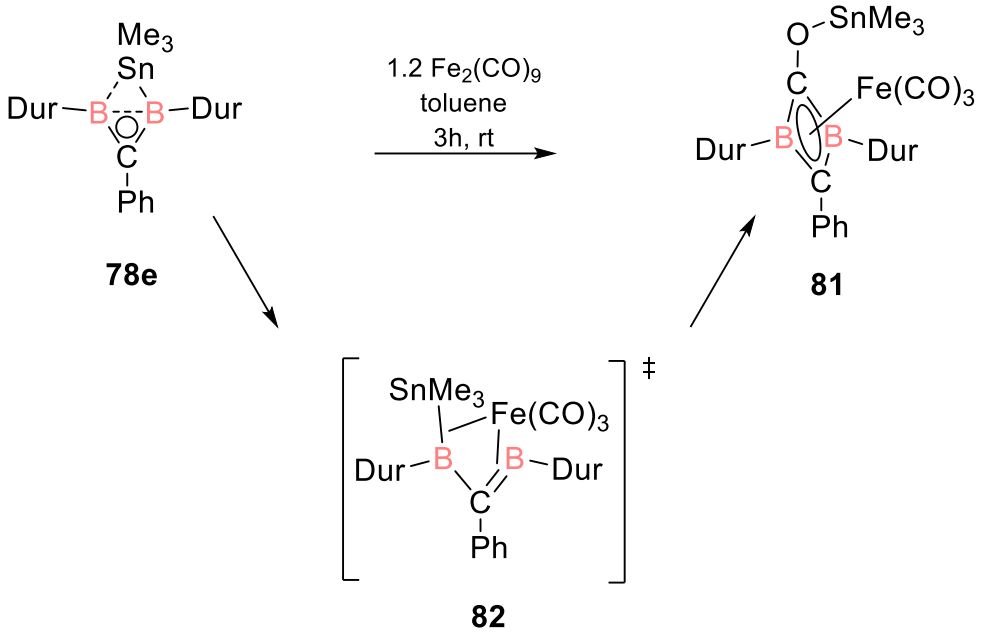

78e **81** **82**

Scheme 41. Synthesis of four-membered $Fe(CO)_3$ complex **81** starting from Me_3Sn bridged diborirane **78e** after addition of 1.2 equivalents of $Fe_2(CO)_9$ *via* transient diborirane complex **82**.

The formally 2π aromatic nature of 1,3-diborete in **81** results in little backdonation from the iron center to the ligand (in contrast to **80**): For the oxygen bearing ring carbon, the ^{13}C NMR signal of the now endocyclic CO moiety is significantly more deshielded (δ = 257.7 ppm) than the CO ligands in $Fe(CO)_3$ (δ = 211.6 ppm).
With these findings, the first examples of the employment of cyclic B_2C moieties as π- and σ-ligands for different metals were disclosed. Furthermore, the fundamental possibility of non-classical diborirane **55e** to activate small molecules like carbon monoxide, albeit in the coordination sphere of an iron species, was demonstrated. In sight of this proof-of concept, various heteroatom-containing multiple bonds might be considered as a next step to either react with the non-classical diborirane **55e** or its iron complex **79**. Several new boron-containing heterocycles can thus be envisaged. Similarly, the formation of several B_2C-based metal complexes should be possible in adaption to the here reported procedures.

Metal complexes of conjugated olefins are known for over a century and have found vast application in catalysis. The boron-containing dianionic derivative of the simplest conjugated olefin, namely butadiene, with internal B-B bonds has been known for a long time as well. The corresponding transition metal complexes, however, remain conspicously absent. The steric cumbersome Me_3Si groups at the anionic carbon centers of diboratabutadiene **18c** (see Chapter 1.1.2) presumably hinder the attack of transition metal electrophiles and may favour electron or proton transfer instead. The synthesis of the first perarylated diboratabutadiene with less bulky phenyl substituents, was anticipated to overcome these problems and was thus defined as the third central target of this work. The required 1,2-dibenzyl-diborane(4) precursor **82** was synthesized from 1,2-diduryl-1,2-dichlorodiborane(4) and two equivalents of benzyl Grignard. Deprotonation in benzylic position using $LiNMe_2$ gives first perarylated diboratabutadiene **18d**, prepared in adaption to the protocol reported by Berndt and coworkers (Scheme 42). The diboratabutadiene **18d** crystallizes as a contact ion pair in s-*trans* geometry in contrast to the Me_3Si-derivative **18c** previously reported by Berndt *et al.* (s-*cis*).[84]

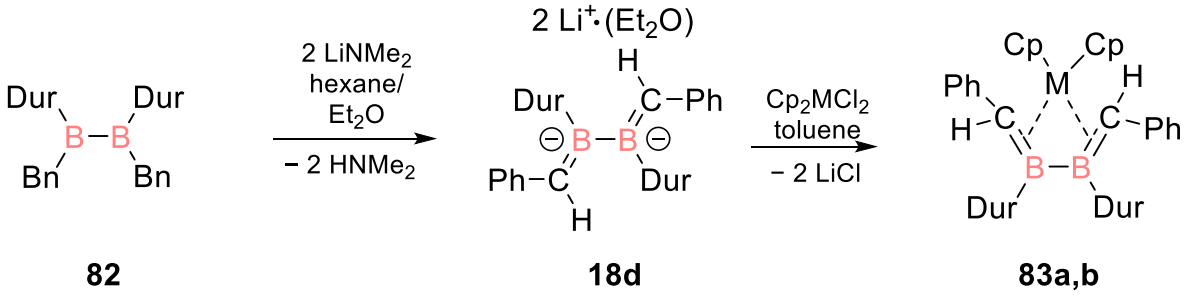

82 **18d** **83a,b**

Scheme 42. Synthesis of perarylated diboratabutadiene **18d** starting from 1,2-dibenzyl-1,2-diduryl-diborane(4) **82** and formation of butadiene metallocene complexes **83a** (M = Zr) and **83b** (M = Hf) from **18d** and Cp_2MCl_2.

The near-coplanarity of the phenyl substituents with the CBBC scaffold in **18d** results in extended conjugation as visualized by UV-Vis experiments and therefore suggests interesting options with regards to the construction of extended conjugated systems.

As anticipated on grounds of the lower steric demand of the phenyl groups, the treatment of diboratabutadiene **18d** with zirconocene- and hafnocene chlorides indeed gives rise to the first transition metal complexes of 2,3-diboratabutadienes **83a,b** with considerable ligand to metal π-interaction as elaborated with multinuclear NMR experiments, x-ray diffraction studies and DFT computations. Both complexes adapt an s-*gauche* geometry in between the well-known s-*cis* and s-*trans* geometries for reported all-carbon butadiene metallocene complexes.

The addition of two equivalents N-heterocyclic carbene to metal complexes **83** results in the oxidative cleavage of the B-B bond under formation of two E/Z isomers of NHC stabilized methyleneboranes **84** and transient metallocenes **85** (Scheme 43).

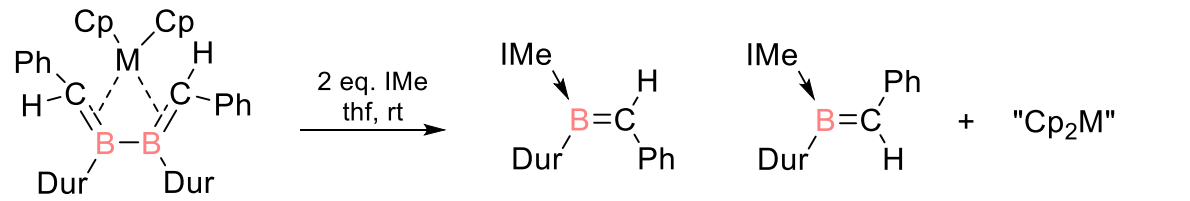

83a,b Z-**84** E-**84** (not isolated) **85a,b** (not observed)

4 : 1

Scheme 43. NHC induced oxidative bond cleavage of diboratabutadienes **83** to generate E/Z isomers of methyleneborane **84** under formation of transient metallocene **85** (**a**: M = Zr; **b**: M = Hf; IMe = 1,3,4,5-tetramethylimidazol-2-ylidene).

Transient metallocenes **85** presumably form hydrogen bridged dimeric metallocene species **[85']**, capable of hydrogenating the generated methyleneboranes **84** to benzyl borane **86** (Scheme 44).

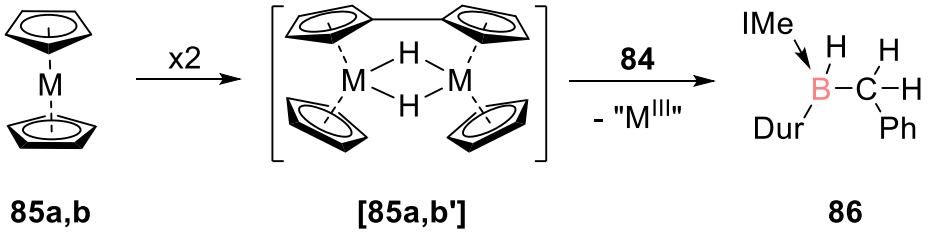

85a,b **[85a,b']** **86**

Scheme 44. Synthesis of benzyl borane **86** starting from metallocene **85** *via* hydrogen bridged dimer **[85']** (**a**: M = Zr; **b**: M = Hf; IMe = 1,3,4,5-tetramethylimidazol-2-ylidene).

With the reported work on the first 2,3-diboratabutadiene transition metal complexes, containing a B-B bond, a missing species in the emerging field of B=C ligands was disclosed including a notable first reactivity. The novel diboratabutadiene transition metal complexes **83** thus show susceptibility to redox reactions and as a logical next step could be further investigated in this regard. In this context, catalytic activity can be anticipated, e.g. in Ziegler-Natta polymerization or dehydrocoupling of main group hydrides of type R_nEH_m to (polymeric) compounds with E-E bonds.

5 Supporting Information

5.1 Diboriranide σ-Complexes of d- and p-Block Metals

Supporting Information

Diboriranide σ-Complexes of d- and p-Block Metals

*P. Grewelinger, T. Wiesmeier, C. Präsang, B. Morgenstern, D. Scheschkewitz**

WILEY-VCH

SUPPORTING INFORMATION

Table of Contents

SUPPORTING INFORMATION

1. Experimental Procedures

1.1. General considerations

All manipulations were carried out under a protective atmosphere of argon applying standard Schlenk or glovebox techniques. The glassware was pre-dried in oven at 125 °C and heated *in vacuo* prior to use. Solvents were dried and degassed by reflux over sodium/benzophenone under argon. [D_6]-benzene (C_6D_6) and [D_8]-thf (thf-d_8) were dried over potassium mirror and distilled under argon prior to use. 1,2-Dichloro-1,2-diduryldiborane(4) was prepared according to published procedures.[S1] All other chemicals were obtained commercially and used as received. The NMR spectra were recorded on a Bruker Avance III HD 400 spectrometer at 300 K (^{1}H: 400.13 MHz, ^{7}Li: 155.50 MHz, ^{11}B: 128.38 MHz, ^{13}C: 100.61 MHz, ^{31}P: 161.98 MHz, ^{119}Sn: 149.21 MHz). The VT-NMR spectra were recorded on a Bruker Avance III HD 300 spectrometer (^{13}C: 75.47 MHz). The ^{1}H and ^{13}C{^{1}H} NMR spectra were referenced to the residual proton and natural abundance ^{13}C resonances of the deuterated solvent and chemical shifts were reported relative to $SiMe_4$ (thf-d_8: δH = 3.58 ppm and δC = 67.21 ppm, C_6D_6: δH = 7.16 ppm and δC = 128.06 ppm, toluene-d_8: δC = 20.43 ppm).[S2] Following abbreviations were used for the multiplicities: s – singlet, d – doublet, t – triplet, m – multiplet. Melting points were determined under argon in NMR tubes and are uncorrected. The molten samples were examined by NMR spectroscopy to confirm whether decomposition had occurred upon melting. Elemental analyses were performed in triplicate for each sample using Leco CHN-900 analyzer and mean values are given below for each compound. Crystallographic data of the structures reported in this paper have been deposited with the Cambridge Crystallographic Data Centre, CCDC, 12 Union Road, Cambridge CB21EZ, UK. (Fax: +44-1223-336-033; E-Mail: deposit@ccdc.cam.ac.uk, http://www.ccdc.cam.ac.uk).

2. Synthetic methods and analytic data

2.1. Synthesis of 1-benzyl-2-chloro-1,2-diduryldiborane(4) 1

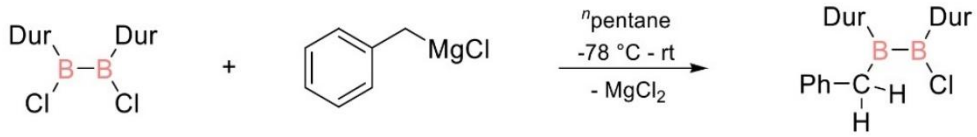

1

358.59 g/mol 150.89 g/mol 414.63 g/mol

1,2-Dichloro-1,2-diduryldiborane(4) **1** (2.45 g, 6.83 mmol) is dissolved in pentane (350 ml) and 6.8 mL of benzylmagnesium chloride solution in Et_2O[S3] (1 M, 6.8 ml, 6.8 mmol) added dropwise at −78 °C over a period of 15 min. The stirring mixture is slowly brought to room temperature overnight. The resulting suspension is filtered leading to a clear green solution, which is concentrated at reduced pressure. Storage at −20 °C overnight results in the precipitation of a pale green solid. The product is rinsed with minimum quantities of pentane and dried *in vacuo* to yield 2.58 g (6.22 mmol, 97%) of 1-benzyl-2-chloro-1,2-diduryldiborane(4) **1** as a colorless solid.

^{1}H NMR (400.13 MHz, C_6D_6, 300 K): δ = 1.85, 1.89, 1.90, 1.96 (each s, 6H, Dur-C$\underline{H}_3$), 3.51 (s, 2H, Ph-C$\underline{H}_2$), 6.71, 6.80 (each s, 1H, Dur-H), 6.91-6.96 (m, 1H, *p*-Ph-H), 7.01-7.04 (m, 4H, *o/m*-Ph-H) ppm. **^{11}B NMR** (128.38 MHz, C_6D_6, 300 K): δ = 93.2, 89.1 (each br s) ppm. **^{13}C NMR**: (100.61 MHz, C_6D_6, 300 K): δ =18.9, 19.0, 19.3, 19.8 (each s, Dur-$\underline{C}H_3$), 41.1 (br s, Ph-$\underline{C}H_2$), 125.3, 128.4, 129.3, 129.9, 131.1, 131.6, 132.3, 133.6, 134.0 (each s, Dur-C and Ph-C), 139.6 (br s, *ipso*-Dur-C). **Elemental analysis:** Calcd. for ($C_{27}H_{33}B_2Cl$): C, 78.2; H, 8.0. Found: C, 72.1; H, 6.4.

2.2. Synthesis of 1-phenyl-2,3-diduryldiborirane 2

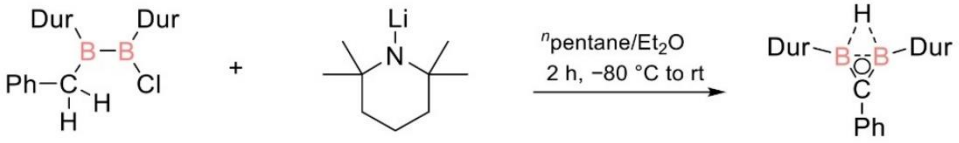

1 **2**

414.63 g/mol 147.22 g/mol 376.16 g/mol

At −80 °C, a solution of 2.58 g (6.22 mmol) of 1-benzyl-2-chloro-1,2-diduryldiborane(4) **1** in 15 mL of Et_2O (15 ml) is added dropwise to a suspension of 0.911 g (6.19 mmol) of lithium tetramethylpiperidide 30 mL of pentane during 10 min. After 2 h of stirring the reaction mixture

is warmed to room temperature, filtered and dried *in vacuo* affording a pale-yellow solid, which is rinsed with minimum quantities of hexane in order to remove tetramethylpiperidine. The solid is redissolved in 40 mL of toluene, filtered and concentrated to approx. 8 mL at reduced pressure. Storing the solution at −23 °C, yields 1.989 g (5.59 mmol, 85%) of colorless crystals of **2** obtained in two to three fractions.

^{1}H NMR (400.13 MHz, C_6D_6, 300 K): δ = 2.14, 2.33 (each s, 12H, Dur-C$\underline{H}_3$), 6.99 (s, 2H, Dur-H), 7.06 (tt ^{3}J = 7.3 Hz ^{4}J = 2 Hz, 1H, *p*-Ph-H), 7.15-7.19 (m, 2H, *m*-Ph-H), 7.40 (brs, 1H, B-H-B), 7.71 – 7.73 (*o*-Ph-H) ppm. **^{11}B NMR** (128.38 MHz, C_6D_6, 300 K): δ = 25.7 (br s) ppm. **^{13}C NMR**: (100.61 MHz, C_6D_6, 300 K): δ = 20.0, 20.1 (each s, Dur-$\underline{C}H_3$), 128.9, 132.3, 133.2, 133.7, 134.7 (each s, Dur-C or Ph-C). **^{13}C NMR**: (75.47 MHz, toluene-d_8, 213 K): δ = 20.3 (s, 2 Dur-$\underline{C}H_3$), 131.8, 132.7, 133.1, 133.7, 134.1, 137.1, 137.9 (each s, Dur-C or Ph-C), 135.7 (br s, B_2C). **Elemental analysis:** Calcd. for ($C_{27}H_{32}B_2$): C, 85.6; H, 8.5. Found: C, 84.4; H, 7.2. **Mp**.: 173 °C (partial decomposition).

2.3. Synthesis of 1-phenyl-2,3-diduryldiboriranide 3

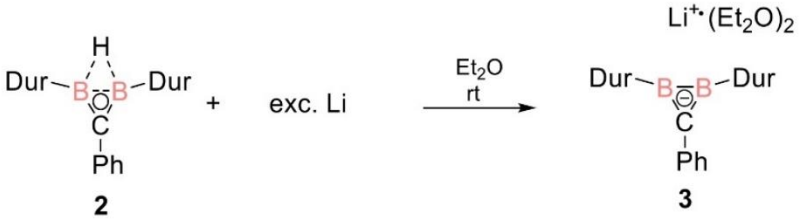

2 376.16 g/mol

3 449.27 g/mol

Approximately 50 mL of Et_2O are added to a solid mixture of 2.080 g (5.53 mmol) of diborirane **2** and 100 mg (14.49 mmol) of lithium powder at room temperature. The reaction mixture is stirred over night while warming to ambient temperature. Filtration and evaporation of volatiles *in vacuo* affords a yellow solid. Rinsing with a minimum amount of Et_2O and drying *in vacuo* yields 1.490 g (3.32 mmol, 60%) of 1-phenyl-2,3-diduryldiboriranide **3** as pale yellow powder.

The coordinated Et_2O molecules can be removed by rinsing the solid with hexane. Pale yellow crystals of **3** were obtained by storing the solution at −20 °C in a Et_2O/thf 1:1 mixture over night.

^{1}H NMR (400.13 MHz, thf-d_8, 300 K): δ = 2.14, 2.19 (each s, 12H, Dur-C$\underline{H}_3$), 6.48 (s, 2H, Dur-H), 6.68 (tt ^{3}J = 7.2 Hz ^{4}J = 1.4 Hz, 1H, *p*-Ph-H)), 6.94 – 6.98 (m, 2H, *m*-Ph-H), 7.19 – 7.21 (m, 2H, *o*-Ph-H) ppm. **^{11}B NMR** (128.38 MHz, thf-d_8, 300 K): δ = 44.2 (br s) ppm. **^{7}Li NMR** (155.50 MHz, thf-d_8, 300 K): δ = −0.46 (br s) ppm. **^{13}C NMR**: (75.47 MHz, thf-d_8, 203 K): δ = 19.9, 20.2 (each s, Dur-$\underline{C}H_3$), 121.5, 126.3, 127.3, 130.1, 130.6, 132.3, 144.9, 154.0 (each s, Dur-C and Ph-C), 151.9 (br s, B_2C). **Elemental analysis:** Calcd. for ($C_{31}H_{41}B_2LiO$): C, 81.2; H, 9.0. Found: C, 80.4; H, 8.4. **Mp**.: 253 °C (partial decomposition).

2.4. Synthesis of 1-phenyl-2,3-diduryl-gold-triphenylphosphine-diboriranide 4

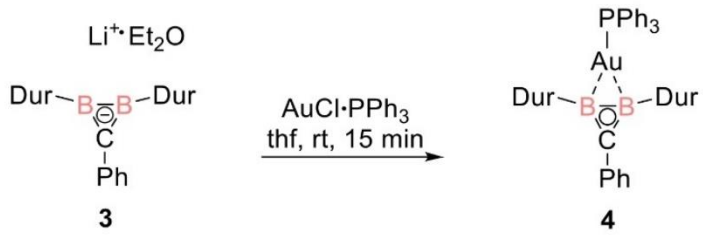

3 **4**

449.27 g/mol 836.42 g/mol

A solution of 110 mg (0.22 mmol) gold chloride(triphenylphosphine) in 5 mL of thf is added in a single portion to a yellow solution of 100 mg (0.22 mmol) of diboriranide **3** in 4 mL of thf. The mixture is stirred for 15 minutes, dried *in vacuo,* extracted with Et_2O and concentrated under reduced pressure after filtration. Colorless crystals of 1-phenyl-2,3-diduryl-gold-triphenylphosphine-diboriranide **4** (85 mg, 0.10 mmol, 47%) were obtained by storing the solution at −25 °C overnight.

^{1}H NMR (400.1 MHz, thf-d_8, 300 K): δ = 2.07, 2.11 (each s, 12H, Dur-C$\underline{H}_3$), 6.73 (s, 2H, Dur-H), 6.80 (tt ^3J = 7.2 Hz ^4J = 1.3 Hz, 1H, *p*-Ph-H)), 6.95 – 6.98 (m, 2H, *m*-Ph-H), 6.93 – 7.06 (m, 6H, *o/m*-PPh-H), 7.13 – 7.15 (m, 2H, *o*-Ph-H), 7.16 – 7.24 (m, 6H, *o/m*-PPh-H), 7.30 – 7.34 (m, 3H, *p*-PPh-H) ppm. **^{11}B NMR** (128.4 MHz, thf-d_8, 300 K): δ = 37.9 (br s) ppm. **^{31}P NMR** (161.98 MHz, thf-d_8, 300 K): δ = 52.2 (s) ppm. **^{13}C NMR**: (75.47 MHz, thf-d_8, 213 K): δ = 20.2, 20.4 (each s, Dur-$\underline{C}H_3$), 125.8, 128.6, 130.2, 130.7, 132.1, 132.9, 134.4, (each s, Dur-C and Ph-C), 129.8 (d, J = 11.1 Hz, PPh_3-C), 130.3 (d, $^1J_{CP}$ = 50.0 Hz, *ipso*-PPh_3-C), 134.9 (d, J = 15.7 Hz, PPh3-C), 139.4 (d, J = 12.6 Hz), 143.6 (d, $^3J_{CP}$ = 3.4 Hz, *ipso*-Dur-C), 147.8 (br d, $^3J_{CP}$ = 18.0 Hz, B_2C). **Elemental analysis:** Calcd. for ($C_{45}H_{46}B_2AuP$): C, 64.6; H, 5.5. Found: C, 65.7; H, 5.6.

2.5. Synthesis of 1-phenyl-2,3-diduryl-(bis)diboriranide-cuprate 5

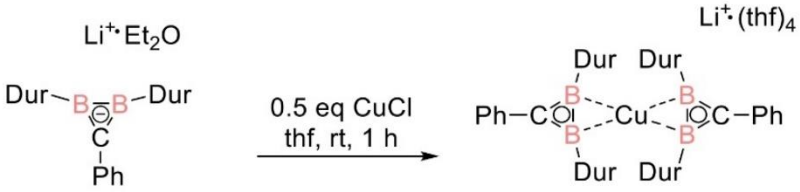

3 **5**

449.27 g/mol 1093.13 g/mol

A suspension of 11 mg (0.11 mmol) copper chloride in 5 mL of thf is added in a single portion to a yellow solution of 100 mg (0.22 mmol) of diboriranide **3** in 4 mL of thf. The mixture is stirred for 1 hour, dried *in vacuo*, extracted with Et_2O and concentrated under reduced pressure after

filtration. Colorless crystals of 1-phenyl-2,3-diduryl-(bis)diboriranide-cuprate **5** (92 mg, 0.09 mmol, 39%) were obtained by storing the solution at −25 °C overnight.

^{1}H NMR (400.1 MHz, thf-d_8, 223 K): δ = 1.72, 2.01 (each s, 12H, Dur-C$\underline{H}_3$), 6.44 (s, 2H, Dur-H), 6.48 – 6.55 (m, 1H, *p*-Ph-H), 6.65 – 6.75 (m, 4H, o/*m*-Ph-H). **^{7}Li NMR** (155.50 MHz, thf-d_8, 300 K): δ = −0.20 (s) ppm. **^{11}B NMR** (128.4 MHz, thf-d_8, 300 K): δ = 34.7 (br s) ppm. **^{13}C NMR**: (75.47 MHz, thf-d_8, 223 K): δ = 19.9, 20.8 (each s, Dur-$\underline{C}H_3$), 123.5, 127.6, 128.5, 130.0, 130.8, 134.8, 141.0, 146.2 (each s, Dur-C and Ph-C), 153.9 (br s, B_2C). **Elemental analysis:** Calcd. for ($C_{70}H_{103}B_4CuLiO_4$): C, 75.0; H, 9.2. Found: C, 73.2; H, 7.9.

2.6. Synthesis of 1-phenyl-2,3-diduryl-diboriranide-chlorocuprate 6

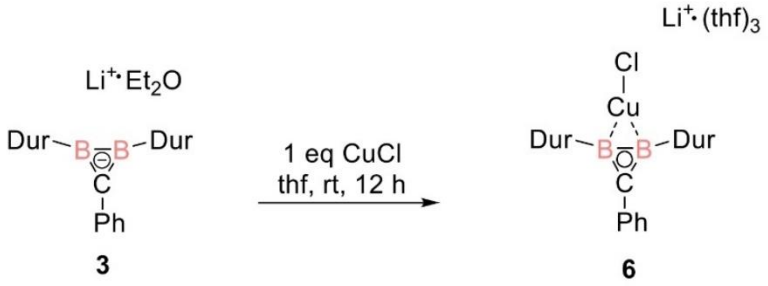

3 449.27 g/mol

6 687.34 g/mol

A suspension of 25 mg (0.25 mmol) copper chloride in 5 mL of thf is added in a single portion to a yellow solution of 113 mg (0.25 mmol) of diboriranide **3** in 4 mL of thf. The mixture is stirred for 12 hours, dried *in vacuo,* rinsed with a minimum amount of Et_2O, extracted with a thf/toluene mixture and concentrated under reduced pressure after filtration. Colorless crystals of 1-phenyl-2,3-diduryl-diboriranide-chlorocuprate **6** (51 mg, 0.10 mmol, 42%) were obtained by storing the solution at −25 °C overnight.

^{1}H NMR (400.1 MHz, thf-d_8, 223 K): δ = 2.18, 2.25 (each s, 12H, Dur-C$\underline{H}_3$), 6.67 (s, 2H, Dur-H), 6.82 – 6.89 (m, 1H, *p*-Ph-H), 6.97 – 7.00 (m, 2H, *m*-Ph-H), 7.13 – 7.15 (m, 2H, *o*-Ph-H). **^{7}Li NMR** (155.50 MHz, thf-d_8, 300 K): δ = −0.40 (s) ppm. **^{11}B NMR** (128.4 MHz, thf-d_8, 300 K): δ = 34.4 (br s) ppm. **^{13}C NMR**: (75.47 MHz, thf-d_8, 223 K): δ = 20.2, 20.5 (each s, Dur-$\underline{C}H_3$), 124.2, 128.0, 128.7, 130.5, 131.7, 133.6, 140.3, 145.8 (each s, Dur-C and Ph-C), 151.1 (br s, B_2C). **Elemental analysis:** Calcd. for ($C_{31}H_{41}B_2CuClLiO$): C, 66.8; H, 7.4. Found: C, 65.9; H, 7.0.

2.7. Synthesis of 1-phenyl-2,3-diduryl-diboriranide-chlorozincate 7

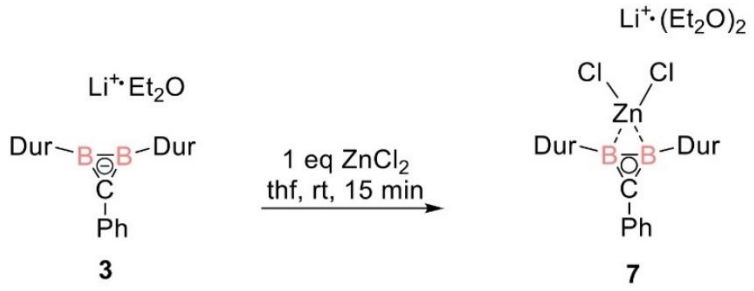

3 **7**

449.27 g/mol 668.63 g/mol

A solution of 30 mg (0.22 mmol) zinc chloride in 5 mL of thf is added in a single portion to a yellow solution of 100 mg (0.22 mmol) of diboriranide **3** in 4 mL of thf. The mixture is stirred for 15 minutes, dried *in vacuo,* extracted with Et_2O and concentrated under reduced pressure after filtration. Colorless crystals of 1-phenyl-2,3-diduryl-diboriranide-chlorozincate **7** (109 mg, 0.21 mmol, 96%) were obtained by storing the solution at −25 °C overnight.

^{1}H NMR (400.1 MHz, thf-d_8, 223 K): δ = 2.08, 2.16 (each s, 12H, Dur-C$\underline{H}_3$), 6.69 (s, 2H, Dur-H), 6.86 (tt ^3J = 7.4 Hz ^4J = 1.3 Hz, 1H, *p*-Ph-H)), 6.96 – 7.00 (m, 2H, *m*-Ph-H), 7.11 – 7.14 (m, 2H, *o*-Ph-H).**^{11}B NMR** (128.4 MHz, thf-d_8, 300 K): δ = 32.9 (br s) ppm. **^{13}C NMR**: (75.47 MHz, thf-d_8, 223 K): δ = 20.2, 20.6 (each s, Dur-$\underline{C}H_3$), 125.7, 128.3, 130.4, 131.1, 132.3, 136.0, 138.3, 139.0 (each s, Dur-C and Ph-C), 144.0 (br s, B_2C). **Elemental analysis:** Calcd. for ($C_{35}H_{51}B_2ZnLiO_2$): C, 62.8; H, 7.7. Found: C, 60.8; H, 6.8.

2.8. Synthesis of 1-phenyl-2,3-diduryl-diboriranide-trimethylstannane 8

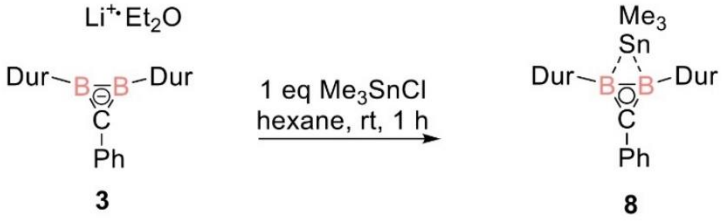

3 **8**

449.27 g/mol 540.98 g/mol

A solution of 44 mg (0.22 mmol) trimethyltin chloride in 5 mL of hexane is added in a single portion to a pale-yellow suspension of 100 mg (0.22 mmol) of diboriranide **3** in 4 mL of hexane. The mixture is stirred for 1 hour, dried *in vacuo,* washed with a minimum amount of hexane, extracted with toluene and concentrated under reduced pressure after filtration. Colorless crystals of 1-phenyl-2,3-diduryl-diboriranide-trimethylstannane **8** (59 mg, 0.11 mmol, 50%) were obtained by storing the solution at −25 °C overnight.

^{1}H NMR (400.1 MHz, C_6D_6, 223 K): δ = 2.08, 2.16 (each s, 12H, Dur-C$\underline{H}_3$), 6.69 (s, 2H, Dur-H), 6.86 (tt ^{3}J = 7.4 Hz ^{4}J = 1.3 Hz, 1H, *p*-Ph-H)), 6.96 – 7.00 (m, 2H, *m*-Ph-H), 7.11 – 7.14 (m, 2H, *o*-Ph-H). **^{11}B NMR** (128.4 MHz, C_6D_6, 300 K): δ = 34.0 (br s) ppm. **^{13}C NMR**: (75.47 MHz, toluene-d_8, 233 K): δ = −3.2 (s, $Sn(CH_3)_3$), 20.2, 20.3 (each s, Dur-$\underline{C}H_3$), 129.0, 131.0, 132.0, 133.7, 135.2, 135.3 136.0, 138.8, (each s, Dur-C and Ph-C), 144.5 (br s, B_2C). **^{119}Sn NMR** (149.21 MHz, C_6D_6, 300 K): δ = −38.0 (br s) ppm. **Elemental analysis:** Calcd. for ($C_{30}H_{40}B_2Sn$): C, 66.6; H, 7.5. Found: C, 67.1; H, 7.3.

2.9. Elemental analysis: detailed data

1: Measured Values: 1) C: 72.1, H: 6.3; 2) C: 72.2, H: 6.3; 3) C: 72.1, H: 6.5

2: Measured Values: 1) C: 80.6, H: 8.4; 2) C: 80.1, H: 8.3

3: Measured Values: 1) C: 84.2, H: 7.2; 2) C: 84.6, H: 7.6; 3) C: 84.1, H: 6.9

4: Measured Values: 1) C: 64.6, H: 5.6; 2) C: 66.5, H: 5.8; 3) C: 65.9, H: 5.4

5: Measured Values: 1) C: 73.2, H: 8.1; 2) C: 73.4, H: 8.0; 3) C: 73.1, H: 7.6

6: Measured Values: 1) C: 65.8, H: 7.3; 2) C: 66.0, H: 7.1; 3) C: 65.8, H: 6.5

7: Measured Values: 1) C: 62.3, H: 7.0; 2) C: 60.8, H: 6.9; 3) C: 59.4, H: 6.6

8: Measured Values: 1) C: 67.3, H: 7.4; 2) C: 66.9, H: 7.2; 3) C: 67.1, H: 7.1

3. NMR Spectra

3.1. NMR spectra of 1-benzyl-2-chloro-1,2-diduryldiborane(4) 1

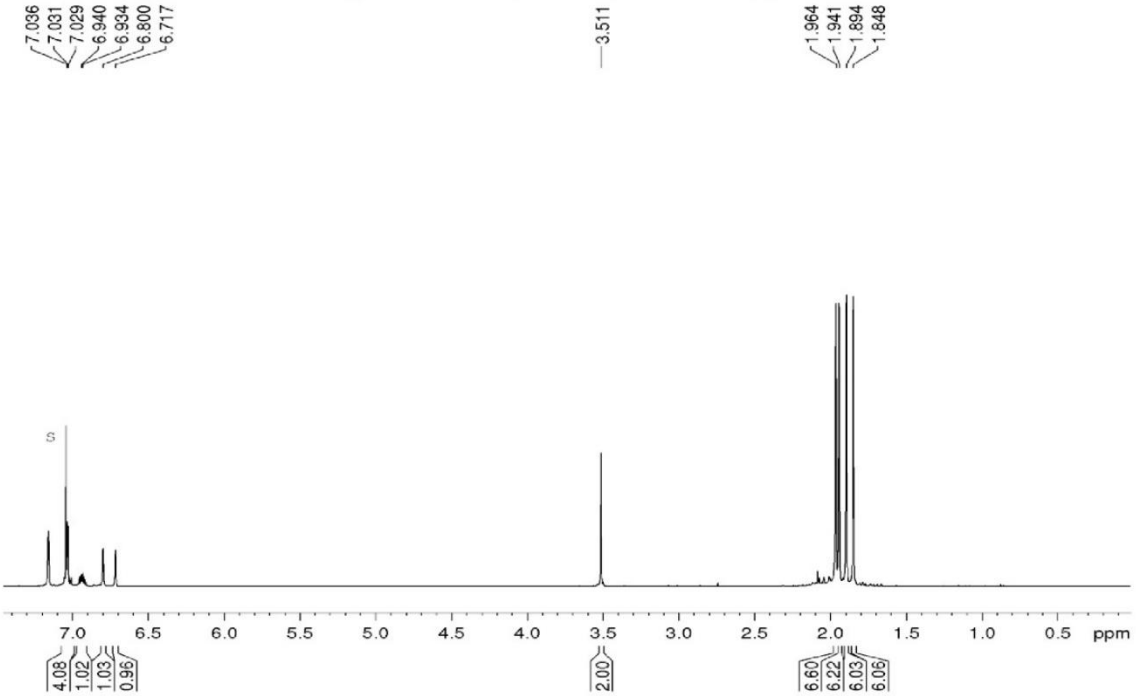

Figure S1. ^{1}H-NMR spectrum (400.1 MHz) of 1-benzyl-2-chloro-1,2-diduryldiborane(4) **1** in C_6D_6 (=s).

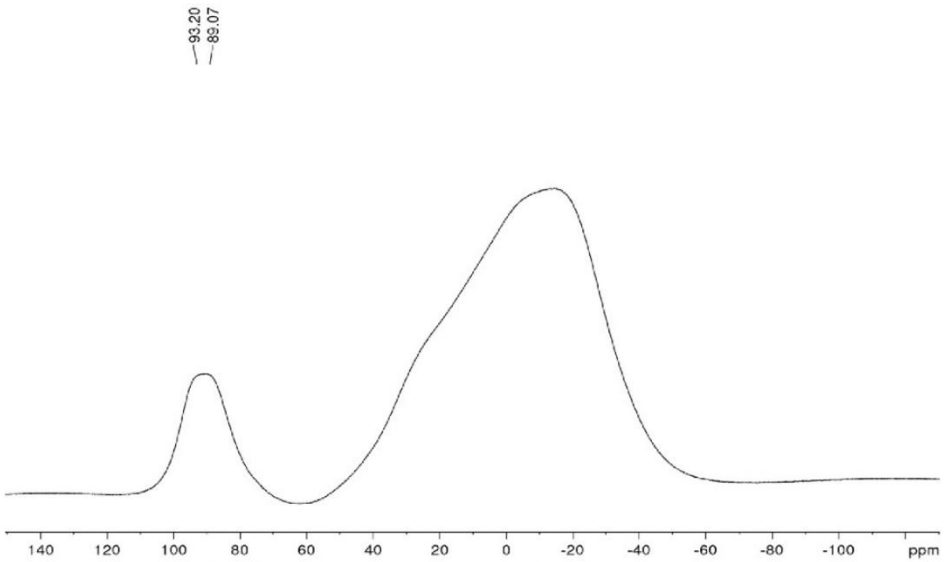

Figure S2. Baseline corrected ^{11}B-NMR spectrum (128.4 MHz) of 1-benzyl-2-chloro-1,2-diduryldiborane(4) **1** (glass peak from 60 to −50 ppm).

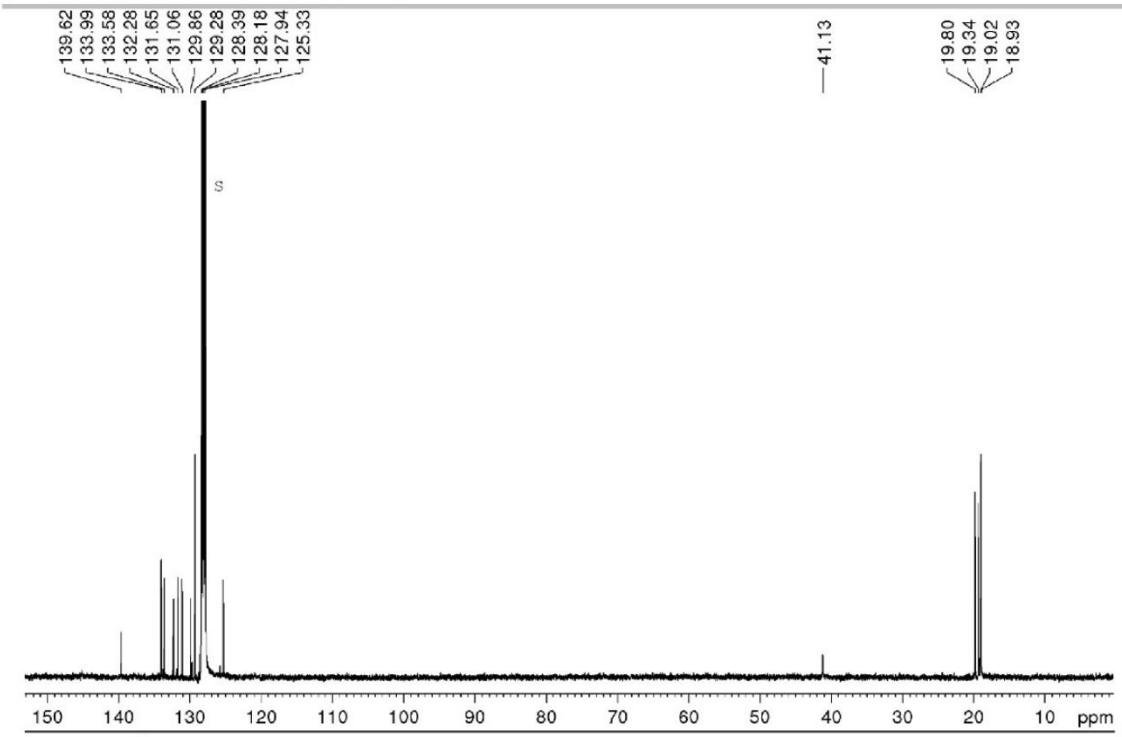

Figure S3. ^{13}C-NMR spectrum (100.61 MHz) of 1-benzyl-2-chloro-1,2-diduryldiborane(4) **1** in C_6D_6 (=s).

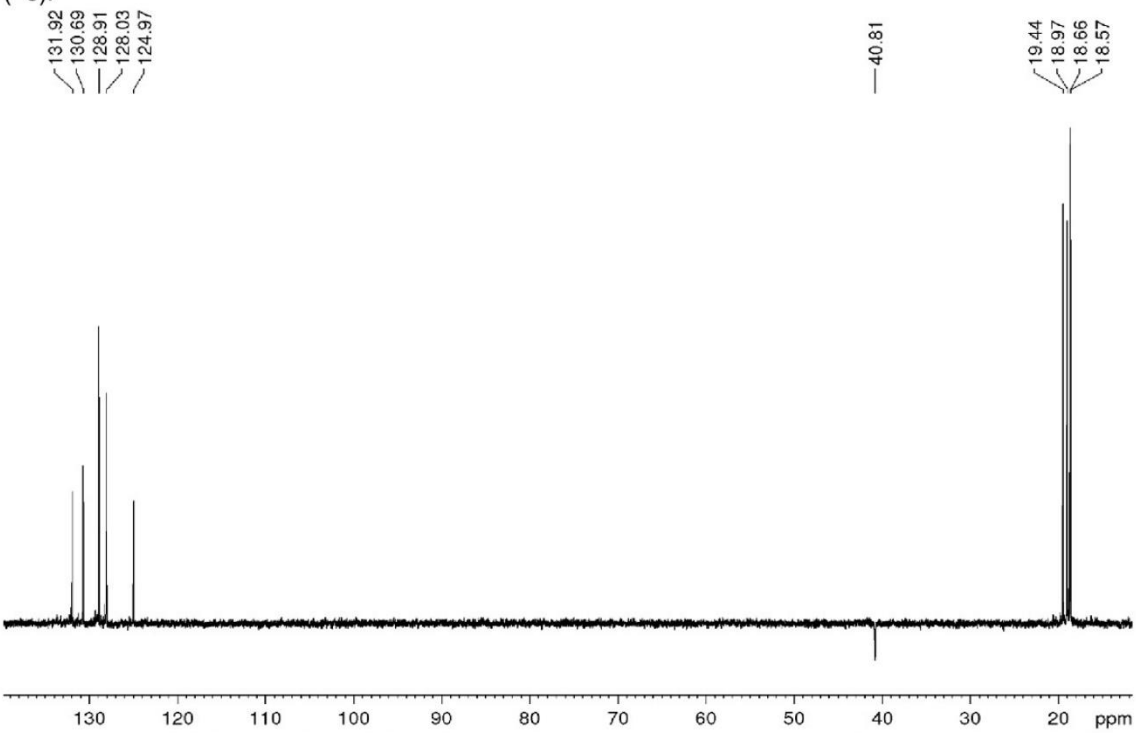

Figure S4. DEPT-135 spectrum (100.61 MHz) of 1-benzyl-2-chloro-1,2-diduryldiborane(4) **1** in C_6D_6.

3.2. NMR Spectra of 1-phenyl-2,3-diduryldiborirane 2

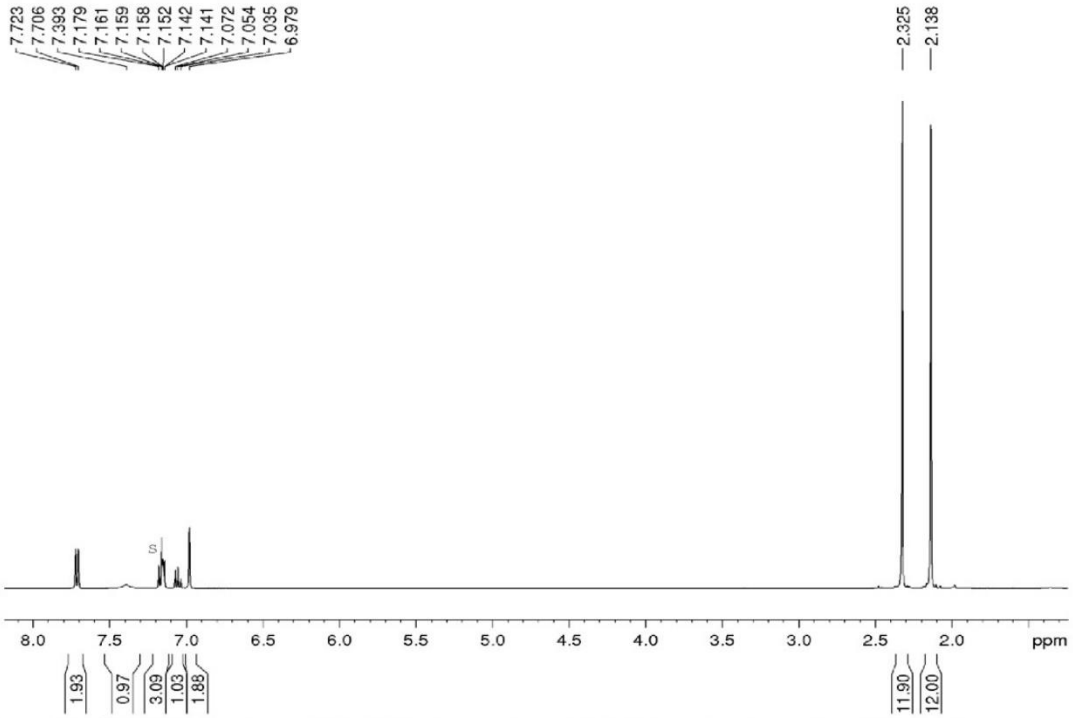

Figure S5. ^{1}H-NMR spectrum (400.1 MHz) of 1-phenyl-2,3-diduryldiborirane **2** in C_6D_6 (=s).

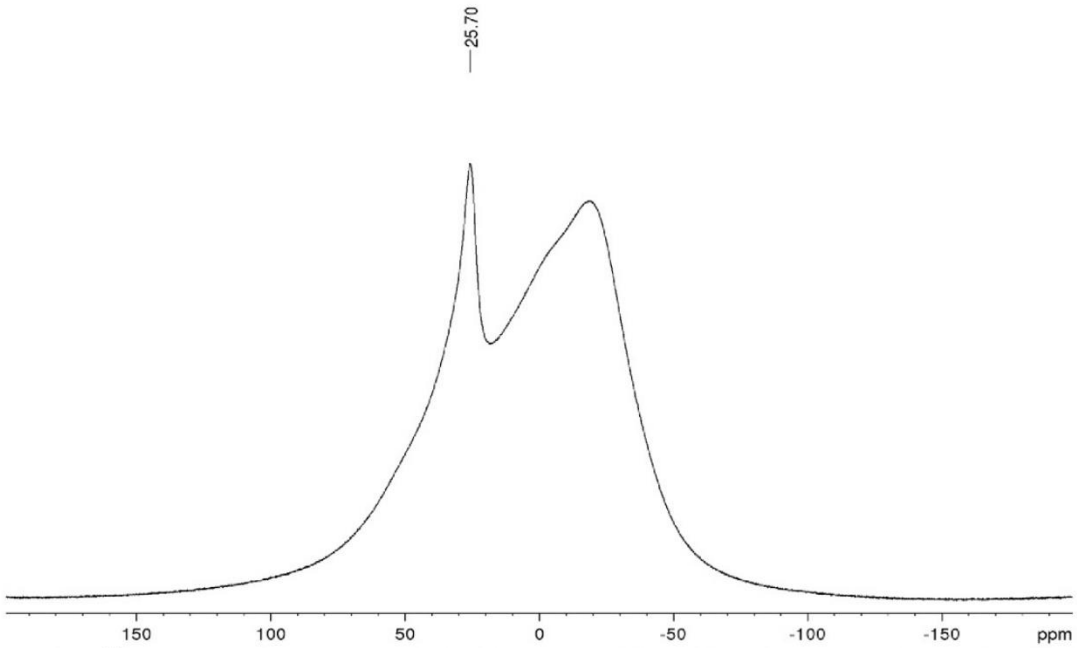

Figure S6. ^{11}B-NMR spectrum (128.4 MHz) of 1-benzyl-2-chloro-1,2-diduryldiborane(4) **2** (glass peak from 70 to −50 ppm).

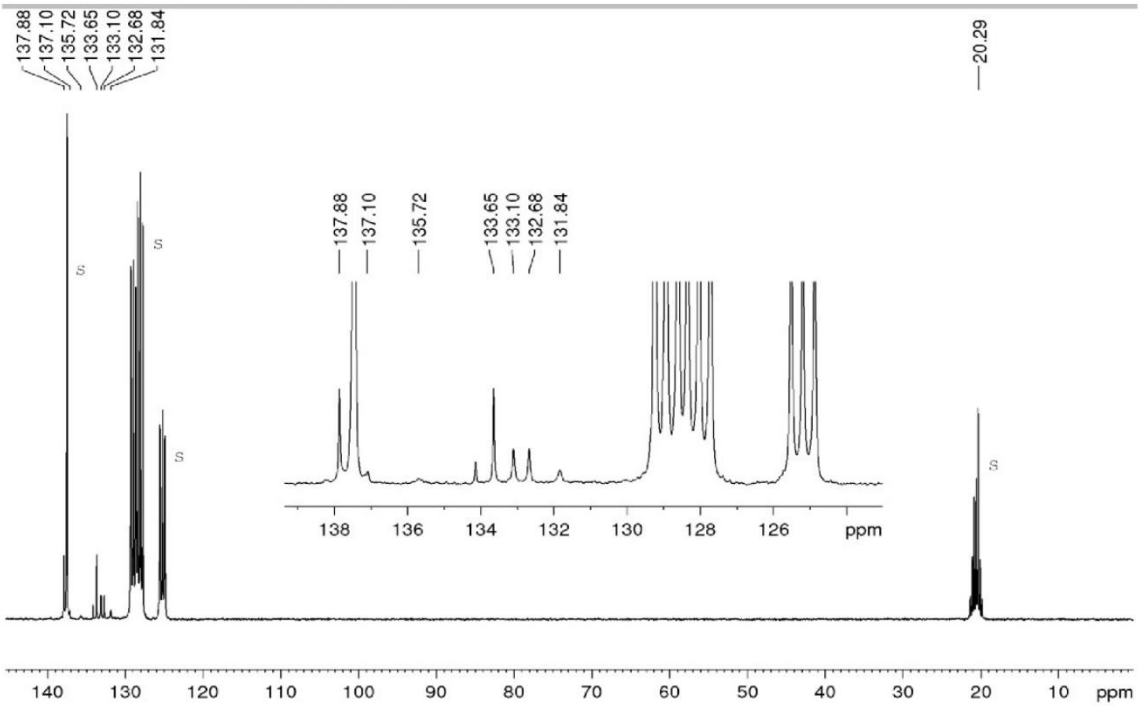

Figure S7. ^{13}C-NMR spectrum (75.47 MHz) of 1-benzyl-2-chloro-1,2-diduryldiborane(4) **2** at 213 K in toluene-d_8 (=s).

3.3. NMR spectra of 1-phenyl-2,3-diduryldiboriranide(4) 3

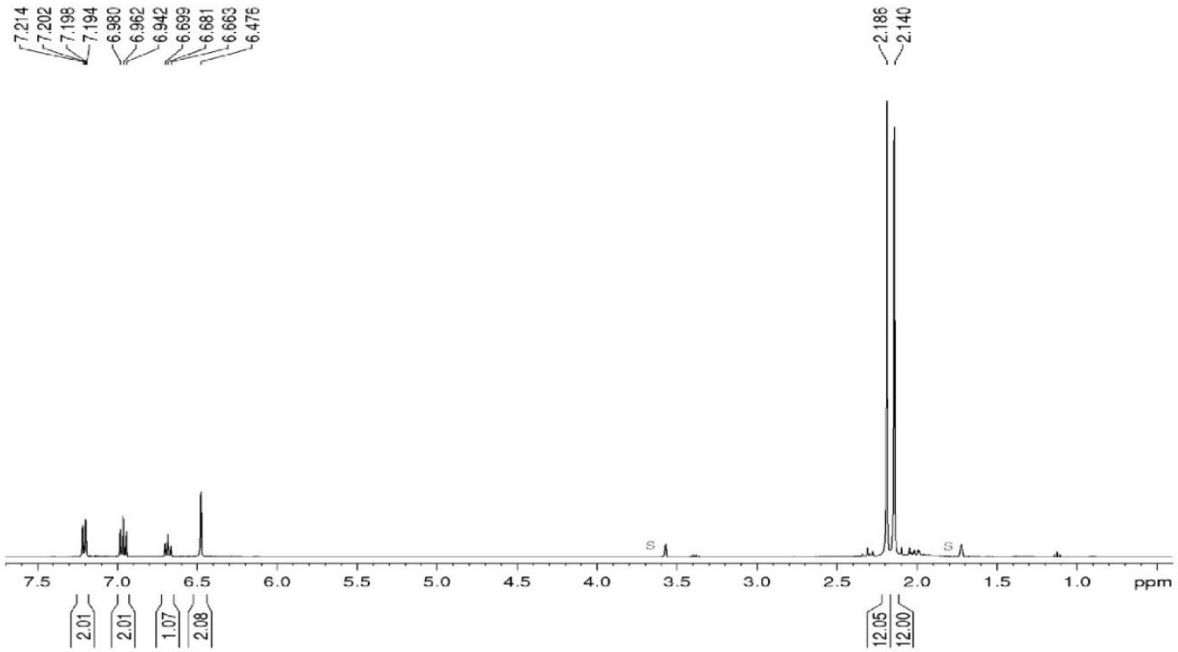

Figure S8. ^{1}H-NMR spectrum (400.1 MHz) of 1-phenyl-2,3-diduryldiboriranide(4) **3** in thf-d_8 (=s).

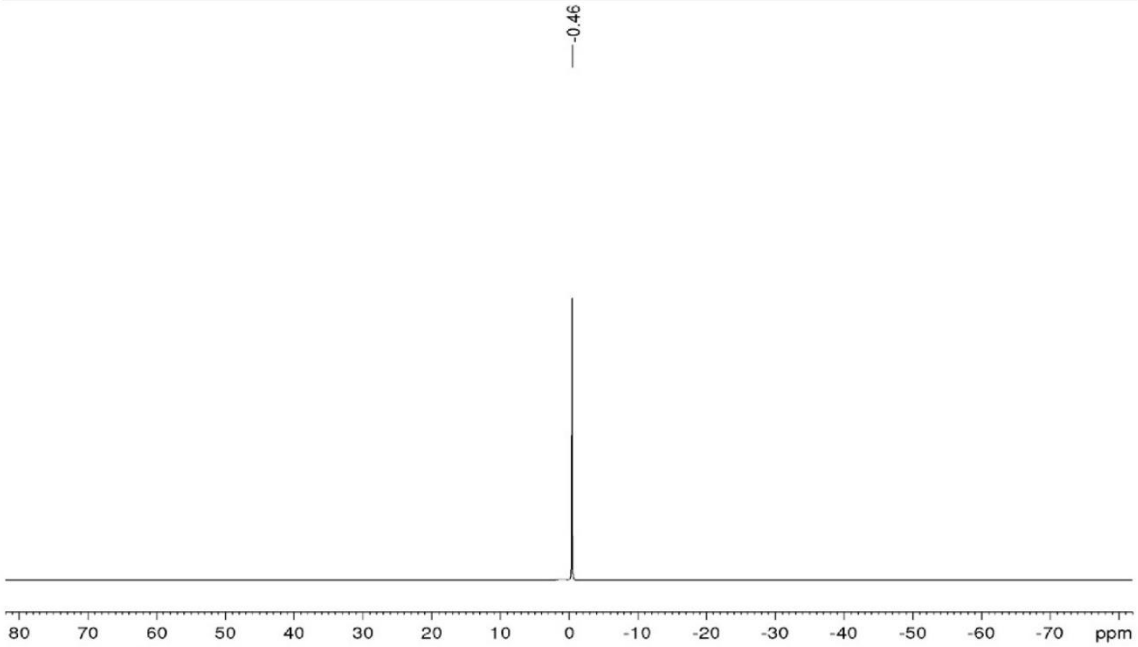

Figure S9. ^{7}Li-NMR spectrum (155.50 MHz) of 1-phenyl-2,3-diduryldiboriranide(4) **3** in thf-d_8.

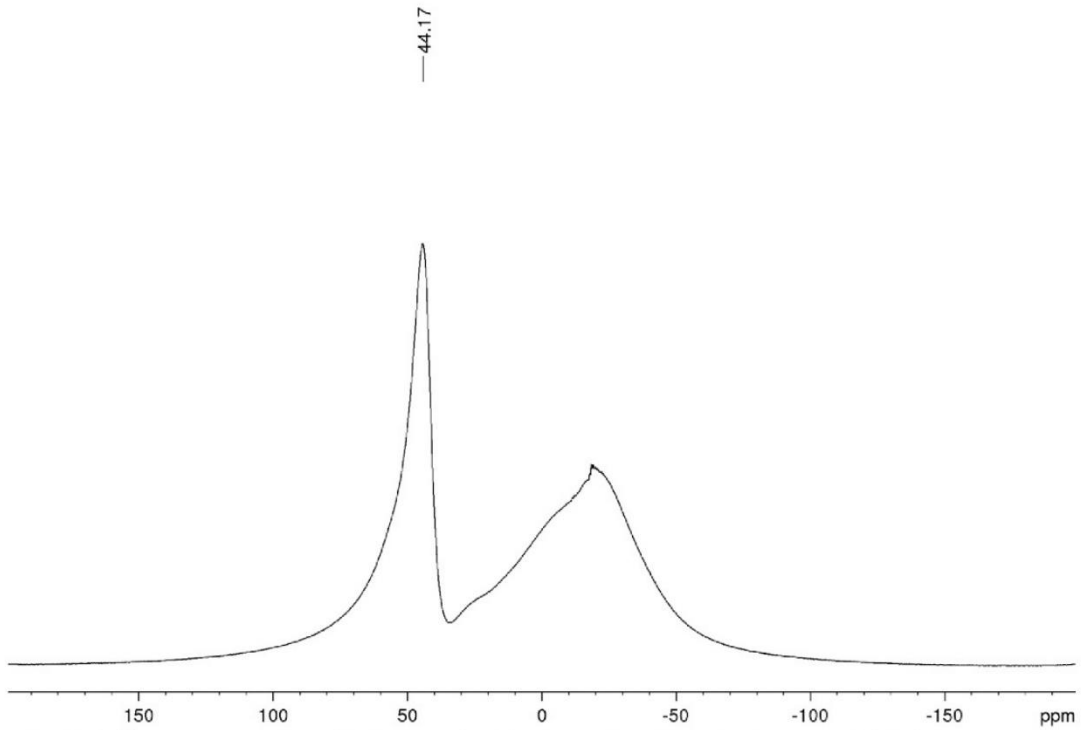

Figure S10. ^{11}B-NMR spectrum (128.4 MHz) of 1-phenyl-2,3-diduryldiboriranide(4) **3** (glass peak from 70 to −50 ppm) in thf-d_8.

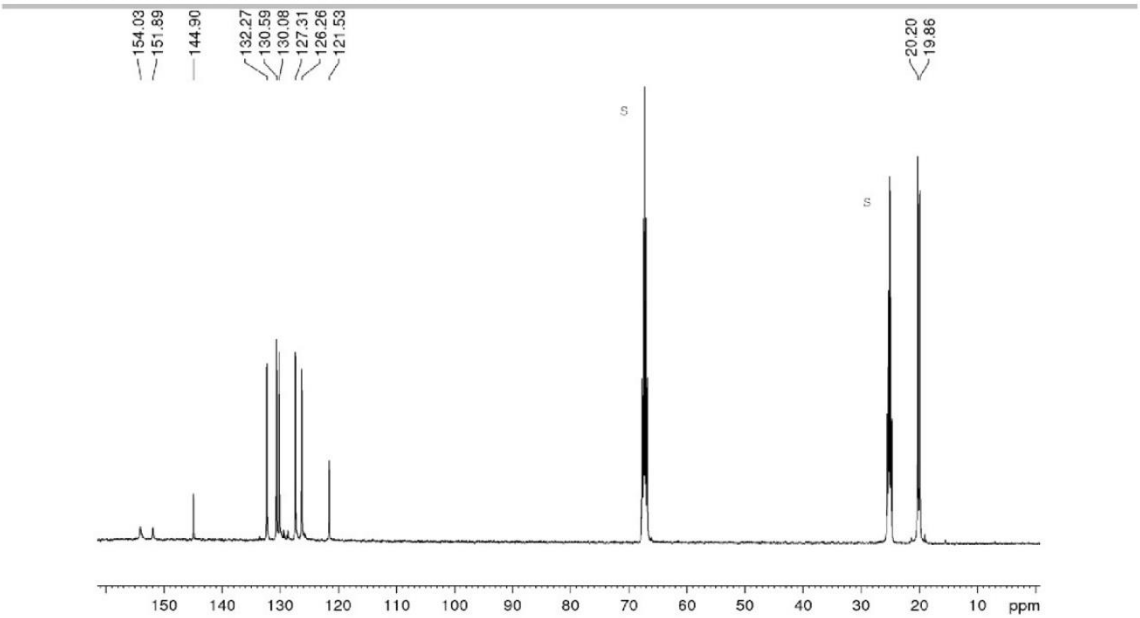

Figure S11. ^{13}C-NMR spectrum (75.47 MHz) of 1-phenyl-2,3-diduryldiboriranide(4) **3** at 203 K in thf-d_8 (=s).

3.4. NMR spectra of 1-phenyl-2,3-diduryl-gold-triphenylphosphine-diboriranide 4

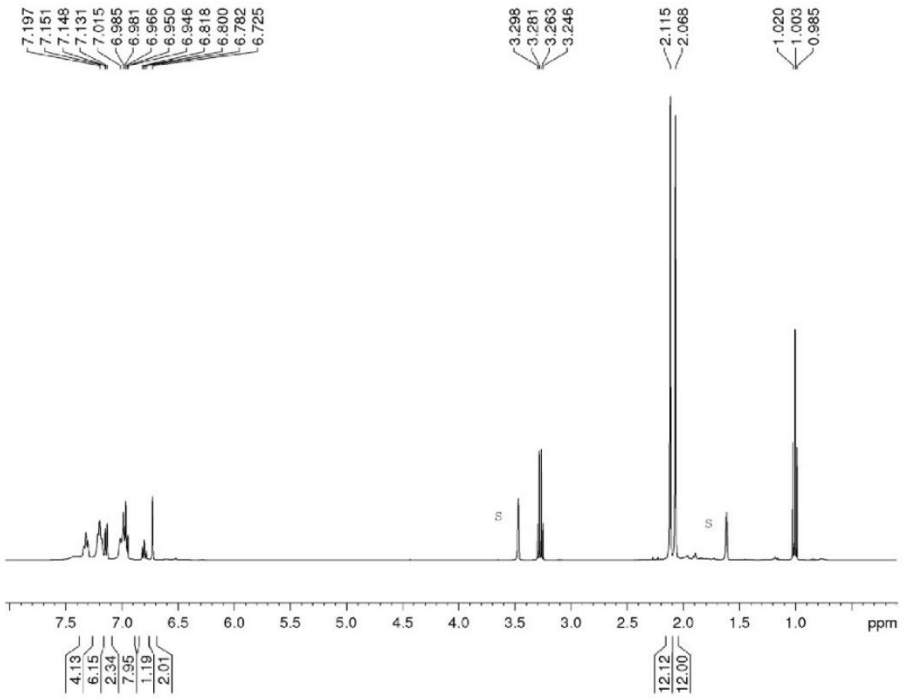

Figure S12. ^{1}H-NMR spectrum (400.1 MHz) of 1-phenyl-2,3-diduryl-gold-triphenylphosphine-diboriranide **4** in thf-d_8 (=s).

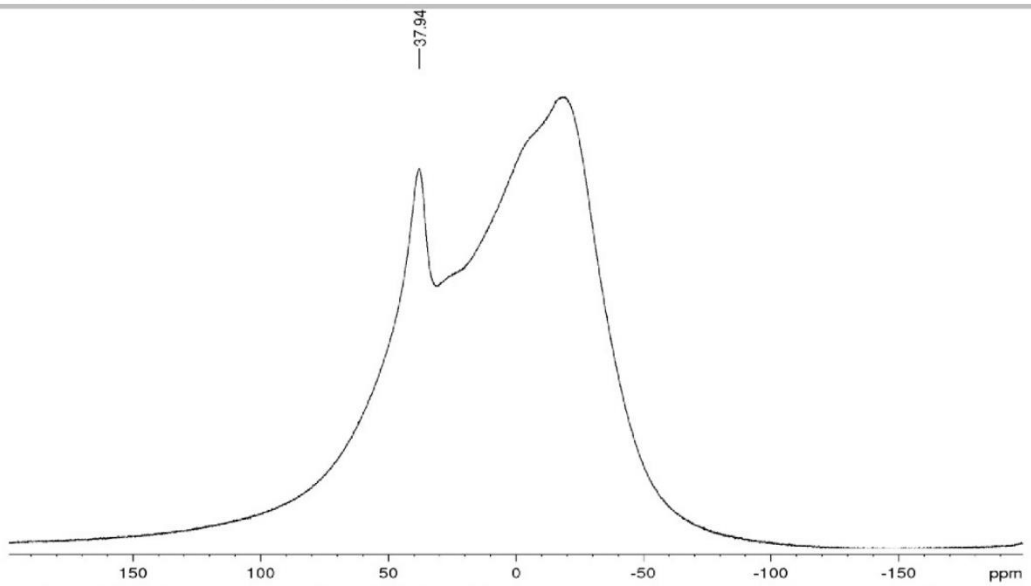

Figure S13. ^{11}B-NMR spectrum (128.4 MHz) of 1-phenyl-2,3-diduryl-gold-triphenylphosphine-diboriranide **4** (glass peak from 70 ppm to −50 ppm).

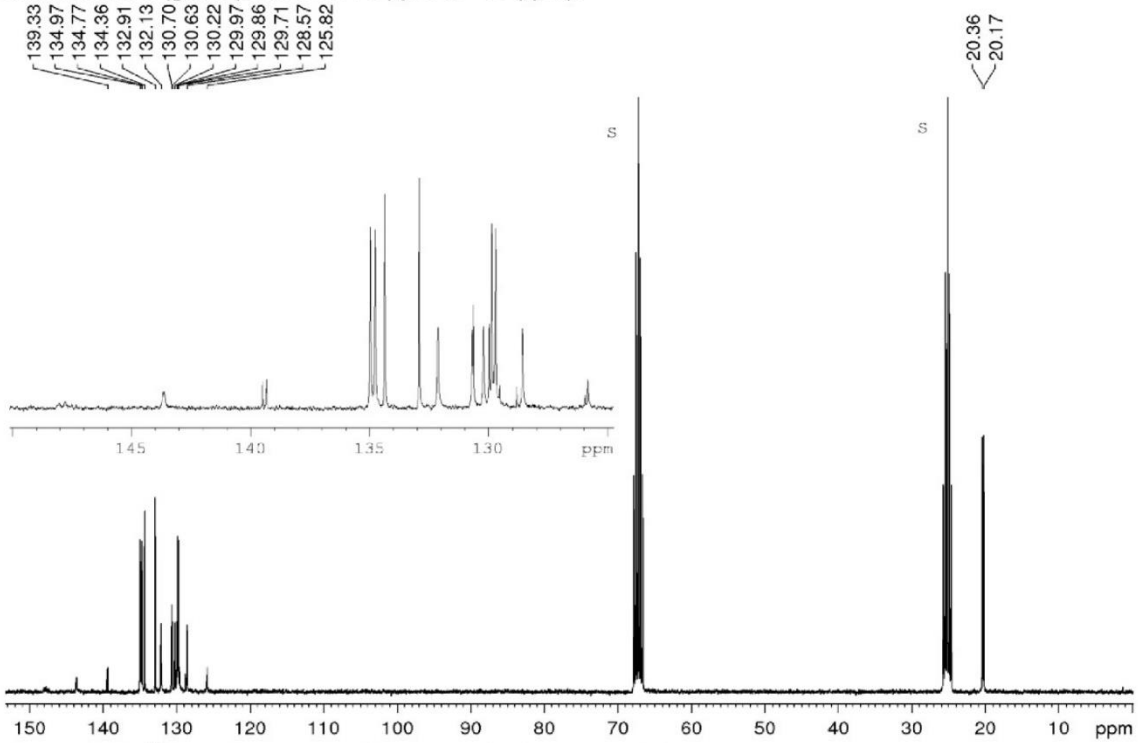

Figure S14. ^{13}C-NMR spectrum (75.47 MHz) of 1-phenyl-2,3-diduryl-gold-triphenylphosphine-diboriranide **4** at 213 K in thf-d_8 (=s).

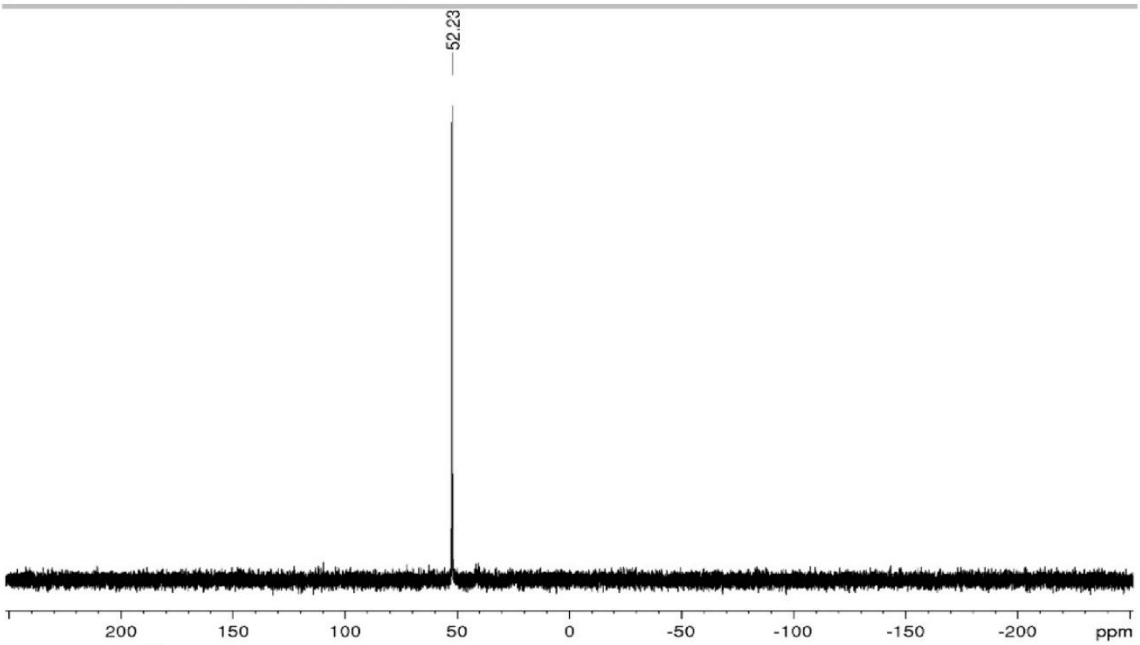

Figure S15. ^{31}P-NMR spectrum (161.98 MHz) of 1-phenyl-2,3-diduryl-gold-triphenylphosphine-diboriranide **4**.

3.5. NMR spectra of 1-phenyl-2,3-diduryl-(bis)diboriranide-cuprate 5

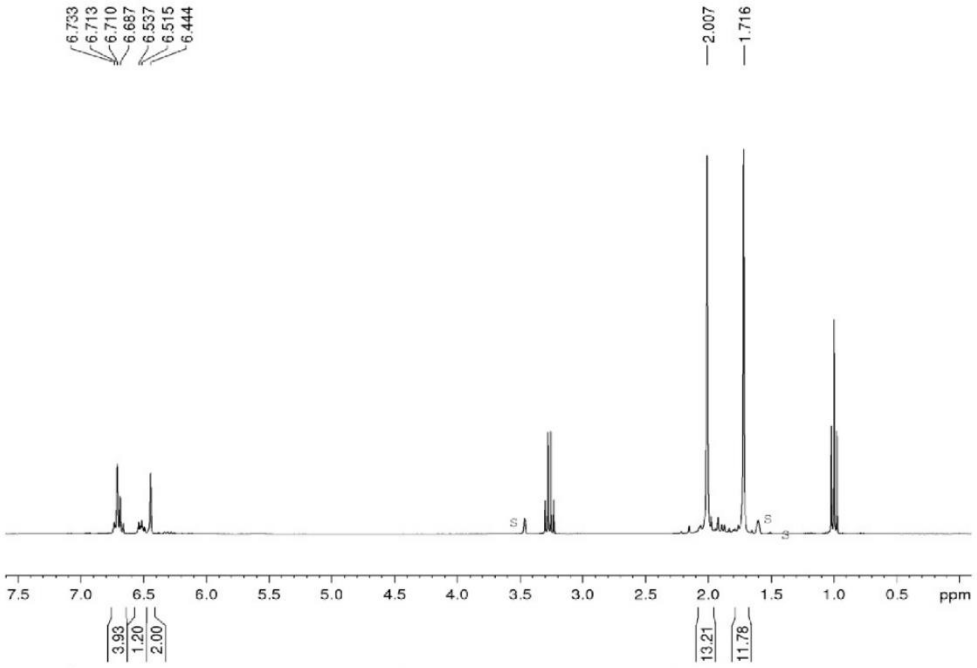

Figure S16. ^{1}H-NMR spectrum (400.1 MHz) of 1-phenyl-2,3-diduryl-(bis)diboriranide-cuprate **5** in thf-d_8 (=s).

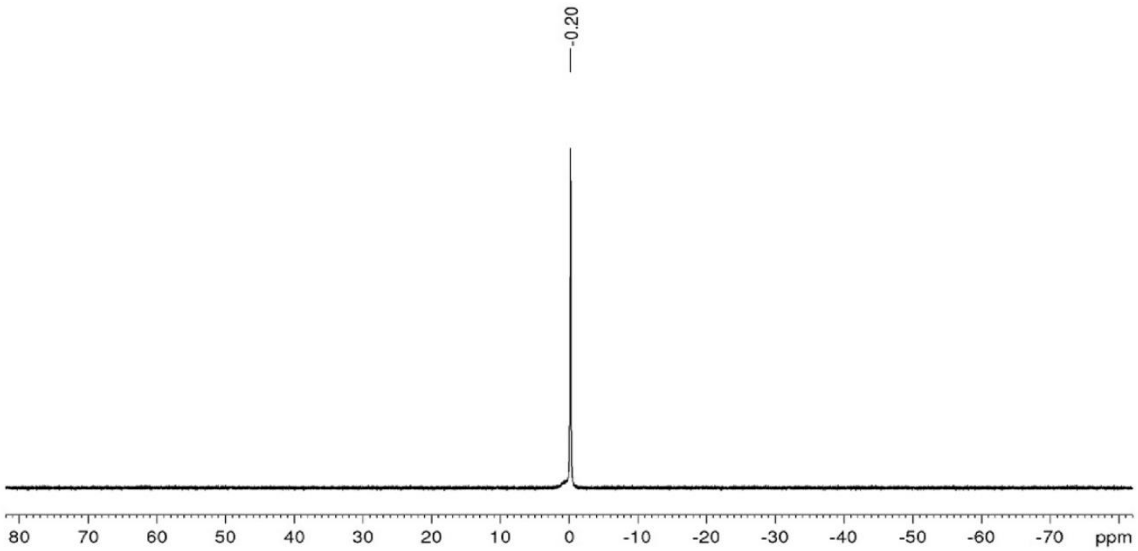

Figure S17. ^{7}Li-NMR spectrum (155.50 MHz) of 1-phenyl-2,3-diduryl-(bis)diboriranide-cuprate **5**.

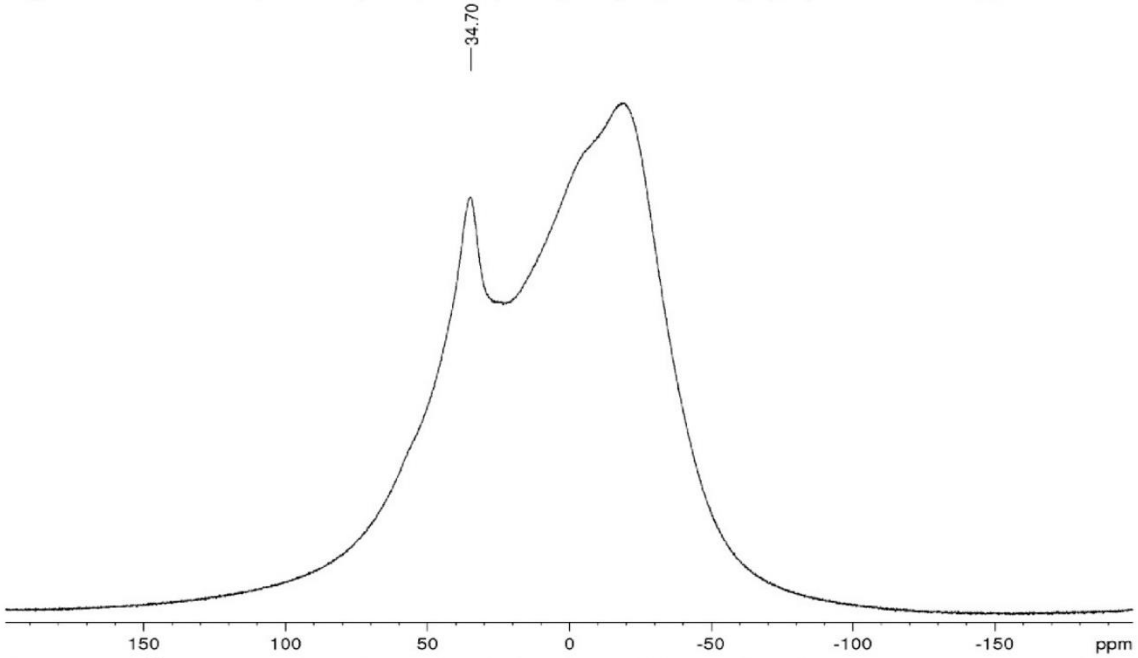

Figure S18. ^{11}B-NMR spectrum (128.4 MHz) of 1-phenyl-2,3-diduryl-(bis)diboriranide-cuprate **5** (glass peak from 70 to −50 ppm).

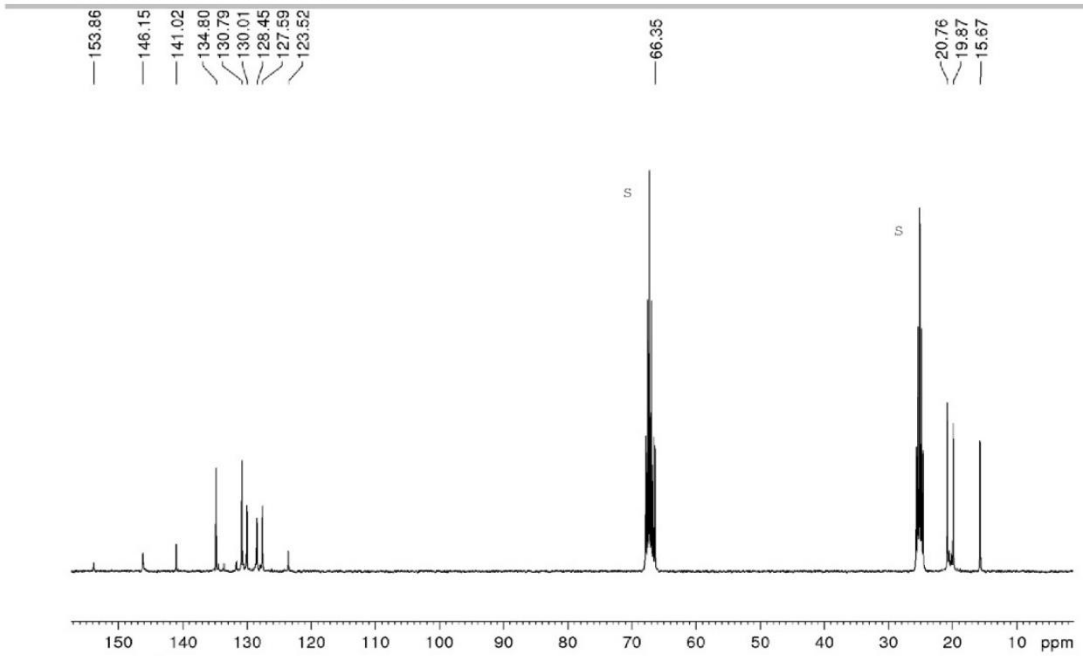

Figure S19. ^{13}C-NMR spectrum (75.47 MHz) of 1-phenyl-2,3-diduryl-(bis)diboriranide-cuprate **5** at 223 K in thf-d_8 (= s).

3.6. NMR spectra of 1-phenyl-2,3-diduryl-diboriranide-chlorocuprate 6

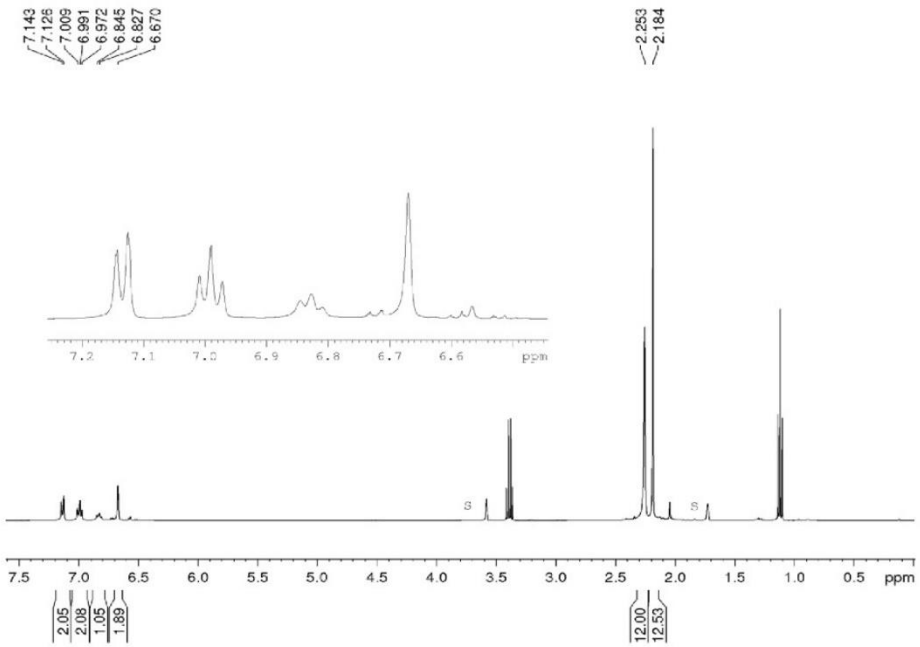

Figure S20. ^{1}H-NMR spectrum (400.1 MHz) of 1-phenyl-2,3-diduryl-diboriranide-chlorocuprate **6** in thf-d_8 (=s).

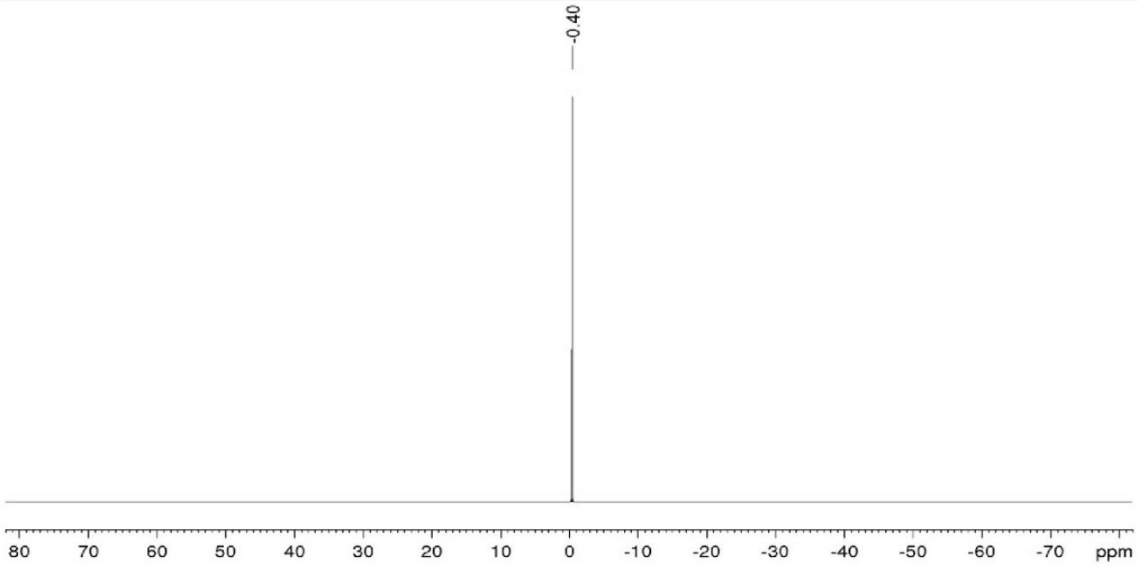

Figure S21. ^{7}Li-NMR spectrum (155.50 MHz) of 1-phenyl-2,3-diduryl-diboriranide-chlorocuprate **6**.

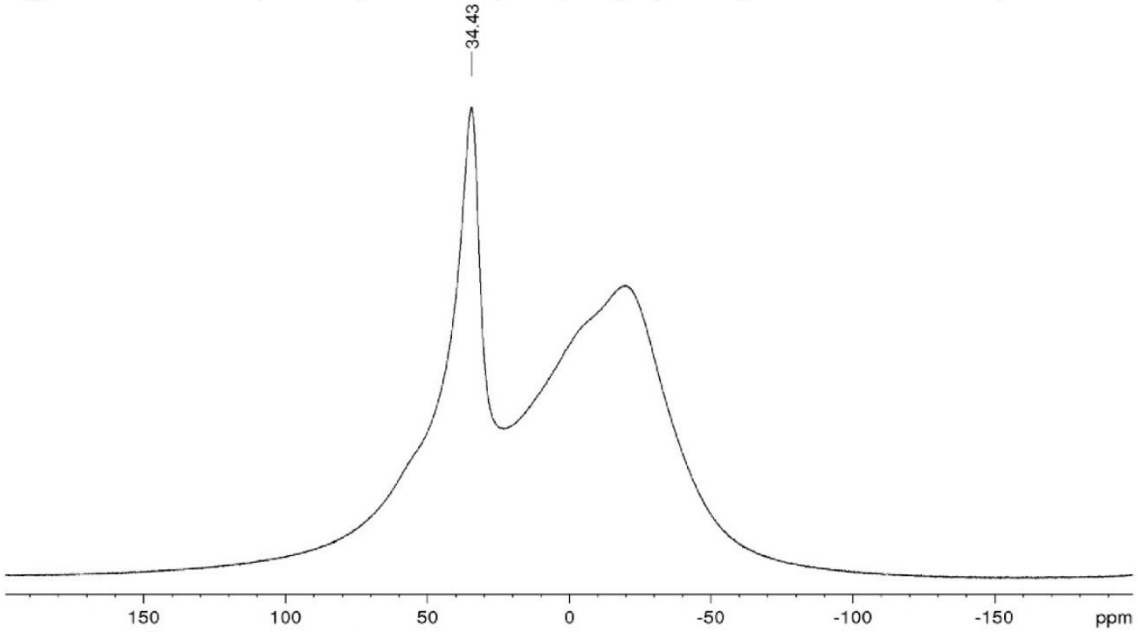

Figure S22. ^{11}B-NMR spectrum (128.4 MHz) of 1-phenyl-2,3-diduryl-diboriranide-chlorocuprate **6** (glass peak from 70 to −50 ppm).

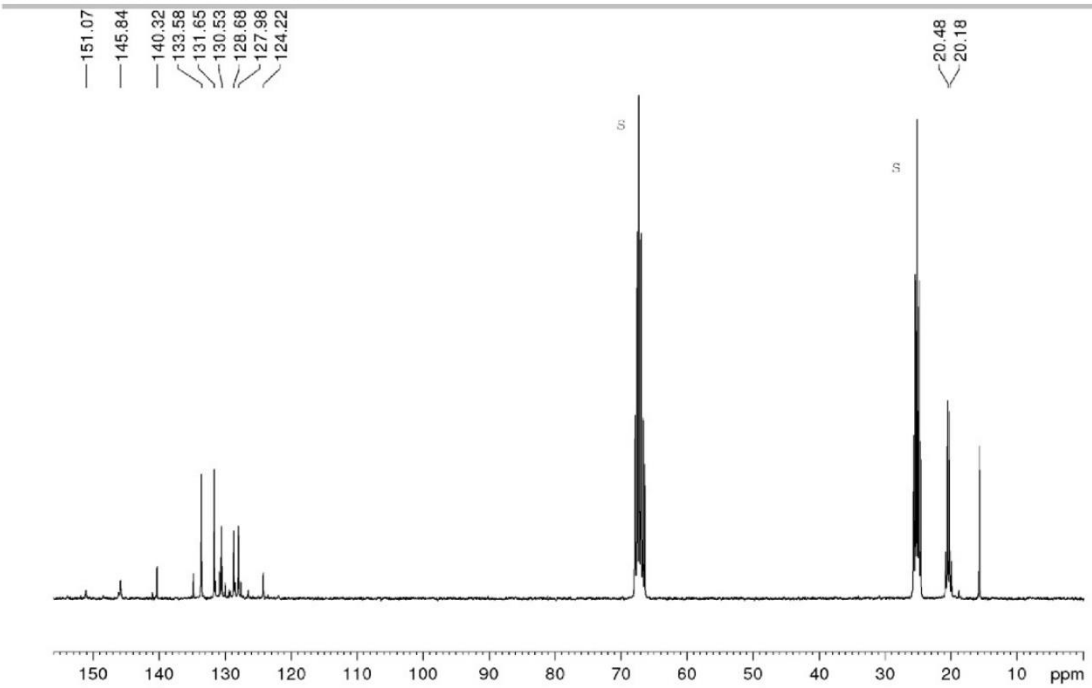

Figure S23. ^{13}C-NMR spectrum (75.47 MHz) of 1-phenyl-2,3-diduryl-diboriranide-chlorocuprate **6** at 223 K in thf-d_8 (=s).

3.7. NMR spectra of 1-phenyl-2,3-diduryl-diboriranide-chlorozincate 7

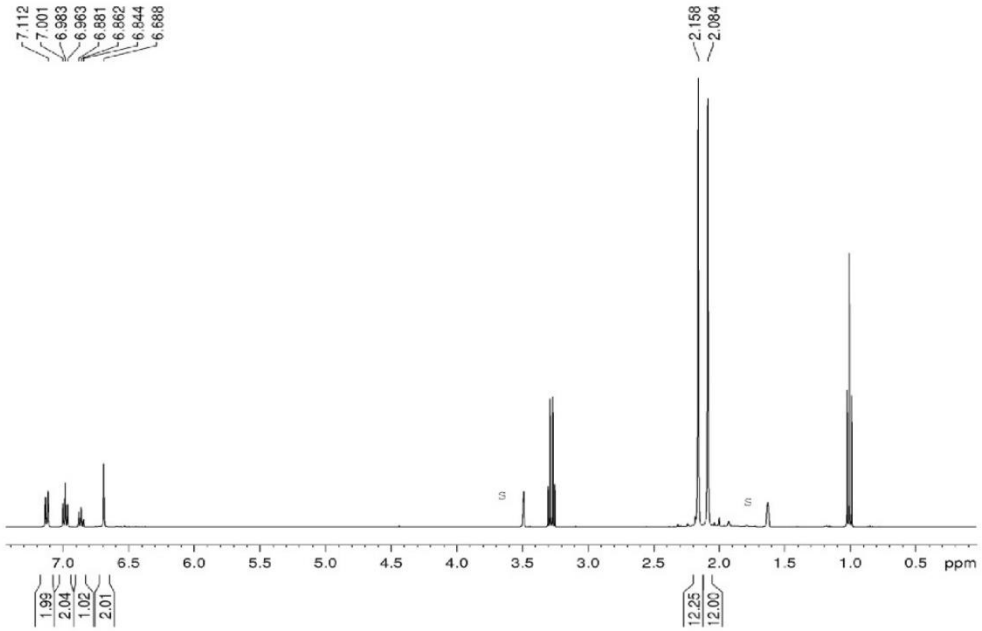

Figure S24. ^{1}H-NMR spectrum (400.1 MHz) of 1-phenyl-2,3-diduryl-diboriranide-chlorozincate **7** in thf-d_8 (=s).

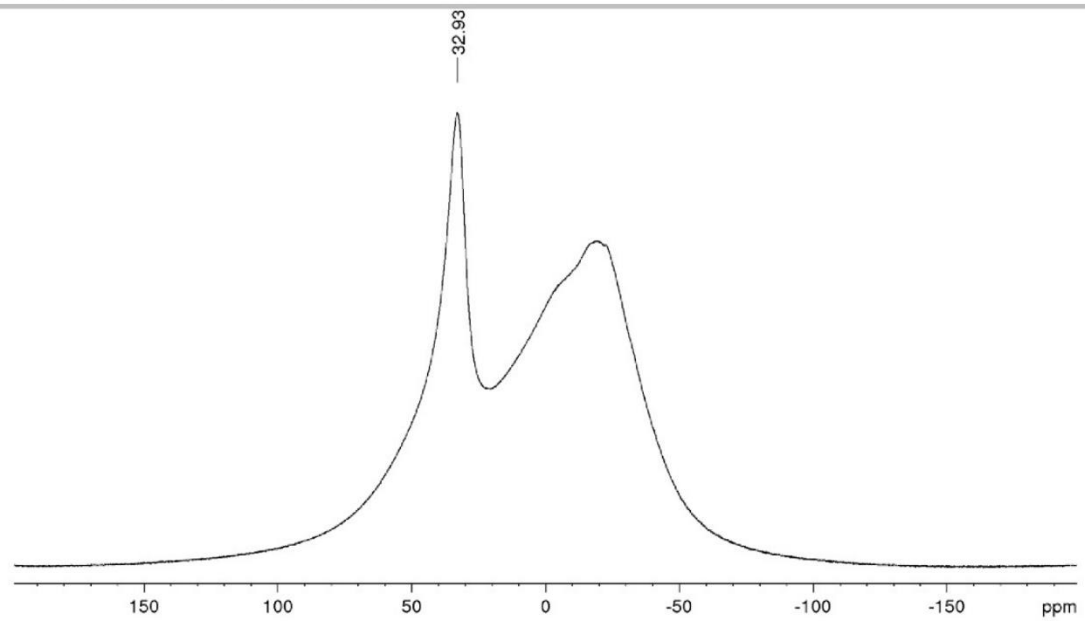

Figure S25. ^{11}B-NMR spectrum (128.4 MHz) of 1-phenyl-2,3-diduryl-diboriranide-chlorozincate **7** (glass peak from 70 to −50 ppm).

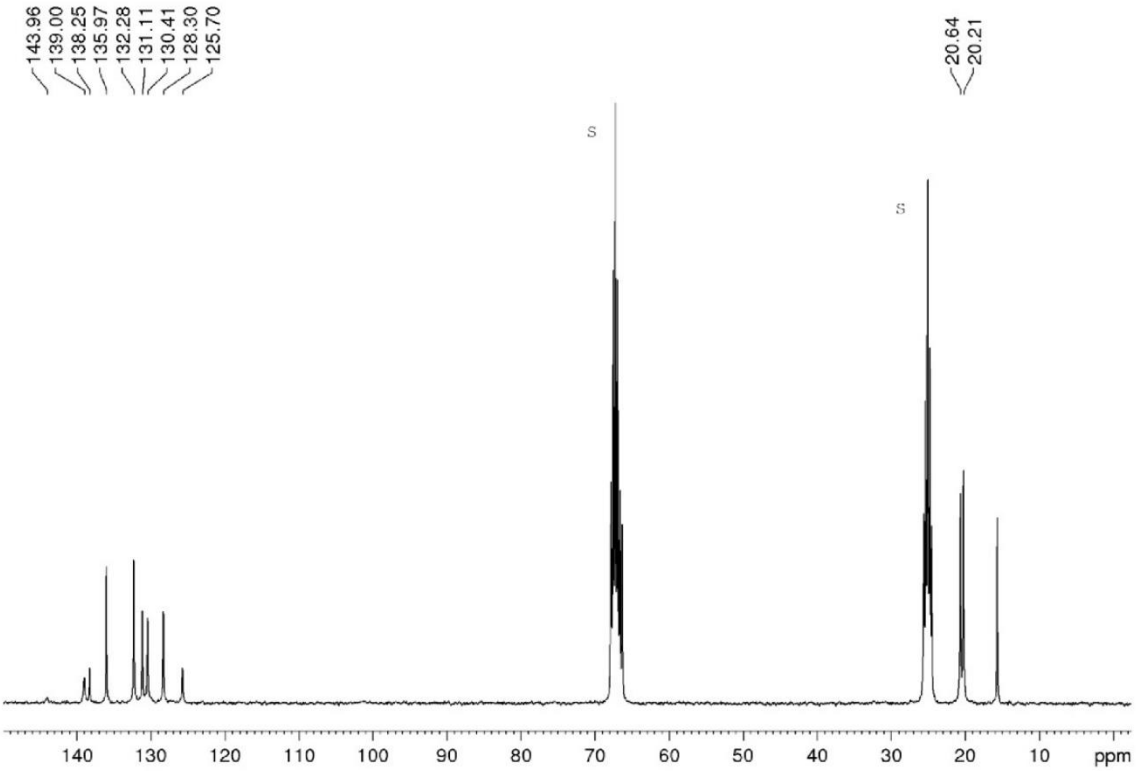

Figure S26. ^{13}C-NMR spectrum (75.47 MHz) of 1-phenyl-2,3-diduryl-diboriranide-chlorozincate **7** at 223 K in thf-d_8 (=s).

3.8. NMR spectra of 1-phenyl-2,3-diduryl-diboriranide-trimethylstannane 8

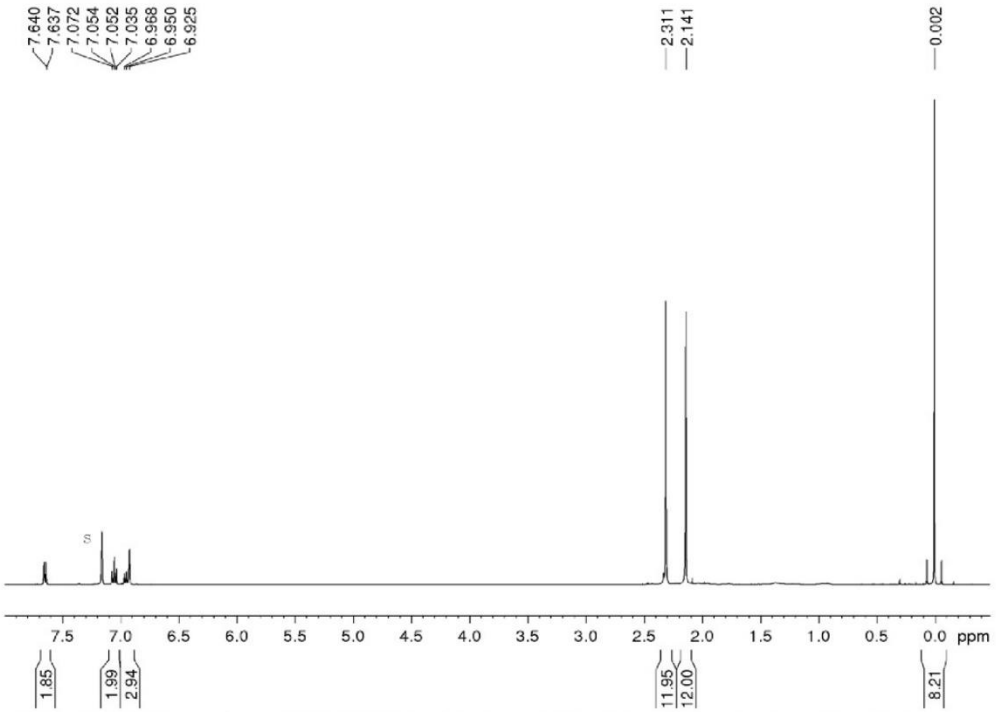

Figure S27. ^{1}H-NMR spectrum (400.1 MHz) of 1-phenyl-2,3-diduryl-diboriranide-trimethylstannane **8** in C_6D_6 (=s).

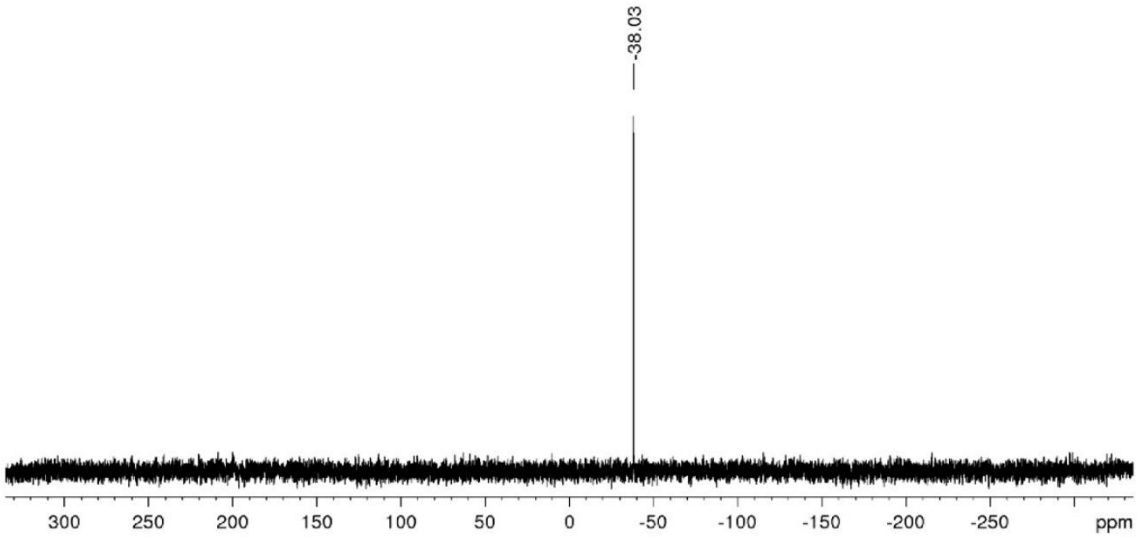

Figure S28. ^{119}Sn-NMR (149.21 MHz) spectrum of 1-phenyl-2,3-diduryl-diboriranide-trimethylstannane **8** in C_6D_6.

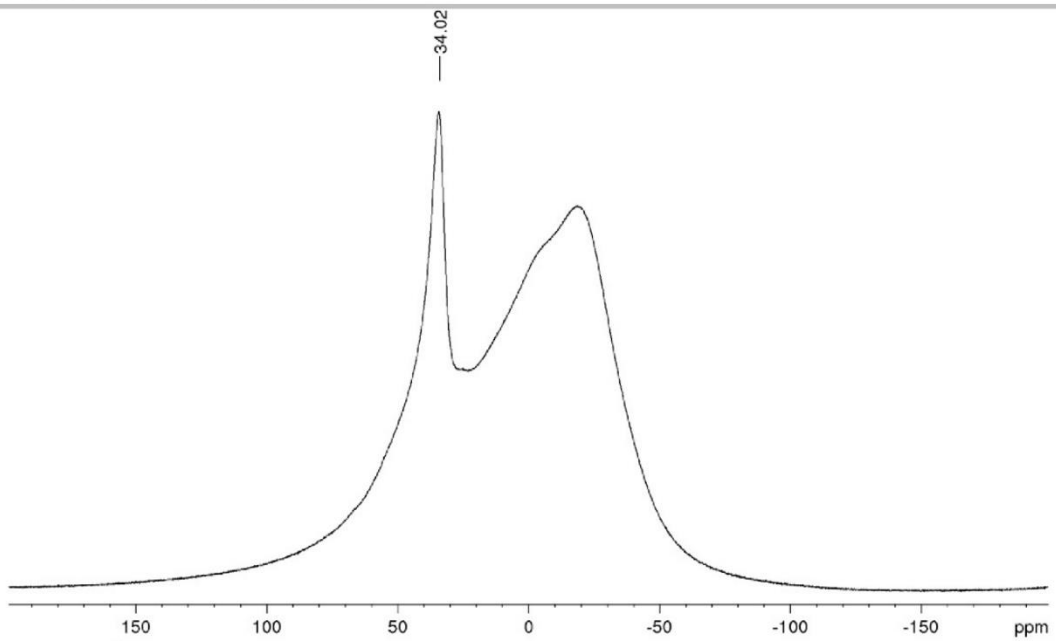

Figure S29. ^{11}B-NMR spectrum (128.4 MHz) of 1-phenyl-2,3-diduryl-diboriranide-trimethylstannane **8** (glass peak from 70 to −50 ppm).

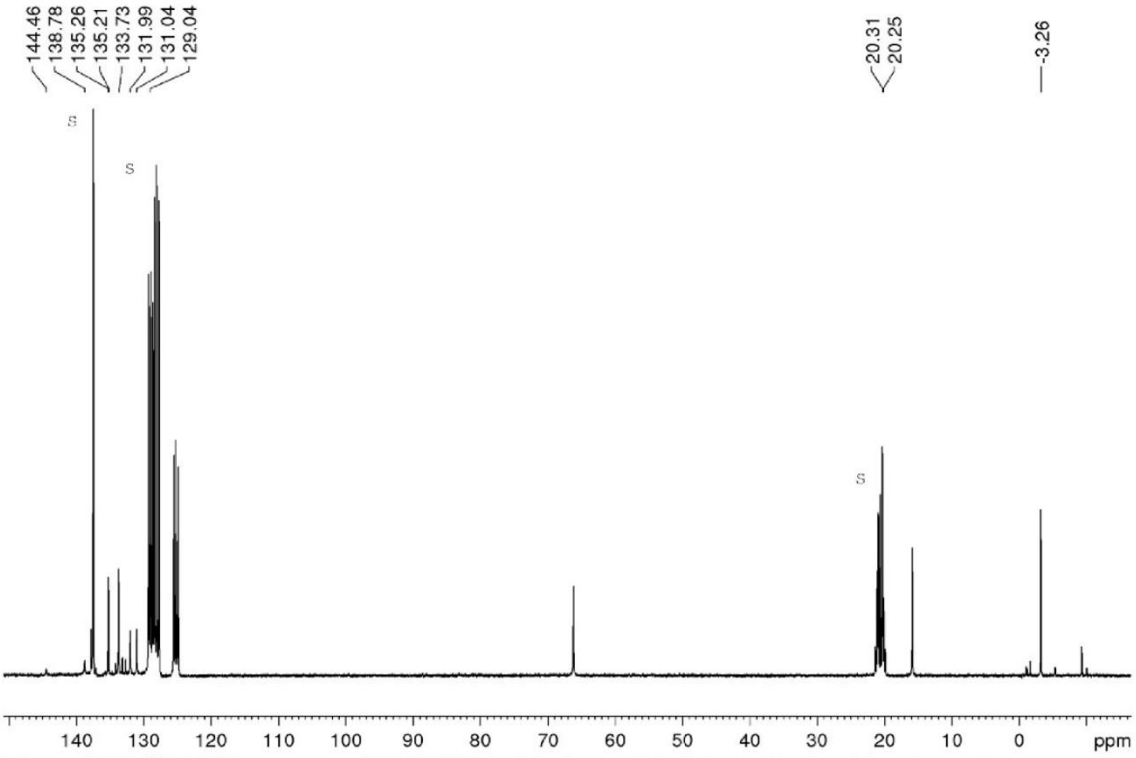

Figure S30. ^{13}C-NMR spectrum (75.47 MHz) of 1-phenyl-2,3-diduryl-diboriranide-trimethylstannane **8** at 233 K in toluene-d_8 (=s).

4. Crystallographic data

The data set was collected using a Bruker D8 Venture diffractometer with a microfocus sealed tube and a Photon II detector. Monochromated $Mo_{K\alpha}$ radiation (λ = 0.71073 Å) was used. Data were collected at 133(2) K and corrected for absorption effects using the multi-scan method. The structure was solved by direct methods using SHELXT [S4] and was refined by full matrix least squares calculations on F^2 (SHELXL2018 [S5]) in the graphical user interface Shelxle [S6].

Acknowledgment: Instrumentation and technical assistance for this work were provided by the Service Center X-ray Diffraction, with financial support from Saarland University and German Science Foundation (project number INST 256/506-1).

4.1. Crystal structure of 1-benzyl-2-chloro-1,2-diduryldiborane(4) 1

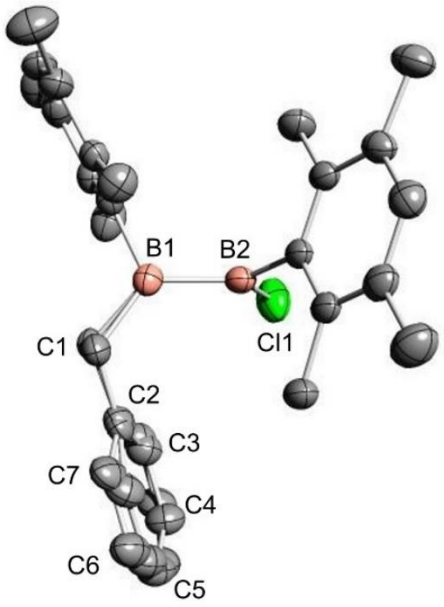

Refinement: All non H-atoms were located in the electron density maps and refined anisotropically. C-bound H atoms were placed in positions of optimized geometry and treated as riding atoms. Their isotropic displacement parameters were coupled to the corresponding carrier atoms by a factor of 1.2 (CH, CH2) or 1.5 (CH3). *Disorder:* The benzyl ring (C1A-C7A, C1B-C7B) is split over two positions. Its occupancy factors refined to 0.77 for the major (A) component. For the refinement of the disorder some similarity restraints were applied to the anisotropic displacement parameters of the disordered atoms.

SUPPORTING INFORMATION

Table S1. Crystal data and structure refinement for sh4878_a.

CCDC Deposition Number	2269482	
Identification code	sh4878_a	
Empirical formula	C27 H33 B2 Cl	
Formula weight	414.60	
Temperature	133(2) K	
Wavelength	0.71073 Å	
Crystal system	Monoclinic	
Space group	$P2_1/n$	
Unit cell dimensions	a = 11.6099(6) Å	a= 90°.
	b = 14.1606(7) Å	b= 92.579(2)°.
	c = 14.8880(7) Å	g = 90°.
Volume	2445.2(2) $Å^3$	
Z	4	
Density (calculated)	1.126 Mg/m^3	
Absorption coefficient	0.167 mm^{-1}	
F(000)	888	
Crystal size	0.300 x 0.200 x 0.080 mm^3	
Theta range for data collection	1.986 to 26.730°.	
Index ranges	-14<=h<=14, -17<=k<=17, -18<=l<=18	
Reflections collected	26610	
Independent reflections	5184 [R(int) = 0.0652]	
Completeness to theta = 25.242°	99.8 %	
Absorption correction	Semi-empirical from equivalents	
Max. and min. transmission	0.7455 and 0.7019	
Refinement method	Full-matrix least-squares on F^2	
Data / restraints / parameters	5184 / 312 / 343	
Goodness-of-fit on F^2	1.040	
Final R indices [I>2sigma(I)]	R1 = 0.0505, wR2 = 0.1328	
R indices (all data)	R1 = 0.0730, wR2 = 0.1494	
Extinction coefficient	n/a	
Largest diff. peak and hole	0.281 and -0.422 $e.Å^{-3}$	

4.2. Crystal structure of 1-phenyl-2,3-diduryldiborirane 2

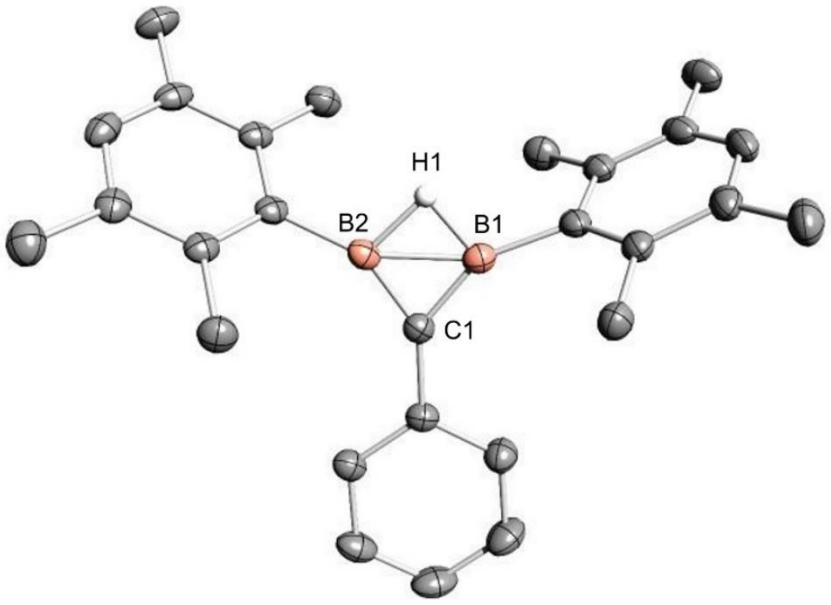

Refinement: All non H-atoms were located on the electron density maps and refined anisotropically. C-bound H atoms were placed in positions of optimized geometry and treated as riding atoms. Their isotropic displacement parameters were coupled to the corresponding carrier atoms by a factor of 1.2 (CH) or 1.5 (CH3). H1 was located on the electron density maps. Its isotropic displacement parameter was coupled on its parent atom by a factor of -1.2.

Table S2. Crystal data and structure refinement for sh4726_a.

CCDC Deposition Number	2269486	
Identification code	sh4726_a	
Empirical formula	C27 H32 B2	
Formula weight	378.14	
Temperature	133(2) K	
Wavelength	0.71073 Å	
Crystal system	Triclinic	
Space group	P-1	
Unit cell dimensions	a = 7.4892(3) Å	a= 76.726(2)°.
	b = 10.5117(5) Å	b= 78.055(2)°.
	c = 14.7867(7) Å	g = 85.874(2)°.
Volume	1108.07(9) Å^3	
Z	2	

Density (calculated)	1.133 Mg/m^3
Absorption coefficient	0.062 mm^{-1}
F(000)	408
Crystal size	0.309 x 0.265 x 0.142 mm^3
Theta range for data collection	1.991 to 27.170°.
Index ranges	-9<=h<=9, -13<=k<=13, -18<=l<=18
Reflections collected	22477
Independent reflections	4859 [R(int) = 0.0412]
Completeness to theta = 25.242°	99.5 %
Absorption correction	Semi-empirical from equivalents
Max. and min. transmission	0.7455 and 0.7164
Refinement method	Full-matrix least-squares on F^2
Data / restraints / parameters	4859 / 0 / 273
Goodness-of-fit on F^2	1.024
Final R indices [I>2sigma(I)]	R1 = 0.0473, wR2 = 0.1074
R indices (all data)	R1 = 0.0701, wR2 = 0.1219
Extinction coefficient	n/a
Largest diff. peak and hole	0.202 and -0.197 $e.Å^{-3}$

4.3. Crystal structure of 1-phenyl-2,3-diduryldiboriranide 3

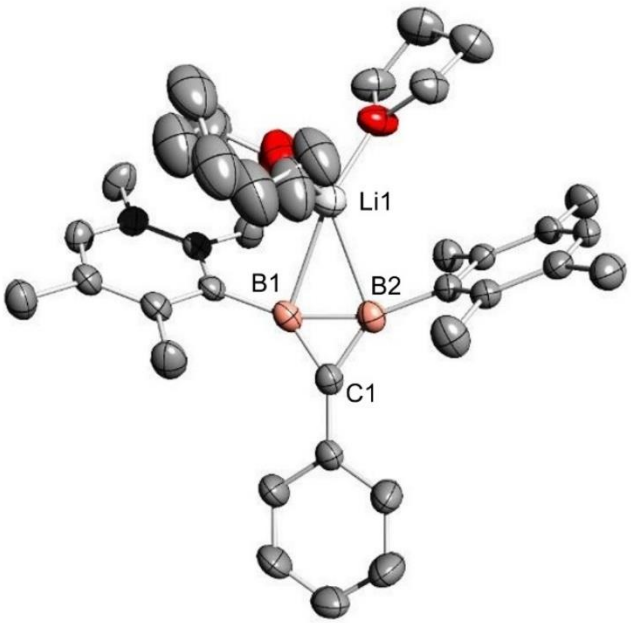

SUPPORTING INFORMATION

Refinement: All non H-atoms were located in the electron density maps and refined anisotropically. C-bound H atoms were placed in positions of optimized geometry and treated as riding atoms. Their isotropic displacement parameters were coupled to the corresponding carrier atoms by a factor of 1.2 (CH, CH2) or 1.5 (CH3). *Disorder*: One of the both Li1 coordinated thf molecules is split over two positions. Its occupancy factors refined to 0.54 for the major component.

Table S3. Crystal data and structure refinement for sh5077_a.

CCDC Deposition Number	2269489	
Identification code	sh5077_a	
Empirical formula	C35 H47 B2 Li O2	
Formula weight	528.28	
Temperature	153(2) K	
Wavelength	0.71073 Å	
Crystal system	Monoclinic	
Space group	$P2_1/c$	
Unit cell dimensions	a = 15.0363(5) Å	a= 90°.
	b = 13.6944(4) Å	b= 108.8270(10)°.
	c = 16.2642(5) Å	g = 90°.
Volume	3169.83(17) $Å^3$	
Z	4	
Density (calculated)	1.107 Mg/m^3	
Absorption coefficient	0.065 mm^{-1}	
F(000)	1144	
Crystal size	0.220 x 0.180 x 0.160 mm^3	
Theta range for data collection	1.990 to 25.024°.	
Index ranges	-17<=h<=17, -16<=k<=16, -19<=l<=18	
Reflections collected	24033	
Independent reflections	5597 [R(int) = 0.0591]	
Completeness to theta = 25.024°	99.8 %	
Absorption correction	Semi-empirical from equivalents	
Max. and min. transmission	0.7456 and 0.6895	
Refinement method	Full-matrix least-squares on F^2	
Data / restraints / parameters	5597 / 184 / 415	
Goodness-of-fit on F^2	1.025	
Final R indices [I>2sigma(I)]	R1 = 0.0640, wR2 = 0.1532	
R indices (all data)	R1 = 0.0943, wR2 = 0.1764	
Extinction coefficient	n/a	
Largest diff. peak and hole	0.569 and -0.381 $e.Å^{-3}$	

4.4. Crystal structure of 1-phenyl-2,3-diduryl-gold-triphenylphosphine-diboriranide 4

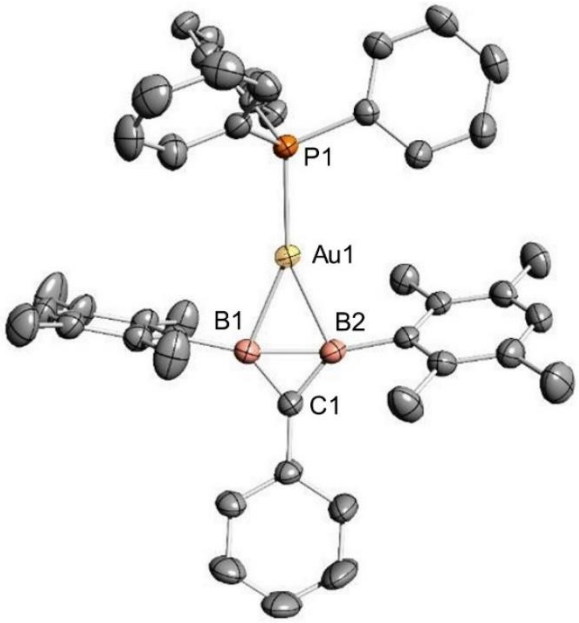

Refinement: All non H-atoms were located in the electron density maps and refined anisotropically. C-bound H atoms were placed in positions of optimized geometry and treated as riding atoms. Their isotropic displacement parameters were coupled to the corresponding carrier atoms by a factor of 1.2 (CH) or 1.5 (CH3).

Table S4. Crystal data and structure refinement for sh5002_a.

CCDC Deposition Number	2269491	
Identification code	sh5002_a	
Empirical formula	C45 H46 Au B2 P	
Formula weight	836.37	
Temperature	153(2) K	
Wavelength	0.71073 Å	
Crystal system	Monoclinic	
Space group	$P2_1/n$	
Unit cell dimensions	a = 11.7189(4) Å	a= 90°.
	b = 16.7177(6) Å	b= 101.4250(10)°.
	c = 20.5533(7) Å	g = 90°.
Volume	3946.9(2) $Å^3$	
Z	4	
Density (calculated)	1.408 Mg/m^3	

Absorption coefficient	3.797 mm^{-1}
F(000)	1680
Crystal size	0.220 x 0.160 x 0.100 mm^3
Theta range for data collection	2.022 to 28.718°.
Index ranges	-15<=h<=15, -22<=k<=22, -27<=l<=27
Reflections collected	97154
Independent reflections	10204 [R(int) = 0.0594]
Completeness to theta = 25.242°	100.0 %
Absorption correction	Semi-empirical from equivalents
Max. and min. transmission	0.7458 and 0.6326
Refinement method	Full-matrix least-squares on F^2
Data / restraints / parameters	10204 / 0 / 450
Goodness-of-fit on F^2	1.048
Final R indices [I>2sigma(I)]	R1 = 0.0225, wR2 = 0.0490
R indices (all data)	R1 = 0.0297, wR2 = 0.0523
Extinction coefficient	n/a
Largest diff. peak and hole	0.334 and -0.738 $e.Å^{-3}$

4.5. Crystal structure of 1-phenyl-2,3-diduryl-(bis)diboriranide-cuprate 5

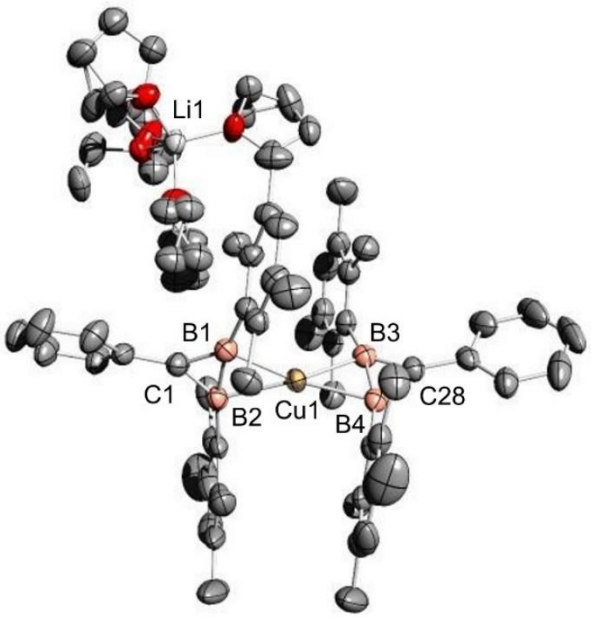

Refinement: All non H-atoms were located in the electron density maps and refined anisotropically. C-bound H atoms were placed in positions of optimized geometry and treated

as riding atoms. Their isotropic displacement parameters were coupled to the corresponding carrier atoms by a factor of 1.2 (CH, CH2) or 1.5 (CH3). *Disorder*: The Li1 cation is surrounded by four coordinated thf molecules. One of them is split over two positions (refined occupancy factors = 0.62 for the major component) and at two further thf molecules only one carbon atom is split over two positions (refined occupancy factors = 0.68 and 0.76, respectively). The fourth thf molecule shares its position with one coordinated diethyl ether molecule, with refined occupancy factors of 0.50 for each molecule.

Table S5. Crystal data and structure refinement for sh5069_a.

CCDC Deposition Number	2269493	
Identification code	sh5069_a	
Empirical formula	C70 H95 B4 Cu Li O4	
Formula weight	1114.17	
Temperature	153(2) K	
Wavelength	0.71073 Å	
Crystal system	Monoclinic	
Space group	$P2_1/n$	
Unit cell dimensions	a = 15.3464(6) Å	a= 90°.
	b = 20.6197(7) Å	b= 92.395(2)°.
	c = 20.5566(9) Å	g = 90°.
Volume	6499.2(4) $Å^3$	
Z	4	
Density (calculated)	1.139 Mg/m^3	
Absorption coefficient	0.382 mm^{-1}	
F(000)	2396	
Crystal size	0.280 x 0.260 x 0.200 mm^3	
Theta range for data collection	1.983 to 26.372°.	
Index ranges	-19<=h<=19, -25<=k<=22, -25<=l<=25	
Reflections collected	147163	
Independent reflections	13274 [R(int) = 0.0701]	
Completeness to theta = 25.242°	99.9 %	
Absorption correction	Semi-empirical from equivalents	
Max. and min. transmission	0.7456 and 0.7146	
Refinement method	Full-matrix least-squares on F^2	
Data / restraints / parameters	13274 / 262 / 842	
Goodness-of-fit on F^2	1.027	
Final R indices [I>2sigma(I)]	R1 = 0.0524, wR2 = 0.1313	
R indices (all data)	R1 = 0.0757, wR2 = 0.1478	
Extinction coefficient	n/a	

Largest diff. peak and hole	0.526 and -0.342 e.Å^{-3}

4.6. Crystal structure of 1-phenyl-2,3-diduryl-diboriranide-chlorocuprate 6

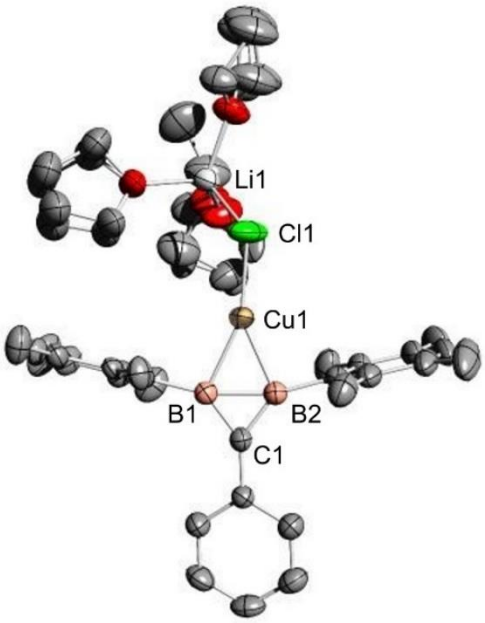

Refinement: All non H-atoms were located in the electron density maps and refined anisotropically. C-bound H atoms were placed in positions of optimized geometry and treated as riding atoms. Their isotropic displacement parameters were coupled to the corresponding carrier atoms by a factor of 1.2 (CH, CH2) or 1.5 (CH3). Disorder: The Li1 is surrounded by three coordinated thf molecules. Two of these thf molecules are split over two positions with refined occupancy factors of 0.60 and 0.57, respectively for the major component. The third thf molecule shares its position with a diethyl ether molecule. Their occupancy factors were each constrained to 0.5.

Table S6. Crystal data and structure refinement for 5067_a.

CCDC Deposition Number	2269495
Identification code	5067_a
Empirical formula	C39 H56 B2 Cl Cu Li O3
Formula weight	700.38
Temperature	153(2) K
Wavelength	0.71073 Å
Crystal system	Monoclinic
Space group	$P2_1/c$
Unit cell dimensions	a = 18.7166(4) Å a= 90°.

	b = 12.4415(3) Å	b= 116.3480(10)°.
	c = 18.7007(4) Å	g = 90°.
Volume	3902.30(15) $Å^3$	
Z	4	
Density (calculated)	1.192 Mg/m^3	
Absorption coefficient	0.662 mm^{-1}	
F(000)	1492	
Crystal size	0.220 x 0.180 x 0.080 mm^3	
Theta range for data collection	2.039 to 25.681°.	
Index ranges	-22<=h<=22, -15<=k<=15, -22<=l<=22	
Reflections collected	61137	
Independent reflections	7386 [R(int) = 0.0442]	
Completeness to theta = 25.242°	99.7 %	
Absorption correction	Semi-empirical from equivalents	
Max. and min. transmission	0.7458 and 0.7188	
Refinement method	Full-matrix least-squares on F^2	
Data / restraints / parameters	7386 / 533 / 568	
Goodness-of-fit on F^2	1.031	
Final R indices [I>2sigma(I)]	R1 = 0.0594, wR2 = 0.1608	
R indices (all data)	R1 = 0.0701, wR2 = 0.1706	
Extinction coefficient	n/a	
Largest diff. peak and hole	1.111 and -0.831 $e.Å^{-3}$	

4.7. Crystal structure of 1-phenyl-2,3-diduryl-diboriranide-chlorozincate 7

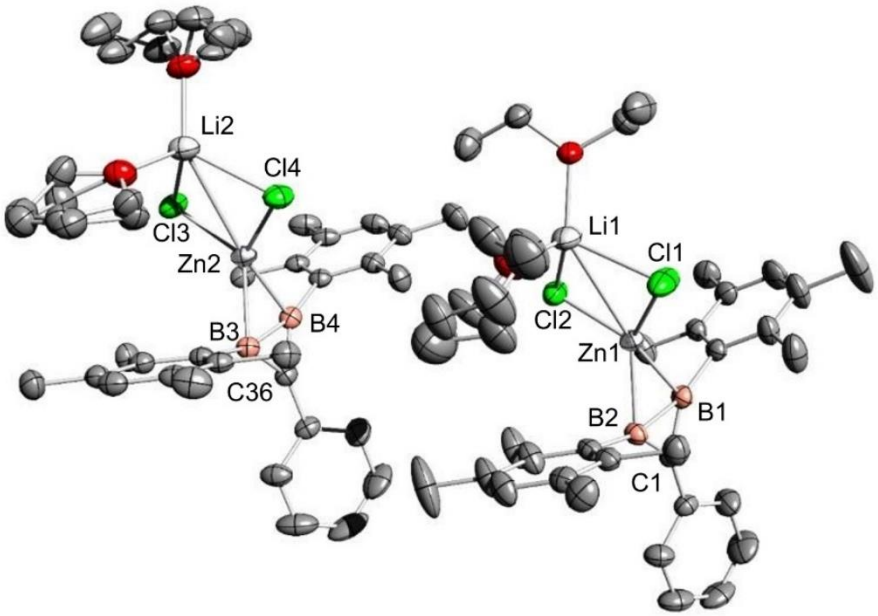

Two independent molecules share one unit cell. *Refinement:* All non H-atoms were located in the electron density maps and refined anisotropically. C-bound H atoms were placed in positions of optimized geometry and treated as riding atoms. Their isotropic displacement parameters were coupled to the corresponding carrier atoms by a factor of 1.2 (CH, CH2) or 1.5 (CH3). *Disorder*: One thf and one diethyl ether share their coordination position of Li1. The occupancy factors refined to 0.7 for thf and 0.3 for diethyl ether. Li2 is coordinated from one thf and one diethyl ether, which are each split over two positions. The occupancy factors refined to 0.54 and 0.78, respectively for the major component.

Table S7. Crystal data and structure refinement for sh5079_a.

CCDC Deposition Number	2269501	
Identification code	sh5079_a	
Empirical formula	C70 H98.58 B4 Cl4 Li2 O4 Zn2	
Formula weight	1333.73	
Temperature	153(2) K	
Wavelength	0.71073 Å	
Crystal system	Triclinic	
Space group	P-1	
Unit cell dimensions	a = 12.0502(3) Å	a= 96.6320(10)°.
	b = 12.5284(2) Å	b= 90.4900(10)°.
	c = 25.0060(6) Å	g = 103.8560(10)°.
Volume	3638.20(14) Å^3	

Z	2
Density (calculated)	1.217 Mg/m^3
Absorption coefficient	0.850 mm^{-1}
F(000)	1409
Crystal size	0.220 x 0.180 x 0.100 mm^3
Theta range for data collection	1.953 to 27.910°.
Index ranges	-15<=h<=15, -16<=k<=16, -32<=l<=32
Reflections collected	151836
Independent reflections	17374 [R(int) = 0.0411]
Completeness to theta = 25.242°	99.9 %
Absorption correction	Semi-empirical from equivalents
Max. and min. transmission	0.7456 and 0.7107
Refinement method	Full-matrix least-squares on F^2
Data / restraints / parameters	17374 / 305 / 910
Goodness-of-fit on F^2	1.044
Final R indices [I>2sigma(I)]	R1 = 0.0344, wR2 = 0.0837
R indices (all data)	R1 = 0.0450, wR2 = 0.0899
Extinction coefficient	n/a
Largest diff. peak and hole	0.468 and -0.428 $e.Å^{-3}$

4.8. Crystal structure of 1-phenyl-2,3-diduryl-diboriranide-trimethylstannane 8

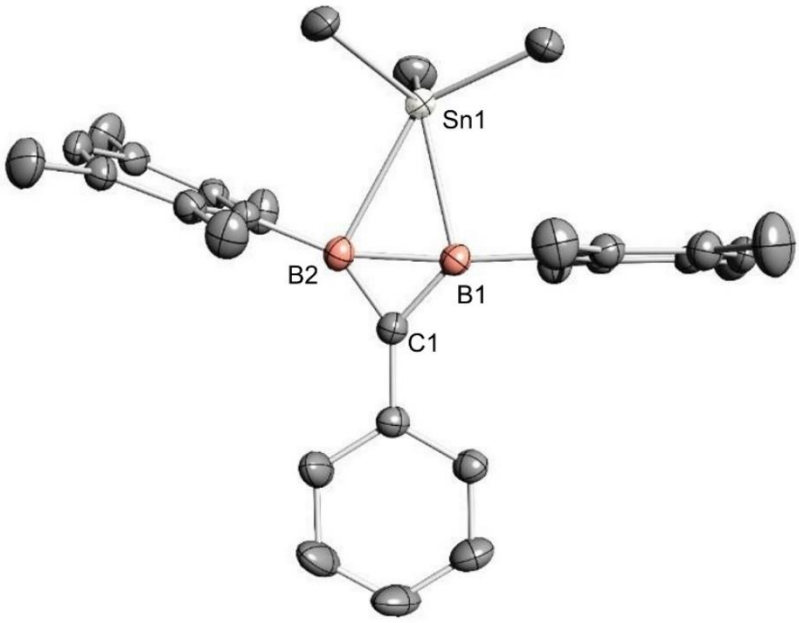

Refinement: All non H-atoms were located in the electron density maps and refined anisotropically. C-bound H atoms were placed in positions of optimized geometry and treated as riding atoms. Their isotropic displacement parameters were coupled to the corresponding carrier atoms by a factor of 1.2 (CH) or 1.5 (CH3).

Table S8. Crystal data and structure refinement for sh5001_a.

CCDC Deposition Number	2269505	
Identification code	sh5001_a	
Empirical formula	C30 H40 B2 Sn	
Formula weight	540.93	
Temperature	153(2) K	
Wavelength	0.71073 Å	
Crystal system	Triclinic	
Space group	P-1	
Unit cell dimensions	a = 9.1041(3) Å	a= 111.6920(10)°.
	b = 11.9303(4) Å	b= 102.8680(10)°.
	c = 14.3871(5) Å	g = 94.6600(10)°.
Volume	1392.26(8) $Å^3$	
Z	2	
Density (calculated)	1.290 Mg/m^3	

Absorption coefficient	0.933 mm^{-1}
F(000)	560
Crystal size	0.210 x 0.120 x 0.100 mm^3
Theta range for data collection	1.907 to 27.904°.
Index ranges	-11<=h<=10, -15<=k<=15, -18<=l<=18
Reflections collected	37342
Independent reflections	6619 [R(int) = 0.0462]
Completeness to theta = 25.242°	99.5 %
Absorption correction	Semi-empirical from equivalents
Max. and min. transmission	0.7456 and 0.7068
Refinement method	Full-matrix least-squares on F^2
Data / restraints / parameters	6619 / 0 / 309
Goodness-of-fit on F^2	1.068
Final R indices [I>2sigma(I)]	R1 = 0.0220, wR2 = 0.0567
R indices (all data)	R1 = 0.0237, wR2 = 0.0578
Extinction coefficient	n/a
Largest diff. peak and hole	0.381 and -0.545 $e.Å^{-3}$

5. DFT Calculations

Computations were carried out with the Gaussian 09 program package.[S7] Structural optimizations and frequency analyses were performed at the BP86/def2SVP level of theory[S8,S9] including the dispersion correction by Grimme.[S10] Single point calculations were run with the the Gaussian 09 program package at the B3LYP/def2TZVPP level of theory.[S8,S9] Pictures of Kohn-Sham orbitals were displayed with ChemCraft.[S11] NBO calculations were run with the NBO 7.0 program package at the B3LYP/def2TZVPP level of theory.[S12]

5.1. Molecular orbitals of 1-phenyl-2,3-diduryldiborirane 2

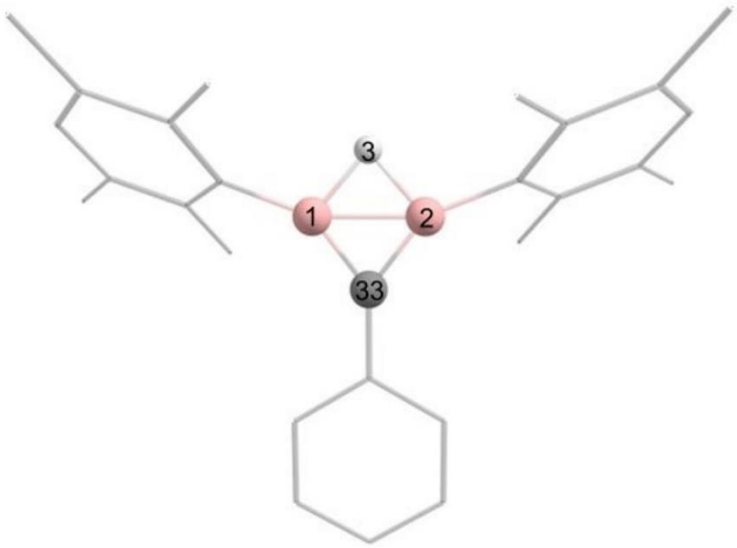

Table S9. Coordinates of the optimized structure of 1-phenyl-2,3-diduryldiborirane **2**.

5	0.903249064	-0.108445008	-0.092341007
5	-0.874733062	-0.148203011	-0.084821006
1	0.032113002	-1.121240081	0.213011016
6	2.367797171	-0.602840045	0.136393010
6	2.890441208	-1.688766122	-0.618728047
6	4.215692306	-2.132927152	-0.389145028
6	4.990328358	-1.471713104	0.581600040
6	4.501686325	-0.387102028	1.330433097
6	3.171784230	0.054765004	1.109503078
6	5.378920363	0.289947021	2.356493167
6	2.633714189	1.208009089	1.925619138

6	2.044758147	-2.367212171	-1.672918121
6	-2.325941166	-0.676548049	0.154934011
6	-2.804934203	-1.836229131	-0.515971037
6	-4.503926327	-0.405380029	1.260062091
6	-3.174870228	0.041762003	1.046279075
6	-2.686421196	1.263211092	1.791357128
6	-5.425017416	0.334094024	2.201166156
6	-0.009870001	0.977101072	-0.437687031
6	-0.040125003	2.372021170	-0.843948059
6	1.161270085	3.109800223	-0.998075071
6	1.131671080	4.460882319	-1.371539099
6	-1.271221089	3.032485220	-1.088100080
6	4.794553345	-3.292921237	-1.165127084
6	-1.927924139	-2.596917188	-1.483443106
6	-4.133440296	-2.278904162	-0.299181022
6	-4.952362357	-1.553603114	0.584249043
6	-4.666197334	-3.503500253	-1.004483074
6	-1.299618095	4.383096317	-1.463522107
6	-0.098752007	5.102979368	-1.603596113

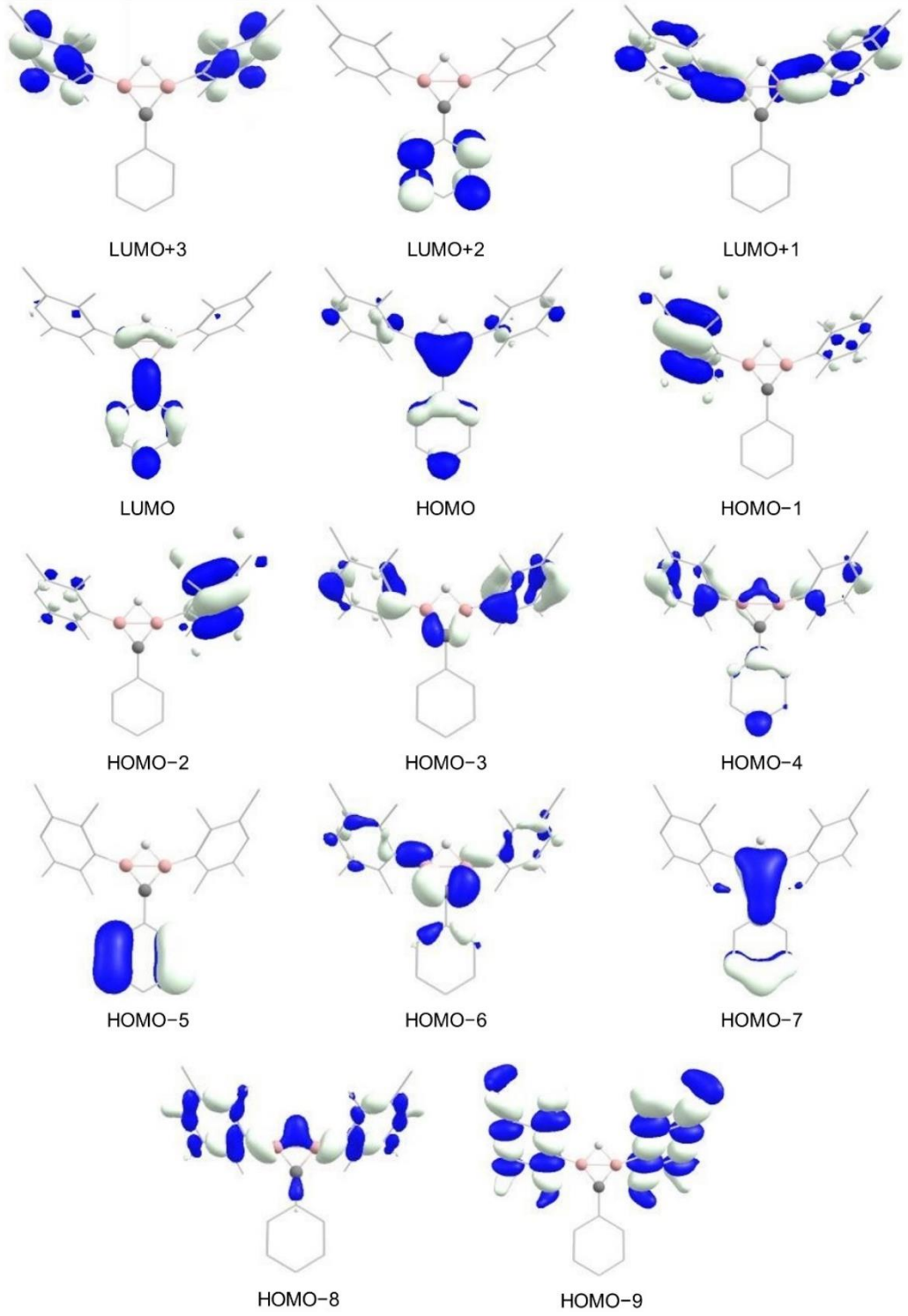

Figure S31. Selected molecular orbitals of 1-phenyl-2,3-diduryldiborirane **2**.

5.2. Molecular orbitals of 1-phenyl-2,3-diduryldiboriranide 3

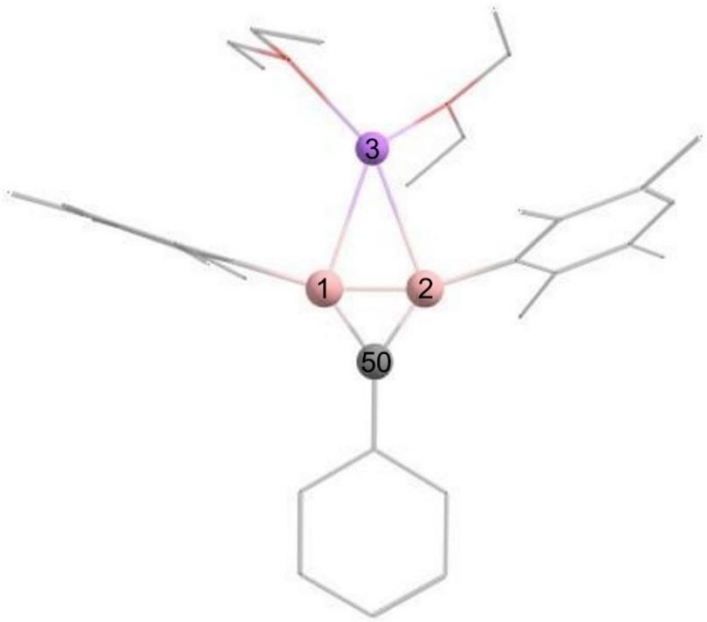

Table S10. Coordinates of the optimized structure of 1-phenyl-2,3-diduryldiboriranide **3**.

5	0.858189060	0.841515061	-0.323354023
5	-0.781055057	0.893113065	-0.193570014
3	-0.055156004	-1.427132101	0.212444015
6	-2.293121165	0.492297035	-0.065634004
6	-2.946419213	0.497146036	1.192231087
6	-4.286196310	0.072483005	1.303022091
6	-4.977510357	-0.306154022	0.147723010
6	-4.385287317	-0.241257018	-1.119359083
6	-3.038973219	0.159144011	-1.225612086
6	-2.415408174	0.315619023	-2.591862185
6	-5.192820371	-0.577853041	-2.348117170
6	-4.974953357	0.043321003	2.643859189
6	-2.238444164	1.017229075	2.420641176
6	2.337667168	0.317149023	-0.376076027
6	3.231450235	0.603983041	0.689739051
6	4.533024328	0.061989005	0.692896048
6	4.944726355	-0.734208054	-0.381841027
6	4.116133295	-0.967444069	-1.483766105

6	2.814068205	-0.428699031	-1.483748108
6	1.957898141	-0.580530043	-2.717249194
6	4.620352333	-1.770445128	-2.656249192
6	5.483901403	0.347822025	1.827797131
6	2.832314204	1.541210111	1.805320131
6	0.074039006	2.069458151	-0.321166023
6	0.103366008	3.521290256	-0.390397028
6	-1.082653079	4.278105307	-0.289019021
6	-1.054796077	5.671892414	-0.337725024
6	0.161815012	6.346597482	-0.490876035
6	1.349072096	5.613424414	-0.594996045
6	1.319277094	4.219406305	-0.544915039
8	-1.460466103	-2.786656199	-0.303890022
6	-2.466011177	-3.093149221	0.670499050
6	-1.965851141	-2.802739202	2.064973146
6	-1.945590140	-3.076658222	-1.618079118
6	-0.884328061	-2.834121202	-2.665230192
8	1.296607093	-2.278687162	1.422302104
6	2.277407162	-3.156828226	0.861520062
6	1.794287130	-3.719979268	-0.453914033
6	1.758299129	-1.740742123	2.665641194
6	0.753110053	-0.776481055	3.250551232

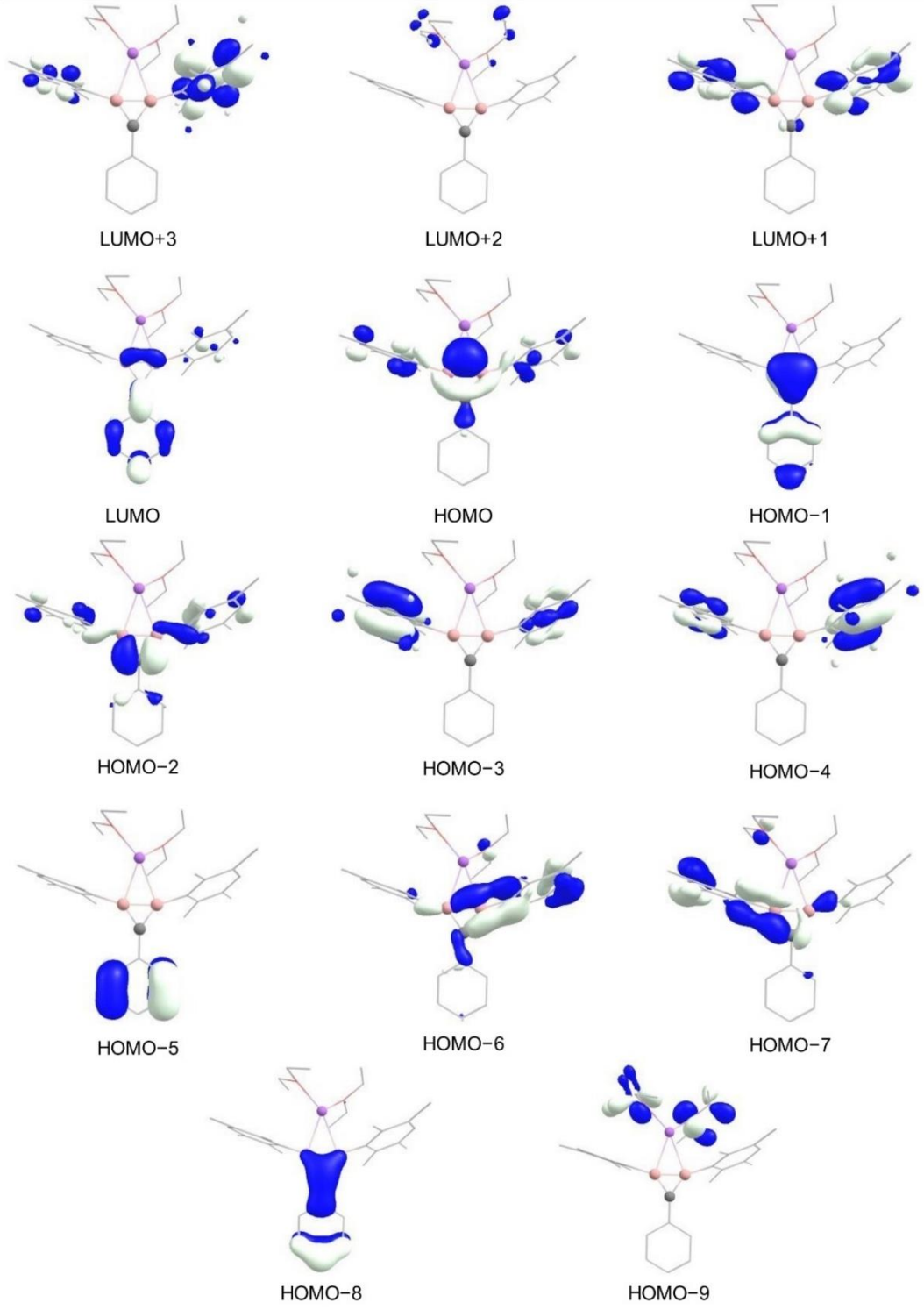

Figure S32. Selected molecular orbitals of 1-phenyl-2,3-diduryldiboriranide **3**.

5.3. Molecular orbitals of 1-phenyl-2,3-diduryl-gold-triphenylphosphine-diboriranide 4

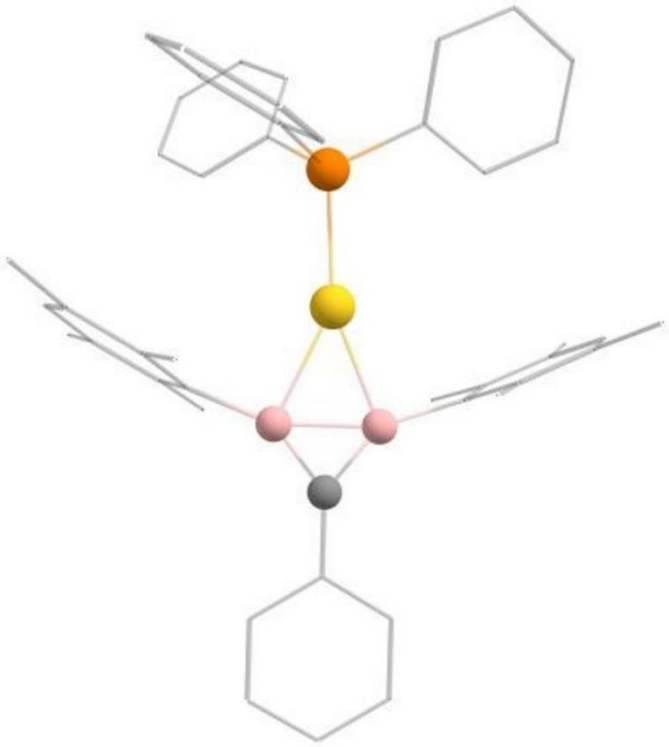

Table S11. Coordinates of the optimized structure of 1-phenyl-2,3-diduryl-gold-triphenylphosphine-diboriranide **4**.

79	0.124171003	0.079807065	0.002408062
15	-2.183550184	0.383059914	-0.027929940
6	3.229037277	-0.574133751	0.319238085
6	4.651582400	-0.851362663	0.459518095
6	5.127869532	-2.182874721	0.567687102
6	6.499021643	-2.449779639	0.691550113
6	5.600176409	0.202754485	0.481589097
6	1.100336272	-2.573051050	0.051757066
6	1.038403314	-3.219727102	-1.215014025
6	0.155573335	-4.312660248	-1.406115038
6	-0.651608692	-4.733168340	-0.332243962
6	-0.605361733	-4.112323293	0.931153130
6	0.288535248	-3.031904146	1.130007145
6	1.863933338	-2.700368006	-2.369364107

6	0.056041379	-4.998036306	-2.749119138
6	-1.514393768	-4.571807390	2.046002211
6	0.338827200	-2.334357090	2.469568238
6	2.124663996	2.096760358	-0.108469946
6	2.154686957	2.627210400	-1.428768042
6	1.848860835	3.994121479	-1.646225055
6	1.519136746	4.801702509	-0.541269976
6	1.474983784	4.297508469	0.772732115
6	1.788514907	2.934327396	0.992292132
6	2.462692045	1.722389357	-2.599487127
6	1.063814686	5.191172503	1.918688202
6	1.701480945	2.346802344	2.381927236
6	-2.699611357	2.131301000	-0.136277948
6	-4.009239480	2.540413933	0.200166076
6	-4.354299607	3.899005006	0.129366071
6	-3.394994607	4.850636143	-0.265856957
6	-2.087965485	4.445830211	-0.586528982
6	-1.734864356	3.088295142	-0.521513976
6	-2.983261173	-0.569684217	-1.366291037
6	-2.479078040	-1.871597269	-1.593265054
6	-3.058195021	-2.678857374	-2.582876126
6	-4.119905133	-2.186073418	-3.364041178
6	-4.606476263	-0.884312361	-3.150695167
6	-4.044065286	-0.073716259	-2.149222091
6	-2.927439191	-0.254640188	1.523199171
6	-3.822961172	-1.341201336	1.544608175
6	-4.274659167	-1.850598405	2.775142260
6	-3.839674182	-1.278124328	3.982033351
6	-2.946599197	-0.190345185	3.961137348
6	-2.485738201	0.316660886	2.738059259
5	1.931639233	-1.238250897	0.187201075
5	2.300949125	0.544084262	0.108225070
6	6.971045527	-0.064326431	0.606039107
6	7.427005653	-1.391819494	0.711577111
6	1.857046789	4.573985521	-3.041124155

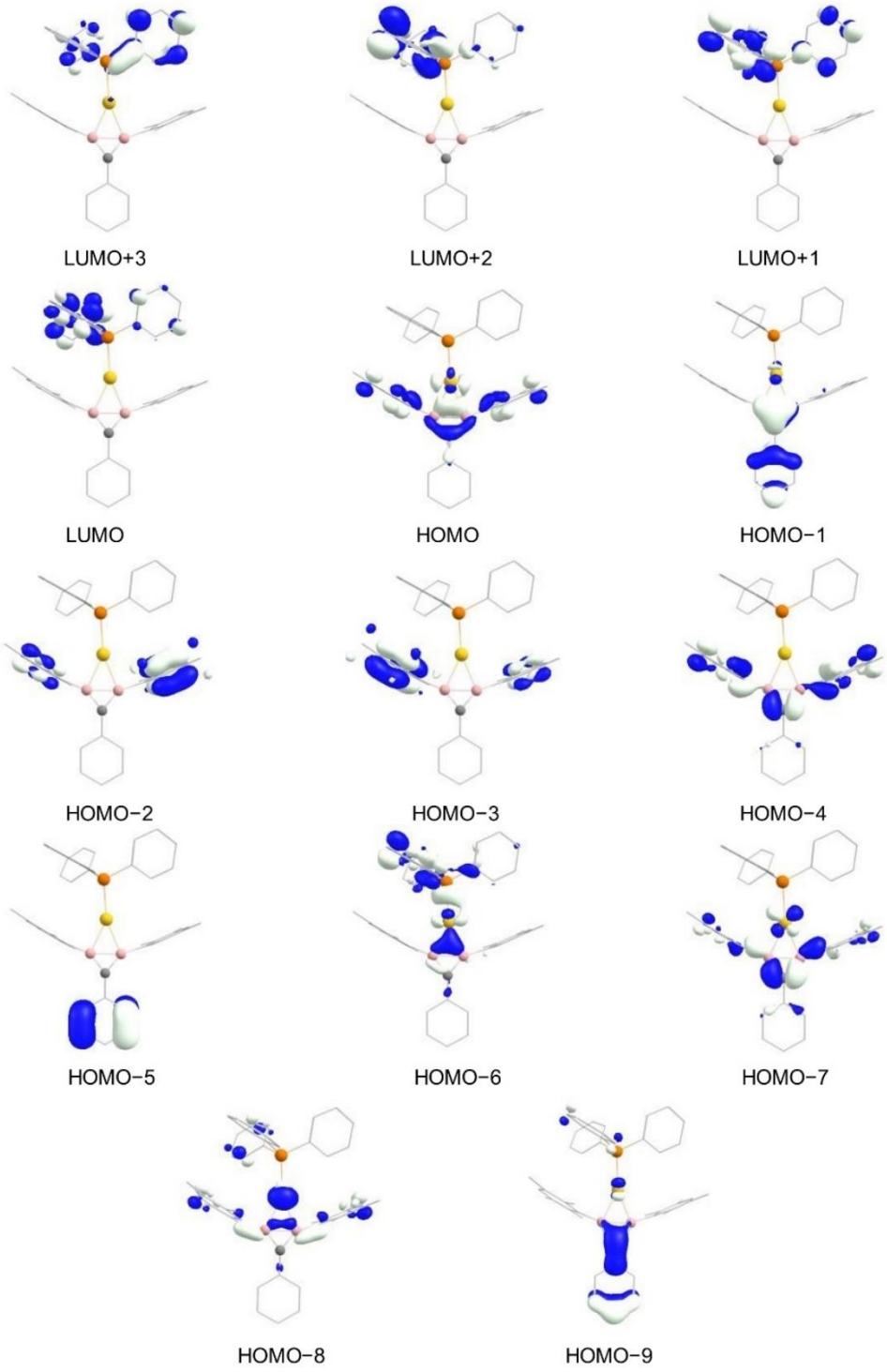

Figure S33. Selected molecular orbitals of gold-triphenylphosphine-diboriranide **4**.

5.4. Molecular orbitals of 1-phenyl-2,3-diduryl-(bis)diboriranide-cuprate 5

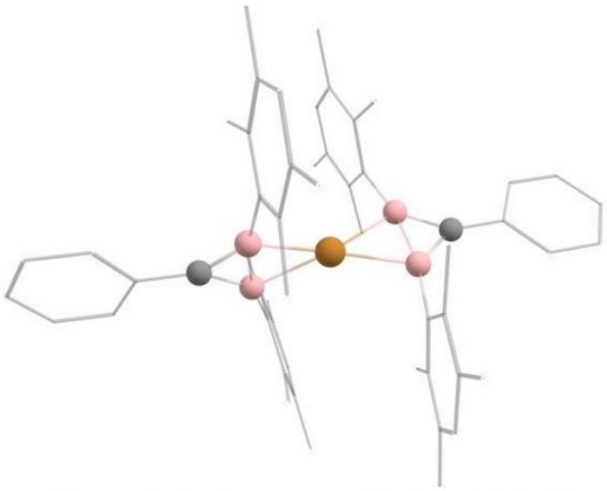

Table S12. Coordinates of the optimized structure of 1-phenyl-2,3-diduryl-(bis)diboriranide-cuprate **5**.

29	0.005379046	-0.028811002	-0.042770072
6	2.025519188	-0.403768037	-2.074559218
6	2.154119203	0.730112047	-2.921411280
6	2.162678206	0.555312033	-4.326298378
6	1.974260180	-1.891137145	-4.022312360
6	1.961998180	-1.715185132	-2.617330258
6	1.922585175	-2.878238212	-1.653703187
6	1.911773173	-3.266007240	-4.651486402
6	2.056472189	-0.750387061	-4.844881419
6	2.292521215	1.729308116	-5.272241447
6	2.315439221	2.084053140	-2.270349234
6	1.148640127	0.196644010	2.558020115
6	0.813832100	-0.941441072	3.339998173
6	0.308497065	-0.764013057	4.651168266
6	0.153342059	0.546379039	5.143698303
6	0.510024089	1.686884119	4.397180247
6	1.019339127	1.509263103	3.088131155
6	1.468009159	2.668527189	2.228767094
6	0.350026082	3.062270221	5.007288293
6	-0.058427965	-1.943314138	5.524682342
6	1.050612111	-2.309566168	2.743738130

6	3.098740270	-0.109645019	0.523026968
6	4.525826369	-0.121124025	0.774783989
6	5.455820454	-0.280341039	-0.287583089
6	6.837265550	-0.285427045	-0.045859072
6	7.329713558	-0.131705036	1.264476022
6	6.423331517	0.027266979	2.330476099
6	5.041698409	0.032372984	2.089621079
6	-1.769350091	-2.294129157	-0.024831071
6	-1.469622070	-3.132474219	-1.131579151
6	-1.333985067	-4.528563322	-0.934866134
6	-1.501206078	-5.046727360	0.363797957
6	-1.833767102	-4.237634296	1.468703038
6	-1.978528105	-2.843526195	1.270035023
6	-2.377832134	-1.901433129	2.382147103
6	-2.034474116	-4.873362342	2.827419135
6	-1.025417045	-5.463295400	-2.083610219
6	-1.350852058	-2.495417176	-2.496261251
6	-1.391655047	2.411325180	-0.589259113
6	-1.465460049	3.272196243	0.539771970
6	-1.101788017	4.633795335	0.404953960
6	-0.690415985	5.101163369	-0.859035130
6	-0.650910988	4.275191308	-1.999173215
6	-1.004895017	2.910730213	-1.861920205
6	-1.153054016	5.589257418	1.577205043
6	-1.967819087	2.692947200	1.842009064
6	-3.106716178	0.162640023	-0.454000102
5	1.773734171	0.004753994	1.137432010
5	2.075186193	-0.209446023	-0.523764107
5	-1.987093099	-0.760540046	-0.240915087
5	-1.854558085	0.924789076	-0.441196101
6	-4.546538282	0.259452035	-0.585990110
6	-5.370177349	-0.895606046	-0.506645106
6	-5.182532319	1.514199126	-0.785889123
6	-6.764772447	-0.799715032	-0.620365115
6	-6.577127412	1.609194142	-0.899577135
6	-7.376995493	0.453034059	-0.817502130
6	-1.025866021	1.959671144	-3.035777290
6	-0.243267954	4.857475351	-3.334641307

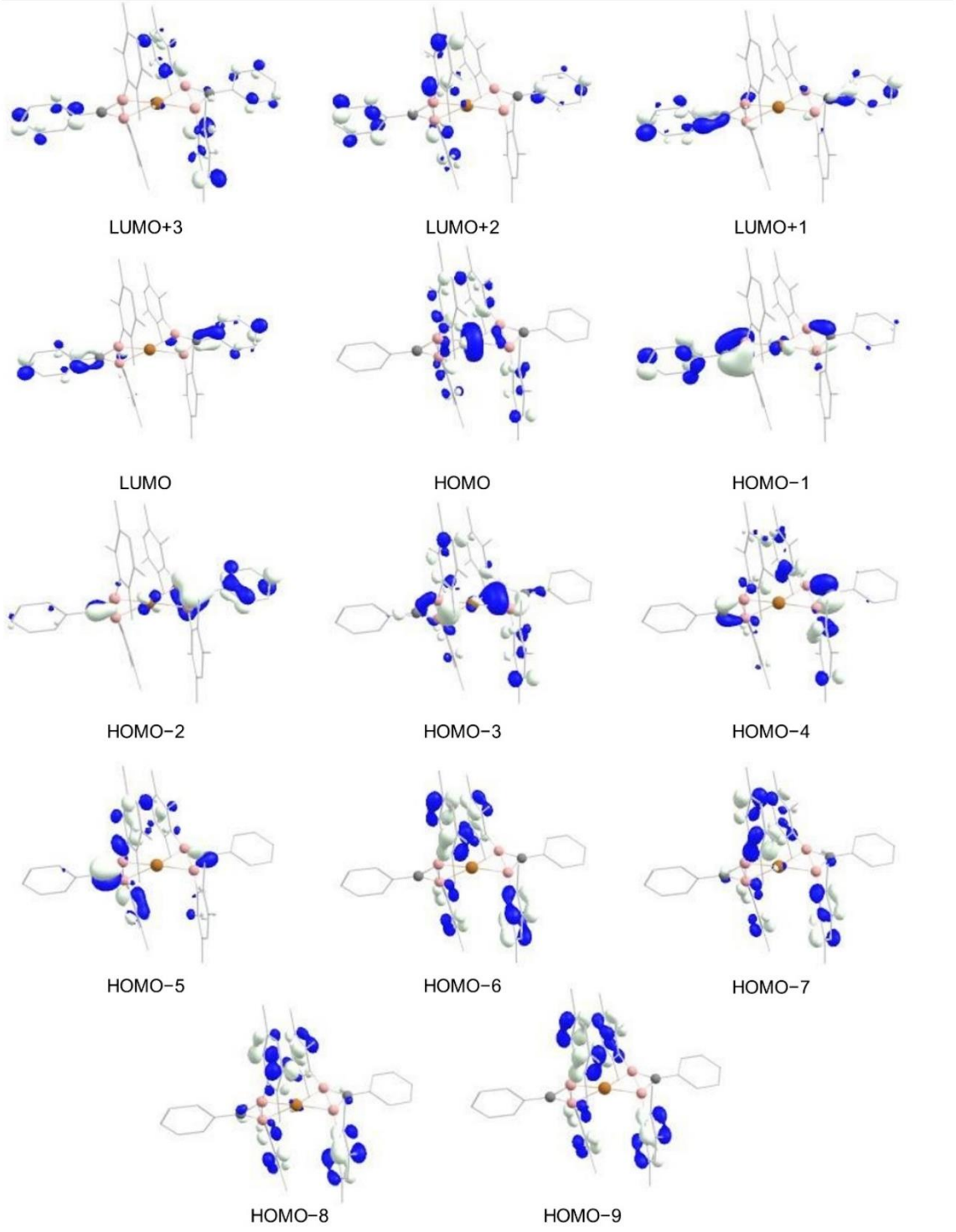

Figure S34. Selected molecular orbitals of (bis)diboriranide-cuprate **5**.

5.5. Molecular orbitals of 1-phenyl-2,3-diduryl-diboriranide-chlorocuprate 6

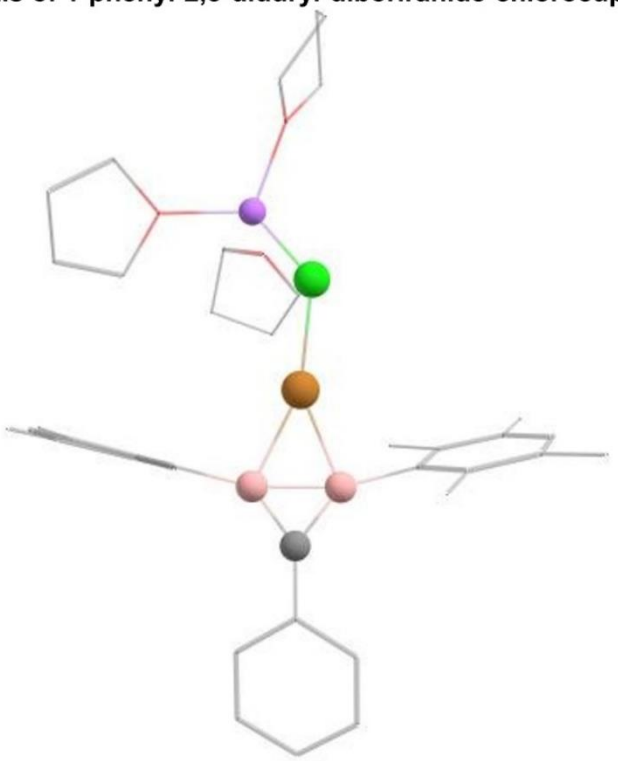

Table S13. Coordinates of the crystal structure of 1-phenyl-2,3-diduryl-diboriranide-chlorocuprate **6**.

29	-0.420704358	0.408054614	-0.676462481
17	1.474307485	1.286730216	-1.142136454
5	-1.854098859	-1.083894005	-0.359355751
5	-2.452472558	0.536241437	-0.295143426
3	3.347512099	0.778395957	0.181542290
6	-0.966611541	-2.392385646	-0.447252829
6	-0.612605170	-2.933974869	-1.688624821
6	0.152167160	-4.101433222	-1.753723206
6	0.570373010	-4.689830559	-0.582087751
6	0.246008924	-4.187686727	0.654399922
6	-0.547222728	-3.033642716	0.729973625
6	-0.958426344	-2.474082030	2.071075369
6	0.763138968	-4.878585369	1.908964385
6	0.538299349	-4.710382539	-3.081425040
6	-1.067542237	-2.260776301	-2.965845897

6	-2.598696594	2.107057496	-0.268713691
6	-2.456332102	2.807195139	0.940567723
6	-2.645873391	4.198078355	0.976099747
6	-2.946654660	4.843452112	-0.205122497
6	-3.078833527	4.191843848	-1.412769029
6	-2.908020995	2.797371160	-1.457525438
6	-3.063589433	2.029068803	-2.729575389
6	-3.390299884	4.975664518	-2.672190926
6	-2.514940948	4.982177436	2.255959396
6	-2.110026958	2.078568948	2.214860379
6	-3.227886533	-0.673073122	-0.149167587
6	-4.580417977	-1.131143866	0.130331787
6	-4.840286859	-2.454341205	0.502507097
6	-6.117031077	-2.872091093	0.817797347
6	-7.175770552	-1.981783890	0.767419885
6	-6.949886428	-0.680066093	0.381118224
6	-5.670474061	-0.257714786	0.074243898
8	2.739222629	0.878084839	2.040928374
6	3.295949459	0.141459298	2.973792869
6	2.133155957	-0.561874587	3.754996382
6	1.182247047	0.584436440	3.761096219
6	1.706794069	1.343328792	2.562396765
8	3.868730072	-1.015032492	-0.074537436
6	5.011200776	-1.512957750	-0.779692288
6	4.733749297	-2.887473783	-1.075252043
6	3.674430707	-3.306169740	0.142572885
6	2.971913020	-2.104487891	0.236623186
8	4.780339702	1.989615268	-0.252190328
6	5.227952841	1.943949272	-1.610320633
6	6.045559922	3.144795206	-1.825026999
6	6.669701045	3.321184694	-0.410758064
6	5.453299665	3.039987535	0.438206019

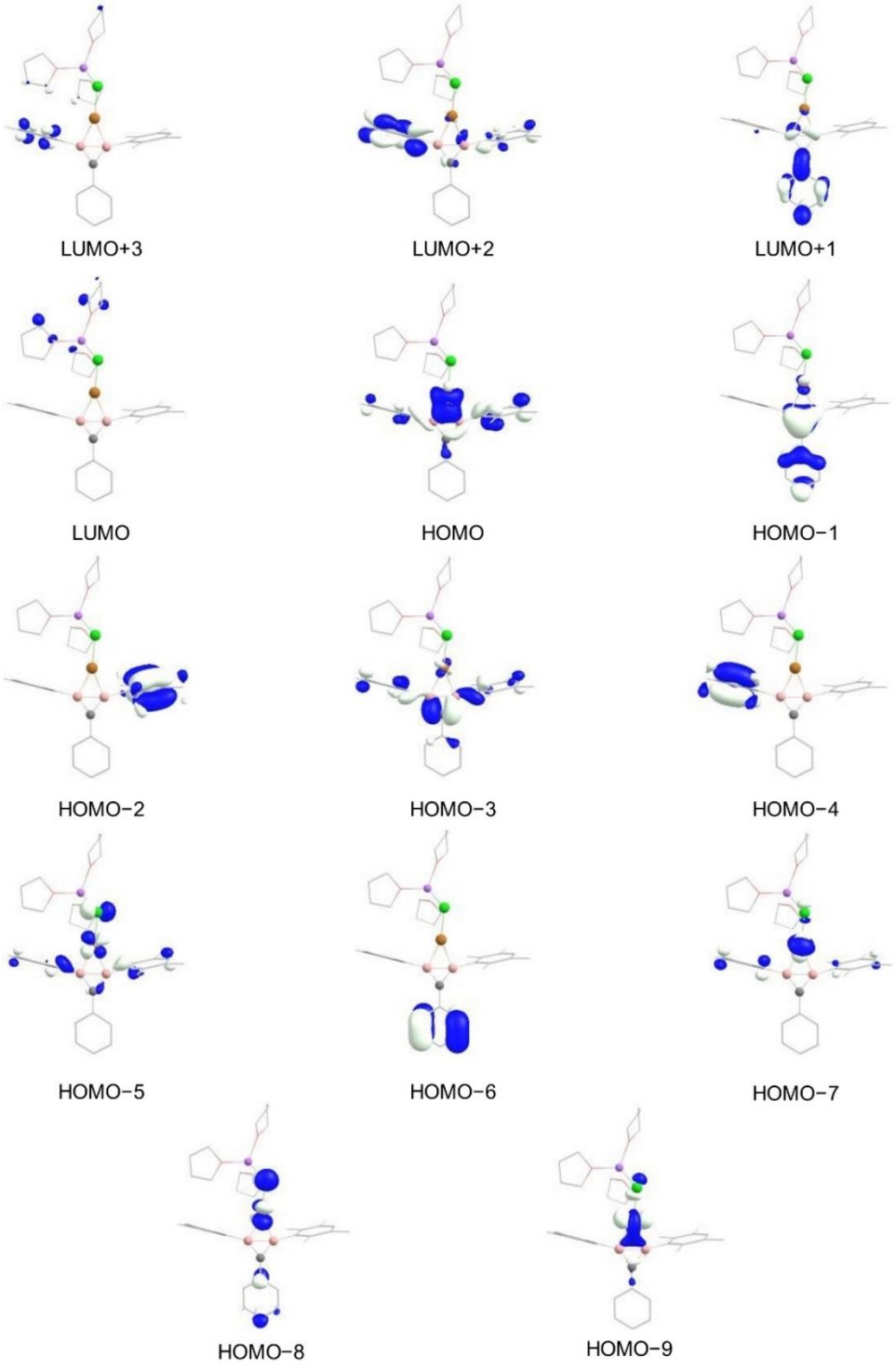

Figure S35. Selected molecular orbitals of diboriranide-chlorocuprate **6**.

5.6. Molecular orbitals of 1-phenyl-2,3-diduryl-diboriranide-chlorozincate 7

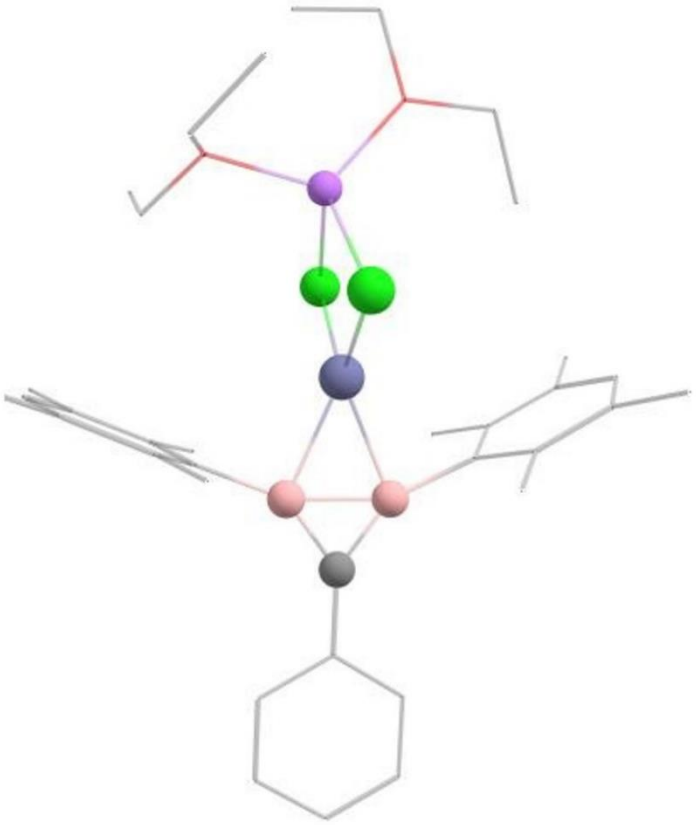

Table S14. Coordinates of the optimized structure of 1-phenyl-2,3-diduryl-diboriranide-chlorozincate **7**.

17	-1.410545103	0.434925031	1.724481126
30	0.014063001	0.209711015	-0.056028004
5	2.080087152	0.886636063	-0.009496001
5	1.913988140	-0.830198060	0.008061001
17	-1.395858101	0.205842015	-1.852381134
6	1.532635111	2.360441168	-0.034071002
6	1.266708091	3.025823217	1.197688085
6	0.672040046	4.310651311	1.182852087
6	0.367643027	4.903808354	-0.056827004
6	0.618723046	4.264661305	-1.284456093
6	1.207718089	2.976449212	-1.276542094
6	1.486948106	2.263485164	-2.578837186

6	0.343227025	5.024833361	2.472357177
6	1.593381114	2.346654169	2.506839181
6	1.220500090	-2.240908161	-0.004722000
6	0.991757070	-2.891051207	-1.251325089
6	0.350648025	-4.153961298	-1.274124092
6	-0.057514004	-4.730290341	-0.055375004
6	0.140114010	-4.095534293	1.184795083
6	0.792233059	-2.837897204	1.214244088
6	1.030633072	-2.134986154	2.530089182
6	-0.355953025	-4.733483343	2.460203177
6	0.099755007	-4.877859349	-2.577214183
6	1.414529104	-2.206824161	-2.530412181
6	3.171826226	-0.079126006	0.036223003
6	4.617115335	-0.238160017	0.080629006
6	5.204174372	-1.528707108	0.087147006
6	6.597163491	-1.683983122	0.128495009
6	7.433551523	-0.552661040	0.165767012
6	6.866260494	0.735330052	0.160669012
6	5.473297379	0.891111066	0.117843009
6	0.246674018	4.931177354	-2.586927184
3	-2.978207213	0.129035009	-0.096670007
8	-4.313506312	1.532997110	-0.319370023
6	-5.711768407	1.230353090	-0.427882031
6	-5.900382419	-0.056905004	-1.212865089
6	-4.054668294	2.885933206	0.108877008
6	-2.611310190	3.271609237	-0.157064011
8	-3.538258256	-1.735705123	0.377256027
6	-2.717785198	-2.736630195	-0.275002020
6	-3.127870223	-2.876312208	-1.728077123
6	-3.698574265	-1.981231143	1.784846126
6	-4.629029332	-0.939676070	2.381485172

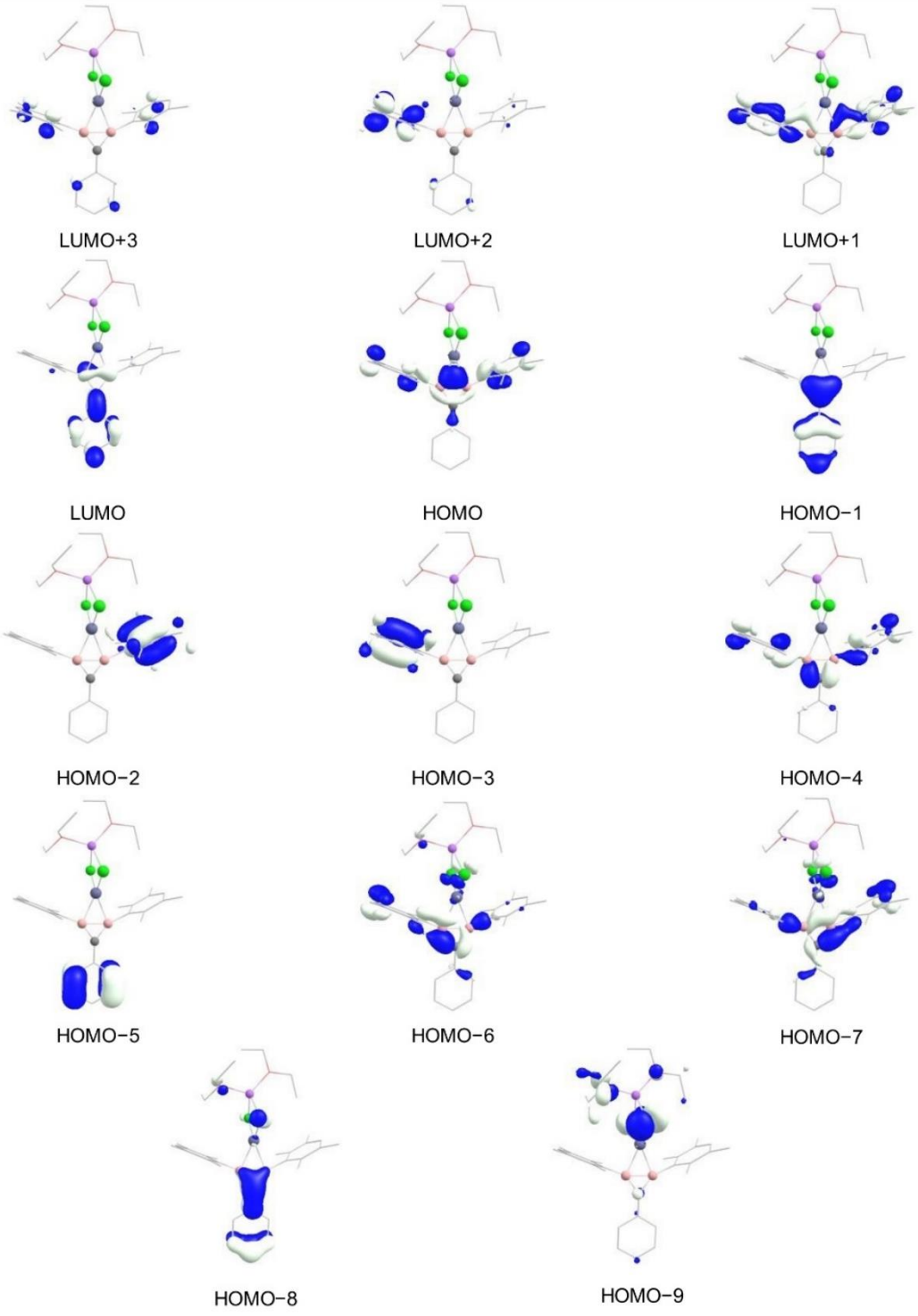

Figure S36. Selected molecular orbitals of 1-phenyl-2,3-diduryl-diboriranide-chlorozincate **7**.

5.7. Molecular orbitals of 1-phenyl-2,3-diduryl-diboriranide-trimethylstannane 8

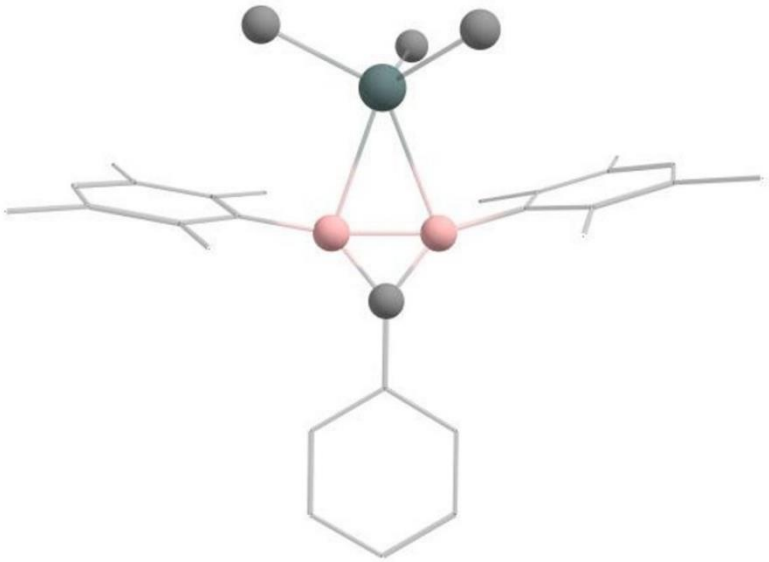

Table S15. Coordinates of the optimized structure of 1-phenyl-2,3-diduryl-diboriranide-trimethylstannane **8**.

50	0.085922034	-1.847930140	-0.554779003
6	-0.054434922	1.596222113	0.078936045
6	-0.172015907	3.038743217	0.237037057
6	-1.444779987	3.658534281	0.309807062
6	-1.556068974	5.049822386	0.444604071
6	-0.399254879	5.848783404	0.508995076
6	0.871058201	5.246946361	0.438654071
6	0.984215188	3.855789259	0.304317061
6	-2.402655114	0.006166035	0.152504050
6	-2.930191162	-0.564035996	1.341659138
6	-4.301216266	-0.916376999	1.404151139
6	-5.111161321	-0.691725974	0.276025059
6	-4.611877279	-0.120585939	-0.908365028
6	-3.242047174	0.236556065	-0.971365029
6	-2.043722102	-0.801543027	2.541784221
6	-4.883721320	-1.525552036	2.657257232
6	-5.518809321	0.094021091	-2.096402110

6	-2.680350125	0.825844101	-2.244482124
6	2.430543236	0.168459970	0.150957050
6	3.256414299	0.384689972	-0.987686030
6	4.633745391	0.057763927	-0.925896030
6	5.155457420	-0.458788119	0.274400059
6	2.991245267	-0.303290073	1.369889140
6	2.688086268	0.986988024	-2.251725121
6	5.529007466	0.264616928	-2.124370112
6	-1.793137116	-2.759182173	-1.194831046
6	1.424465127	-2.155479183	-2.250194121
5	-0.889427002	0.397551039	0.056426044
5	0.910108132	0.514617019	0.061857044
6	4.369732363	-0.626953118	1.428984142
6	2.148729204	-0.391393066	2.620748230
6	0.829917067	-3.061629239	1.092398116
6	4.990044396	-1.128467166	2.711570233

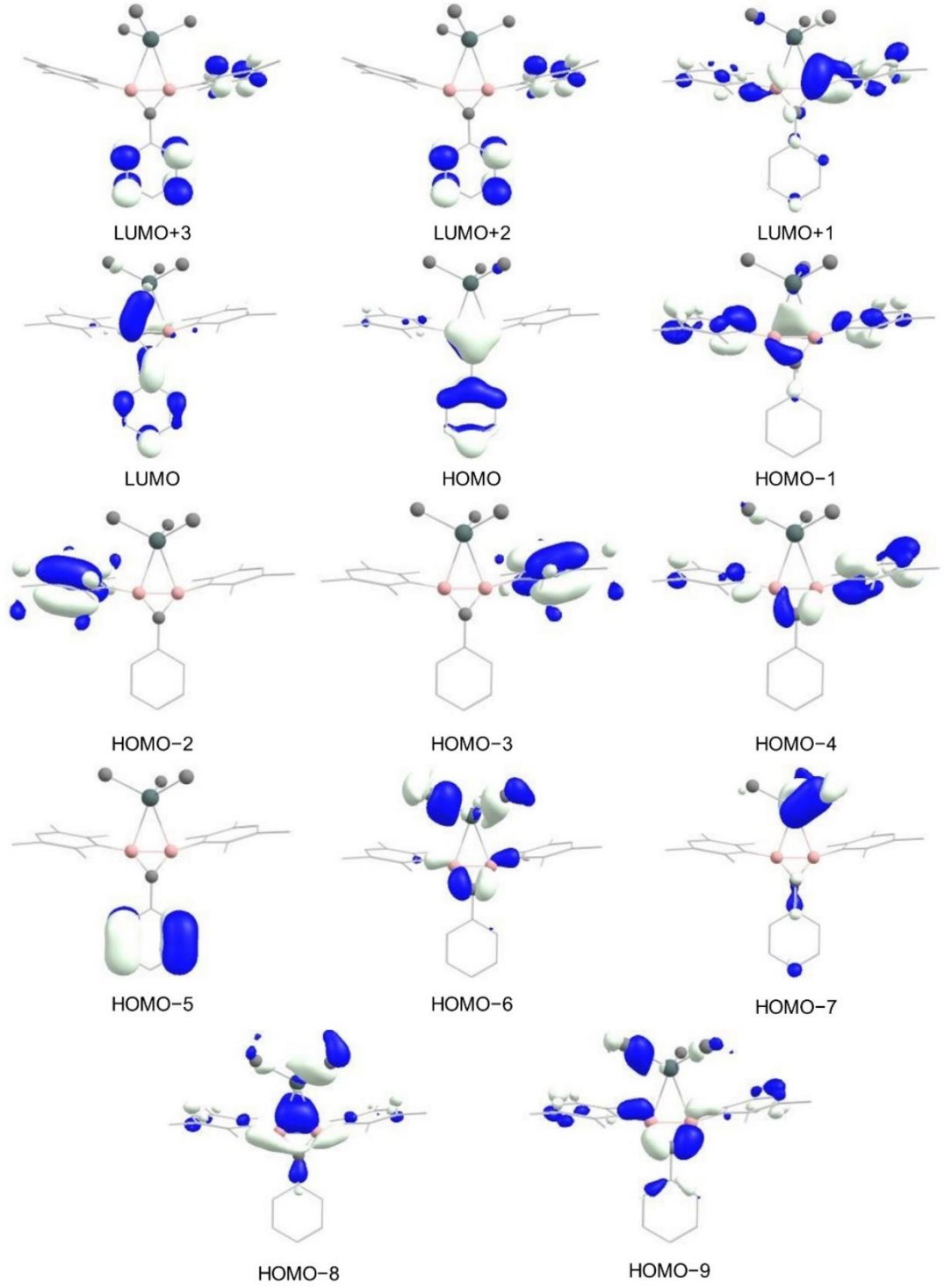

Figure S37. Selected molecular orbitals of 1-phenyl-2,3-diduryldiboriranide-trimethylstannane **8**.

5.8. Natural bond orbital (NBO) analysis of diborirane 2 and diboriranide 3

3c2e Bonds (excerpts from NBO output)

5.8.1. Diborirane **2**

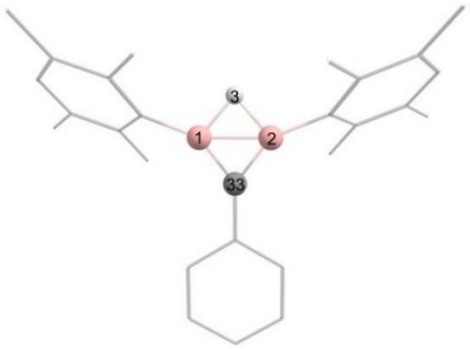


```
NATURAL BOND ORBITAL ANALYSIS:

                          Occupancies       Lewis Structure    Low   High
        Max    Occ      -------------------  -----------------   occ   occ
  Cycle  Ctr   Thresh    Lewis   non-Lewis     CR  BD  nC  LP    (L)   (NL)
 ================================================================================
    1     2     1.90   191.69606  12.30394     29  62   0  11    11     13
    2     2     1.66   193.03199  10.96801     29  64   0   9     9     13
    3     2     1.65   194.31990   9.68010     29  66   0   7     7     13
    4     2     1.63   195.53549   8.46451     29  68   0   5     5     13
    5     2     1.62   196.79444   7.20556     29  70   0   3     3     13
    6     2     1.61   197.29291   6.70709     29  71   0   2     2     13
    7     3     1.61   199.24059   4.75941     29  71   2   0     0      9
 --------------------------------------------------------------------------------

 Structure accepted: No low occupancy Lewis orbitals

 ------------------------------------------------------
   Core                     57.99950 ( 99.999% of  58)
   Valence Lewis           141.24110 ( 96.740% of 146)
  ==================      ============================
   Total Lewis             199.24059 ( 97.667% of 204)
  ------------------------------------------------------
   Valence non-Lewis         4.47509 (  2.194% of 204)
   Rydberg non-Lewis         0.28432 (  0.139% of 204)
  ==================      ============================
   Total non-Lewis           4.75941 (  2.333% of 204)
 ------------------------------------------------------

     (Occupancy)   Bond orbital / Coefficients / Hybrids
 ------------------ Lewis ------------------------------------------------------101.
(1.95588) 3C ( 1) B  1- B  2- H  3
              ( 27.62%)   0.5256* B  1 s( 24.76%)p 3.02( 74.89%)d 0.01(  0.24%)
                                       f 0.00(  0.10%)
                                    0.0000  0.4976  0.0037  0.0082 -0.0013
                                   -0.6675 -0.0201 -0.0179 -0.5290  0.0075
                                    0.0117  0.1497 -0.0116 -0.0042  0.0092
```

```
                                    0.0216 -0.0016 -0.0070 -0.0122 -0.0065
                                    0.0178 -0.0004 -0.0343 -0.0117 -0.0056
                                    0.0259  0.0075  0.0002  0.0090 -0.0080
                                   -0.0117
               ( 28.17%)   0.5308* B  2 s( 25.38%)p 2.93( 74.27%)d 0.01(  0.24%)
                                             f 0.00(  0.11%)
                                    0.0000  0.5037  0.0031  0.0088 -0.0012
                                    0.6852  0.0214  0.0171 -0.5011  0.0078
                                    0.0114  0.1448 -0.0117 -0.0045 -0.0094
                                   -0.0208  0.0026  0.0069 -0.0129 -0.0048
                                    0.0186 -0.0004 -0.0352 -0.0088 -0.0052
                                   -0.0268  0.0067  0.0007 -0.0091  0.0092
                                   -0.0112
               ( 44.21%)   0.6649* H  3 s( 99.39%)p 0.01(  0.60%)d 0.00(  0.01%)
                                    0.9970 -0.0026 -0.0007 -0.0020  0.0000
                                    0.0728 -0.0009 -0.0260  0.0005 -0.0001
                                    0.0002 -0.0053 -0.0027 -0.0074

102. (1.91932) 3C ( 1) B  1- B  2- C 33
               ( 24.51%)   0.4951* B  1 s(  0.00%)p 1.00( 99.69%)d 0.00(  0.17%)
                                             f 0.00(  0.14%)
                                    0.0000  0.0050  0.0003  0.0002 -0.0002
                                    0.0245 -0.0046  0.0011 -0.2960 -0.0176
                                   -0.0020 -0.9530 -0.0004 -0.0111  0.0091
                                    0.0074  0.0257  0.0219  0.0119 -0.0117
                                   -0.0064  0.0035 -0.0070  0.0076  0.0241
                                   -0.0057  0.0074 -0.0239  0.0054 -0.0025
                                   -0.0091
               ( 24.25%)   0.4925* B  2 s(  0.00%)p 1.00( 99.68%)d 0.00(  0.17%)
                                             f 0.00(  0.14%)
                                    0.0000  0.0052  0.0006 -0.0002 -0.0003
                                   -0.0229  0.0053 -0.0007 -0.3012 -0.0175
                                   -0.0016 -0.9514  0.0025 -0.0111 -0.0108
                                   -0.0064 -0.0284 -0.0189  0.0088 -0.0134
                                   -0.0057  0.0045 -0.0060  0.0085  0.0245
                                    0.0061  0.0080 -0.0237 -0.0065  0.0032
                                   -0.0091
               ( 51.24%)   0.7158* C 33 s(  0.00%)p 1.00( 99.74%)d 0.00(  0.16%)
                                             f 0.00(  0.10%)
                                    0.0000  0.0011 -0.0020  0.0013  0.0000
                                    0.0052 -0.0002  0.0002 -0.2886  0.0108
                                    0.0011 -0.9554  0.0333  0.0024 -0.0001
                                    0.0000 -0.0006 -0.0001  0.0317  0.0022
                                   -0.0078 -0.0013 -0.0234 -0.0001  0.0158
                                   -0.0004  0.0236  0.0123  0.0006 -0.0004
                                    0.0055

Summary of Natural Population Analysis:

                                     Natural Population
               Natural     -----------------------------------------------
  Atom No      Charge         Core      Valence    Rydberg      Total
 ----------------------------------------------------------------------
    B  1     0.49038      1.99997     2.49318    0.01647     4.50962
    B  2     0.48118      1.99997     2.50242    0.01643     4.51882
    H  3     0.10243      0.00000     0.89058    0.00699     0.89757
    C 33    -0.62571      1.99998     4.59842    0.02730     6.62571
```

Wiberg bond index matrix in the NAO basis:

	Atom	1	2	3	4	5	6	7	8	9
1.	B	0.0000	0.5333	0.4601	0.9398	0.0115	0.0115	0.0044	0.0111	0.0139
2.	B	0.5333	0.0000	0.4720	0.0216	0.0066	0.0006	0.0032	0.0010	0.0079
3.	H	0.4601	0.4720	0.0000	0.0021	0.0030	0.0002	0.0017	0.0001	0.0050
33.	C	1.2763	1.2683	0.0185	0.0105	0.0132	0.0004	0.0056	0.0004	0.0122

5.8.2. Diboriranide **3**

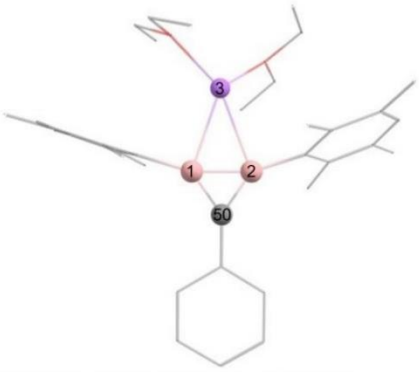

NATURAL BOND ORBITAL ANALYSIS:

Cycle	Max Ctr	Occ Thresh	Occupancies Lewis	Occupancies non-Lewis	Lewis Structure CR	Lewis Structure BD	Lewis Structure nC	Lewis Structure LP	Low occ (L)	High occ (NL)
1	2	1.90	277.08032	12.91968	40	90	0	15	11	13
2	2	1.84	277.06417	12.93583	40	90	0	15	11	13
3	2	1.82	277.88812	12.11188	40	91	0	14	10	12
4	2	1.67	280.47545	9.52455	40	95	0	10	6	12
5	2	1.66	280.47545	9.52455	40	95	0	10	6	12
6	2	1.65	281.11192	8.88808	40	96	0	9	5	12
7	2	1.64	281.74755	8.25245	40	97	0	8	4	12
8	2	1.62	282.95774	7.04226	40	99	0	6	2	12
9	2	1.61	282.95774	7.04226	40	99	0	6	2	12
10	2	1.60	283.54347	6.45653	40	100	0	5	1	12
11	3	1.60	284.43282	5.56718	40	100	1	4	0	10

Structure accepted: No low occupancy Lewis orbitals

Core	79.99930	(99.999% of 80)
Valence Lewis	204.43352	(97.349% of 210)
Total Lewis	284.43282	(98.080% of 290)
Valence non-Lewis	5.14379	(1.774% of 290)
Rydberg non-Lewis	0.42339	(0.146% of 290)
Total non-Lewis	5.56718	(1.920% of 290)

```
     (Occupancy)   Bond orbital / Coefficients / Hybrids
 ------------------ Lewis ----------------------------------------------------145.
(1.90715) 3C ( 1) B  1- B  2- C 50
              ( 24.42%)   0.4942* B  1 s(  0.05%)p99.99( 99.74%)d 2.11(  0.10%)
                                                 f 2.62(  0.12%)
                                        0.0000  0.0193 -0.0084  0.0027 -0.0015
                                       -0.0800  0.0042  0.0043 -0.0489 -0.0135
                                       -0.0068 -0.9937  0.0222  0.0209  0.0003
                                        0.0001  0.0025  0.0239  0.0116 -0.0145
                                        0.0006  0.0030 -0.0034 -0.0035  0.0213
                                        0.0053 -0.0014 -0.0213  0.0152 -0.0041
                                        0.0000
              ( 24.33%)   0.4933* B  2 s(  0.02%)p99.99( 99.76%)d 4.90(  0.10%)
                                                 f 6.06(  0.12%)
                                        0.0000  0.0114 -0.0073  0.0038 -0.0001
                                       -0.0746 -0.0038  0.0006 -0.0543 -0.0007
                                        0.0006 -0.9941  0.0194  0.0199  0.0023
                                       -0.0014 -0.0030 -0.0251  0.0114 -0.0133
                                        0.0009 -0.0007 -0.0006  0.0041  0.0208
                                        0.0073  0.0020 -0.0237 -0.0119 -0.0010
                                       -0.0027
              ( 51.25%)   0.7159* C 50 s(  0.02%)p99.99( 99.74%)d 8.70(  0.14%)
                                                 f 5.87(  0.10%)
                                        0.0000  0.0126 -0.0023  0.0016  0.0000
                                       -0.0727  0.0015 -0.0003 -0.0636  0.0016
                                        0.0014 -0.9933  0.0378  0.0037  0.0022
                                        0.0002 -0.0005  0.0005  0.0372  0.0021
                                       -0.0021 -0.0002 -0.0072  0.0006  0.0233
                                        0.0018  0.0050  0.0200 -0.0007  0.0021
                                        0.0014

Summary of Natural Population Analysis:

                                     Natural Population
              Natural     -----------------------------------------
  Atom No     Charge        Core      Valence    Rydberg      Total
 ----------------------------------------------------------------------
    B  1    0.20398      1.99997     2.77697    0.01909     4.79602
    B  2    0.18602      1.99997     2.79489    0.01912     4.81398
   Li  3    0.86785      1.99997     0.11975    0.01243     2.13215
    C 50   -0.59606      1.99998     4.57055    0.02553     6.59606

Wiberg bond index matrix in the NAO basis:

     Atom    1       2       3       4       5       6       7       8       9
     ---- ------  ------  ------  ------  ------  ------  ------  ------  ------
   1.  B  0.0000  1.0580  0.0178  0.0247  0.0147  0.0008  0.0091  0.0001  0.0008
   2.  B  1.0580  0.0000  0.0182  0.9130  0.0122  0.0129  0.0031  0.0009  0.0130
   3. Li  0.0178  0.0182  0.0000  0.0081  0.0018  0.0014  0.0005  0.0004  0.0014
  50.  C  1.2689  1.2616  0.0037  0.0152  0.0157  0.0005  0.0080  0.0000  0.0005
```

References

[S1] R. Hunold, *Dissertation,* Universität Marburg, **1988**; b) H. Hommer, H. Nöth, J. Knizek, W. Ponikwar, H. Schwenk-Kircher, *Eur. J. Inorg. Chem.* **1998**, 1519 – 1527.

[S2] G. R. Fulmer, A. J. M. Miller, N. H. Sherden, H. E. Gottlieb, A. Nudelman, B. M. Stoltz, J. E. Bercaw, K. I. Goldberg, *Organometallics* **2010**, *29*, 2176 – 2179.

[S3] Purchased at Sigma Aldrich

[S4] G. M. Sheldrick, *Acta Cryst.* **2015**, *A71*, 3 − 8.

[S5] G. M. Sheldrick, *Acta Cryst.* **2015**, *C71*, 3 − 8.

[S6] C. B. Hübschle, G. M. Sheldrick, B. Dittrich, *J. Appl. Crystallogr.* **2011**, *44*, 1281 − 1284.

[S7] Gaussian 09, Revision A.02, M. J. Frisch, G. W. Trucks, H. B. Schlegel, G. E. Scuseria, M. A. Robb, J. R. Cheeseman, G. Scalmani, V. Barone, G. A. Petersson, H. Nakatsuji, X. Li, M. Caricato, A. Marenich, J. Bloino, B. G. Janesko, R. Gomperts, B. Mennucci, H. P. Hratchian, J. V. Ortiz, A. F. Izmaylov, J. L. Sonnenberg, D. Williams-Young, F. Ding, F. Lipparini, F. Egidi, J. Goings, B. Peng, A. Petrone, T. Henderson, D. Ranasinghe, V. G. Zakrzewski, J. Gao, N. Rega, G. Zheng, W. Liang, M. Hada, M. Ehara, K. Toyota, R. Fukuda, J. Hasegawa, Ishida, M. T. Nakajima, Y. Honda, O. Kitao, H. Nakai, T. Vreven, K. Throssell, J. A. Montgomery Jr, J. E. Peralta, F. Ogliaro, M. Bearpark, J. J. Heyd, E. Brothers, K. N. Kudin, V. N. Staroverov, T. Keith, R. Kobayashi, J. Normand, K. Raghavachari, A. Rendell, J. C. Burant, S. S. Iyengar, J. Tomasi, M. Cossi, J. M. Millam, M. Klene, C. Adamo, R. Cammi, J. W. Ochterski, R. L. Martin, K. Morokuma, O. Farkas, J. B. Foresman, D. J. Fox, Gaussian, Inc., Wallingford CT, **2016**.

[S8] a) J. P. Perdew, *Phys. Rev. B* **1986**, *33*, 8822 – 8824; b) A. D. Becke, *Phys. Rev. A* **1988**, *38*, 3098 – 3100.

[S9] a) A. Schäfer, H. Horn, R. Ahlrichs, *J. Chem. Phys.* **1992**, *97*, 2571 – 2577; b) A. Schäfer, C. Huber, R. Ahlrichs, *J. Chem. Phys.* **1994**, *100*, 5829 – 5835; c) F. Weigend, R. Ahlrichs, *Phys. Chem. Chem. Phys.* **2005**, *7*, 3297 – 3305; d) F. Weigend, *Phys. Chem. Chem. Phys.* **2006**, *8*, 1057 – 1065.

[S10] S. Grimme, J. Antony, S. Ehrlich, H. Krieg, *J. Chem. Phys.* **2010**, *132*, 154104.

[S11] Chemcraft - graphical software for visualization of quantum chemistry computations. https://www.chemcraftprog.com

[S12] NBO 7.0. E. D. Glendening, J, K. Badenhoop, A. E. Reed, J. E. Carpenter, J. A. Bohmann, C. M. Morales, P. Karafiloglou, C. R. Landis, and F. Weinhold, Theoretical Chemistry Institute, University of Wisconsin, Madison, **2018**.

5.2 π-Complexes of Non-Classical Diboriranes: Side-on vs. End-on Carbonylative Ring Expansion

π-Complexes Derived from Non-Classical Diboriranes: Side-on vs. End-on Carbonylative Ring Expansion

Philipp Grewelinger, Carsten Präsang, Michael Zimmer, Bernd Morgenstern, and David Scheschkewitz*

*Krupp-Chair for General and Inorganic Chemistry, Saarland University, 66123 Saarbrücken, Germany

Supporting Information

Table of Contents

1. General remarks

All manipulations were carried out under argon with standard Schlenk or glovebox techniques. The glassware was pre-dried in oven at 125 °C and heated in vacuo prior to use. Hexane, toluene and tetrahydrofuran were taken from a solvent purification system (Innovative Technology PureSolv MD7). Benzene-d_6 was dried over potassium mirror and distilled prior to use. Non-classical diborirane **1** and tin-bridged non-classical diborirane **4** were prepared according to the published procedures.[12] All other chemicals were obtained commercially and used as received. The NMR spectra were recorded on a Bruker Avance III HD 400 spectrometer at 300 K (^{1}H: 400.13 MHz, ^{11}B: 128.38 MHz, ^{13}C: 100.61 MHz, ^{119}Sn: 149.21 MHz). The VT-NMR spectra were recorded on a Bruker Avance III HD 300 spectrometer (^{13}C: 75.47 MHz). The ^{1}H and ^{13}C{1H} NMR spectra were referenced to the residual proton and natural abundance ^{13}C resonances of the deuterated solvent and chemical shifts were reported relative to $SiMe_4$ (C_6D_6: δH = 7.16 ppm and δC = 128.06 ppm, toluene-d_8: δC = 20.43 ppm).[30] The following abbreviations were used for the multiplicities: s – singlet, d – doublet, t – triplet, m – multiplet. Melting points were determined under argon in NMR tubes and are uncorrected. The molten samples were examined by NMR spectroscopy to confirm whether decomposition had occurred upon melting. UV/Vis spectra were recorded on a Shimadzu UV-2600 spectrometer in quartz cells with a path length of 0.1 cm. Elemental analysis was performed in triplicate for each sample using an elementar vario Micro Cube analyzer and mean values are given below for each compound. In all cases the actual value is lower than the calculated one should be. A possible explanation could be the presence of $Fe_x(CO)_y$ species as well as traces of grease. Infrared spectra were measured with a Shimadzu IRAffinity-1S in a platinum ATR diamond cell and in BaF_2 cells with 1mM hexane solutions. Crystallographic data of the structures reported in this paper have been deposited with the Cambridge Crystallographic Data Centre, CCDC, 12 Union Road, Cambridge CB21EZ, UK. (Fax: +44-1223-336-033; E-Mail: deposit@ccdc.cam.ac.uk, http://www.ccdc.cam.ac.uk)

2. Experimental procedure, data and spectra

2.1 Diborirane $Fe(CO)_3$ complex **2**

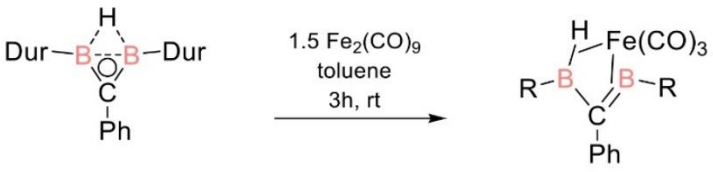

1 **2**

378.17 g/mol 548.10 g/mol

At ambient temperature 100 mL toluene is added to a mixture of non-classical diborirane **1** (1.06 g, 2.87 mmol) and $Fe_2(CO)_9$ (1.60 g, 4.31 mmol). The solution turns to dark red. After 3 h of stirring, all volatiles are removed in vacuo at room temperature. The solid residue is redissolved in 40 mL hexane and filtered. Removing of the solvent yields to 1.50 g (98%) of a brown-orange powder. The powder is redissolved to give a room temperature-saturated solution and stored at −25 °C. Diborirane $Fe(CO)_3$ complex **2** is obtained as red orange crystals (780 mg, 50%).

^{1}H NMR (400 MHz, C_6D_6, 300K): δ 7.33-7.31 (m, Ph-H, 2H), 7.03-6.98 (m, Ph-H, 2H), 6.94-6.89 (m, Ph-H, 1H), 6.91(s, Dur-H, 2H), 2.20 (s, Dur-CH_3, 12H), 2.01 (s, Dur-CH_3, 12H), −11.37 (br s, B-H, 1H).

^{11}B NMR (128.38 MHz, C_6D_6, 300 K): δ = 68.4 (br s) ppm.

^{11}B CP/MAS solid-state-NMR (79 MHz, 13 kHz): δ 85.1 (B=C), 50.6 (B-H) ppm.

^{13}C{ 1H} NMR (100.61 MHz, C_6D_6, 300 K): δ = 211.2 (s, COs), 139.2, 136.6, 134.6, 134.2, 130.6, 128.8, 126.3 (each s, Ar-C), 48.9 (s, B_2C), 21.0, 19.9 (each s, Dur-CH_3).

^{13}C{ 1H} NMR (75.47 MHz, tol-d_8, 213 K): 211.2 (s, COs), 138.8, 136.5, 136.2 (br s, Dur_{ipso}-C), 134.4, 134.0, 130.7, 126.3 (each s, Ar-C), 48.9 (s, B_2C), 20.9, 19.9 (each s, Dur-CH_3).

UV/Vis (hexane): λmax(ε) = 294 nm (15600 $M^{-1}cm^{-1}$), 420 nm (1445 $M^{-1}cm^{-.1}$).

Elemental analysis: calc. for $C_{30}H_{32}B_2FeO_3$: C, 69.6%; H, 6.2%. Found: C, 68.3%; H, 5.2%.

Melting point: 145 °C (partial decomposition to non-classical diborirane **1**)

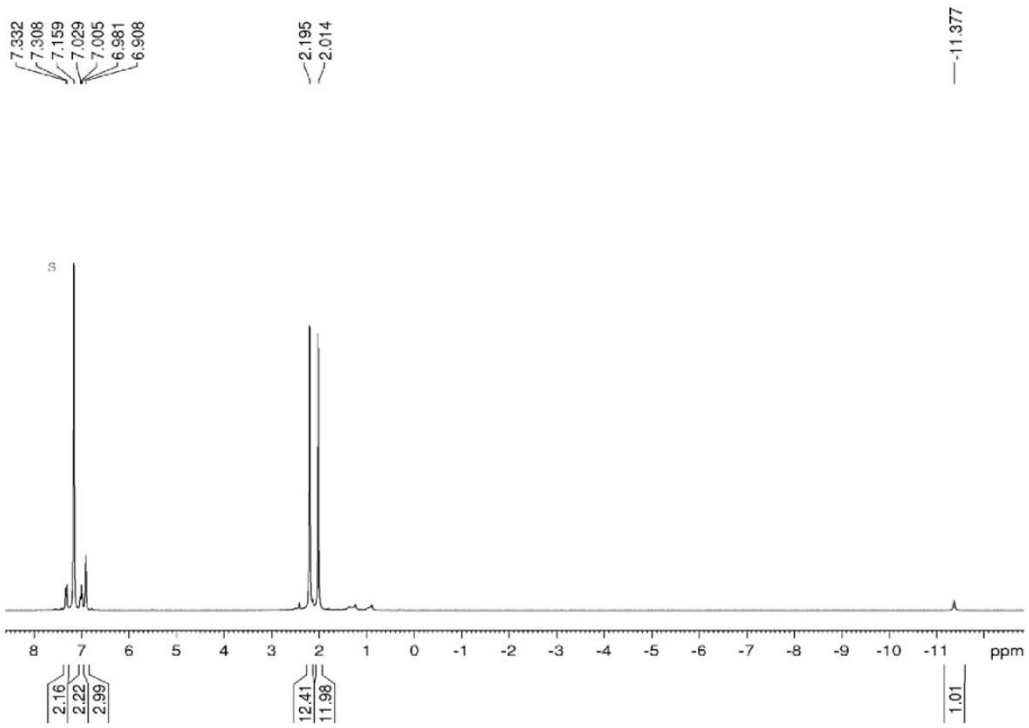

Figure S1. ^{1}H-NMR spectrum (400.1 MHz) of diborirane $Fe(CO)_3$ complex **2** in C_6D_6 (=s).

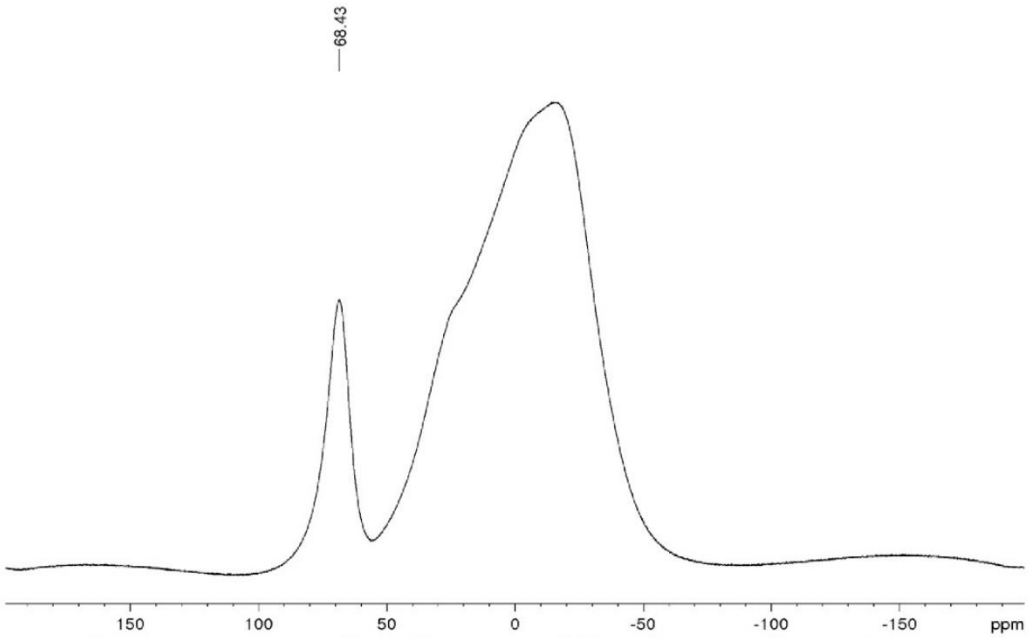

Figure S2. Baseline corrected ^{11}B-NMR spectrum (128.4 MHz) of diborirane $Fe(CO)_3$ complex **2** (glass peak from 50 to −50 ppm).

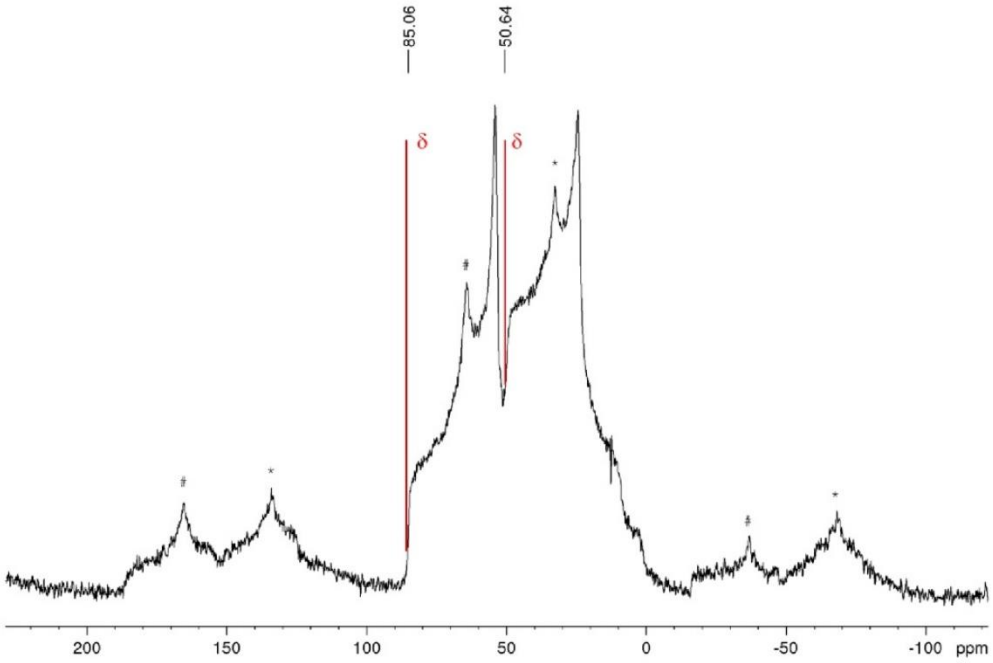

Figure S3. ^{11}B CP/MAS SS-NMR (79 MHz, 13 kHz) of diborirane $Fe(CO)_3$ complex **2**. Spin sidebands marked with # and *.

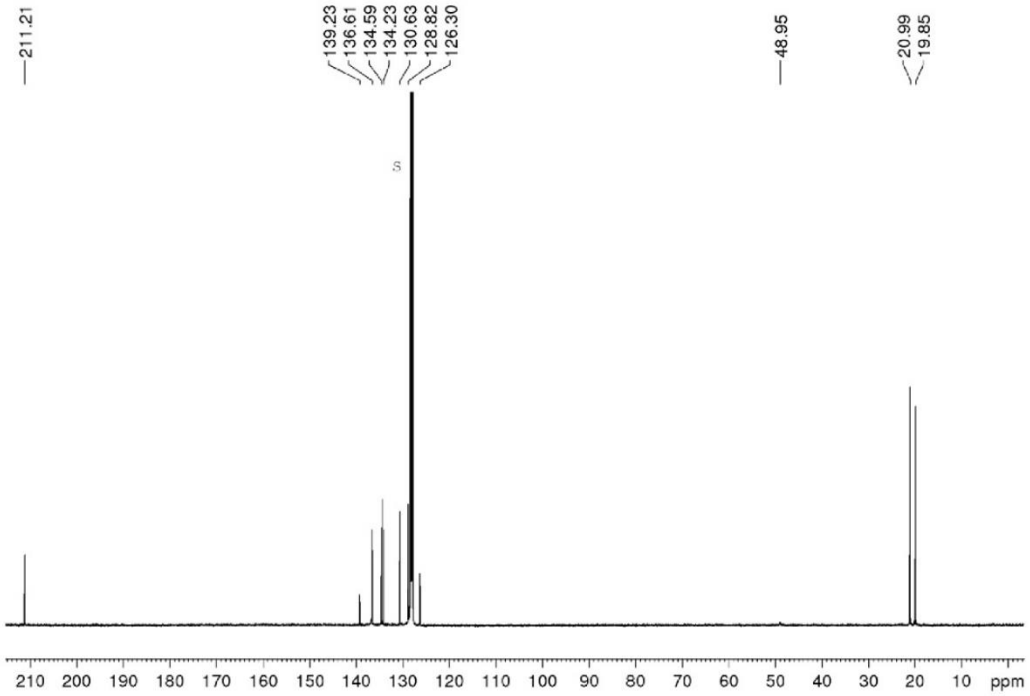

Figure S4. ^{13}C-NMR spectrum (100.61 MHz) of diborirane $Fe(CO)_3$ complex **2** in C_6D_6 (=s).

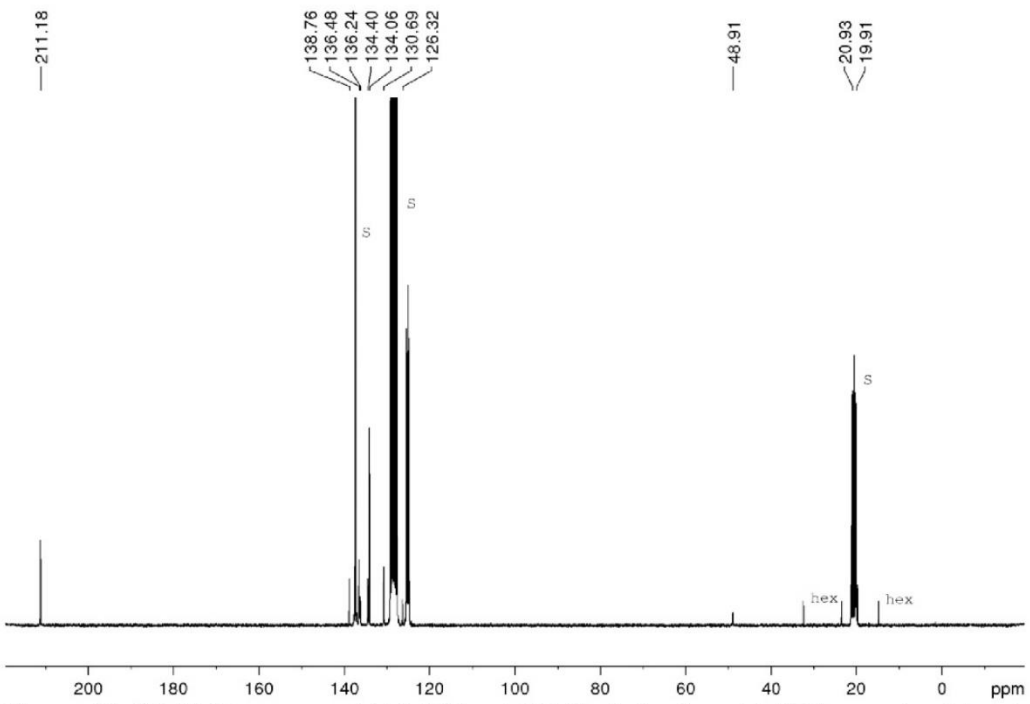

Figure S5. ^{13}C-NMR spectrum (75.47 MHz at 213 K) of diborirane $Fe(CO)_3$ complex **2** in tol-d8 (=s) with traces of hexane (=hex at14.3, 23.1, 32.1 ppm).

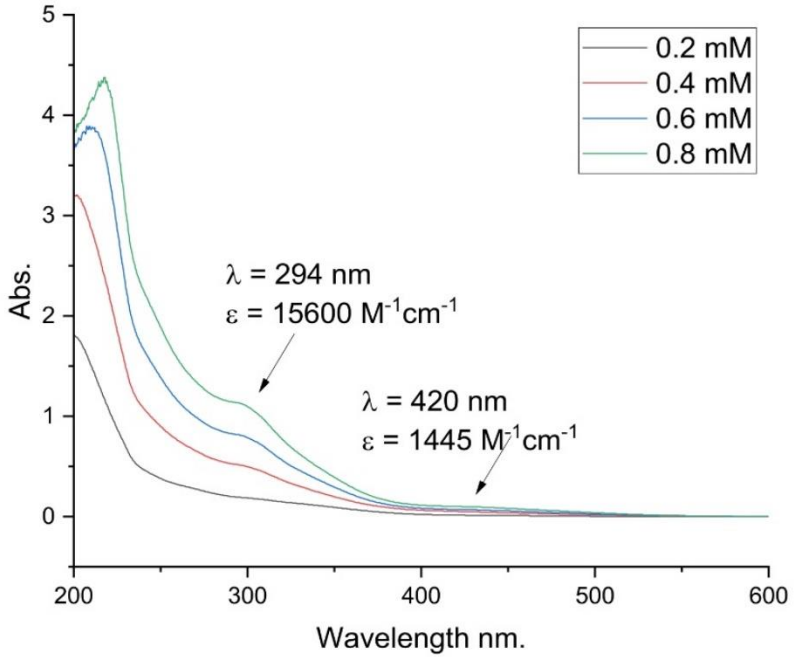

Fig S6. UV/Vis spectrum of diborirane $Fe(CO)_3$ complex **2** in hexane.

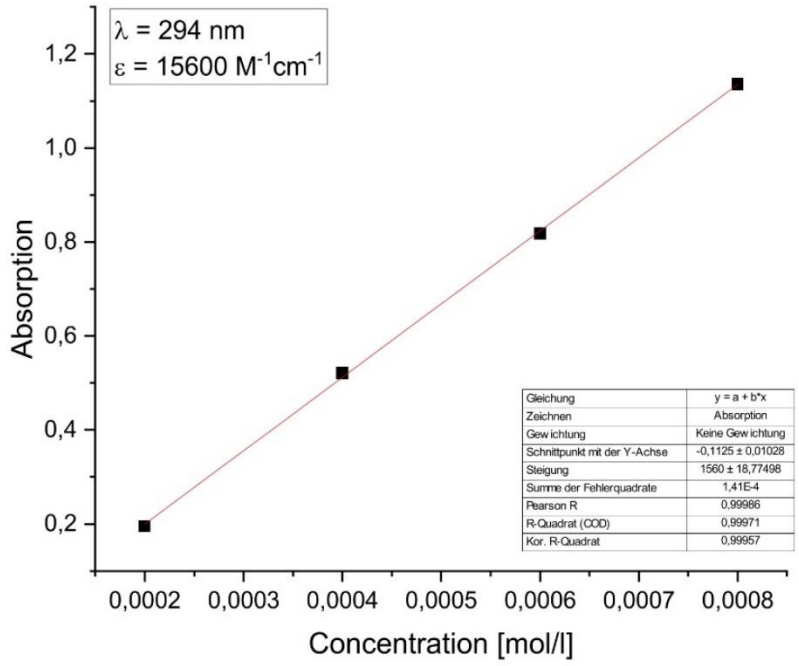

Fig S7. Determination of ε (15600 $M^{-1}cm^{-1}$) by linear regression of absorptions (λ = 294 nm) of diborirane $Fe(CO)_3$ complex **2** against concentration.

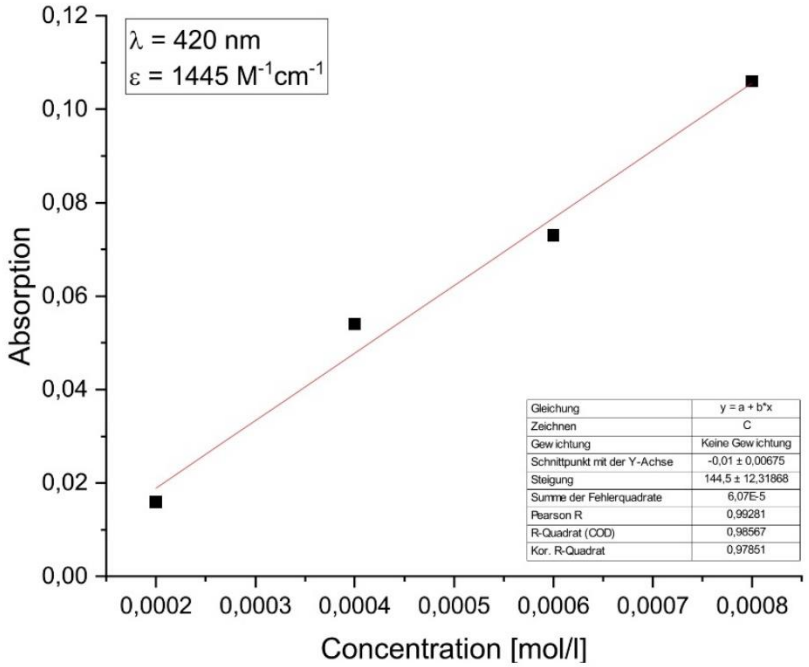

Fig S8. Determination of ε (1445 $M^{-1}cm^{-1}$) by linear regression of absorptions (λ = 420 nm) of diborirane $Fe(CO)_3$ complex **2** against concentration.

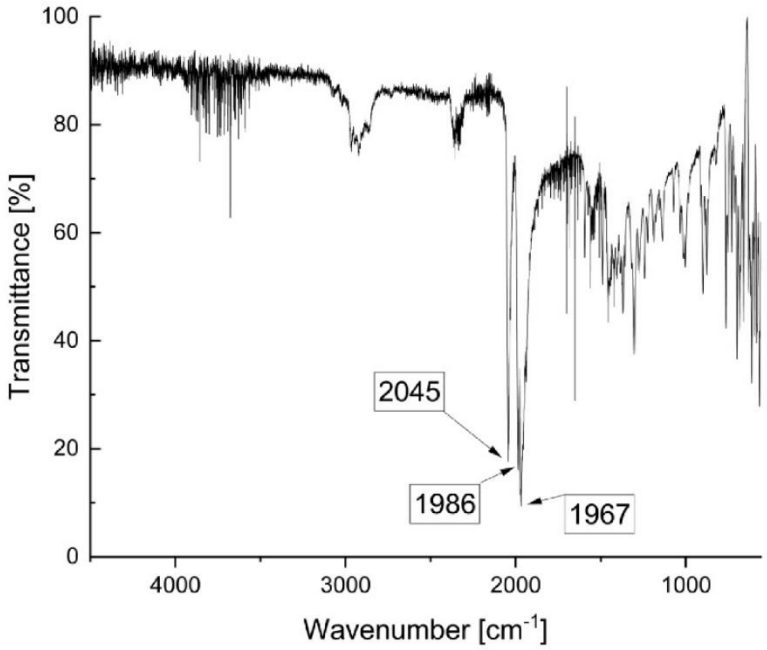

Fig S9. IR spectrum of diborirane $Fe(CO)_3$ complex **2** in the solid state. (The CO_2 stretching band at 2400 cm^{-1} is due to imperfect background subtraction).

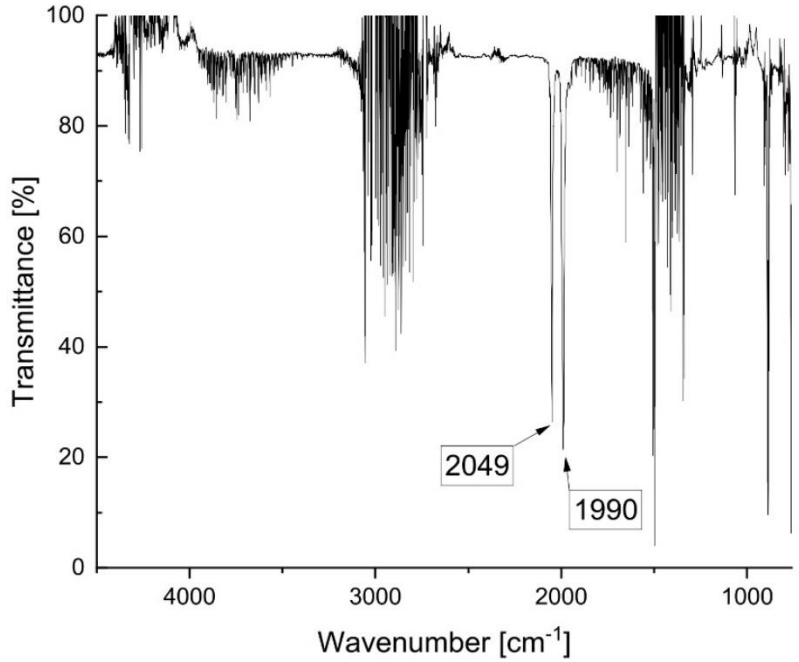

Fig S10. IR spectrum of diborirane $Fe(CO)_3$ complex **2** in 1 mM hexane solution (superimposed signals around 1500 and 3000 cm^{-1} from hexane due to imperfect background substraction)[31].

2.2 Oxadiborolane $Fe(CO)_3$ complex **3**.

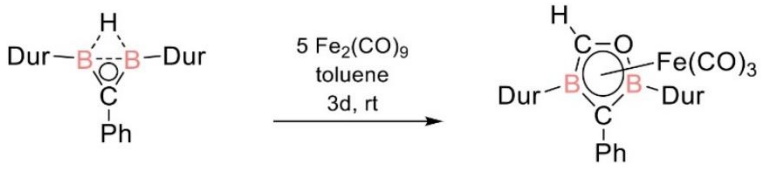

1 **3**

378.17 g/mol 576.10 g/mol

At ambient temperature 100 mL toluene is added to a mixture of non-classical diborirane **1** (200 mg, 0.53 mmol) and $Fe_2(CO)_9$ (1.0 g, 2.69 mmol). The solution turns dark-red. After 3 d of stirring, all volatiles are removed in vacuo at room temperature. The solid residue is redissolved in 40 mL hexane and filtered. The filtrate is concentration to saturation and stored at −25 °C to give oxadiborolane $Fe(CO)_3$ complex **3** as red orange crystals (80 mg, 26%).

^{1}H NMR (400 MHz, C_6D_6, 300K): δ 7.56-7.53 (m, Ph-H, 2H), 7.02, 7.01 (each s, Dur-H, 1H), 6.79-6.77 (m, Ph-H, 3H), 5.50 (s, HC-O, 1H), 2.48 (br s, Dur-CH_3, 6H), 2.41, 2.20, 2.13 (each s, Dur-CH_3, 6H).

^{11}B NMR (128.38 MHz, C_6D_6, 300 K): δ = 34.5 (br s, B-O) 26.2 (br s, B-C) ppm.

^{13}C{^{1}H} NMR (100.61 MHz, C_6D_6, 300 K): δ = 207.5 (s, COs), 141.8 (s, Ar-C), 140.1 (br s, Dur_{ipso}-C), 134.6, 134.4, 133.9, 132.4, 130.2, 126.8 (each s, Ar-C), 21.5, (br s, Dur-CH_3), 20.7, 20.3 (each s, Dur-CH_3).

^{13}C{^{1}H} NMR (100.61 MHz, tol-d_8, 213 K): 206.8 (br s, COs), 141.4, 141.3, 138.8, 136.5, 135.5, 134.6, 134.3, 134.2, 133.9, 133.6, 132.2, 130.7, 126.8 (each s, Ar-C), 109.0 (br s, B_2C-Ph), 90.0 (br s, BCO), 22.7, 21.9 (each s, Dur-CH_3).

UV/Vis (hexane): λmax(ε) = 243 nm (26025 $M^{-1}cm^{-1}$), 320 nm (8310 $M^{-1}cm^{-1}$), 403 nm (2450 $M^{-1}cm^{-1}$).

Elemental analysis: calc. for $C_{31}H_{32}B_2FeO_4$: C, 68.2%; H, 5.9%. Found: C, 67.4%; H, 5.4%.

Melting point: 235 °C (slight decomposition)

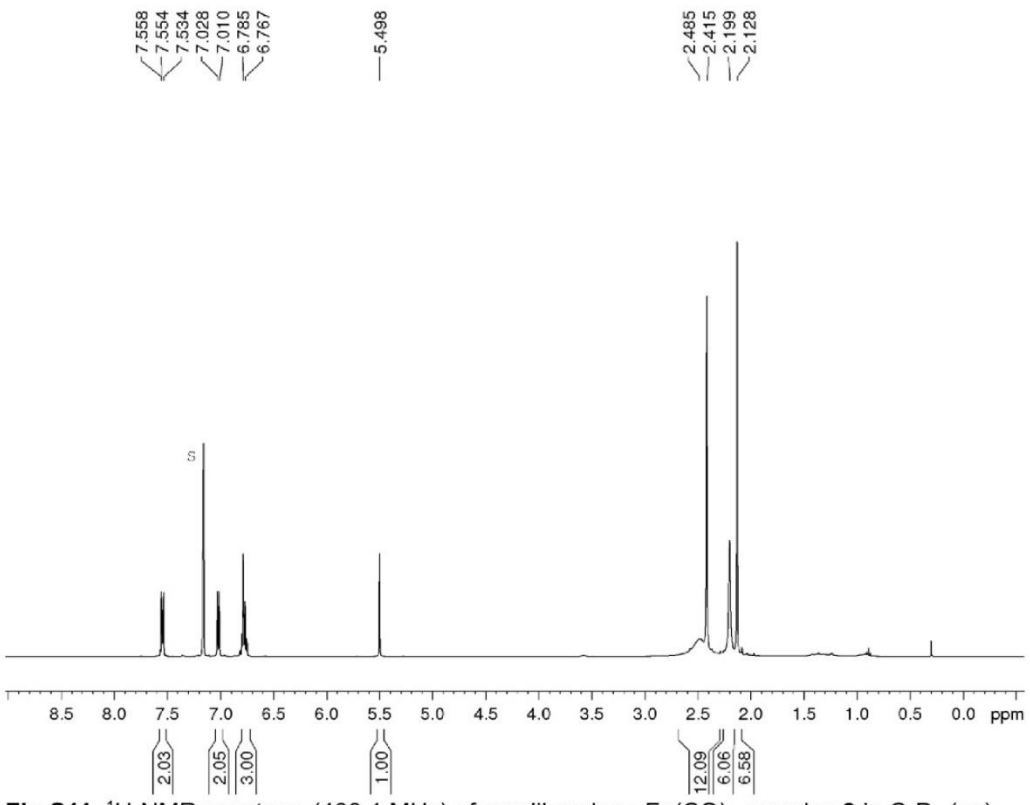

Fig S11. ^{1}H-NMR spectrum (400.1 MHz) of oxadiborolane $Fe(CO)_3$ complex **3** in C_6D_6 (=s).

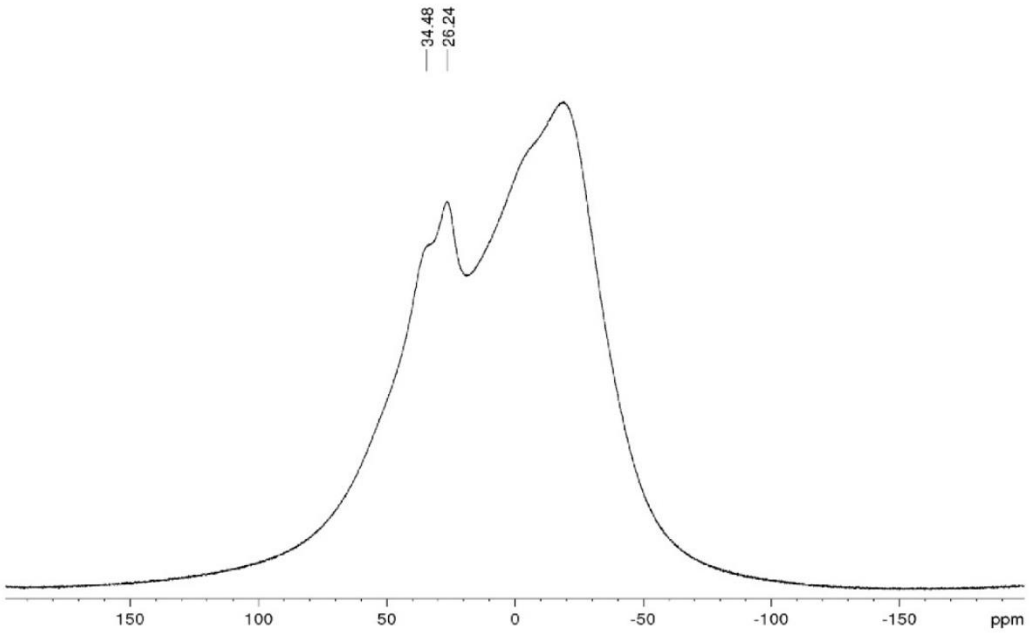

Fig S12. ^{11}B-NMR spectrum (128.4 MHz) of oxadiborolane $Fe(CO)_3$ complex **3** (glass peak from 100 to −100 ppm).

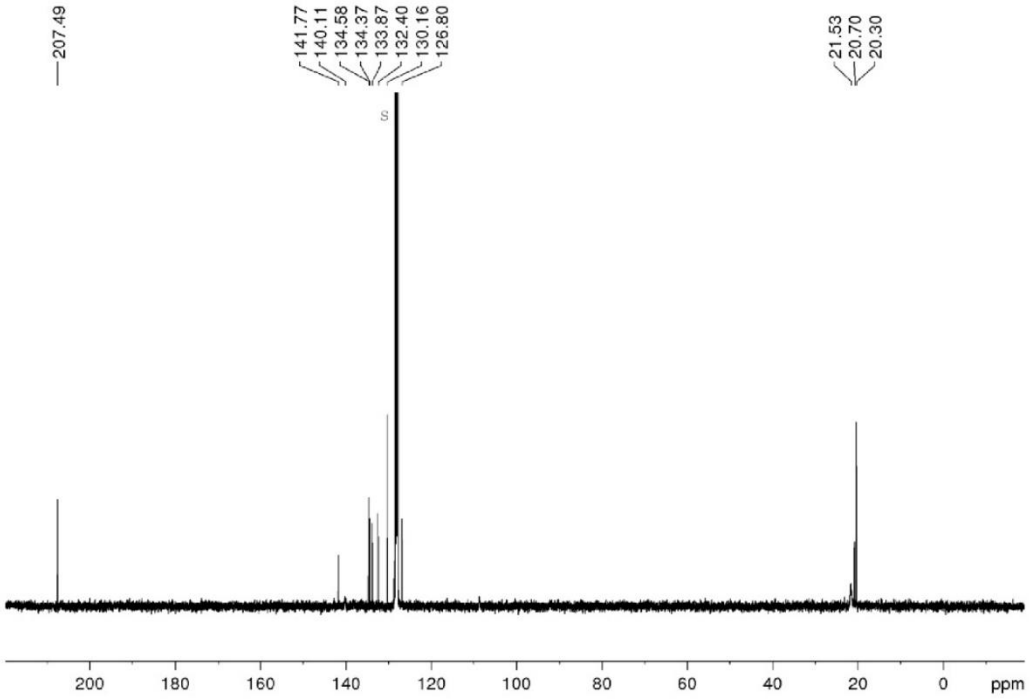

Figure S13. ^{13}C-NMR spectrum (100.61 MHz) of oxadiborolane Fe(CO)$_3$ complex **3** in C_6D_6 (=s).

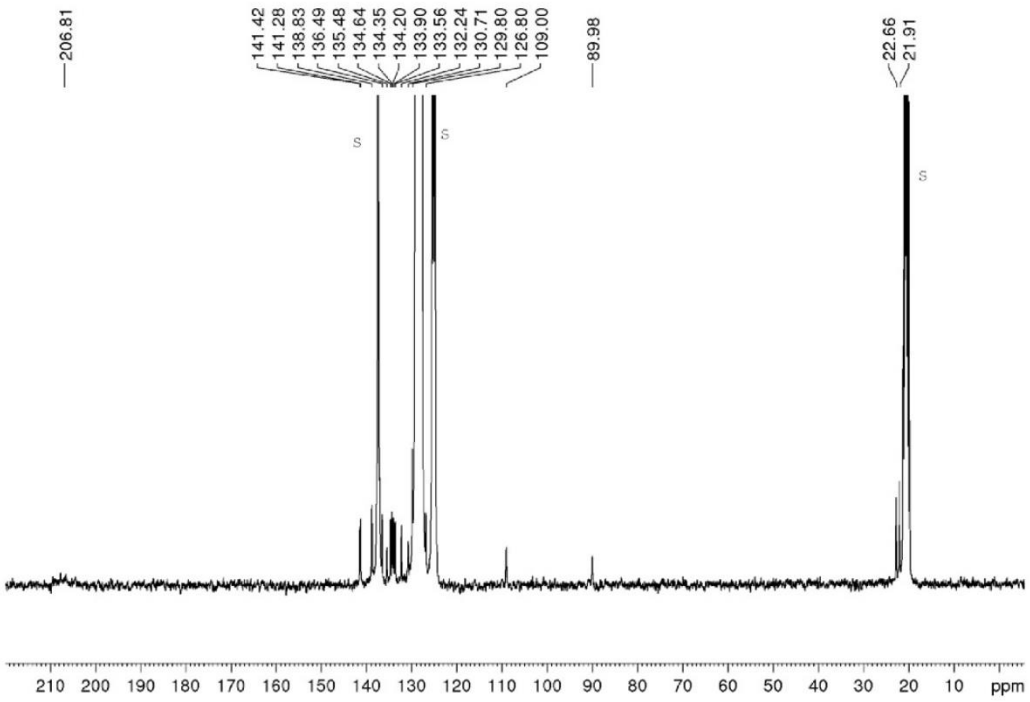

Figure S14. ^{13}C-NMR spectrum (75.47 MHz at 213 K) of oxadiborolane Fe(CO)$_3$ complex **3** in tol-d8 (=s).

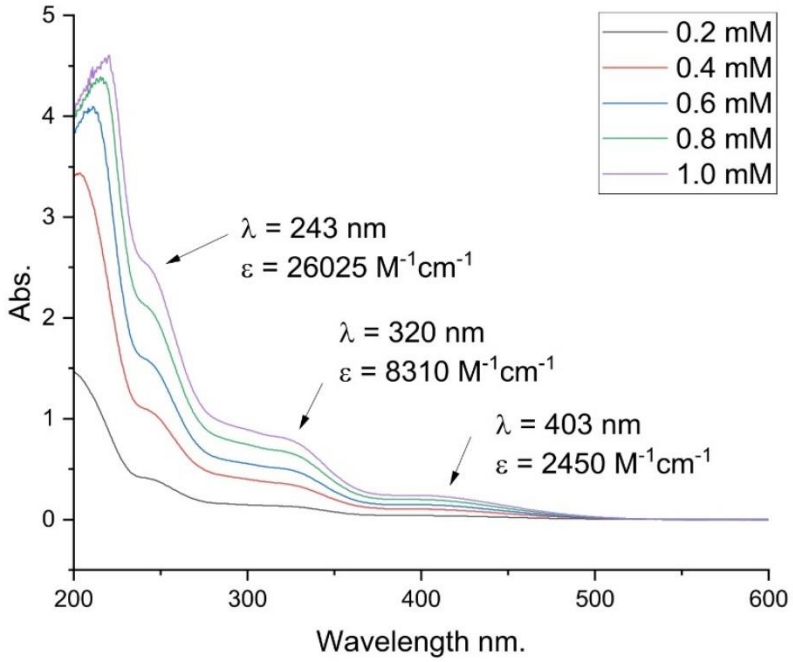

Fig S15. UV/Vis spectrum of oxadiborolane $Fe(CO)_3$ complex **3** in hexane.

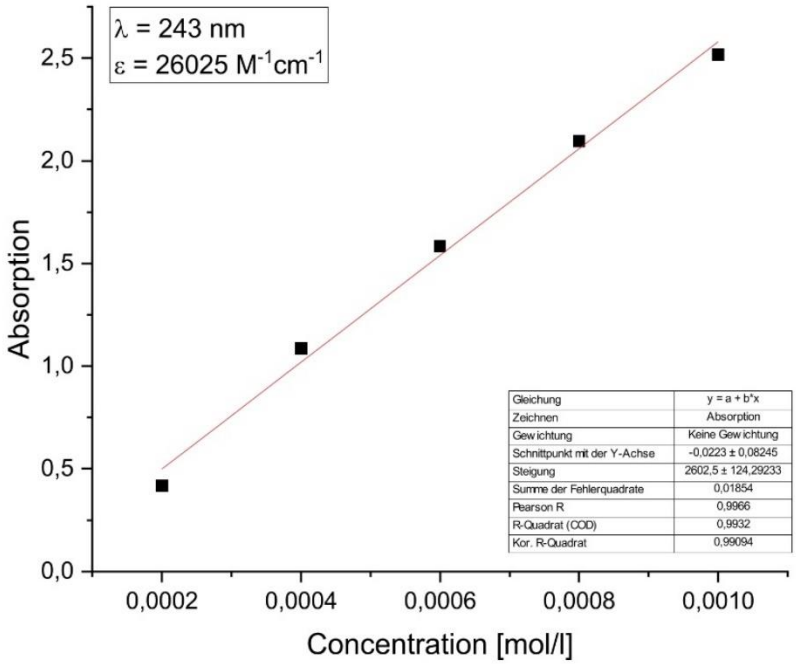

Fig S16. Determination of ε (26025 $M^{-1}cm^{-1}$) by linear regression of absorptions (λ = 243 nm) of oxadiborolane $Fe(CO)_3$ complex **3** against concentration.

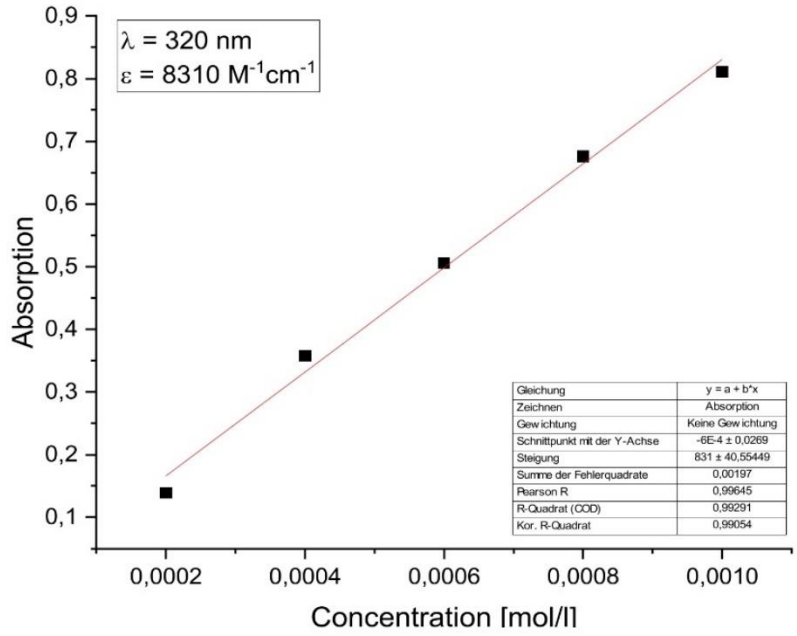

Fig S17. Determination of ε (8310 $M^{-1}cm^{-1}$) by linear regression of absorptions (λ = 320 nm) of oxadiborolane $Fe(CO)_3$ complex **3** against concentration.

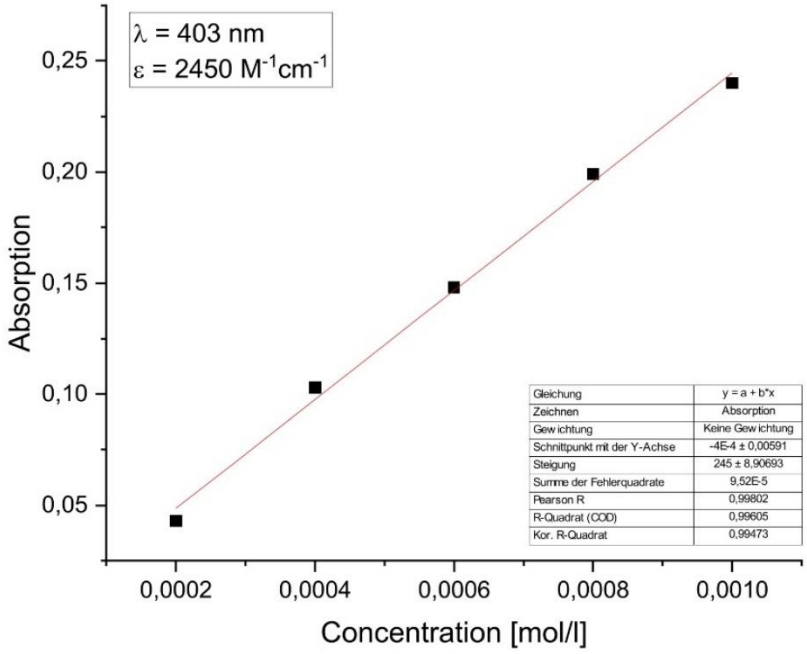

Fig S18. Determination of ε (2450 $M^{-1}cm^{-1}$) by linear regression of absorptions (λ = 403 nm) of oxadiborolane $Fe(CO)_3$ complex **3** against concentration.

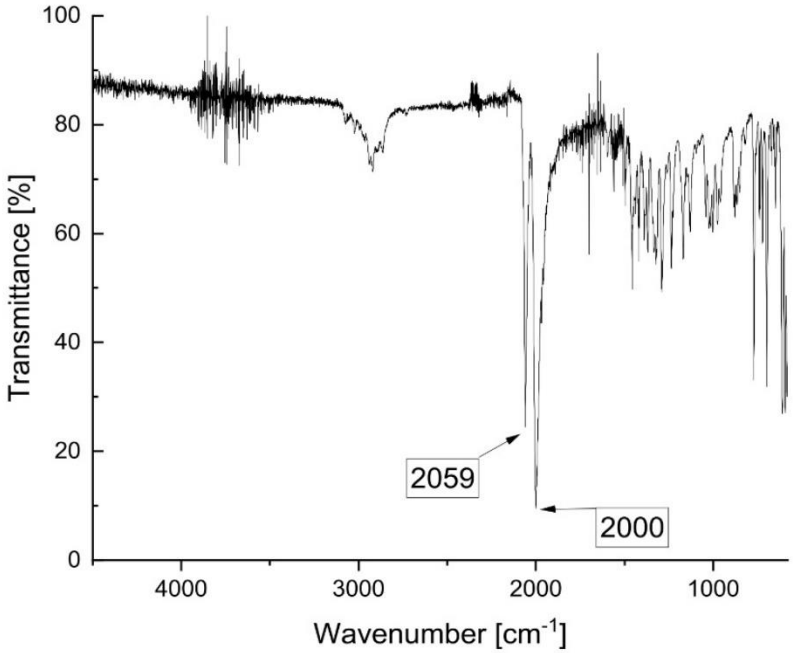

Fig S19. IR spectrum of oxadiborolane $Fe(CO)_3$ complex **3** in the solid state (The CO_2 stretching band at 2400 cm^{-1} is due to imperfect background subtraction)..

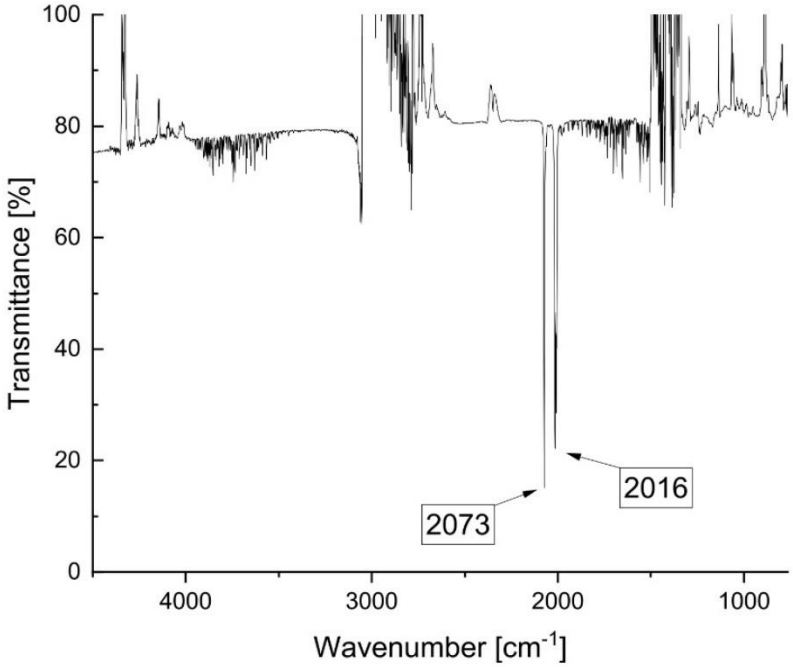

Fig S20. IR spectrum of oxadiborolane $Fe(CO)_3$ complex **3** in 1 mM hexane solution (superimposed signals around 1500 and 3000 cm^{-1} from hexane due to imperfect background substraction)[31].

2.3 1,3-Diborete $Fe(CO)_3$ complex **5**

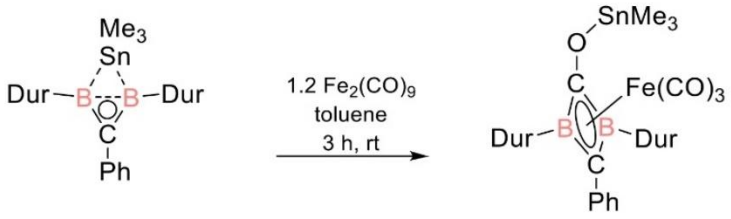

4 540.98 g/mol

5 723.90 g/mol

At ambient temperature 20 mL toluene is added to a mixture of tin bridged non-classical diborirane **4** (200 mg, 0.46 mmol) and $Fe_2(CO)_9$ (200 mg,0.55 mmol). The solution turns dark-brown. After stirring for three hours, all volatiles are removed in vacuo at room temperature. The solid residue is redissolved in 30 mL hexane and filtered. The filtrate is condensed to saturation and stored at −25 °C to give 1,3-diborete $Fe(CO)_3$ complex **5** as dark brown crystals (110 mg, 33%).

^{1}H NMR (400 MHz, C_6D_6, 300K): δ 8.04-8.02 (m, Ph-H, 2H), 7.25-7.21 (m, Ph-H, 2H), 7.16-7.13 (m, Ph-H, 1H), 6.83 (s, Dur-H, 2H), 2.26 (br s, Dur-CH_3, 12H), 2.06 (s, Dur-CH_3, 12H), 0.04 (s, $SnMe_3$, 9H).

^{11}B NMR (128.38 MHz, C_6D_6, 300 K): δ = −17.7 (br s) ppm.

^{13}C{ 1H} NMR (100.61 MHz, C_6D_6, 300 K): δ = 211.6 (s, COs),143.4, 139.7, 133.7, 132.6, 131.5, 129.1, 126.9, 126.3 (each s, Ar-C), 20.5, 19.9 (s, Dur-CH_3) 19.2 (br s, Dur-CH_3), −2.9 (s, $SnMe_3$).

^{13}C{ 1H} NMR (75.47 MHz, tol-d_8, 213 K): 257.7 (s, B_2C-O), 211.7 (s, COs), 143.0, 139.6, 139.3, 133.5, 133.4, 132.3, 131.2, 126.8 (each s, Ar-C), 111.2 (s, B_2C-Ph), 20.7, 17.7 (each s, Dur-CH_3), −3.1 (s, $SnMe_3$).

^{119}Sn NMR (149.21 MHz, C_6D_6, 300 K): δ = 191.3 (s) ppm.

UV/Vis (hexane): λmax(ε) = 248 nm (24535 $M^{-1}cm^{-1}$), 405 nm (3345 $M^{-1}cm^{-1}$).

Elemental analysis: calc. for $C_{34}H_{40}B_2FeO_4Sn$: C, 57.6%; H, 5.7%. Found: C, 57.3%; H, 5.7%.

Melting point: 168 °C (decomposition)

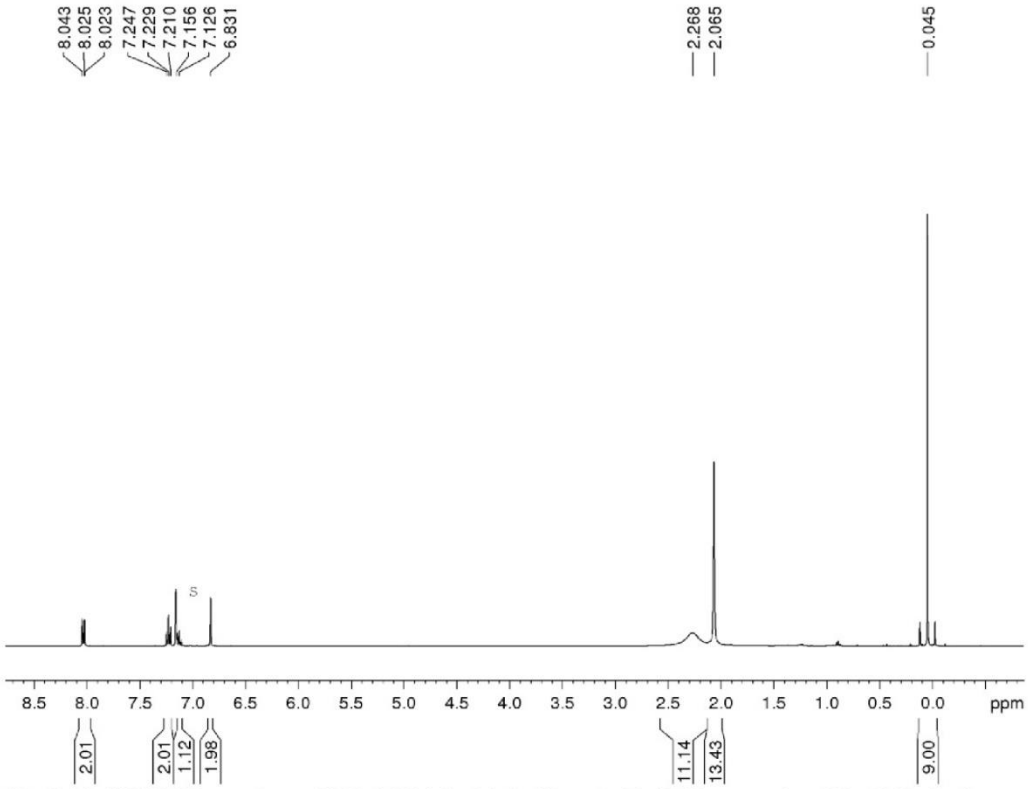

Fig S21. ^{1}H-NMR spectrum (400.1 MHz) of 1,3-diborete Fe(CO)$_3$ complex **5** in C_6D_6 (=s).

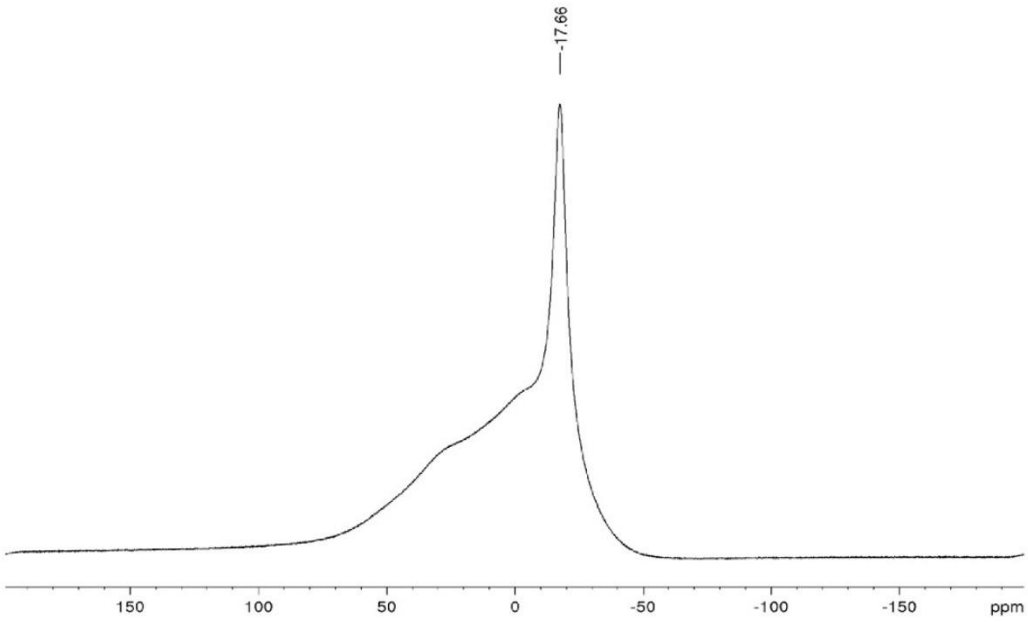

Fig S22. ^{11}B-NMR spectrum (128.4 MHz) of 1,3-diborete Fe(CO)$_3$ complex **5** (glass peak from 60 to −50 ppm).

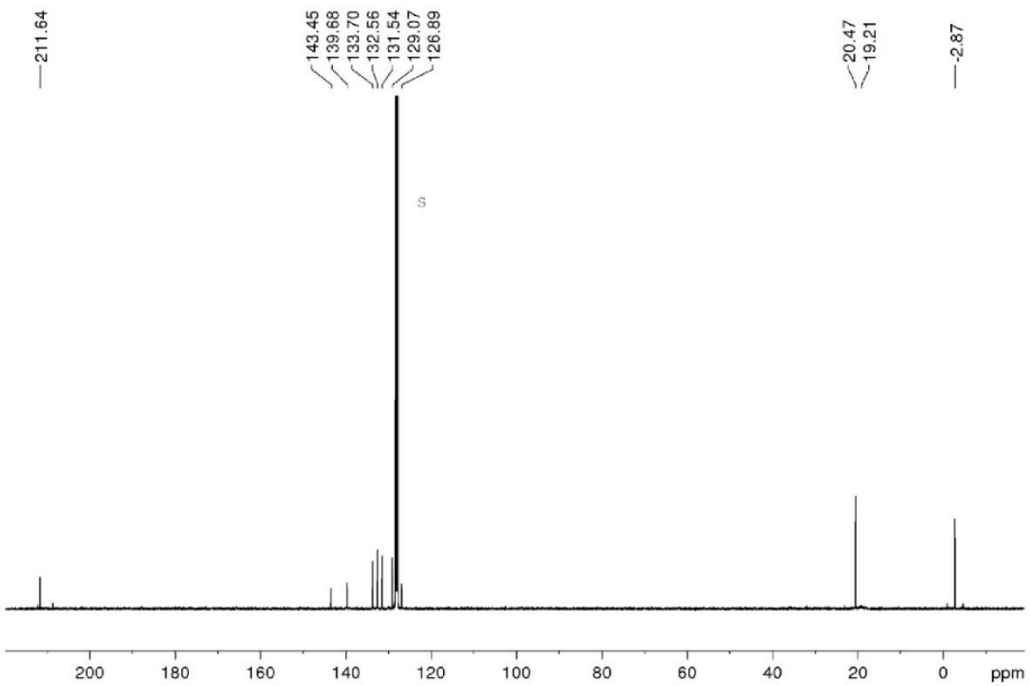

Fig S23. ^{13}C-NMR spectrum (100.61 MHz) of 1,3-diborete Fe(CO)$_3$ complex **5** in C_6D_6 (=s).

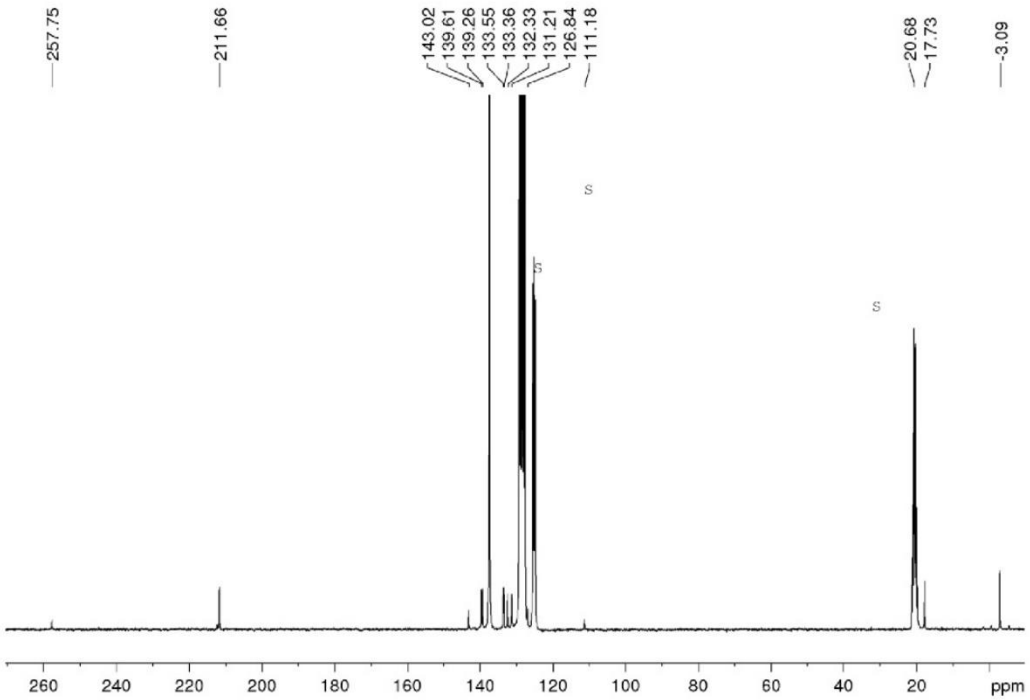

Fig S24. ^{13}C-NMR spectrum (75.47 MHz at 213 K) of 1,3-diborete Fe(CO)$_3$ complex **5** in tol-d8 (=s).

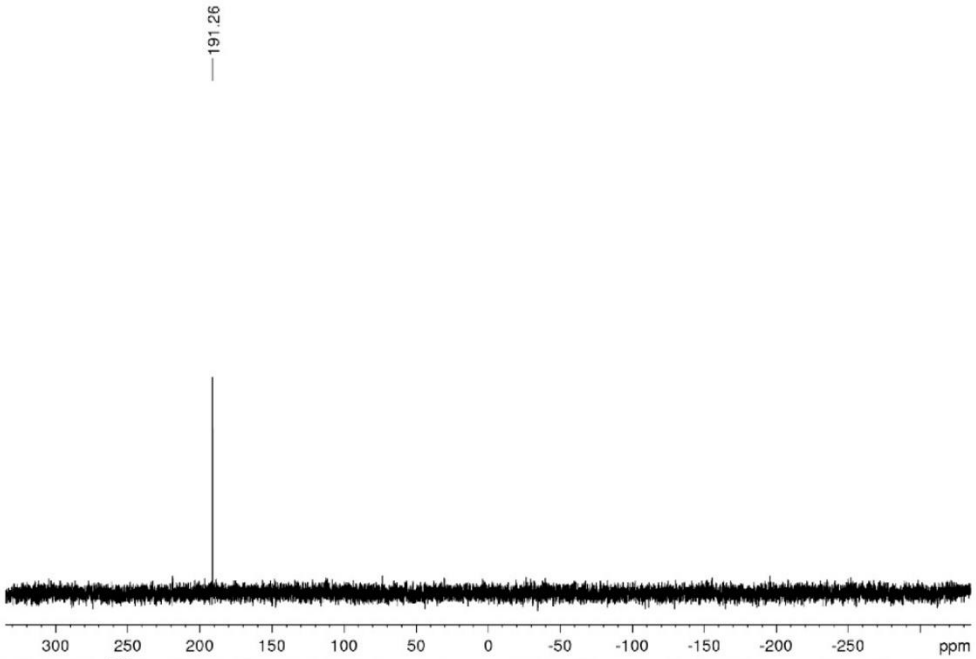

Fig S25. ^{119}Sn-NMR (149.21 MHz) spectrum of 1,3-diborete Fe(CO)$_3$ complex **5** in C_6D_6.

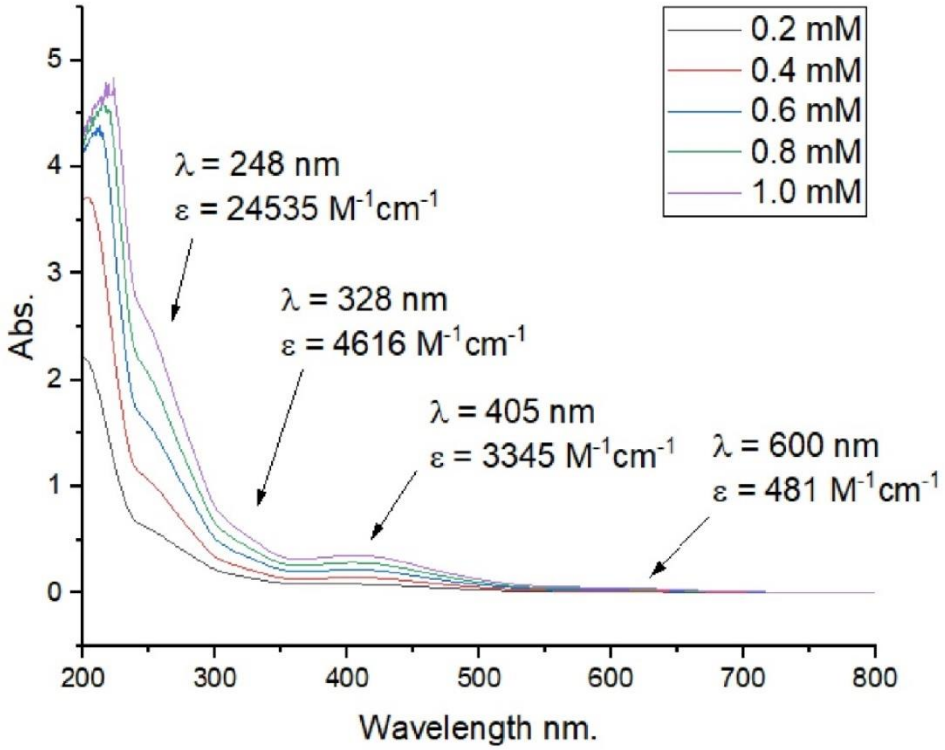

Fig S26. UV/Vis spectrum of 1,3-diborete Fe(CO)$_3$ complex **5** in hexane.

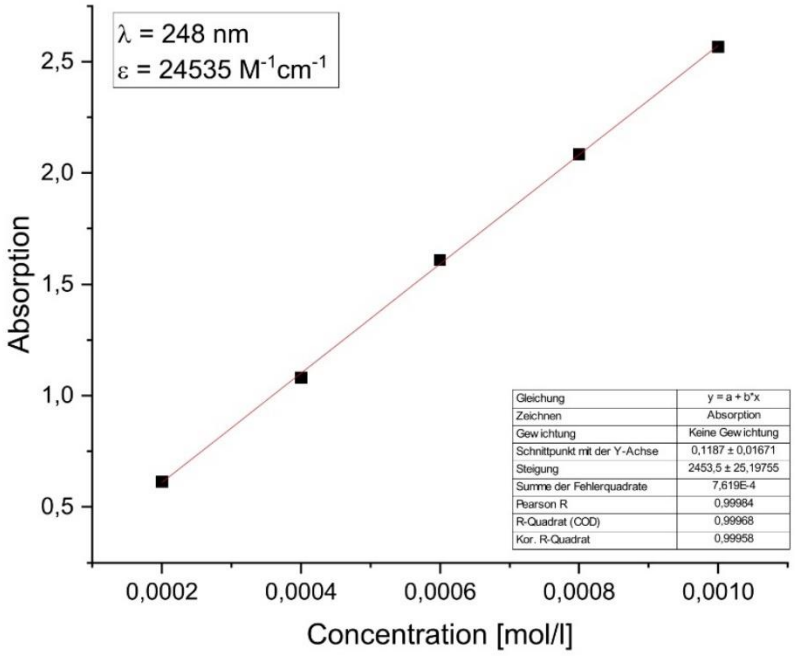

Fig S27. Determination of ε (24535 $M^{-1}cm^{-1}$) by linear regression of absorptions (λ = 248 nm) of 1,3-diborete $Fe(CO)_3$ complex **5** against concentration.

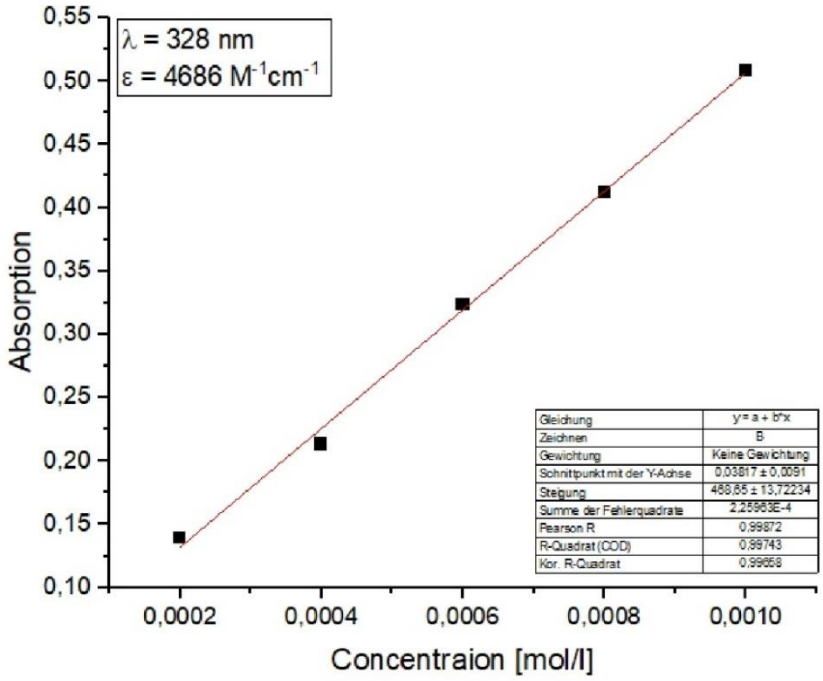

Fig S28. Determination of ε (4686 $M^{-1}cm^{-1}$) by linear regression of absorptions (λ = 328 nm) of 1,3-diborete $Fe(CO)_3$ complex **5** against concentration.

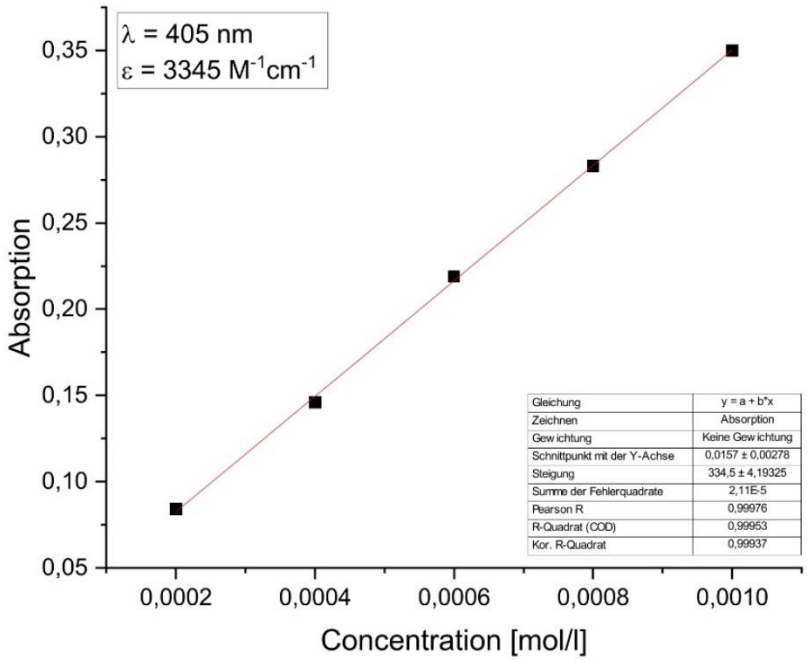

Fig S29. Determination of ε (3345 $M^{-1}cm^{-1}$) by linear regression of absorptions (λ = 405 nm) of 1,3-diborete $Fe(CO)_3$ complex **5** against concentration.

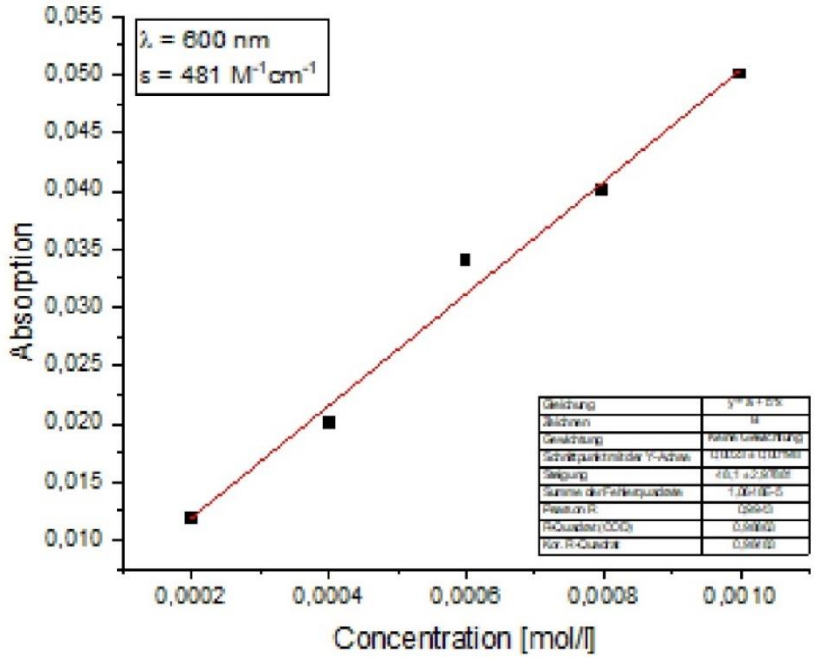

Fig S30. Determination of ε (481 $M^{-1}cm^{-1}$) by linear regression of absorptions (λ = 600 nm) of 1,3-diborete $Fe(CO)_3$ complex **5** against concentration.

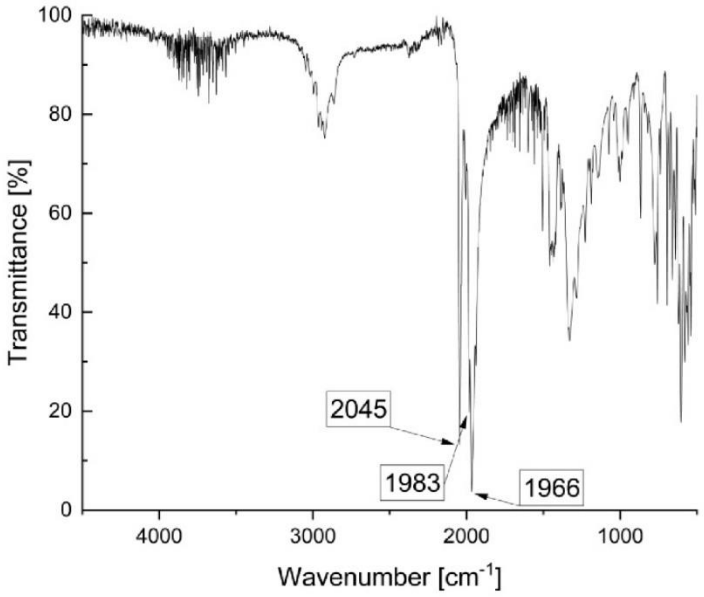

Fig S31. IR spectrum of 1,3-diborete $Fe(CO)_3$ complex **5** in the solid state.

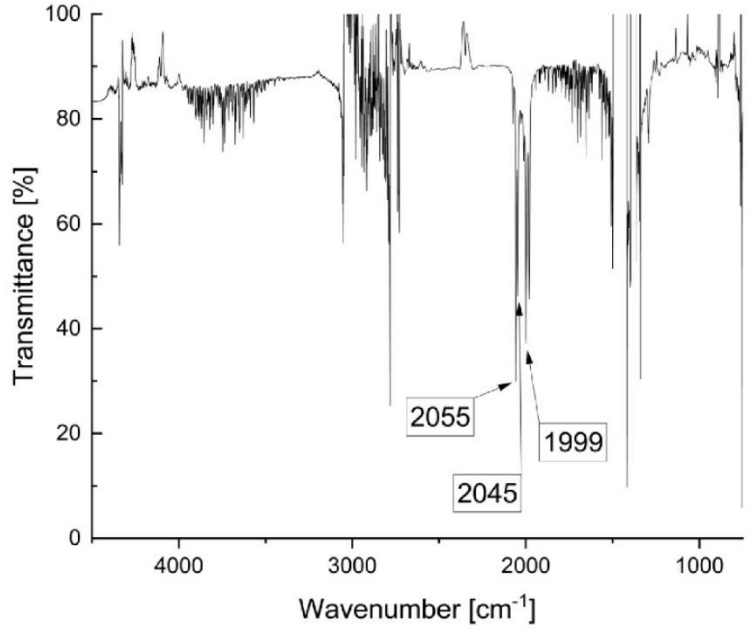

Fig S32. IR spectrum of 1,3-diborete $Fe(CO)_3$ complex **5** in 1 mM hexane solution (superimposed signals around 1500 and 3000 cm^{-1} from hexane due to imperfect background substraction)[31].

3. Details on crystallographic studies

The data set was collected using a Bruker D8 Venture diffractometer with a microfocus sealed tube and a Photon II detector. Monochromated MoKα radiation (λ = 0.71073 Å) was used. Data were collected at 133(2) K and corrected for absorption effects using the multi-scan method. The structure was solved by direct methods using SHELXT[32] and was refined by full matrix least squares calculations on F2 (SHELXL2018)[33] in the graphical user interface Shelxle[34].

Acknowledgment: Instrumentation and technical assistance for this work were provided by the Service Center X-ray Diffraction, with financial support from Saarland University and German Science Foundation (project number INST 256/506-1).

3.1 Molecular structure of diborirane $Fe(CO)_3$ complex **2** in the solid state

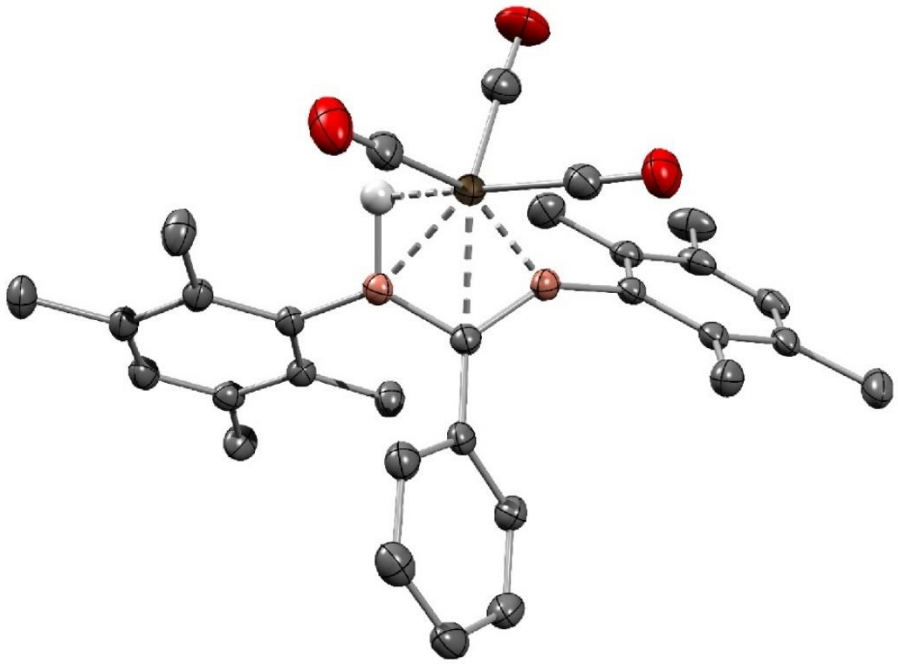

Refinement: All non H-atoms were located in the electron density maps and refined anisotropically. C-bound H atoms were placed in positions of optimized geometry and treated as riding atoms. Their isotropic displacement parameters were coupled to the corresponding carrier atoms by a factor of 1.2 (CH) or 1.5 (CH3). The B1 bonded H-atom H1 was located in the electron density maps and its positional parameters were refined using isotropic displacement parameters, which were set at 1.2 times the Ueq value of B1.

Table S1. Crystal data and structure refinement for sh5393_a.

Identification code	sh5393_a	
CCDC number	2357653	
Empirical formula	C30 H32 B2 Fe O3	
Formula weight	518.02	
Temperature	143(2) K	
Wavelength	0.71073 Å	
Crystal system	Triclinic	
Space group	P-1	
Unit cell dimensions	a = 8.9119(2) Å	α = 101.7840(10)°.
	b = 12.3028(3) Å	β = 96.3730(10)°.
	c = 12.8635(3) Å	γ = 101.5830(10)°.
Volume	1335.43(5) Å3	
Z	2	
Density (calculated)	1.288 Mg/m3	
Absorption coefficient	0.594 mm-1	
F(000)	544	
Crystal size	0.220 x 0.160 x 0.020 mm3	
Theta range for data collection	2.363 to 27.134°.	
Index ranges	-11<=h<=11, -15<=k<=15, -16<=l<=15	
Reflections collected	28379	
Independent reflections	5909 [R(int) = 0.0322]	
Completeness to theta = 25.242°	99.9 %	
Absorption correction	Semi-empirical from equivalents	
Max. and min. transmission	0.7455 and 0.7106	
Refinement method	Full-matrix least-squares on F2	
Data / restraints / parameters	5909 / 0 / 336	
Goodness-of-fit on F2	1.064	
Final R indices [I>2sigma(I)]	R1 = 0.0326, wR2 = 0.0828	
R indices (all data)	R1 = 0.0378, wR2 = 0.0862	
Extinction coefficient	n/a	
Largest diff. peak and hole	0.385 and -0.301 e.Å-3	

3.2 Molecular structure of oxadiborolane $Fe(CO)_3$ complex **3** in the solid state

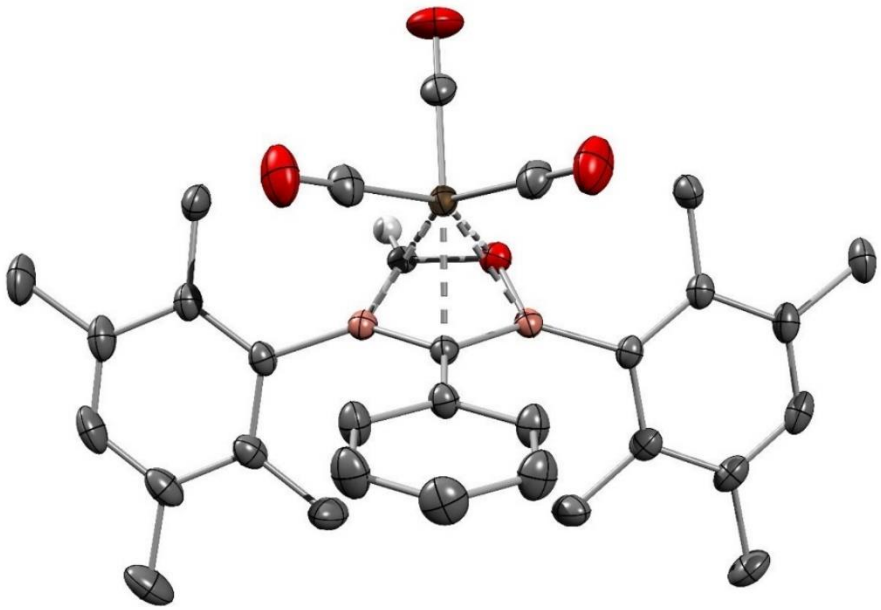

Refinement: All non H-atoms were located in the electron density maps and refined anisotropically. C-bound H atoms were placed in positions of optimized geometry and treated as riding atoms. Their isotropic displacement parameters were coupled to the corresponding carrier atoms by a factor of 1.2 (CH, CH2) or 1.5 (CH3). The C-bound H-atom H28 was located in the electron density maps. Its isotropic displacement parameters were coupled to C28 by a factor of 1.2. In addition, a restraint of 1.00 (0.01) Å was used for the C-H bond length.

Table S2. Crystal data and structure refinement for sh5285_a.

Identification code	sh5285_a	
CCDC number	2357652	
Empirical formula	C31 H32 B2 Fe O4	
Formula weight	546.03	
Temperature	143(2) K	
Wavelength	0.71073 Å	
Crystal system	Triclinic	
Space group	P-1	
Unit cell dimensions	a = 11.1006(3) Å	α = 92.8560(10)°.
	b = 11.6086(3) Å	β = 103.8400(10)°.
	c = 11.7024(3) Å	γ = 104.9170(10)°.
Volume	1404.86(6) Å3	

Z	2
Density (calculated)	1.291 Mg/m3
Absorption coefficient	0.571 mm-1
F(000)	572
Crystal size	0.230 x 0.110 x 0.010 mm3
Theta range for data collection	2.284 to 27.921°.
Index ranges	-14<=h<=14, -15<=k<=15, -15<=l<=15
Reflections collected	49513
Independent reflections	6732 [R(int) = 0.0389]
Completeness to theta = 25.242°	99.9 %
Absorption correction	Semi-empirical from equivalents
Max. and min. transmission	0.7456 and 0.7066
Refinement method	Full-matrix least-squares on F2
Data / restraints / parameters	6732 / 1 / 355
Goodness-of-fit on F2	1.067
Final R indices [I>2sigma(I)]	R1 = 0.0347, wR2 = 0.0851
R indices (all data)	R1 = 0.0421, wR2 = 0.0903
Extinction coefficient	n/a
Largest diff. peak and hole	0.438 and -0.304 e.Å-3

3.3 Molecular structure of 1,3-diborete $Fe(CO)_3$ complex **5** in the solid state

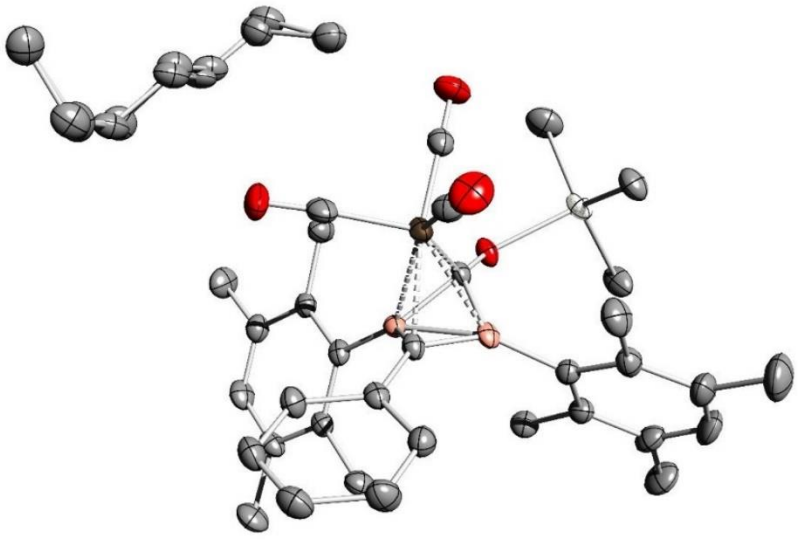

Refinement: All non H-atoms were located in the electron density maps and refined anisotropically. C-bound H atoms were placed in positions of optimized geometry and treated

as riding atoms. Their isotropic displacement parameters were coupled to the corresponding carrier atoms by a factor of 1.2 (CH, CH2) or 1.5 (CH3).

Disorder: the n-hexane solvent molecule is located over a twofold axis, and hence a PART-1 instruction was used for the refinement in SHELX.

Table S3. Crystal data and structure refinement for 5330_a.

Identification code	5330_a	
CCDC number	2357648	
Empirical formula	C37 H47 B2 Fe O4 Sn	
Formula weight	751.90	
Temperature	143(2) K	
Wavelength	0.71073 Å	
Crystal system	Monoclinic	
Space group	C2/c	
Unit cell dimensions	a = 30.8795(10) Å	α = 90°.
	b = 12.5704(4) Å	β = 124.0490(10)°.
	c = 23.0731(13) Å	γ = 90°.
Volume	7420.8(5) Å3	
Z	8	
Density (calculated)	1.346 Mg/m3	
Absorption coefficient	1.099 mm-1	
F(000)	3096	
Crystal size	0.280 x 0.020 x 0.010 mm3	
Theta range for data collection	2.131 to 27.113°.	
Index ranges	-39<=h<=39, -16<=k<=14, -29<=l<=29	
Reflections collected	50190	
Independent reflections	8191 [R(int) = 0.0770]	
Completeness to theta = 25.242°	99.9 %	
Absorption correction	Semi-empirical from equivalents	
Max. and min. transmission	0.7455 and 0.6753	
Refinement method	Full-matrix least-squares on F2	
Data / restraints / parameters	8191 / 73 / 446	
Goodness-of-fit on F2	1.017	
Final R indices [I>2sigma(I)]	R1 = 0.0373, wR2 = 0.0678	
R indices (all data)	R1 = 0.0634, wR2 = 0.0775	
Extinction coefficient	n/a	
Largest diff. peak and hole	0.627 and -0.588 e.Å-3	

4. Computational details

Computations were carried out with the Gaussian 16 program package.[35] Structural optimizations and frequency analyses were performed at the BP86/def2SVP level of theory[36,37] including the dispersion correction by Grimme.[38] Single point calculations were run with the Gaussian 16 program package at the B3LYP/def2TZVPP level of theory.[36,37] Pictures of Kohn-Sham orbitals were displayed with ChemCraft.[39]

4.1 Coordinates of optimized structures

Coordinates of diborirane $Fe(CO)_3$ complex 2:

NImag = 0

Absolute energy: −2700.8587784 Hartree

ΔG = −2700.406850 Hartree

26	-0.214972974	-0.869109077	1.763653159
8	-1.542716096	0.903472033	3.674605298
6	0.064994025	0.653425035	0.322019056
6	0.407186030	2.085947145	0.437341065
6	1.622786112	2.492189190	1.034710107
1	2.287596168	1.725533146	1.463009138
6	1.977115118	3.847466291	1.087771112
1	2.928501181	4.145981326	1.555926144
6	1.120423042	4.824953350	0.547966074
1	1.397576049	5.889854438	0.592237074
6	-0.093859039	4.433956309	-0.043540970
1	-0.769955099	5.192581353	-0.468844001
6	-0.448767046	3.077223203	-0.097101974
1	-1.387833107	2.768115167	-0.582070007
6	2.421872212	-0.571528019	-0.619679010
6	3.469525301	-1.451385067	-0.186078980
6	4.765981393	-1.333099039	-0.746998019
6	4.981829391	-0.381600969	-1.758490093
1	5.995578443	-0.283519949	-2.183507125
6	3.956697307	0.431329075	-2.270446131
6	2.656436214	0.325781049	-1.716937090
6	3.256228298	-2.502857144	0.878101095
1	2.199735229	-2.811084185	0.969229100
6	5.914004500	-2.195705089	-0.274277986

1	5.736421505	-3.273505168	-0.482126002
1	6.858490532	-1.911129054	-0.778280025
1	6.074527508	-2.108330078	0.821363091
6	4.252478316	1.402206148	-3.389151210
1	3.683962279	1.154279125	-4.312002279
1	3.967900280	2.440851218	-3.116990191
1	5.329632370	1.399845166	-3.647582227
6	1.564706126	1.159378091	-2.342778136
1	0.556514059	0.852516058	-2.018320113
1	1.678042118	2.236405175	-2.093290119
1	1.605201129	1.082226091	-3.449212214
6	-2.539766151	-0.230880063	-0.621998013
6	-3.708210244	0.472953972	-0.229575983
6	-4.919189330	0.255523939	-0.930339034
6	-4.927184315	-0.660478126	-1.998266110
1	-5.872970403	-0.834131154	-2.539186151
6	-3.779254222	-1.369083161	-2.401774139
6	-2.565364137	-1.148538128	-1.707775090
6	-1.310819037	-1.906470166	-2.078218114
1	-1.230892031	-2.087518177	-3.168370196
1	-0.395206980	-1.357870112	-1.772856097
6	-1.028792048	0.182481988	2.920267242
6	-1.453558043	-2.133070183	1.693592155
5	1.093637116	-0.460516029	0.175955046
1	0.724949103	-1.642226121	0.662862080
5	-1.232375061	-0.038866031	0.163848045
8	-2.275398093	-2.953072257	1.620715151
6	0.989666122	-1.384519097	2.991978247
8	1.718481176	-1.751774114	3.821825309
1	3.845881352	-3.414192205	0.657321081
1	3.580540317	-2.150347116	1.880963167
1	-1.273698020	-2.900008236	-1.578171083
6	-3.856687215	-2.353197234	-3.546129222
1	-3.558598178	-3.376076303	-3.230326199
1	-4.885084290	-2.412766252	-3.953661253

1	-3.180468172	-2.070432202	-4.382310282
6	-3.660284254	1.430426039	0.938087099
1	-4.126730302	2.408403106	0.695519085
1	-4.203330286	1.029441005	1.821772162
1	-2.621022180	1.638950069	1.260776125
6	-6.181208424	0.983979974	-0.533664005
1	-7.036927512	0.684546938	-1.170266051
1	-6.457097470	0.781013956	0.523691071
1	-6.065100427	2.086478058	-0.620145009

Coordinates of oxadiborolane $Fe(CO)_3$ complex 3:

NImag = 0

Absolute energy: −2814.1671690 Hartree

ΔG = −2813.696837 Hartree

26	0.077003000	1.898743000	0.256073000
8	0.810256000	1.368711000	-1.578695000
8	-0.181189000	4.818026000	-0.070835000
8	2.234328000	1.871373000	2.270655000
6	-0.031254000	-0.273877000	-0.025021000
6	-1.275250000	-1.697999000	1.657743000
1	-2.221596000	-1.419868000	1.174099000
6	2.750728000	-0.213719000	-0.816599000
6	3.837555000	0.711601000	-0.751656000
6	5.172101000	0.231275000	-0.691843000
6	5.402800000	-1.153201000	-0.732808000
1	6.441909000	-1.520876000	-0.678712000
6	4.360697000	-2.085063000	-0.865100000
6	3.024848000	-1.614244000	-0.918723000
6	3.648065000	2.212386000	-0.749125000
1	4.063354000	2.673374000	0.172532000
1	4.194888000	2.673161000	-1.599775000
1	2.593549000	2.516966000	-0.839882000
6	4.667394000	-3.561352000	-0.949814000
1	4.146138000	-4.136466000	-0.154556000

1	4.333903000	-3.997009000	-1.916878000
1	5.754130000	-3.752297000	-0.851348000
6	1.931134000	-2.637012000	-1.123820000
1	0.936252000	-2.175483000	-1.243670000
1	2.130313000	-3.246158000	-2.031339000
1	1.862814000	-3.345563000	-0.271077000
6	-2.783588000	-0.121447000	-0.861291000
6	-3.872234000	0.764090000	-0.613120000
6	-3.055218000	-1.492674000	-1.159046000
6	-3.687831000	2.254946000	-0.441579000
1	-4.028836000	2.604085000	0.556719000
1	-2.637575000	2.567433000	-0.561997000
1	-4.291274000	2.813910000	-1.188948000
6	-1.949512000	-2.441329000	-1.566684000
1	-1.688976000	-3.154094000	-0.753636000
1	-2.246383000	-3.049408000	-2.445851000
1	-1.023839000	-1.901442000	-1.838388000
6	-0.593718000	1.440551000	-1.626493000
1	-0.941361000	2.218727000	-2.323246000
6	-1.198325000	1.741935000	1.457125000
6	-0.068215000	3.669232000	0.043127000
6	1.407578000	1.880739000	1.458868000
6	-0.057433000	-1.181308000	1.147937000
6	1.136923000	-1.527089000	1.832912000
1	2.096333000	-1.118627000	1.484255000
6	1.118685000	-2.375053000	2.947887000
1	2.063766000	-2.625217000	3.455673000
5	1.243537000	0.223648000	-0.750977000
5	-1.260039000	0.307293000	-0.825431000
8	-2.001422000	1.612775000	2.284405000
6	-4.378617000	-1.993793000	-1.090888000
6	-5.197856000	0.258468000	-0.541898000
6	-5.420285000	-1.110319000	-0.760150000
6	-4.674885000	-3.450698000	-1.360153000
1	-5.747519000	-3.677792000	-1.200743000

1	-4.422347000	-3.738353000	-2.404398000
1	-4.083221000	-4.121210000	-0.700432000
6	-6.360824000	1.174811000	-0.242649000
1	-6.228122000	1.710129000	0.722417000
1	-6.477539000	1.961593000	-1.019866000
1	-7.313194000	0.611370000	-0.189452000
6	6.337442000	1.186726000	-0.589590000
1	7.299711000	0.641074000	-0.532200000
1	6.388396000	1.870855000	-1.464466000
1	6.261545000	1.837083000	0.308542000
1	-6.450231000	-1.500831000	-0.693093000
6	-1.294437000	-2.548792000	2.772806000
6	-0.098043000	-2.898793000	3.421341000
1	-0.113516000	-3.565929000	4.297616000
1	-2.257362000	-2.936232000	3.141836000

Coordinates of 1,3-diborete $Fe(CO)_3$ complex 5:

NImag = 0

Absolute energy: −3147.6503343 Hartree

ΔG = −3147.101157 Hartree

8	0.982697000	-1.726373000	0.187987000
8	-0.239552000	2.014269000	-3.979575000
8	1.360525000	-2.170361000	-3.238444000
8	-2.950097000	-1.227148000	-3.117958000
5	-1.271367000	-0.327229000	-0.000763000
5	0.174443000	0.810905000	-0.068437000
50	3.074768000	-1.772243000	-0.038447000
26	-0.440211000	-0.191437000	-2.027654000
6	-1.210339000	1.090471000	-0.623393000
6	-2.166555000	2.187450000	-0.726890000
6	-3.510565000	1.939660000	-1.098161000
1	-3.816097000	0.909586000	-1.335993000
6	-4.444590000	2.983181000	-1.142742000
1	-5.486737000	2.772024000	-1.430350000

6	-4.056146000	4.295996000	-0.814785000
1	-4.791166000	5.115519000	-0.848511000
6	-2.725330000	4.554844000	-0.442491000
1	-2.415230000	5.578903000	-0.180300000
6	-1.787434000	3.511816000	-0.401525000
1	-0.749859000	3.708296000	-0.092882000
6	-2.383798000	-1.044731000	0.849973000
6	-2.744440000	-2.398255000	0.583764000
6	-3.856188000	-2.976368000	1.251086000
6	-3.089405000	-0.302294000	1.844815000
6	-2.696475000	1.104331000	2.239886000
1	-3.448657000	1.849492000	1.902536000
1	-1.725098000	1.414543000	1.820943000
1	-2.627181000	1.199115000	3.344086000
6	-1.989271000	-3.262422000	-0.402293000
1	-2.608970000	-3.497384000	-1.295184000
1	-1.719949000	-4.237515000	0.055553000
1	-1.054366000	-2.796073000	-0.750528000
6	1.301459000	1.523029000	0.774110000
6	1.544892000	1.125680000	2.121507000
6	2.607425000	1.726741000	2.849400000
6	3.426451000	2.672422000	2.209026000
1	4.264918000	3.118586000	2.770930000
6	3.197602000	3.089182000	0.886108000
6	2.107500000	2.530681000	0.172515000
6	1.827474000	3.018924000	-1.228484000
1	0.872083000	2.623861000	-1.611551000
1	2.626637000	2.723648000	-1.943341000
1	1.768906000	4.127165000	-1.268817000
6	4.091337000	4.124699000	0.245546000
1	3.526758000	5.041494000	-0.032100000
1	4.550794000	3.748933000	-0.694390000
1	4.910689000	4.427665000	0.926916000
6	2.854434000	1.366070000	4.295479000
1	3.724128000	1.916607000	4.705168000

1	3.046397000	0.279134000	4.428230000
1	1.973056000	1.601754000	4.930366000
6	0.682081000	0.111770000	2.838298000
1	0.137952000	0.585950000	3.683610000
1	1.293516000	-0.701442000	3.281446000
1	-0.070910000	-0.362359000	2.187218000
6	0.221331000	-0.779572000	-0.299435000
6	3.559357000	-0.141186000	-1.365841000
1	2.612626000	0.263107000	-1.771966000
1	4.193149000	-0.508793000	-2.195312000
1	4.072309000	0.651024000	-0.789393000
6	3.808959000	-1.593310000	1.983674000
1	3.803528000	-0.524856000	2.268752000
1	4.838943000	-1.998884000	2.034205000
1	3.153331000	-2.173243000	2.660908000
6	3.287379000	-3.766325000	-0.846213000
1	2.737646000	-4.474598000	-0.196485000
1	4.357836000	-4.051076000	-0.877524000
1	2.861657000	-3.789325000	-1.866512000
6	-0.323491000	1.140828000	-3.219510000
6	0.642072000	-1.381750000	-2.768467000
6	-1.942546000	-0.798402000	-2.726733000
6	-4.192995000	-0.891369000	2.513282000
6	-4.561402000	-2.208471000	2.191489000
6	-4.283495000	-4.396099000	0.960925000
1	-4.514100000	-4.546622000	-0.115964000
1	-3.484866000	-5.128263000	1.211898000
1	-5.185825000	-4.670448000	1.542485000
6	-4.975858000	-0.118999000	3.549261000
1	-4.345008000	0.160661000	4.421533000
1	-5.376096000	0.832966000	3.138568000
1	-5.831404000	-0.711443000	3.929775000
1	-5.428795000	-2.658972000	2.704196000

Coordinates of Tin bridged diborirane $Fe(CO)_3$ complex 6:

NImag = 0

Absolute energy: −3034.3712699 Hartree

ΔG = −3033.827647 Hartree

26	0.135948000	-0.072087000	-1.691430000
8	0.699289000	2.151694000	-3.516255000
6	0.222148000	1.283170000	-0.047646000
6	0.389939000	2.761332000	-0.060971000
6	-0.616308000	3.606601000	-0.583682000
1	-1.516610000	3.155886000	-1.030892000
6	-0.475566000	5.000667000	-0.542868000
1	-1.270178000	5.642075000	-0.955820000
6	0.677081000	5.579780000	0.018957000
1	0.789365000	6.674918000	0.047298000
6	1.685169000	4.750732000	0.540638000
1	2.591034000	5.194756000	0.983218000
6	1.545099000	3.354676000	0.499734000
1	2.330828000	2.706784000	0.918902000
6	-2.502580000	0.703527000	0.508645000
6	-3.716994000	0.432410000	-0.200081000
6	-4.934810000	0.277158000	0.502832000
6	-4.937188000	0.449526000	1.898479000
1	-5.885075000	0.318026000	2.448043000
6	-3.786603000	0.816037000	2.614347000
6	-2.556729000	0.958015000	1.920583000
6	-3.745460000	0.361038000	-1.705599000
1	-3.847979000	-0.679185000	-2.082190000
6	-6.217263000	-0.057074000	-0.222125000
1	-6.110844000	-0.965639000	-0.851989000
1	-7.046895000	-0.232027000	0.490818000
1	-6.529610000	0.762612000	-0.905872000
6	-3.865243000	1.036766000	4.106011000
1	-3.184337000	0.353181000	4.658166000
1	-3.564149000	2.068918000	4.387221000

1	-4.893046000	0.869321000	4.483509000
6	-1.353790000	1.372415000	2.732518000
1	-0.447358000	1.492187000	2.118345000
1	-1.547546000	2.339166000	3.244196000
1	-1.130989000	0.637932000	3.536483000
6	2.707763000	-0.046745000	0.593273000
6	3.913496000	0.303442000	-0.081202000
6	5.158460000	-0.085190000	0.470191000
6	5.174142000	-0.805624000	1.678726000
1	6.145759000	-1.119563000	2.096667000
6	3.999692000	-1.123908000	2.382936000
6	2.753350000	-0.725962000	1.842088000
6	1.483144000	-1.020132000	2.597060000
1	1.515061000	-0.603673000	3.626651000
1	0.606879000	-0.574818000	2.090319000
6	0.472770000	1.256160000	-2.810789000
6	1.574390000	-1.046253000	-2.031775000
5	-1.119336000	0.610244000	-0.179810000
5	1.351054000	0.315320000	-0.045645000
8	2.508832000	-1.689165000	-2.301271000
6	-1.046151000	-0.740164000	-2.834052000
8	-1.720593000	-1.178655000	-3.678128000
1	-4.609540000	0.927008000	-2.110752000
1	-2.827970000	0.787407000	-2.145382000
1	1.294251000	-2.109762000	2.699453000
6	4.064718000	-1.872737000	3.692289000
1	3.485668000	-2.820645000	3.651094000
1	5.109025000	-2.124801000	3.962172000
1	3.633174000	-1.279342000	4.527680000
6	3.891003000	1.122015000	-1.350602000
1	4.521285000	2.031013000	-1.251053000
1	4.286344000	0.550487000	-2.217380000
1	2.872851000	1.466865000	-1.610174000
6	6.450829000	0.264306000	-0.227952000
1	7.325957000	-0.141608000	0.316429000

1	6.477871000	-0.136281000	-1.264078000
1	6.586549000	1.364406000	-0.315365000
50	-0.694537000	-2.196784000	-0.223887000
6	1.059171000	-3.477958000	0.060364000
1	0.812214000	-4.244944000	0.821867000
1	1.300055000	-3.977748000	-0.897776000
1	1.940132000	-2.894617000	0.388466000
6	-1.761278000	-2.190925000	1.691493000
1	-2.816286000	-1.915535000	1.506531000
1	-1.698928000	-3.234653000	2.062552000
1	-1.330529000	-1.506606000	2.441650000
6	-2.082912000	-3.368778000	-1.438100000
1	-1.652319000	-3.618724000	-2.425646000
1	-2.291383000	-4.302976000	-0.878346000
1	-3.030277000	-2.815122000	-1.583286000

Coordinates of CO

NImag = 0

Absolute energy: −113.2244328 Hartree

ΔG = −113.238679 Hartree

6	0.000000000	0.000000000	-0.652816000
8	0.000000000	0.000000000	0.489612000

Coordinates of Me_3Sn analogue of 3:

NImag = 0

Absolute energy: −3147.655461 Hartree

ΔG = −3147.104333 Hartree

26	-0.322599000	-0.770522000	1.527062000
8	-0.664679000	-1.373923000	-0.383750000
8	0.809496000	-3.228270000	2.691433000
8	-2.888354000	-0.740524000	2.980219000
6	-0.621667000	0.962676000	0.205871000
6	-0.201604000	3.389066000	0.746353000
1	0.843394000	3.257565000	0.430840000

6	-3.038356000	-0.301111000	-0.722758000
6	-3.868847000	-1.404637000	-0.354864000
6	-5.259605000	-1.366460000	-0.636745000
6	-5.790828000	-0.252265000	-1.306437000
1	-6.874684000	-0.222667000	-1.512244000
6	-4.987707000	0.810464000	-1.751067000
6	-3.597942000	0.780262000	-1.474078000
6	-3.339350000	-2.650437000	0.321812000
1	-3.827380000	-2.819241000	1.305374000
1	-3.566417000	-3.547563000	-0.293838000
1	-2.248732000	-2.631933000	0.474807000
6	-5.601931000	1.959564000	-2.514641000
1	-5.391678000	2.935846000	-2.027437000
1	-5.194858000	2.033868000	-3.546784000
1	-6.701232000	1.847575000	-2.593983000
6	-2.746927000	1.891970000	-2.044415000
1	-1.668553000	1.720777000	-1.888603000
1	-2.916501000	1.986960000	-3.138342000
1	-2.993409000	2.877185000	-1.594772000
6	2.216812000	1.280367000	-0.227576000
6	3.360039000	1.185822000	0.613022000
6	2.269675000	2.103496000	-1.395095000
6	3.412929000	0.258058000	1.804105000
1	3.355192000	0.813373000	2.765011000
1	2.589598000	-0.476112000	1.789099000
1	4.364026000	-0.311625000	1.828452000
6	1.097319000	2.142236000	-2.353110000
1	0.360564000	2.926382000	-2.069078000
1	1.416509000	2.355868000	-3.391289000
1	0.551199000	1.178859000	-2.367552000
6	0.708400000	-1.024309000	-0.252424000
6	0.397828000	0.369443000	2.654335000
6	0.356783000	-2.266217000	2.223425000
6	-1.897926000	-0.760925000	2.377166000
6	-1.080500000	2.279136000	0.700515000

6	-2.411566000	2.470277000	1.153709000
1	-3.110472000	1.620905000	1.146457000
6	-2.851126000	3.721101000	1.604805000
1	-3.890077000	3.841136000	1.950811000
5	-1.532455000	-0.181618000	-0.296313000
5	0.854630000	0.494170000	-0.043452000
8	0.789080000	1.157469000	3.411494000
6	3.414773000	2.891862000	-1.666415000
6	4.506470000	1.980883000	0.341968000
6	4.504280000	2.824435000	-0.779702000
6	3.483276000	3.799901000	-2.873844000
1	4.428519000	4.377941000	-2.882595000
1	3.433393000	3.229113000	-3.826982000
1	2.642974000	4.526343000	-2.895893000
6	5.717569000	1.927555000	1.243753000
1	5.458880000	2.164606000	2.298214000
1	6.179522000	0.915813000	1.257348000
1	6.494521000	2.645805000	0.915313000
6	-6.166025000	-2.504143000	-0.229887000
1	-7.218657000	-2.296871000	-0.505761000
1	-5.871511000	-3.460393000	-0.714672000
1	-6.131863000	-2.688806000	0.865623000
1	5.394098000	3.445087000	-0.981222000
6	-0.643824000	4.644699000	1.190960000
6	-1.970577000	4.819356000	1.618951000
1	-2.316394000	5.803832000	1.971666000
1	0.058999000	5.492769000	1.209738000
50	2.105331000	-2.534913000	-0.955205000
6	3.715313000	-2.958403000	0.439253000
1	3.327359000	-3.031032000	1.472677000
1	4.180401000	-3.924473000	0.159577000
1	4.477096000	-2.158314000	0.384042000
6	2.896995000	-1.616024000	-2.759674000
1	3.716495000	-2.224961000	-3.189153000
1	2.091035000	-1.503561000	-3.510972000

1	3.281634000	-0.613093000	-2.486659000
6	0.907067000	-4.311063000	-1.317461000
1	0.038704000	-4.049604000	-1.952724000
1	1.510059000	-5.091193000	-1.822136000
1	0.538719000	-4.707562000	-0.350926000

Coordinates of $Fe(CO)_4$ complex of diborirane 1:

NImag = 0

Absolute energy: −3147.6021649 Hartree

ΔG = −3147.054949 Hartree

26	-0.819574000	-0.518712000	2.026731000
8	0.540163000	1.773317000	3.326193000
6	-0.163138000	0.746364000	-0.009859000
6	-0.029021000	2.241696000	-0.073730000
6	-0.961753000	2.979348000	-0.849891000
1	-1.793889000	2.449233000	-1.337192000
6	-0.815191000	4.360784000	-1.042391000
1	-1.546190000	4.904551000	-1.661361000
6	0.263806000	5.043607000	-0.455791000
1	0.382850000	6.128139000	-0.606090000
6	1.191127000	4.330173000	0.324882000
1	2.042726000	4.852494000	0.787791000
6	1.047495000	2.949838000	0.516158000
1	1.790029000	2.410641000	1.115287000
6	2.512800000	0.483341000	-0.299857000
6	3.527993000	0.437567000	0.693442000
6	4.769447000	1.085941000	0.474087000
6	4.980655000	1.756728000	-0.742835000
1	5.944314000	2.267253000	-0.910885000
6	4.004263000	1.797721000	-1.753199000
6	2.761604000	1.153283000	-1.534208000
6	3.284194000	-0.257416000	2.009767000
1	4.137461000	-0.899241000	2.309605000
6	5.847498000	1.068905000	1.532361000

1	6.187318000	0.034140000	1.757006000
1	6.734154000	1.651566000	1.213101000
1	5.489682000	1.494666000	2.494795000
6	4.271744000	2.539534000	-3.041476000
1	4.213491000	1.868245000	-3.925966000
1	3.525426000	3.345549000	-3.211694000
1	5.277742000	3.003788000	-3.036956000
6	1.709389000	1.218723000	-2.620353000
1	0.855914000	0.542701000	-2.421263000
1	1.295185000	2.245705000	-2.719124000
1	2.125611000	0.939671000	-3.610797000
6	-2.981997000	0.320956000	-0.493507000
6	-4.019826000	1.105065000	0.084236000
6	-5.309377000	1.075833000	-0.497739000
6	-5.525671000	0.264796000	-1.628439000
1	-6.535811000	0.235673000	-2.071188000
6	-4.506499000	-0.499887000	-2.225747000
6	-3.210591000	-0.463799000	-1.657751000
6	-2.090165000	-1.267783000	-2.267538000
1	-1.972805000	-1.055368000	-3.350802000
1	-1.117939000	-1.051788000	-1.778961000
6	0.021345000	0.887337000	2.788029000
6	-1.790453000	-1.777093000	1.188532000
5	1.078455000	-0.175168000	-0.144738000
5	-1.580022000	0.311680000	0.131328000
8	-2.495885000	-2.597848000	0.766288000
6	-2.188853000	-0.283441000	3.119645000
8	-3.054080000	-0.159065000	3.887362000
1	3.121558000	0.466680000	2.839050000
1	2.389901000	-0.900168000	1.953353000
1	-2.266819000	-2.360487000	-2.173138000
6	-4.788626000	-1.344040000	-3.444809000
1	-4.558671000	-2.415665000	-3.261220000
1	-5.850849000	-1.271690000	-3.749913000
1	-4.165070000	-1.034596000	-4.311426000

6	-3.740201000	2.017871000	1.252845000
1	-3.932940000	3.078769000	0.983877000
1	-4.382896000	1.784622000	2.127737000
1	-2.684520000	1.955816000	1.580832000
6	-6.430936000	1.905744000	0.078745000
1	-7.377041000	1.747344000	-0.474826000
1	-6.615402000	1.659895000	1.146577000
1	-6.195642000	2.991790000	0.045058000
50	1.327347000	-2.357003000	-0.797342000
6	-0.018933000	-4.046920000	-0.432099000
1	0.479336000	-4.939808000	-0.860963000
1	-0.166301000	-4.214145000	0.652407000
1	-1.005975000	-3.919140000	-0.913693000
6	1.662844000	-2.338482000	-2.965542000
1	2.514373000	-1.668602000	-3.195875000
1	1.908209000	-3.364995000	-3.304587000
1	0.767151000	-1.983776000	-3.512364000
6	3.225428000	-3.055430000	0.035665000
1	3.123138000	-3.269452000	1.117382000
1	3.527007000	-3.985261000	-0.487143000
1	4.005221000	-2.283291000	-0.112835000
6	0.284763000	-1.760868000	2.709062000
8	0.885973000	-2.621823000	3.206578000

4.2 TD-DFT calculations

Excitation energies and oscillator strengths of diborirane $Fe(CO)_3$ complex 2:

136: HOMO, 137: LUMO

Excited State 1: Singlet-A 2.6370 eV 470.17 nm f=0.0272 <S**2>=0.000

130 -> 137 0.15300

136 -> 137 0.64901

136 -> 138 -0.11809

This state for optimization and/or second-order correction.

Total Energy, E(CIS/TDA) = -2702.13119839

Copying the excited state density for this state as the 1-particle RhoCI density.

Excited State 2: Singlet-A 3.0453 eV 407.13 nm f=0.0428 <S**2>=0.000

127 -> 137 -0.13642

128 -> 137 0.13263

135 -> 137 0.63380

Excited State 3: Singlet-A 3.3012 eV 375.57 nm f=0.0033 <S**2>=0.000

128 -> 137 -0.41382

128 -> 138 0.12908

129 -> 137 -0.13158

130 -> 137 0.41431

130 -> 138 -0.10011

132 -> 137 -0.18723

Excited State 4: Singlet-A 3.4988 eV 354.36 nm f=0.0009 <S**2>=0.000

134 -> 137 0.69958

Excited State 5: Singlet-A 3.5282 eV 351.41 nm f=0.0085 <S**2>=0.000

127 -> 137 0.21504

128 -> 137 0.39774

128 -> 138 -0.12325

129 -> 137 -0.21971

130 -> 137 0.30379
132 -> 137 -0.10937
133 -> 137 -0.15198
135 -> 137 -0.11675
136 -> 139 -0.11142

Excited State 6: Singlet-A 3.5585 eV 348.42 nm f=0.0171 <S**2>=0.000
133 -> 137 0.67206

Excited State 7: Singlet-A 3.7205 eV 333.24 nm f=0.0597 <S**2>=0.000
130 -> 139 0.11920
136 -> 138 -0.25869
136 -> 139 0.57960

Excited State 8: Singlet-A 3.7879 eV 327.31 nm f=0.0309 <S**2>=0.000
126 -> 137 0.12983
127 -> 137 -0.20225
130 -> 137 0.16544
130 -> 140 -0.10685
135 -> 137 -0.14624
135 -> 138 -0.10934
135 -> 139 0.10823
136 -> 138 0.39523
136 -> 140 -0.34976

Excited State 9: Singlet-A 3.8573 eV 321.43 nm f=0.1755 <S**2>=0.000
126 -> 137 -0.14985
127 -> 137 0.28479
130 -> 137 -0.17151
132 -> 137 -0.20731
135 -> 137 0.13502
135 -> 138 0.10340
135 -> 139 -0.11967

136 -> 137 0.13827

136 -> 138 0.33573

136 -> 139 0.21022

Excited State 10: Singlet-A 3.9594 eV 313.14 nm f=0.0063 <S**2>=0.000

129 -> 137 -0.11372

130 -> 140 0.14334

132 -> 137 0.16680

136 -> 137 0.10651

136 -> 138 0.24928

136 -> 139 0.17102

136 -> 140 0.50565

Excited State 11: Singlet-A 4.0995 eV 302.44 nm f=0.0443 <S**2>=0.000

132 -> 137 -0.18401

135 -> 138 -0.11536

135 -> 139 0.52073

136 -> 138 0.10047

136 -> 140 0.13262

136 -> 141 0.26870

136 -> 142 -0.11405

136 -> 148 -0.10170

Excited State 12: Singlet-A 4.1641 eV 297.75 nm f=0.0855 <S**2>=0.000

127 -> 137 0.22768

129 -> 137 -0.12355

131 -> 137 0.29861

132 -> 137 0.49261

135 -> 139 0.20840

Excited State 13: Singlet-A 4.2254 eV 293.42 nm f=0.0238 <S**2>=0.000

131 -> 137 -0.27760

135 -> 139 0.24926

135 -> 141 -0.11083
136 -> 141 -0.25503
136 -> 142 0.39945
136 -> 148 0.15499

Excited State 14: Singlet-A 4.2498 eV 291.74 nm f=0.0263 <S**2>=0.000
131 -> 137 0.29553
135 -> 138 -0.15648
135 -> 139 -0.12384
135 -> 140 0.13468
136 -> 138 0.13151
136 -> 141 0.25283
136 -> 142 0.41550
136 -> 143 -0.20081

Excited State 15: Singlet-A 4.2831 eV 289.47 nm f=0.0861 <S**2>=0.000
127 -> 137 -0.12112
129 -> 137 0.17215
130 -> 139 -0.13003
131 -> 137 0.44681
132 -> 137 -0.17358
135 -> 138 0.21446
135 -> 139 0.15744
136 -> 141 -0.20240
136 -> 148 0.11013

Excited State 16: Singlet-A 4.3777 eV 283.22 nm f=0.0429 <S**2>=0.000
127 -> 137 0.13290
129 -> 137 0.39540
130 -> 137 0.25434
131 -> 137 -0.15613
132 -> 137 0.14193
134 -> 139 0.13881

135 -> 138 0.22063
135 -> 140 0.13047
136 -> 137 -0.11099
136 -> 138 0.11322

Excited State 17: Singlet-A 4.3958 eV 282.05 nm f=0.0085 <S**2>=0.000
129 -> 137 -0.10190
134 -> 138 -0.20497
134 -> 139 0.62323
136 -> 146 0.10791

Excited State 18: Singlet-A 4.4468 eV 278.82 nm f=0.1764 <S**2>=0.000
127 -> 137 -0.10793
129 -> 137 -0.17585
130 -> 139 0.10458
130 -> 140 -0.11818
135 -> 138 0.46397
135 -> 140 -0.24953
136 -> 141 0.18433
136 -> 142 0.16262

Excited State 19: Singlet-A 4.4738 eV 277.13 nm f=0.0652 <S**2>=0.000
127 -> 137 -0.12072
130 -> 139 0.13574
135 -> 138 0.25686
135 -> 140 0.51075
136 -> 142 -0.10274
136 -> 144 0.14585

Excited State 20: Singlet-A 4.5179 eV 274.43 nm f=0.0095 <S**2>=0.000
133 -> 138 0.66686
SavETr: write IOETrn= 770 NScale= 10 NData= 16 NLR=1 NState= 20 LETran=

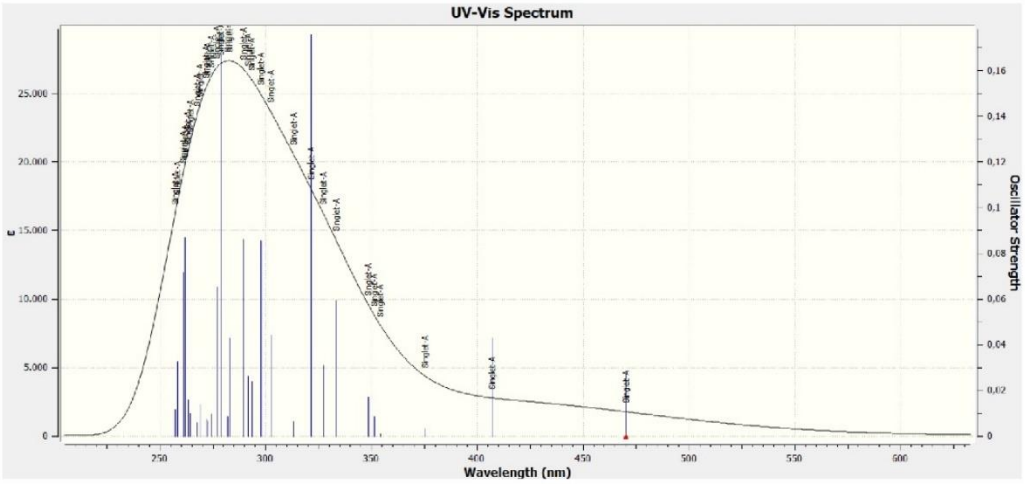

Fig S33. Computed UV/Vis spectrum of diborirane $Fe(CO)_3$ complex **2** in hexane.

Excitation energies and oscillator strengths of oxadiborolane $Fe(CO)_3$ complex 3 in the solid state

143: HOMO, 144: LUMO

Excited State 1: Singlet-A 2.7152 eV 456.62 nm f=0.0217 <S**2>=0.000

135 -> 144 -0.14656

137 -> 144 0.16954

140 -> 144 0.29826

141 -> 144 -0.12021

142 -> 144 0.55238

143 -> 144 -0.10068

This state for optimization and/or second-order correction.

Total Energy, E(CIS/TDA) = -2815.54177306

Copying the excited state density for this state as the 1-particle RhoCI density.

Excited State 2: Singlet-A 3.0422 eV 407.54 nm f=0.0254 <S**2>=0.000

134 -> 144 0.12091

135 -> 144 0.14679

136 -> 144 0.15750

137 -> 144 0.11074

140 -> 144 0.53449

142 -> 144 -0.30486

Excited State 3: Singlet-A 3.0931 eV 400.84 nm f=0.0004 <S**2>=0.000

143 -> 144 0.69613

Excited State 4: Singlet-A 3.1884 eV 388.86 nm f=0.0011 <S**2>=0.000

140 -> 144 0.13358

141 -> 144 0.68657

Excited State 5: Singlet-A 3.3248 eV 372.91 nm f=0.0037 <S**2>=0.000

131 -> 144 0.17953

132 -> 144 0.13022

133 -> 144 -0.12192

134 -> 144 0.19889
135 -> 144 0.25837
136 -> 144 0.43747
137 -> 144 -0.11219
140 -> 144 -0.15604
142 -> 144 0.18126

Excited State 6: Singlet-A 3.4257 eV 361.92 nm f=0.0028 <S**2>=0.000
131 -> 144 -0.13150
133 -> 144 -0.19548
134 -> 144 0.16184
135 -> 144 0.39410
136 -> 144 -0.31804
137 -> 144 0.13913
139 -> 144 -0.25995
142 -> 144 0.11451

Excited State 7: Singlet-A 3.4729 eV 357.00 nm f=0.0062 <S**2>=0.000
132 -> 144 0.13838
133 -> 144 0.10814
134 -> 144 0.34548
136 -> 144 -0.16494
137 -> 144 0.23343
139 -> 144 0.43969
140 -> 144 -0.13710

Excited State 8: Singlet-A 3.6587 eV 338.87 nm f=0.0015 <S**2>=0.000
134 -> 144 -0.13564
135 -> 144 -0.10296
136 -> 144 0.20858
137 -> 144 0.47439
137 -> 145 -0.12602
138 -> 144 0.14932

139 -> 144 -0.20639

140 -> 144 -0.20545

140 -> 145 -0.22352

Excited State 9: Singlet-A 3.7834 eV 327.71 nm f=0.0923 <S**2>=0.000

140 -> 145 -0.22054

142 -> 145 0.54028

142 -> 146 0.26745

142 -> 148 -0.11282

Excited State 10: Singlet-A 3.7913 eV 327.02 nm f=0.0189 <S**2>=0.000

132 -> 144 -0.14149

133 -> 144 -0.21503

134 -> 144 -0.31103

135 -> 144 0.19272

137 -> 144 0.11591

138 -> 144 -0.12273

139 -> 144 0.41457

142 -> 145 -0.13516

Excited State 11: Singlet-A 3.8236 eV 324.26 nm f=0.0054 <S**2>=0.000

143 -> 145 0.69672

Excited State 12: Singlet-A 3.8547 eV 321.64 nm f=0.0029 <S**2>=0.000

137 -> 144 -0.14300

138 -> 144 0.66407

Excited State 13: Singlet-A 3.9097 eV 317.12 nm f=0.0258 <S**2>=0.000

137 -> 144 0.12098

140 -> 145 0.43073

140 -> 146 0.11439

141 -> 145 -0.10778

142 -> 146 0.43760

Excited State 14: Singlet-A 3.9697 eV 312.33 nm f=0.0098 <S**2>=0.000

141 -> 145 0.68164

Excited State 15: Singlet-A 3.9799 eV 311.52 nm f=0.0631 <S**2>=0.000

137 -> 144 0.17332

137 -> 146 -0.12975

140 -> 145 0.39739

140 -> 146 -0.22042

140 -> 147 -0.15139

142 -> 145 0.23921

142 -> 146 -0.27393

142 -> 147 -0.15001

Excited State 16: Singlet-A 4.0931 eV 302.91 nm f=0.0082 <S**2>=0.000

131 -> 145 0.10331

134 -> 145 -0.23872

135 -> 145 -0.11048

136 -> 145 0.46814

136 -> 149 0.13263

137 -> 145 -0.15038

142 -> 147 -0.22286

Excited State 17: Singlet-A 4.1339 eV 299.92 nm f=0.0243 <S**2>=0.000

135 -> 145 0.11381

136 -> 145 -0.10630

137 -> 145 0.10894

140 -> 146 -0.11226

140 -> 147 -0.12950

140 -> 148 0.18572

142 -> 146 0.18745

142 -> 147 -0.34674

142 -> 148 0.38492

142 -> 149 -0.11698

Excited State 18: Singlet-A 4.1823 eV 296.45 nm f=0.0349 <S**2>=0.000
134 -> 145 -0.10382
136 -> 145 0.12605
140 -> 146 -0.16543
140 -> 148 0.10800
142 -> 145 0.10404
142 -> 147 0.39944
142 -> 148 0.39632

Excited State 19: Singlet-A 4.1965 eV 295.45 nm f=0.0031 <S**2>=0.000
142 -> 146 0.10634
143 -> 146 0.67302
143 -> 148 -0.12346

Excited State 20: Singlet-A 4.2495 eV 291.76 nm f=0.0829 <S**2>=0.000
140 -> 146 0.54290
142 -> 145 0.14533
142 -> 146 -0.19909
142 -> 148 0.23981

Excited State 21: Singlet-A 4.2670 eV 290.57 nm f=0.0079 <S**2>=0.000
139 -> 154 0.10049
140 -> 146 0.11275
141 -> 146 0.65518

Excited State 22: Singlet-A 4.3197 eV 287.02 nm f=0.0230 <S**2>=0.000
137 -> 145 -0.11581
137 -> 147 0.16204
139 -> 145 0.16604
140 -> 146 -0.10358
140 -> 147 0.53548

142 -> 147 -0.25119

Excited State 23: Singlet-A 4.3407 eV 285.63 nm f=0.0034 <S**2>=0.000
135 -> 145 -0.17890
137 -> 145 0.13048
139 -> 145 0.55763
140 -> 147 -0.16315
142 -> 145 -0.12154

Excited State 24: Singlet-A 4.3488 eV 285.10 nm f=0.0014 <S**2>=0.000
142 -> 147 0.10668
143 -> 147 0.66766

Excited State 25: Singlet-A 4.3928 eV 282.25 nm f=0.0238 <S**2>=0.000
140 -> 147 0.10837
140 -> 148 0.34701
143 -> 146 0.11247
143 -> 148 0.54397

Excited State 26: Singlet-A 4.4197 eV 280.53 nm f=0.0388 <S**2>=0.000
137 -> 145 0.11474
140 -> 148 0.45703
142 -> 148 -0.25096
142 -> 149 -0.12206
143 -> 147 -0.10897
143 -> 148 -0.36533

Excited State 27: Singlet-A 4.4775 eV 276.91 nm f=0.0465 <S**2>=0.000
135 -> 145 -0.13485
139 -> 145 -0.22695
140 -> 148 0.12244
140 -> 149 0.13600
142 -> 147 -0.15644

142 -> 149 0.48273

142 -> 150 -0.15150

143 -> 149 -0.10680

Excited State 28: Singlet-A 4.4929 eV 275.96 nm f=0.0047 <S**2>=0.000

141 -> 147 0.66239

Excited State 29: Singlet-A 4.5175 eV 274.45 nm f=0.0007 <S**2>=0.000

136 -> 145 0.10567

138 -> 145 0.58961

142 -> 152 -0.11137

142 -> 153 0.16537

Excited State 30: Singlet-A 4.5336 eV 273.48 nm f=0.0128 <S**2>=0.000

133 -> 145 -0.16390

134 -> 145 0.18505

135 -> 145 0.35291

135 -> 146 0.13173

136 -> 145 0.14303

137 -> 145 -0.13997

139 -> 145 0.17222

139 -> 146 -0.10179

142 -> 149 0.28416

SavETr: write IOETrn= 770 NScale= 10 NData= 16 NLR=1 NState= 30 LETran=

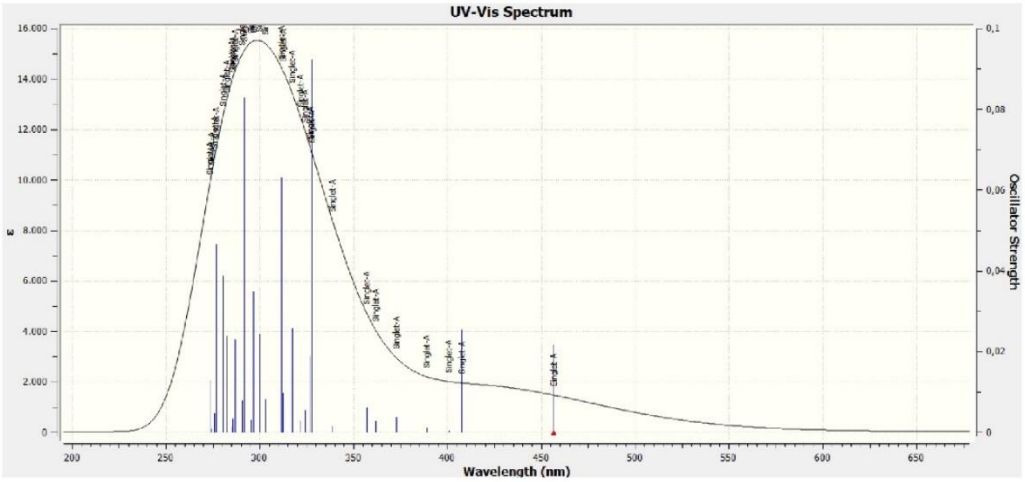

Fig S34. Computed UV/Vis spectrum of oxadiborolane Fe(CO)3 complex **3** in hexane.

Excitation energies and oscillator strengths of 1,3-diborete $Fe(CO)_3$ complex 5:

168: LUMO, 167: HOMO

Excited State 1: Singlet-A 1.9591 eV 632.86 nm f=0.0045 <S**2>=0.000

162 -> 168 -0.15051

164 -> 168 0.20526

167 -> 168 0.63495

This state for optimization and/or second-order correction.

Total Energy, E(TD-HF/TD-DFT) = -3149.11346164

Copying the excited state density for this state as the 1-particle RhoCI density.

Excited State 2: Singlet-A 2.6691 eV 464.51 nm f=0.0177 <S**2>=0.000

153 -> 168 -0.12441

154 -> 168 -0.10190

159 -> 168 -0.21959

160 -> 168 -0.27277

162 -> 168 -0.16184

164 -> 168 0.50965

167 -> 168 -0.15181

Excited State 3: Singlet-A 2.7062 eV 458.15 nm f=0.0018 <S**2>=0.000

166 -> 168 0.69716

Excited State 4: Singlet-A 2.8488 eV 435.22 nm f=0.0232 <S**2>=0.000
154 -> 168 0.18566
157 -> 168 -0.15121
159 -> 168 0.15494
160 -> 168 0.36911
162 -> 168 0.20230
163 -> 168 0.23114
164 -> 168 0.37471
167 -> 168 -0.13605

Excited State 5: Singlet-A 2.9089 eV 426.22 nm f=0.0222 <S**2>=0.000
155 -> 168 -0.13214
156 -> 168 -0.16606
157 -> 168 0.27017
158 -> 168 -0.15157
160 -> 168 -0.18408
163 -> 168 0.52748

Excited State 6: Singlet-A 2.9572 eV 419.26 nm f=0.0005 <S**2>=0.000
165 -> 168 0.69953

Excited State 7: Singlet-A 3.0541 eV 405.96 nm f=0.0101 <S**2>=0.000
156 -> 168 -0.10324
157 -> 168 0.47633
158 -> 168 0.16634
159 -> 168 0.26640
160 -> 168 0.16954
162 -> 168 -0.16695
163 -> 168 -0.22004

Excited State 8: Singlet-A 3.3407 eV 371.13 nm f=0.0066 <S**2>=0.000

157 -> 168 0.20993
158 -> 168 0.18413
160 -> 168 -0.12168
162 -> 168 0.57680
167 -> 168 0.16421

Excited State 9: Singlet-A 3.3607 eV 368.92 nm f=0.0115 <S**2>=0.000
153 -> 168 -0.22400
155 -> 168 0.20289
156 -> 168 0.16071
158 -> 168 0.40647
159 -> 168 -0.12705
162 -> 168 -0.18930
163 -> 168 0.30184
164 -> 168 -0.13826

Excited State 10: Singlet-A 3.7080 eV 334.37 nm f=0.0110 <S**2>=0.000
161 -> 168 0.66029
167 -> 169 -0.14232

Excited State 11: Singlet-A 3.7343 eV 332.02 nm f=0.0174 <S**2>=0.000
159 -> 168 -0.20715
160 -> 168 0.21330
161 -> 168 0.22642
167 -> 169 0.37811
167 -> 170 -0.36240
167 -> 171 0.11515

Excited State 12: Singlet-A 3.8319 eV 323.56 nm f=0.0179 <S**2>=0.000
159 -> 168 -0.25053
160 -> 168 0.18999
164 -> 170 0.13322
167 -> 169 0.21135

167 -> 170 0.51705

Excited State 13: Singlet-A 3.9375 eV 314.88 nm f=0.0463 <S**2>=0.000
158 -> 168 0.11429
159 -> 168 0.30679
160 -> 168 -0.25301
167 -> 169 0.42898
167 -> 170 0.10747
167 -> 172 -0.21007

Excited State 14: Singlet-A 4.0215 eV 308.30 nm f=0.0407 <S**2>=0.000
164 -> 171 0.14525
167 -> 169 -0.13060
167 -> 171 0.62590

Excited State 15: Singlet-A 4.1144 eV 301.34 nm f=0.0059 <S**2>=0.000
159 -> 168 0.10006
164 -> 169 -0.17063
164 -> 172 0.10878
167 -> 169 0.16763
167 -> 172 0.56278
167 -> 173 -0.17279

Excited State 16: Singlet-A 4.2236 eV 293.55 nm f=0.0022 <S**2>=0.000
166 -> 169 0.69605

Excited State 17: Singlet-A 4.2882 eV 289.13 nm f=0.0103 <S**2>=0.000
154 -> 168 -0.25907
159 -> 168 0.18010
164 -> 169 0.36891
167 -> 173 -0.33281
167 -> 174 -0.17079
167 -> 175 0.14815

Excited State 18: Singlet-A 4.3403 eV 285.66 nm f=0.0187 <S**2>=0.000

154 -> 168 -0.19222

159 -> 168 0.12199

164 -> 169 0.25249

164 -> 170 -0.26240

167 -> 170 0.13046

167 -> 172 0.17007

167 -> 173 0.39873

167 -> 175 -0.13297

Excited State 19: Singlet-A 4.3603 eV 284.35 nm f=0.0105 <S**2>=0.000

159 -> 170 -0.11311

162 -> 170 -0.10003

164 -> 169 0.19761

164 -> 170 0.56262

167 -> 170 -0.10625

167 -> 173 0.19275

Excited State 20: Singlet-A 4.3860 eV 282.68 nm f=0.0006 <S**2>=0.000

166 -> 170 0.69040

Excited State 21: Singlet-A 4.4339 eV 279.63 nm f=0.0028 <S**2>=0.000

153 -> 168 -0.10102

154 -> 168 -0.14531

164 -> 174 0.13379

167 -> 174 0.58689

167 -> 177 0.10656

Excited State 22: Singlet-A 4.4687 eV 277.45 nm f=0.0250 <S**2>=0.000

154 -> 168 0.27409

160 -> 169 0.17025

163 -> 169 -0.17507

163 -> 170 0.11739
164 -> 169 0.27141
164 -> 171 0.39127
167 -> 171 -0.12560

Excited State 23: Singlet-A 4.4869 eV 276.33 nm f=0.0145 <S**2>=0.000
154 -> 168 -0.25785
163 -> 169 0.38322
163 -> 170 -0.10784
164 -> 171 0.34133
167 -> 169 -0.13267

Excited State 24: Singlet-A 4.5198 eV 274.31 nm f=0.0006 <S**2>=0.000
166 -> 171 0.67092

Excited State 25: Singlet-A 4.5300 eV 273.70 nm f=0.0022 <S**2>=0.000
165 -> 169 0.64568
165 -> 170 0.21564

Excited State 26: Singlet-A 4.5856 eV 270.37 nm f=0.0202 <S**2>=0.000
153 -> 168 0.14138
159 -> 169 -0.11628
159 -> 170 0.10960
160 -> 169 -0.20846
160 -> 170 0.23894
163 -> 169 -0.11117
164 -> 169 -0.14581
164 -> 170 0.14457
164 -> 171 0.32212
164 -> 172 0.19266

Excited State 27: Singlet-A 4.6017 eV 269.43 nm f=0.0664 <S**2>=0.000
153 -> 168 0.15362

154 -> 168 0.11725
158 -> 168 0.13451
163 -> 169 0.36485
163 -> 170 0.26457
164 -> 169 0.17941
164 -> 171 -0.13138
167 -> 173 -0.12309
167 -> 175 -0.24486

Excited State 28: Singlet-A 4.6063 eV 269.16 nm f=0.0040 <S**2>=0.000
164 -> 177 0.15577
165 -> 169 -0.26221
165 -> 170 0.56041
165 -> 175 0.13255

Excited State 29: Singlet-A 4.6298 eV 267.80 nm f=0.0144 <S**2>=0.000
153 -> 168 0.39153
154 -> 168 -0.13251
155 -> 168 0.11323
156 -> 168 -0.24040
157 -> 168 -0.14960
158 -> 168 0.28901
160 -> 169 0.12673
163 -> 169 -0.14644
163 -> 170 -0.13783

Excited State 30: Singlet-A 4.6468 eV 266.82 nm f=0.0922 <S**2>=0.000
154 -> 168 0.13477
156 -> 168 -0.12581
161 -> 169 0.17994
163 -> 169 0.25300
164 -> 169 0.11797
166 -> 172 -0.14847

167 -> 173 0.10849

167 -> 175 0.40476

167 -> 176 -0.19939

SavETr: write IOETrn= 770 NScale= 10 NData= 16 NLR=1 NState= 30 LETran= 550.

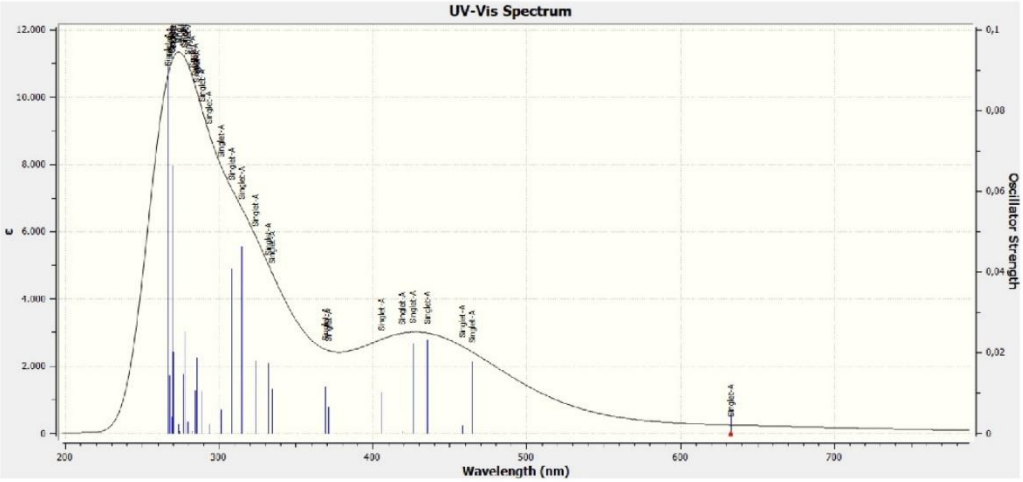

Fig S35. Computed UV/Vis spectrum of 1,3-diborete $Fe(CO)_3$ complex **5** in hexane.

4.3 Molecular orbitals

Selected frontier orbitals of diborirane $Fe(CO)_3$ complex 2

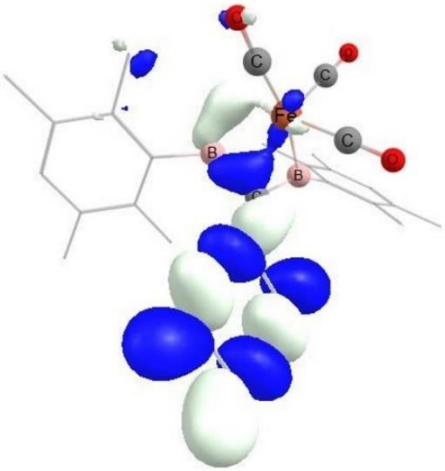

HOMO−18 (−9.64)

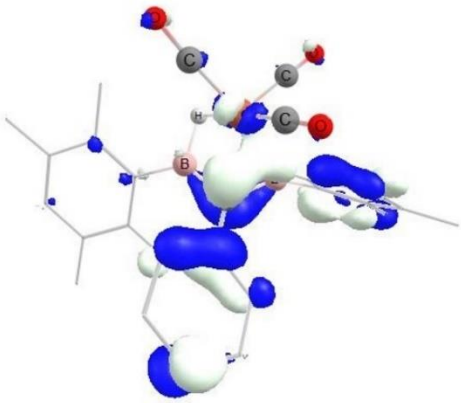

HOMO−1 (−6.18)

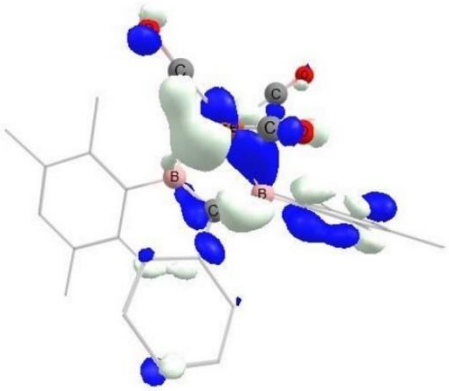

HOMO (−5.95)

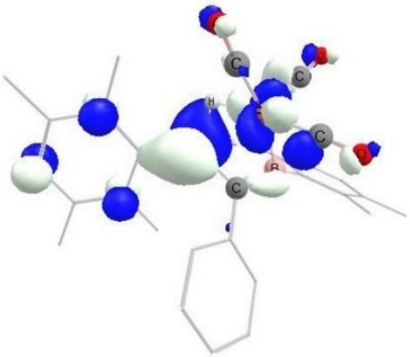

LUMO (−2.22)

Selected frontier orbitals of oxadiborolane $Fe(CO)_3$ complex 3

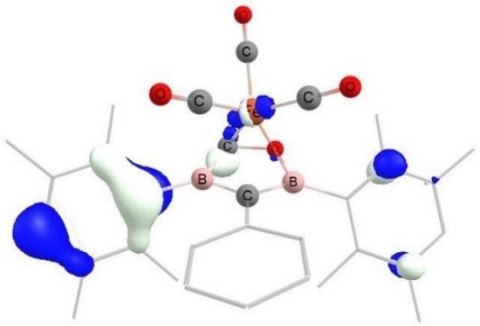

HOMO−3 (−6.23)

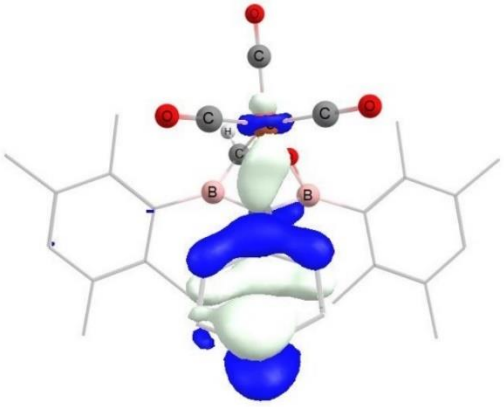

HOMO−1 (−6.18)

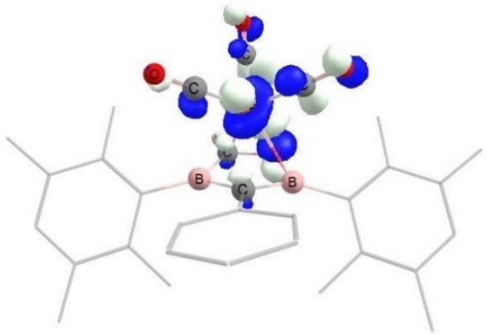

LUMO (−2.47)

Selected frontier orbitals of 1,3-diborete Fe(CO)3 complex 5

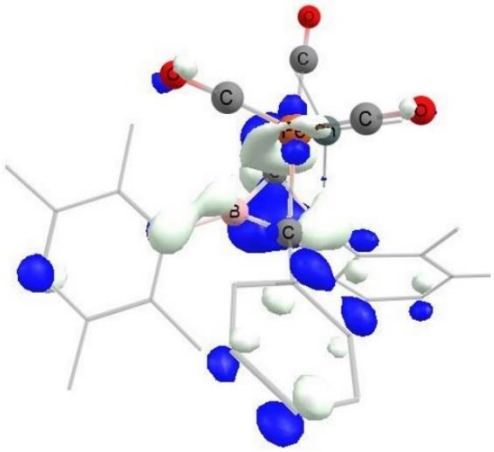

HOMO−5 (−6.82)

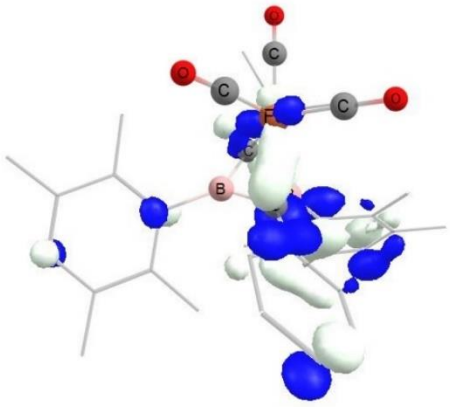

HOMO−2 (−6.19)

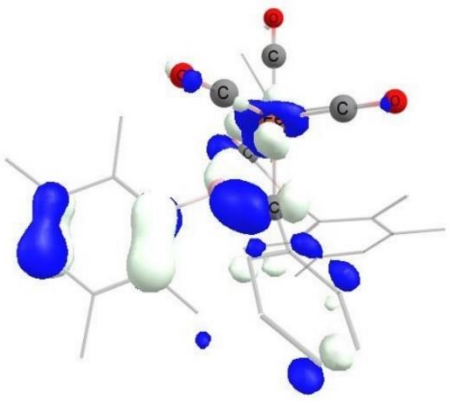

HOMO (−5.77)

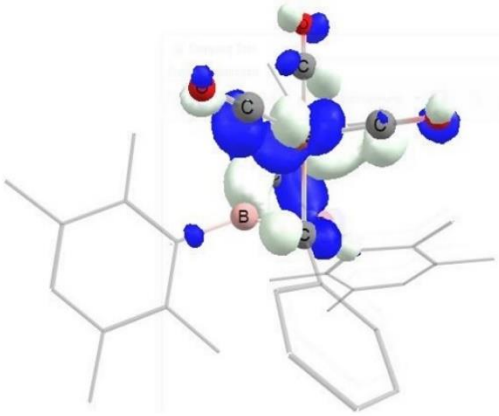

LUMO (−2.63)

4.4 Quantum theory – Atoms in Molecules (QT-AIM)

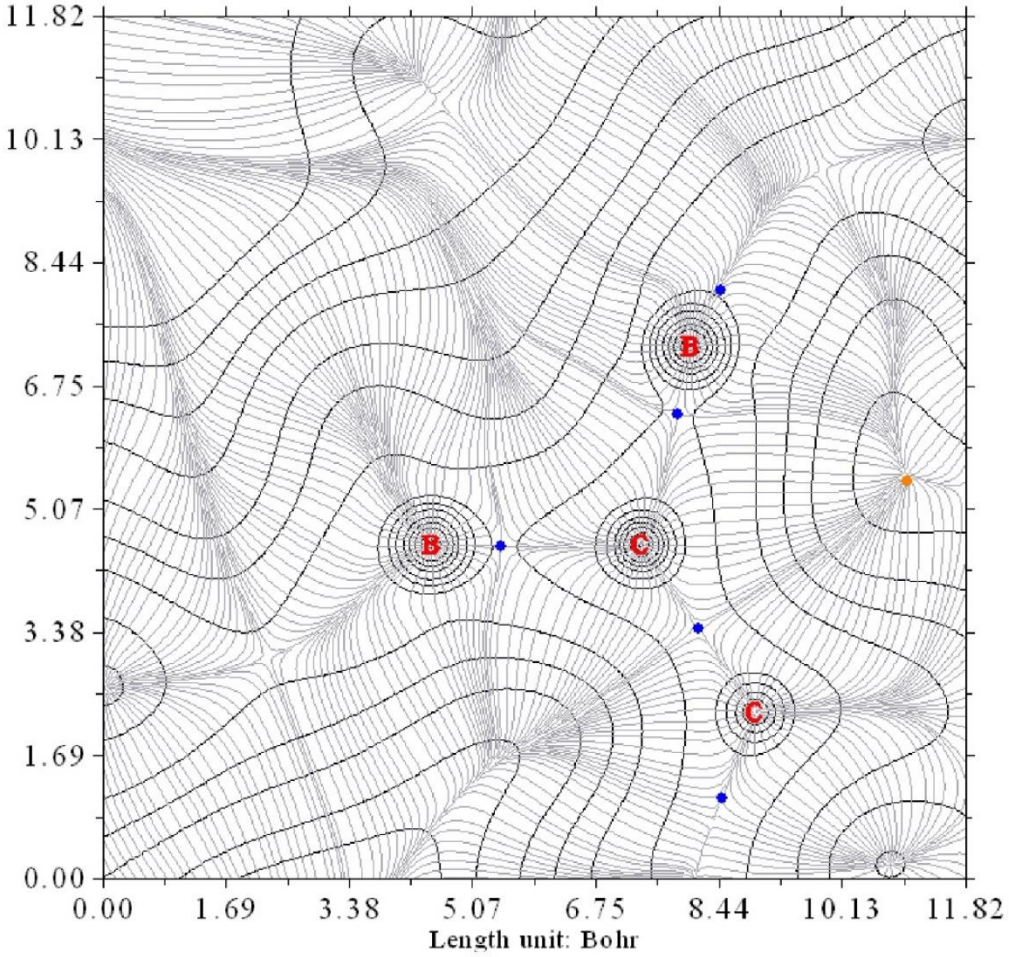

Fig S36. Electron density in the B_2C plane of compound **3** (blue = bond critical point).[40]

5. References

[30] G. R. Fulmer, A. J. M. Miller, N. H. Sherden, H. E. Gottlieb, A. Nudelman, B. M. Stoltz, J. E. Bercaw, K. I. Goldberg, *Organometallics* **2010**, *29*, 2176 – 2179.

[31] L. Benco, T. Demuth, J. Hafner, F. Hutschka, H. Toulhoat, *J. Catal.* **2002**, *205*, 147 – 156.

[32] G. M. Sheldrick, *Acta Cryst.* **2015**, *A71*, 3 − 8.

[33] G. M. Sheldrick, *Acta Cryst.* **2015**, *C71*, 3 − 8.

[34] C. B. Hübschle, G. M. Sheldrick, B. Dittrich, *J. Appl. Crystallogr.* **2011**, *44,* 28 − 28 .

[35] Gaussian 09, Revision A.02, M. J. Frisch, G. W. Trucks, H. B. Schlegel, G. E. Scuseria, M. A. Robb, J. R. Cheeseman, G. Scalmani, V. Barone, G. A. Petersson, H. Nakatsuji, X. Li, M. Caricato, A. Marenich, J. Bloino, B. G. Janesko, R. Gomperts, B. Mennucci, H. P. Hratchian, J. V. Ortiz, A. F. Izmaylov, J. L. Sonnenberg, D. Williams-Young, F. Ding, F. Lipparini, F. Egidi, J. Goings, B. Peng, A. Petrone, T. Henderson, D. Ranasinghe, V. G. Zakrzewski, J. Gao, N. Rega, G. Zheng, W. Liang, M. Hada, M. Ehara, K. Toyota, R. Fukuda, J. Hasegawa, Ishida, M. T. Nakajima, Y. Honda, O. Kitao, H. Nakai, T. Vreven, K. Throssell, J. A. Montgomery Jr, J. E. Peralta, F. Ogliaro, M. Bearpark, J. J. Heyd, E. Brothers, K. N. Kudin, V. N. Staroverov, T. Keith, R. Kobayashi, J. Normand, K. Raghavachari, A. Rendell, J. C. Burant, S. S. Iyengar, J. Tomasi, M. Cossi, J. M. Millam, M. Klene, C. Adamo, R. Cammi, J. W. Ochterski, R. L. Martin, K. Morokuma, O. Farkas, J. B. Foresman, D. J. Fox, Gaussian, Inc., Wallingford CT, **2016**.

[36] a) J. P. Perdew, *Phys. Rev. B* **1986**, *33*, 8822 – 8824; b) A. D. Becke, *Phys. Rev. A* **1988**, *38*, 3098 – 3100.

[37] a) A. Schäfer, H. Horn, R. Ahlrichs, *J. Chem. Phys.* **1992**, *97*, 2571 – 2577; b) A. Schäfer, C. Huber, R. Ahlrichs, *J. Chem. Phys.* **1994**, *100*, 5829 – 5835; c) F. Weigend, R. Ahlrichs, *Phys. Chem. Chem. Phys.* **2005**, *7*, 3297 – 3305; d) F. Weigend, *Phys. Chem. Chem. Phys.* **2006**, *8*, 1057 – 1065.

[38] S. Grimme, J. Antony, S. Ehrlich, H. Krieg, *J. Chem. Phys.* **2010**, *132*, 154104.

[39] Chemcraft - graphical software for visualization of quantum chemistry computations. https://www.chemcraftprog.com

[40] T. Lu, F. Chen, Multiwfn: A Multifunctional Wavefunction Analyzer, *J. Comput. Chem.* **2012**, *33*, 580 – 592.

5.3 2,3-Diboratabutadiene Complexes of Group 4 Metals and their Donor-induced Oxidative Cleavage to Methyleneboranes

Supporting Information

2,3-Diboratabutadiene Complexes of Group 4 Metals and their Donor-induced Oxidative Cleavage to Methyleneboranes

Philipp Grewelinger, Carsten Präsang, Bernd Morgenstern, and David Scheschkewitz*

*Krupp-Chair for General and Inorganic Chemistry, Saarland University, 66123 Saarbrücken, Germany

Supporting Information

Table of Contents

1. General remarks

All manipulations were carried out under argon with standard Schlenk or glovebox techniques. The glassware was pre-dried in oven at 125 °C and heated in vacuo prior to use. Hexane, toluene and tetrahydrofuran were taken from a solvent purification system (Innovative Technology PureSolv MD7). Benzene-d_6 was dried over potassium mirror and distilled prior to use. All other chemicals were obtained commercially and used as received. The NMR spectra were recorded on a Bruker Avance III HD 400 spectrometer at 300 K (^{1}H: 400.13 MHz, ^{11}B: 128.38 MHz, ^{13}C: 100.61 MHz). The VT-NMR spectra were recorded on a Bruker Avance III HD 300 spectrometer (^{13}C: 75.47 MHz). The ^{1}H and ^{13}C{1H} NMR spectra were referenced to the residual proton and natural abundance ^{13}C resonances of the deuterated solvent and chemical shifts were reported relative to $SiMe_4$ (C_6D_6: δ^{1}H = 7.16 ppm and δ^{13}C = 128.06 ppm, toluene-d_8: δ^{13}C = 20.43 ppm).[61] The following abbreviations were used for the multiplicities: s – singlet, d – doublet, t – triplet, m – multiplet. Melting points were determined under argon in NMR tubes. The molten samples were examined by NMR spectroscopy to confirm whether decomposition had occurred upon melting. UV/Vis spectra were recorded on a Shimadzu UV-2600 spectrometer in quartz cells with a path length of 0.1 cm. Elemental analysis was performed in triplicate for each sample using an elementar vario Micro Cube analyzer and mean values are given below for each compound. Crystallographic data of the structures reported in this paper have been deposited with the Cambridge Crystallographic Data Centre, CCDC, 12 Union Road, Cambridge CB21EZ, UK. (Fax: +44-1223-336-033; E-Mail: deposit@ccdc.cam.ac.uk, http://www.ccdc.cam.ac.uk)

2. Experimental procedure, data and spectra

2.1 1,2-Dibenzyldiborane(4) **1**

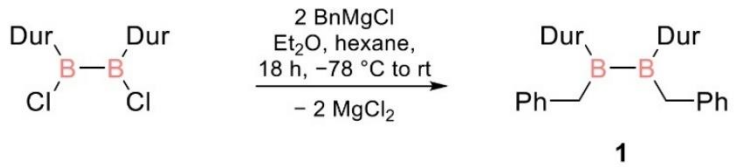

1

358.95 g/mol 470.31 g/mol

Et_2O (150 mL) is added to 13.8 g of magnesium turnings. At 0 °C 2.2 equivalents benzylchloride (21.4 g, 123 mmol) are added dropwise and the mixture is stirred for 4 h. The obtained solution of $PhCH_2MgCl$ in Et_2O is transferred to a dropping funnel. Then 91% of the solution is added dropwise to a solution of 1 equivalent 1,2-dichlorodiborane(4) (20 g, 55.7 mmol) in 150 mL hexane at −74 °C. The reaction is checked for complete conversion after 18h of stirring at room temperature. The excess of Grignard can be used in case of incomplete conversion but is discarded otherwise. After additional stirring if need be, all volatiles are removed in vacuo at room temperature. The solid residue is redissolved in 40 mL hexane and filtered. Removing of the solvent results in 25.1 g (96%) of a pale green powder. The powder is redissolved to give a room temperature-saturated solution and stored at 0 °C. Diborirane(4) **1** is obtained as 20.6 g (79%) colorless crystals.

^{1}H NMR (400 MHz, C_6D_6, 300K): δ = 7.04-7.00 (m, Ph-H, 8H), 6.94 (m, Ph-H, 2H), 6.71 (s, Dur-H, 2H), 3.49 (s, Bn-H, 4H), 1.96, 1.65 (each s, Dur-CH_3, 12H).

^{11}B NMR (128.38 MHz, C_6D_6, 300 K): δ = 100.0 (br s) ppm.

^{13}C{^{1}H} NMR (100.61 MHz, C_6D_6, 300 K): δ = 146.5 (br s Dur-C_{ipso}), 140.1, 133.3, 130.6, 129.7, 129.3, 128.3, 125.1 (each s, Ar-C), 41.4 (br s, B-CH_2), 19.7, 19.1 (each s, Dur-CH_3)

Elemental analysis: calc. for $C_{34}H_{40}B_2$: C, 86.8%; H, 8.6%. Found: C, 84.7%; H, 7.7%.

Melting point: 98 - 100 °C

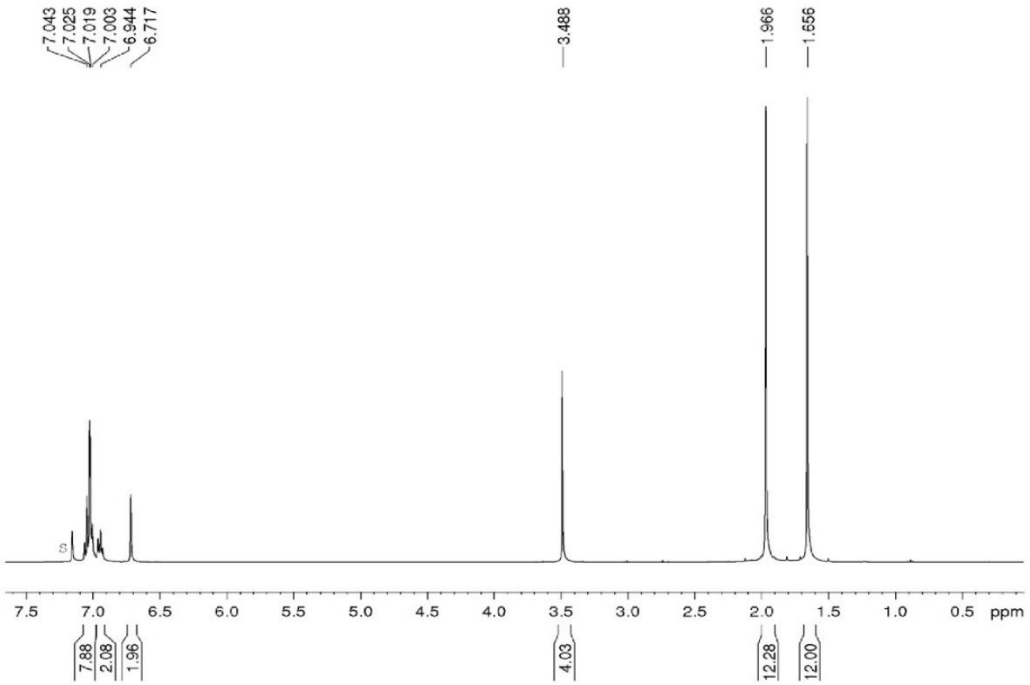

Figure S1. ^{1}H-NMR spectrum (400.1 MHz) of dibenzyldiborane(4) **1** in C_6D_6 (=s).

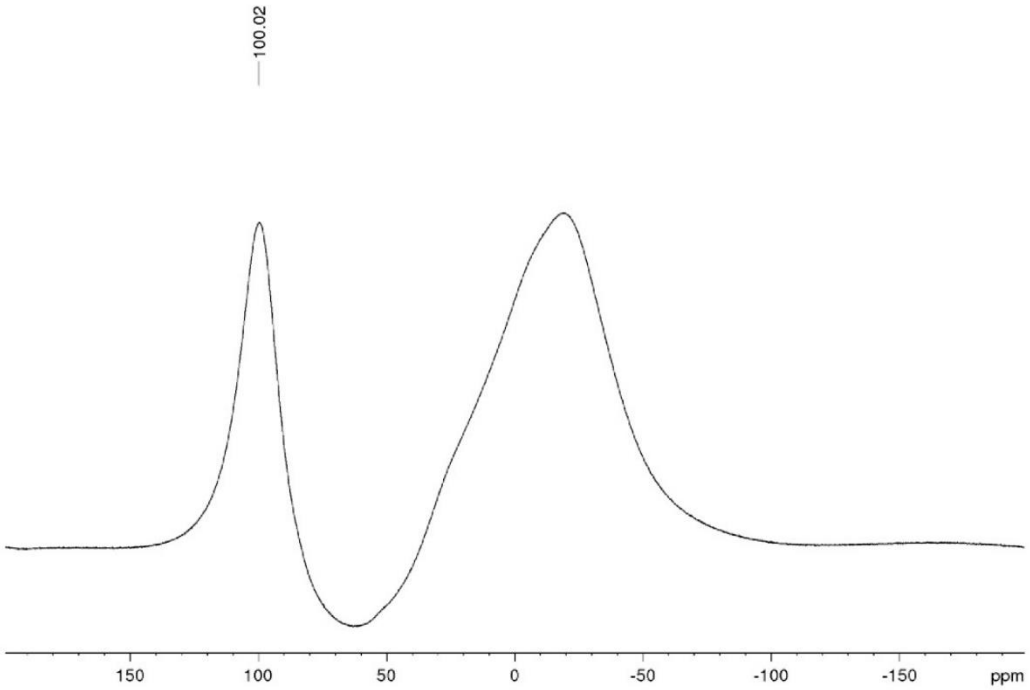

Figure S2. Baseline corrected ^{11}B-NMR spectrum (128.4 MHz) of dibenzyldiborane(4) **1** (glass peak from 50 to −50 ppm).

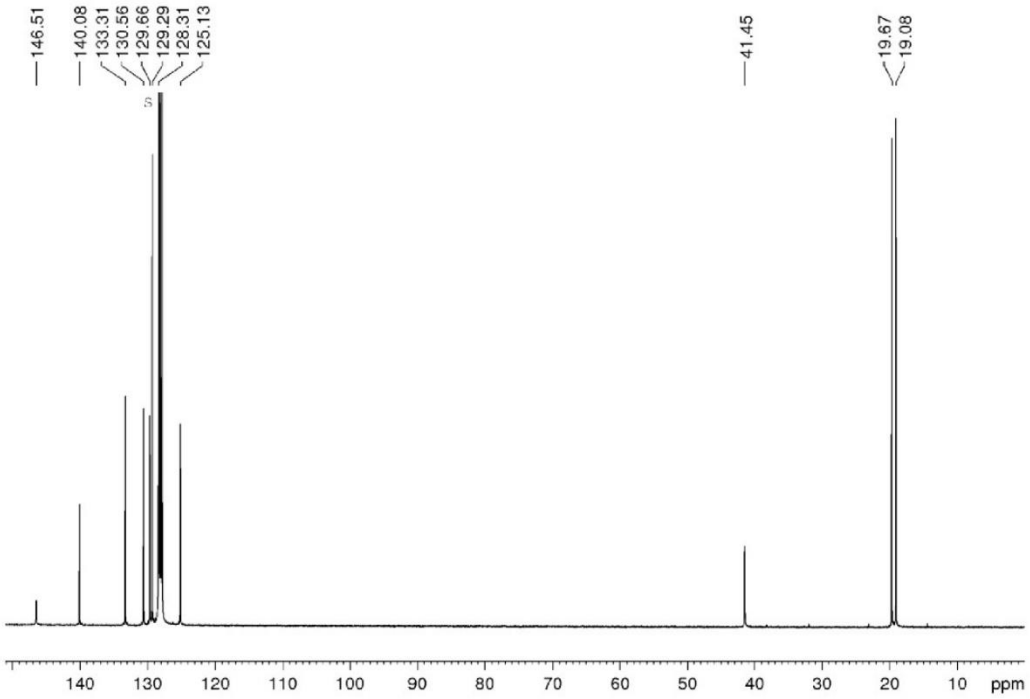

Figure S3. ^{13}C-NMR spectrum (100.61 MHz) of dibenzyldiborane(4) **1**in C_6D_6 (=s).

2.2 Dilithio-2,3-diboratabutadiene **2**.

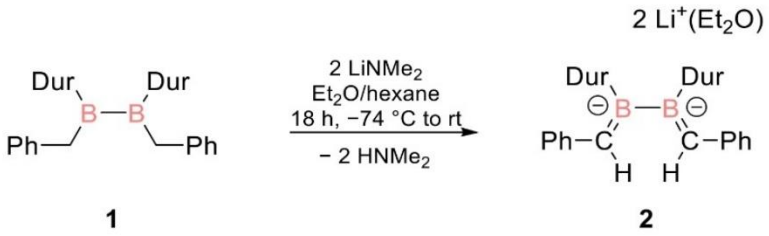

1 **2**

470.31 g/mol 630.42 g/mol

At −74 °C, 2.0 equivalents of $LiNMe_2$ (5.1 g, 100 mmol) are suspended in 150 mL diethylether. A solution of 1,2-dibenzyldiborane(4) **1** (23.5 g, 50 mmol) in 150 ml of hexaneis added to the cooled suspension. The mixture is stirred and allowed to reach ambient temperature overnight. To ensure no coordination of amine to the lithium counter cation, the solvent was removed in vacuo and the residue redispersed in 150 ml diethylether. The process was repeated three times. Washing with hexane and removing of the solvent results in 24.0 g (76%) of a yellow powder. The powder is redissolved in a toluene/Et_2O 1:1 mixture to give a room temperature-saturated solution and stored at 0 °C. Diboratabutadiene **2** is obtained as yellow crystals (17.8 g, 56%)

^{1}H NMR (400 MHz, thf-d_8, 300K): δ = 6.59-6.57 (m, Ph-H, 4H), 6.43-6.39 (m, Ph-H, 4H), 6.29 (s, Dur-H, 1H), 5.91-5.88 (m, Ph-H, 2H), 4.22 (s, BC-H, 2H), 1.99-1.78, 2.13 (each s, Dur-CH_3, 12H).

^{7}Li NMR (116.60 MHz, thf-d_8, 300 K): δ = 0.32 (s) ppm.

^{11}B NMR (128.38 MHz, thf-d_8, 300 K): δ = 58.1 (br s) ppm.

^{13}C{^{1}H} NMR (100.61 MHz, thf-d_8, 300 K): δ = 161.9 (br s Dur-C_{ipso}), 156.9, 134.2, 130.6, 128.2, 126.1, 124.7, 113.8, (each s, Ar-C), 95.4 (br s, B-C-Li), 19.8, 16.6 (each s, Dur-CH_3)

UV/Vis (Et_2O): $\lambda_{max}(\varepsilon)$ = 230 nm (26450 $M^{-1}cm^{-1}$), 305 nm (15010 $M^{-1}cm^{-1}$), 395 nm (27610 $M^{-1}cm^{-1}$).

Elemental analysis: calc. for $C_{34}H_{38}B_2Li_2 + 3{\cdot}C_4H_{10}O$: C, 78.4%; H, 9.7%. Found: C, 78.5%; H, 8.1%.

Melting point: 263 - 265 °C (decomposition)

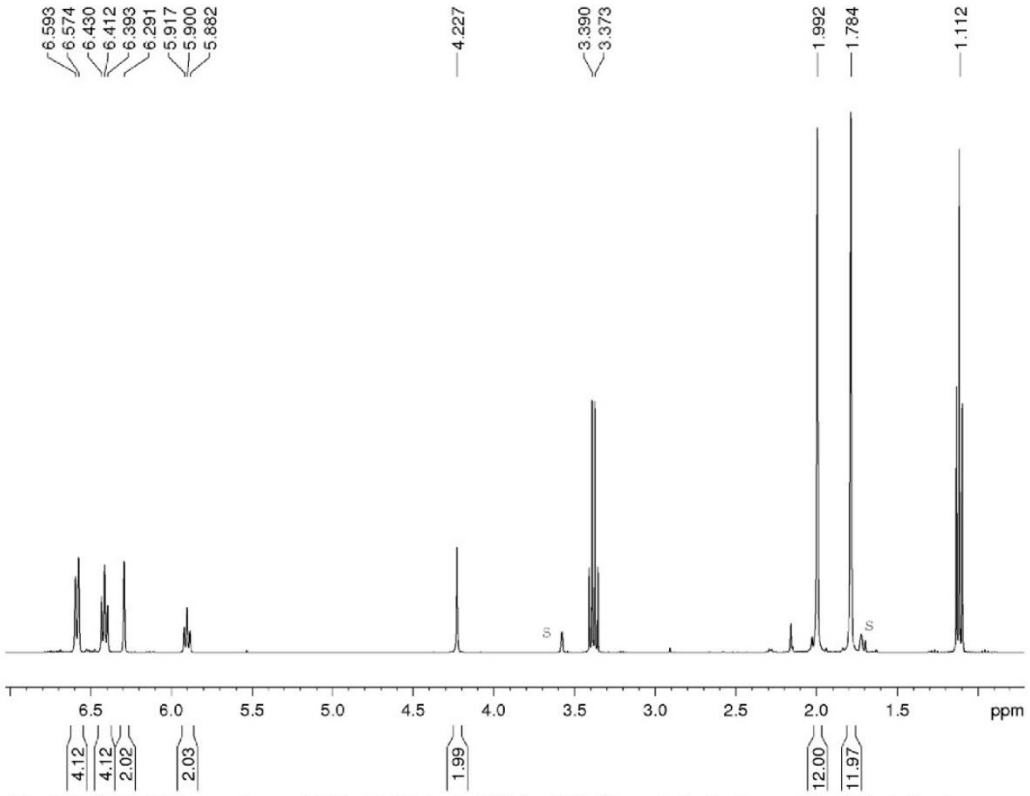

Fig S4. ^{1}H-NMR spectrum (400.1 MHz) of dilithio-2,3-diboratabutadiene **2** in thf-d_8 (=s).

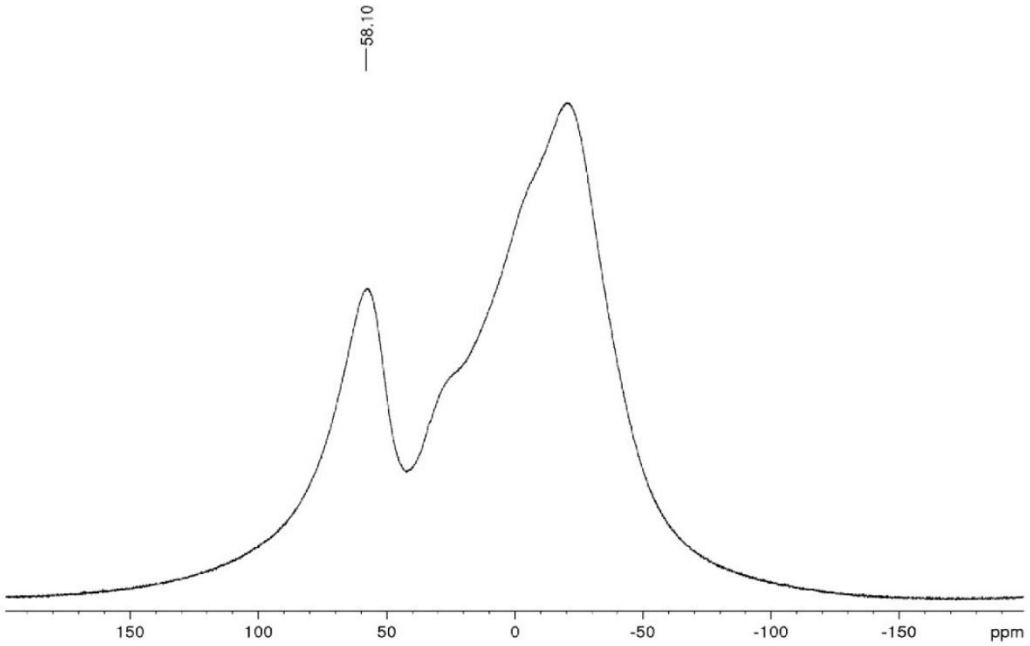

Fig S5. ^{11}B-NMR spectrum (128.4 MHz) of dilithio-2,3-diboratabutadiene **2** (glass peak from 50 to −50 ppm).

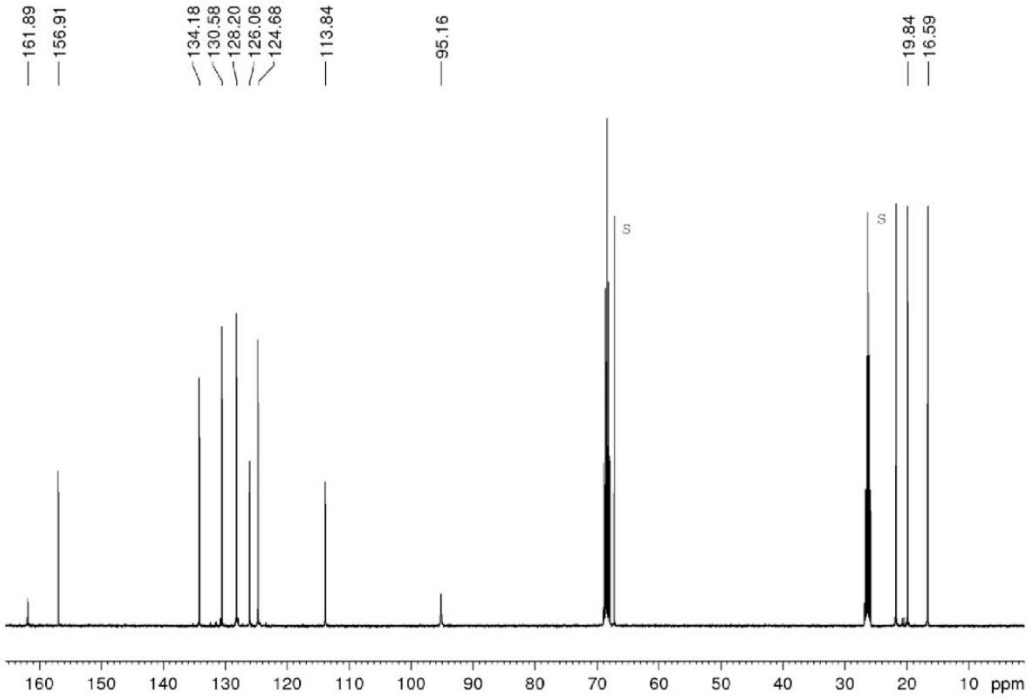

Figure S6. ^{13}C-NMR spectrum (100.61 MHz) of dilithio-2,3-diboratabutadiene **2** in thf-d_8 (=s).

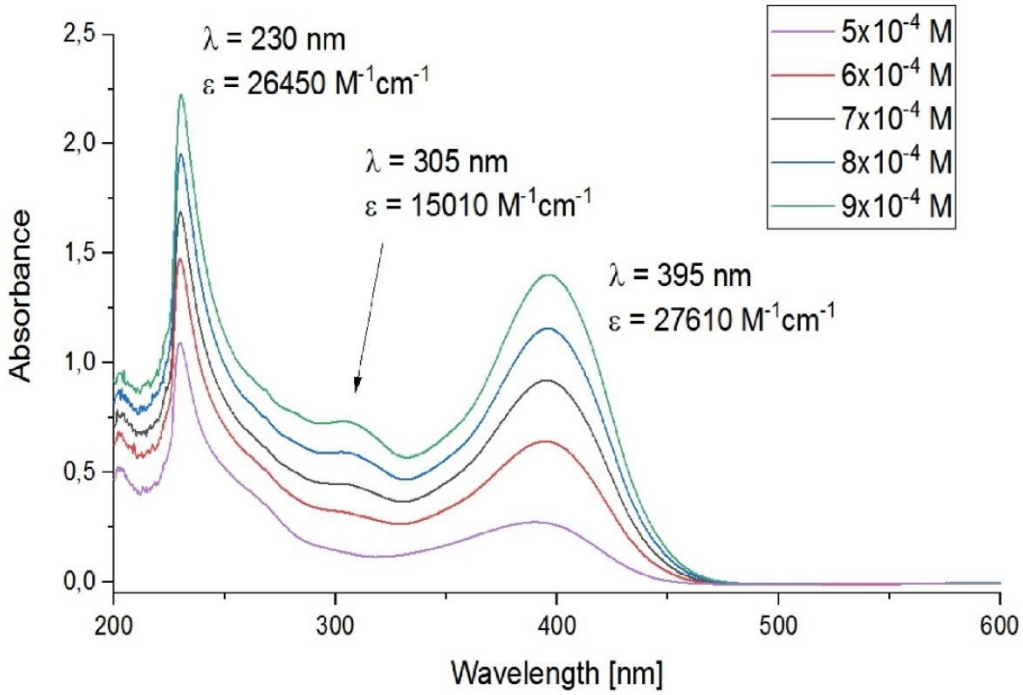

Fig S7. UV/Vis spectrum of dilithio-2,3-diboratabutadiene **2** in diethylether.

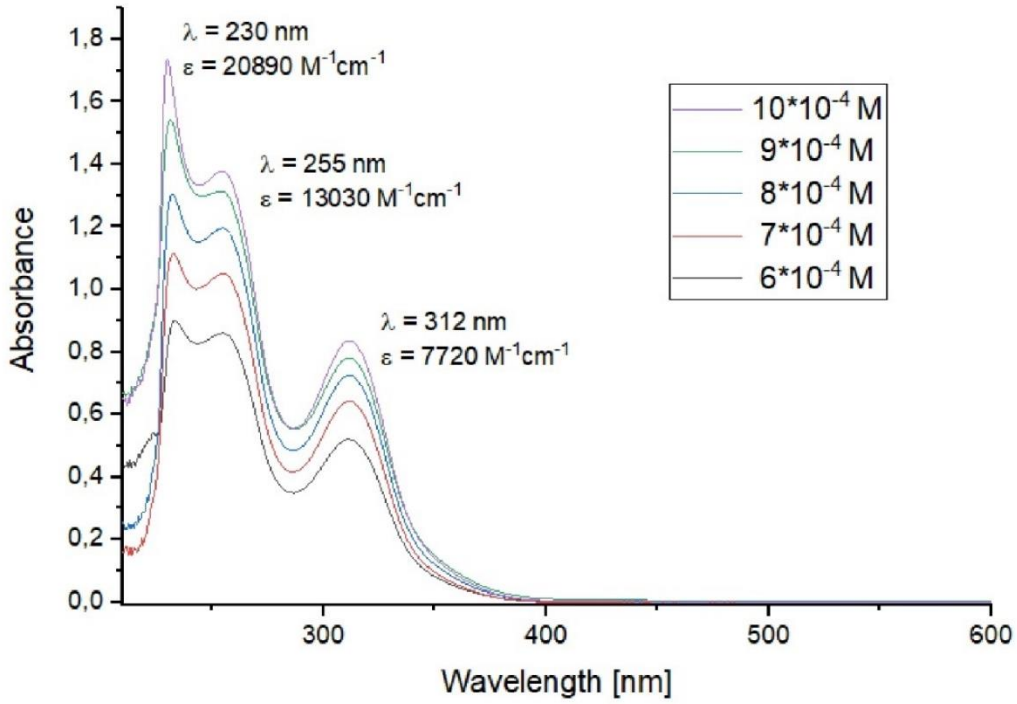

Fig S8. UV/Vis spectrum of 1,4-bis(trimethylsilyl)-2,3-diboratabutadiene in diethylether.

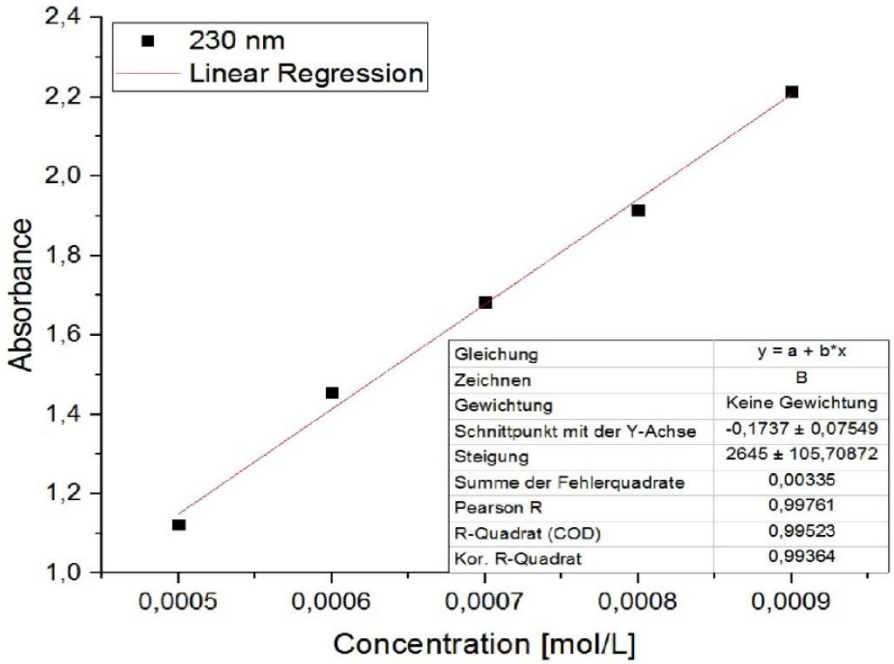

Fig S9. Determination of ε (26450 $M^{-1}cm^{-1}$) by linear regression of absorptions (λ = 230 nm) of dilithio-2,3-diboratabutadiene **2** against concentration.

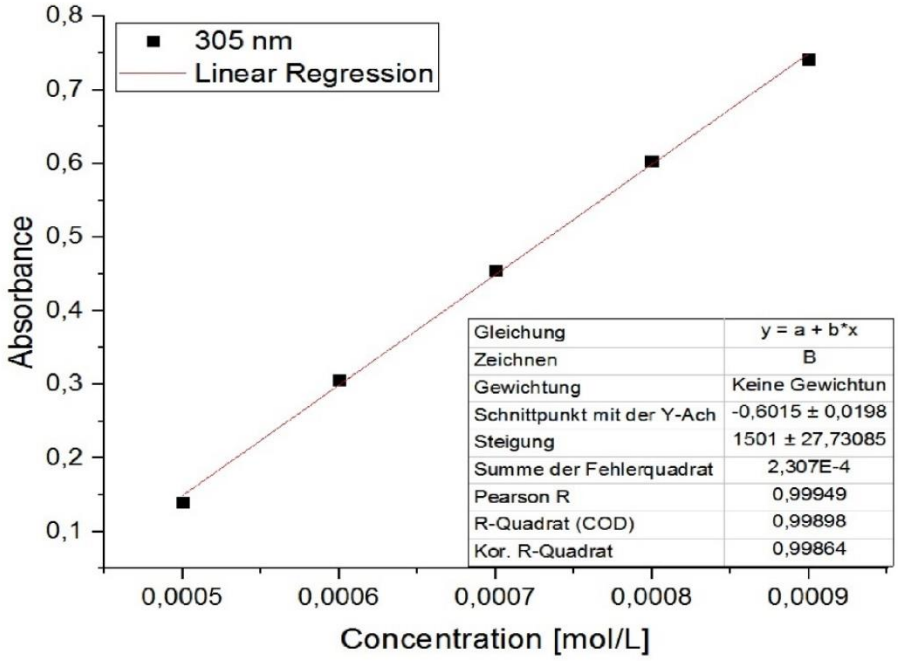

Fig S10. Determination of ε (15010 $M^{-1}cm^{-1}$) by linear regression of absorptions (λ = 305 nm) of dilithio-2,3-diboratabutadiene **2** against concentration.

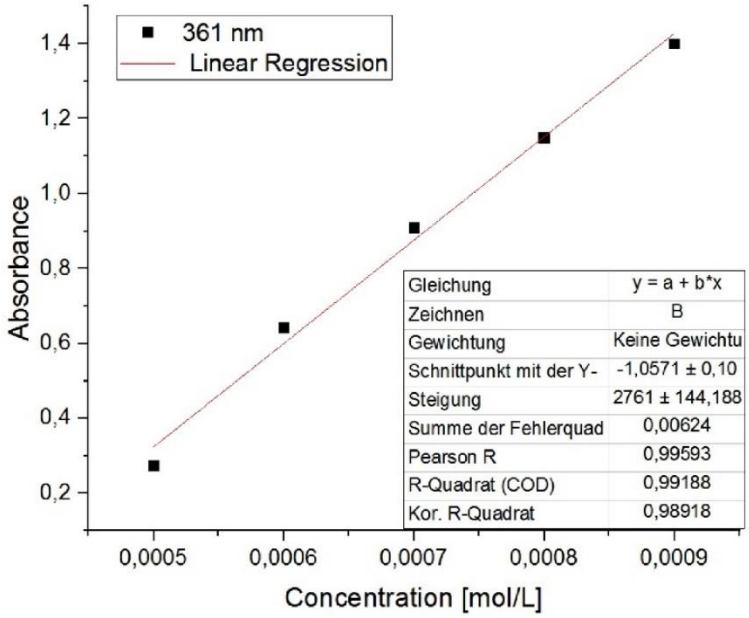

Fig S11. Determination of ε (27610 $M^{-1}cm^{-1}$) by linear regression of absorptions (λ = 361 nm) of dilithio-2,3-diboratabutadiene **2** against concentration.

2.3 2,3-Diboratabutadiene zirconocene complex **3a**

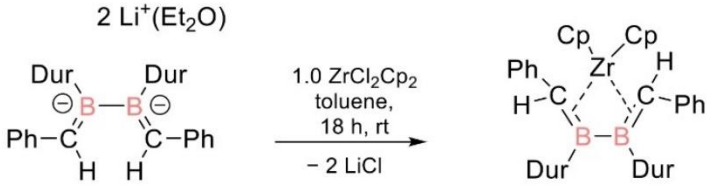

2 **3a**

704.54 g/mol 687.70 g/mol

At ambient temperature, 5.0 g diboratabutadiene **2** (7.1 mmol, 1.0 equiv) are suspended in 50 mL of toluene. A solution of Cp_2ZrCl_2 (2.07 g, 7.1 mmol, 1.0 equiv) in 10 mL of hexane is added dropwise. After stirring for 18 hours, the mixture is filtered and then all volatiles are removed in vacuo at room temperature. Washing with hexane and removing of the solvent results in 4.1 g (84%) of a red powder. The powder is redissolved in toluene to give a room temperature-saturated solution and stored at −25 °C. 2,3-Diboratabutadiene zirconocene complex **3a** is obtained as red crystals (3.1 g, 64%).

^{1}H NMR (400 MHz, C_6D_6, 300K): δ = 7.09-7.07 (m, Ph-H, 4H), 6.94-6.92 (m, Ph-H, 4H), 6.86-6.82 (m, Ph-H, 2H), 6.75 (s, BCH, 2H) 6.72 (s, Dur-H, 2H), 5.72 (s, Cp-H, 10H), 2.46, 2.20, 1.92, 1.72 (each s, Dur-CH_3, 6H)

^{11}B NMR (128.38 MHz, C_6D_6, 300 K): δ = 73.5 (br s) ppm.

^{13}C{^{1}H} NMR (100.61 MHz, C_6D_6, 300 K): δ = 151.4 (s, Ar-C), 146.9 (br s Dur-C_{ipso}), 134.0, 133.4, 132.9, 132.6, 131.3, 128.6, 126.1, 122.6 (each s, Ar-C), 113.3 (s, Cp-C), 90.4 (br s, B-C-Zr), 23.1, 20.5, 20.0 (each s, Dur-CH_3)

UV/Vis (toluene): $\lambda_{max}(\varepsilon)$ = 410 nm (5995 $M^{-1}cm^{-1}$), 460 nm (4255 $M^{-1}cm^{-1}$).

Elemental analysis: calc. for $C_{44}H_{46}B_2Zr$: C, 76.8%; H, 6.7%. Found: C, 75.2%; H, 6.0%.

Melting point: 188 – 190 °C (product mixture)

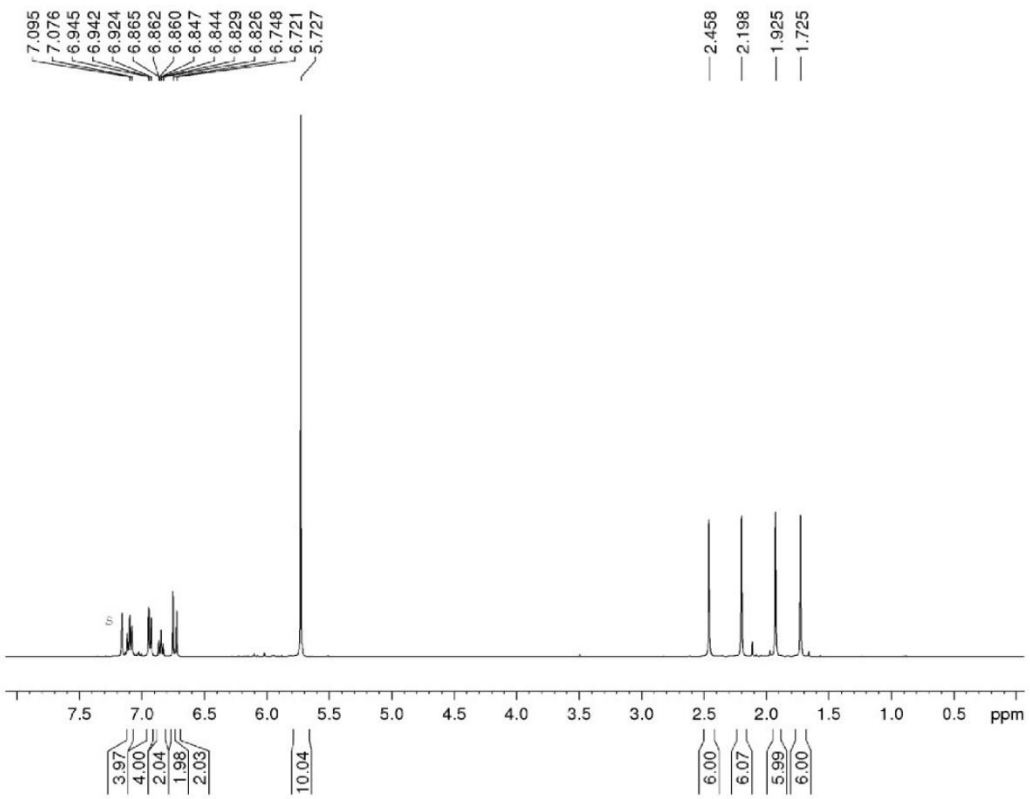

Fig S12. ^{1}H-NMR spectrum (400.1 MHz) of diboratabutadiene zirconocene complex **3** in C_6D_6 (=s).

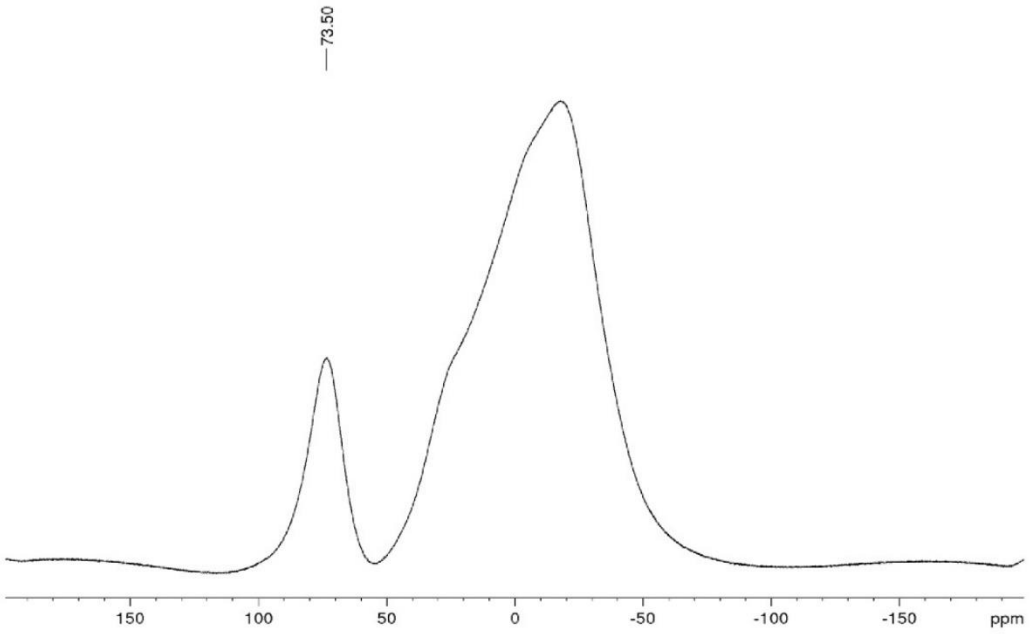

Fig S13. ^{11}B-NMR spectrum (128.4 MHz) of diboratabutadiene zirconocene complex **3** (glass peak from 50 to −50 ppm).

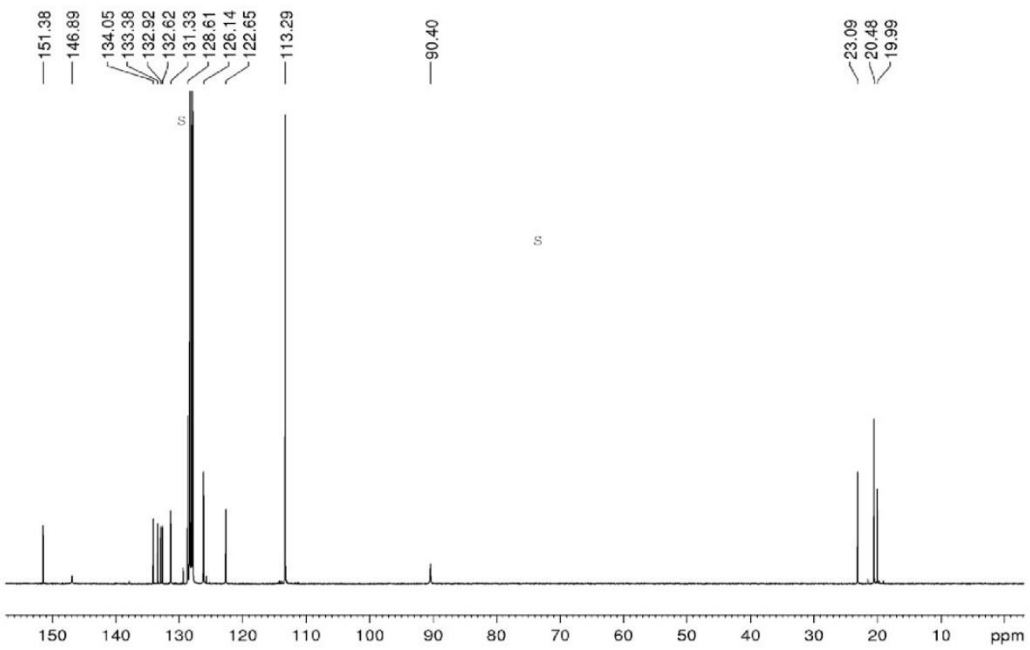

Fig S14. ^{13}C-NMR spectrum (100.61 MHz) of diboratabutadiene zirconocene complex **3** in C_6D_6 (=s).

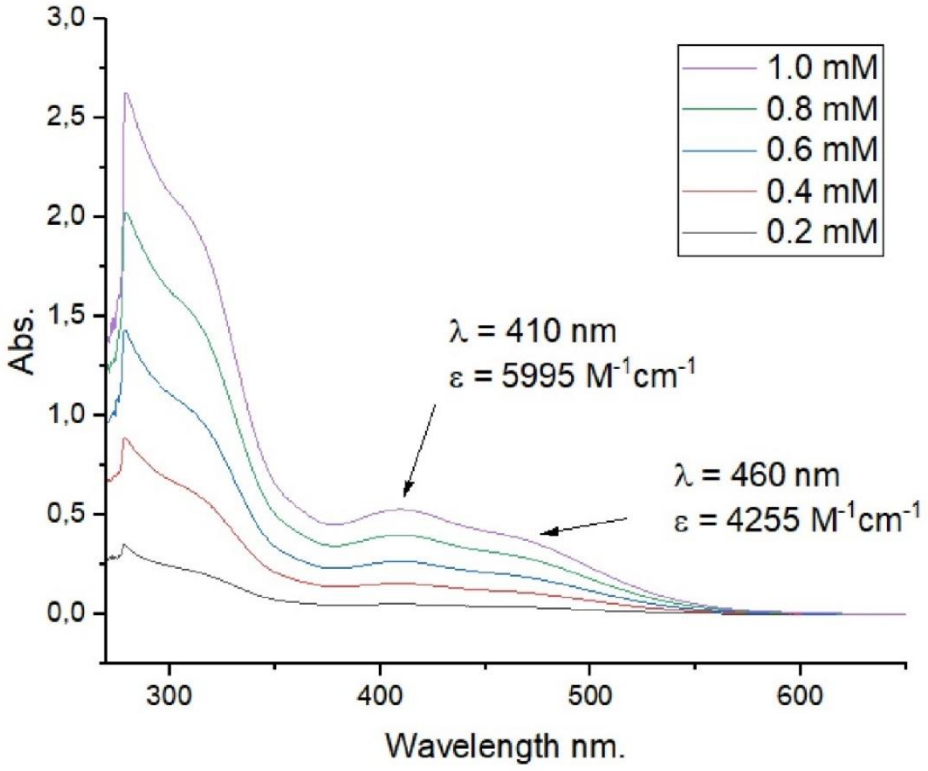

Fig S15. UV/Vis spectrum of diboratabutadiene zirconocene complex **3a** in toluene.

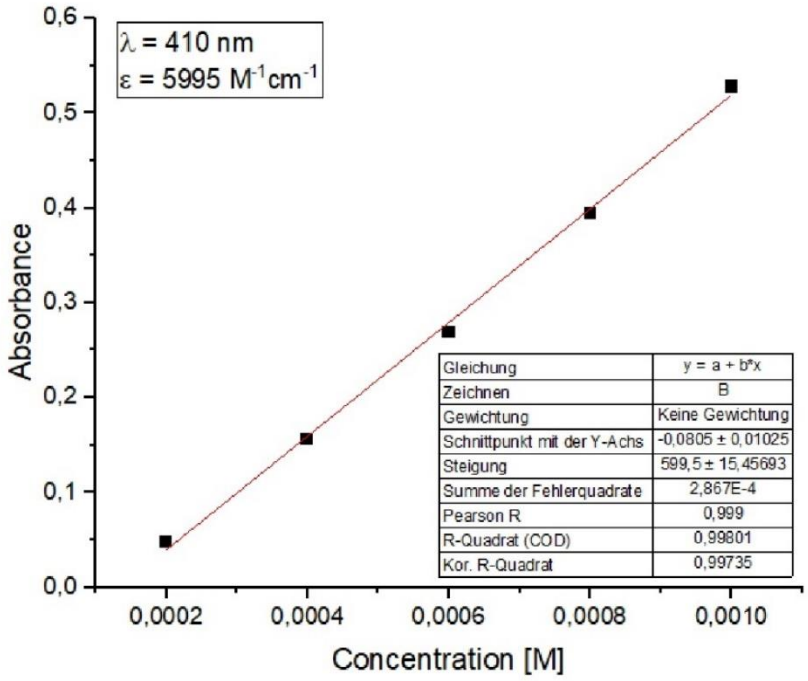

Fig S16. Determination of ε (5995 $M^{-1}cm^{-1}$) by linear regression of absorptions (λ = 410 nm) of diboratabutadiene zirconocene complex **3** against concentration.

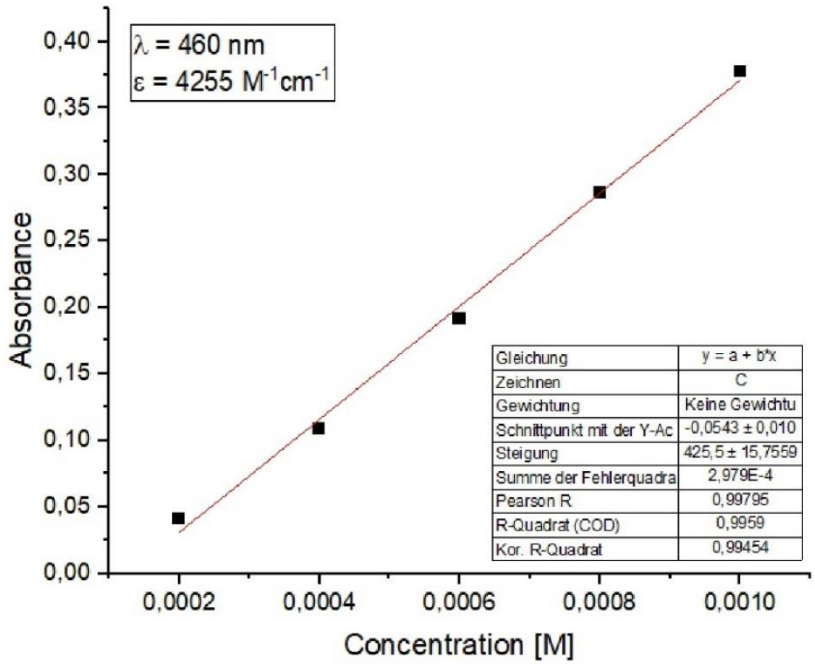

Fig S17. Determination of ε (4255 $M^{-1}cm^{-1}$) by linear regression of absorptions (λ = 460 nm) of diboratabutadiene zirconocene complex **3a** against concentration.

2.4 2,3-Diboratabutadiene hafnocene complex **3b**

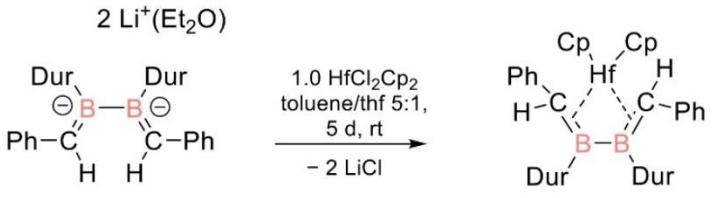

704.54 g/mol

774.95 g/mol

At ambient temperature, 5.0 g diboratabutadiene **2** (7.1 mmol, 1.0 equiv) are suspended in 50 mL of toluene and 10 ml of thf. A solution of Cp_2HfCl_2 (2.07 g, 7.1 mmol, 1.0 equiv) in 5 mL of toluene and 1 mL of thf is added to the solution. After stirring for 5 days, the mixture is filtered and then all volatiles are removed in vacuo at room temperature. Washing with hexane and removing of the solvent results in 4.2 g (76%) of an orange powder. The powder is redissolved in toluene to give a room temperature-saturated solution and stored at −25 °C. 2,3-Diboratabutadiene hafnocene complex **3b** is obtained as orange crystals (3.2 g, 57%).

^{1}H NMR (400 MHz, C_6D_6, 300K): δ = 7.13-7.09 (m, Ph-H, 4H), 6.90-6.89 (m, Ph-H, 4H), 6.84-6.80 (m, Ph-H, 2H), 6.74 (s, BCH, 2H) 6.52 (s, Dur-H, 2H), 5.73 (s, Cp-H, 10H), 2.55, 2.24, 1.89, 1.72 (each s, Dur-CH_3, 6H)

^{11}B NMR (128.38 MHz, C_6D_6, 300 K): δ = 75.5 (br s) ppm.

^{13}C{ 1H} NMR (100.61 MHz, C_6D_6, 300 K): δ = 150.8 (s, Ar-C), 146.0 (br s Dur-C_{ipso}), 134.0, 132.8, 132.7, 132.2, 131.0, 128.4, 126.2, 122.6 (each s, Ar-C), 113.2 (s, Cp-C), 89.7 (br s, B-C-Zr), 23.1, 20.3, 20.2, 19.4 (each s, Dur-CH_3)

UV/Vis (toluene): $\lambda_{max}(\varepsilon)$ = 340 nm (6440 $M^{-1}cm^{-1}$), 380 nm (5425 $M^{-1}cm^{-1}$), 415 nm (4215 $M^{-1}cm^{-1}$).

Elemental analysis: calc. for $C_{44}H_{46}B_2Hf$: C, 68.2%; H, 6.0%. Found: C, 67.1%; H, 5.9%.

Melting point: 198 – 200°C (product mixture)

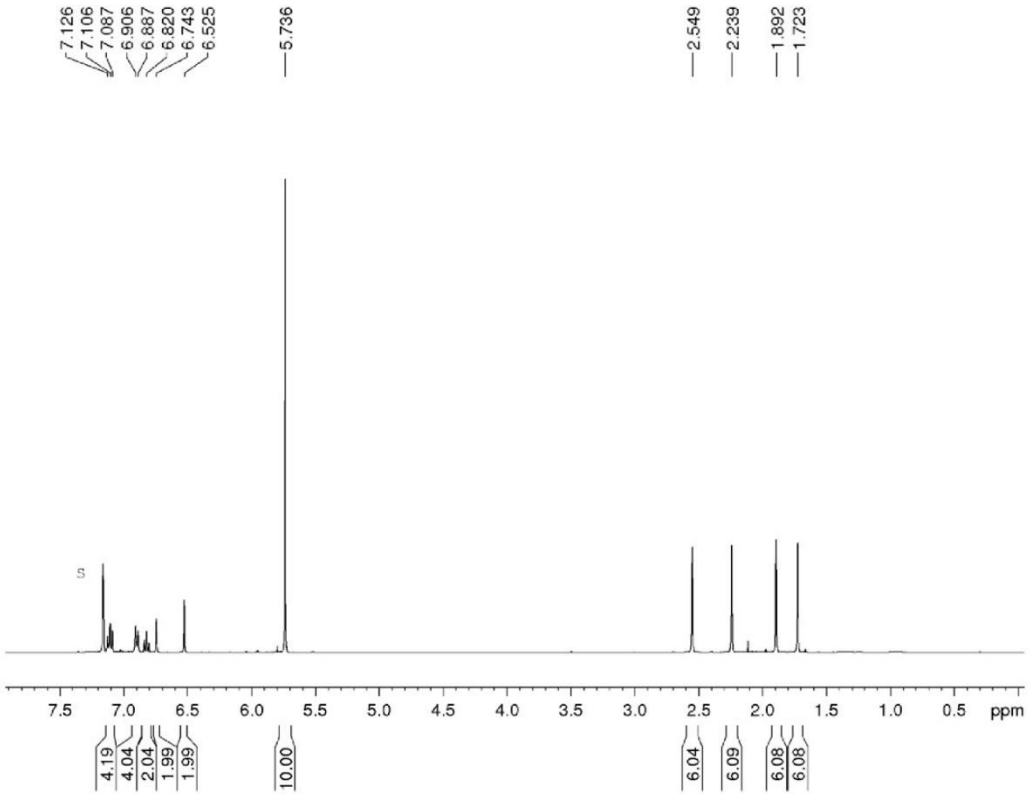

Fig S18. ^{1}H-NMR spectrum (400.1 MHz) of diboratabutadiene hafnocene complex **3b** in C_6D_6 (=s).

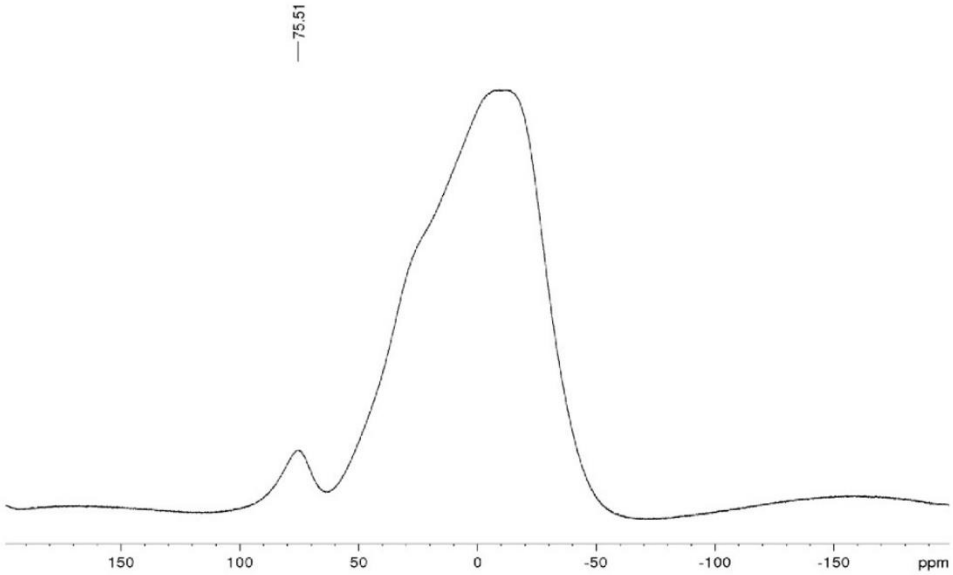

Fig S19. ^{11}B-NMR spectrum (128.4 MHz) of diboratabutadiene hafnocene complex **3b** (glass peak from 50 to −50 ppm).

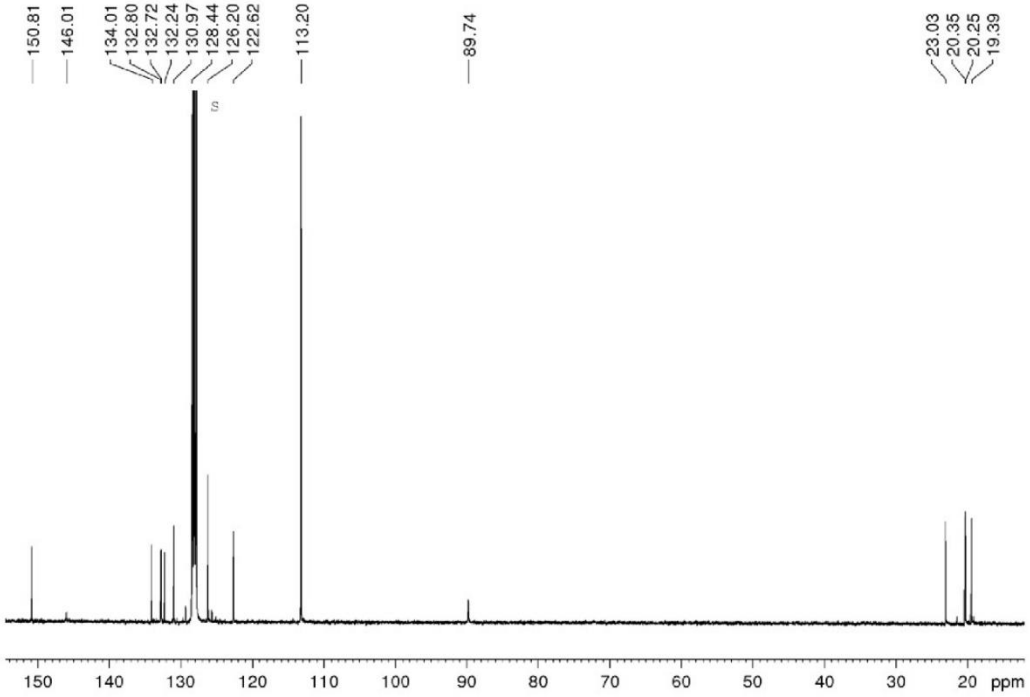

Fig S20. ^{13}C-NMR spectrum (100.61 MHz) of diboratabutadiene hafnocene complex **3b** in C_6D_6 (=s).

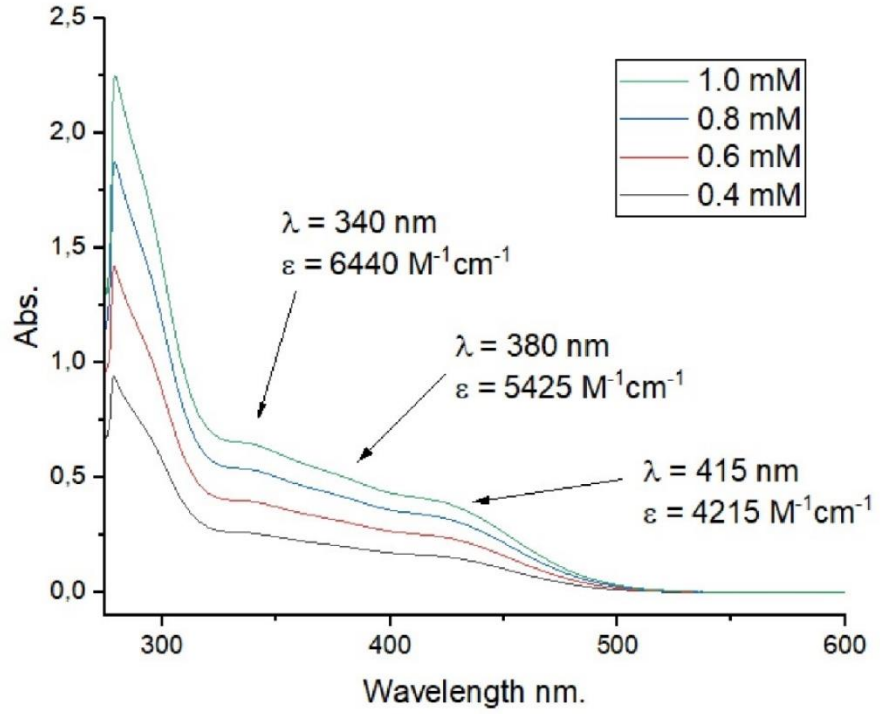

Fig S21. UV/Vis spectrum of diboratabutadiene hafnocene complex **3b** in toluene.

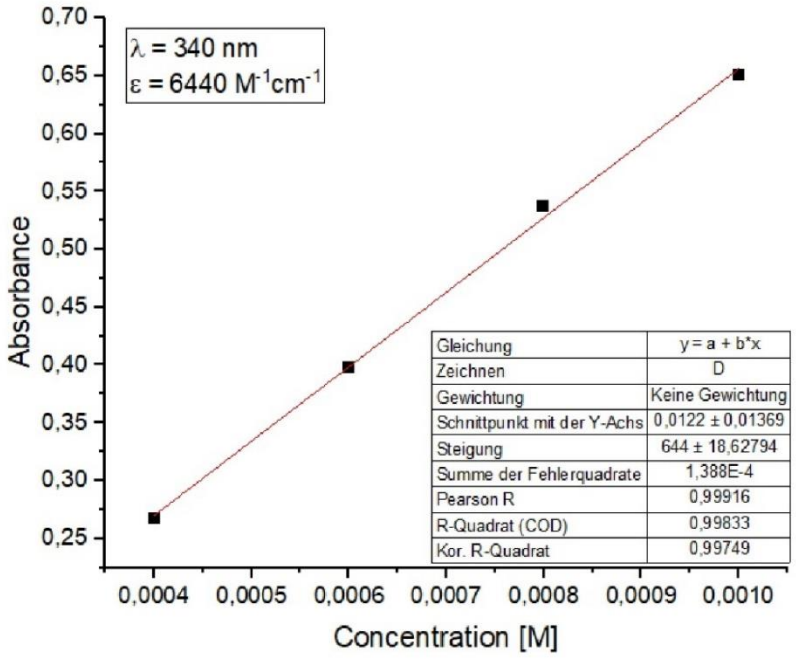

Fig S22. Determination of ε (6440 $M^{-1}cm^{-1}$) by linear regression of absorptions (λ = 340 nm) of diboratabutadiene hafnocene complex **3b** against concentration.

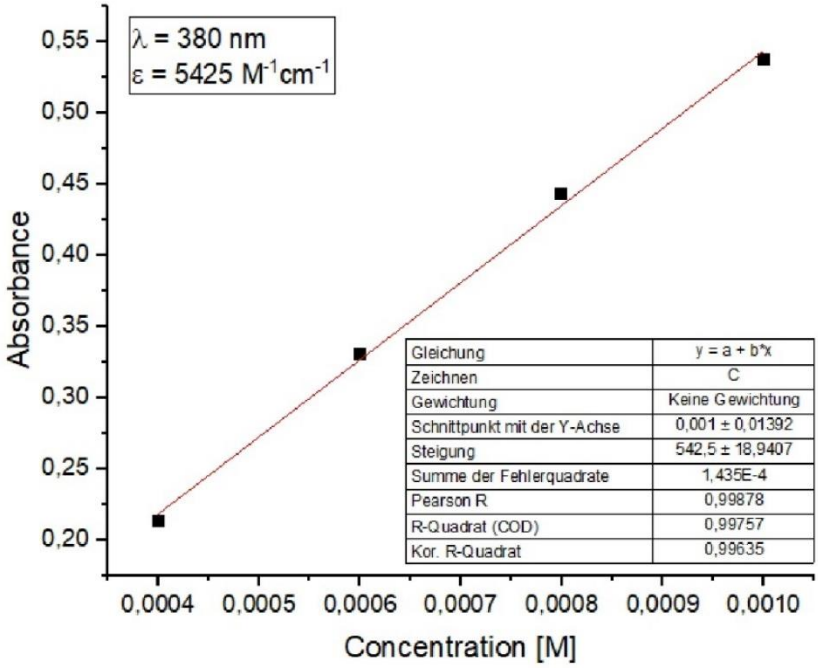

Fig S23. Determination of ε (5425 $M^{-1}cm^{-1}$) by linear regression of absorptions (λ = 380 nm) of diboratabutadiene hafnocene complex **3b** against concentration.

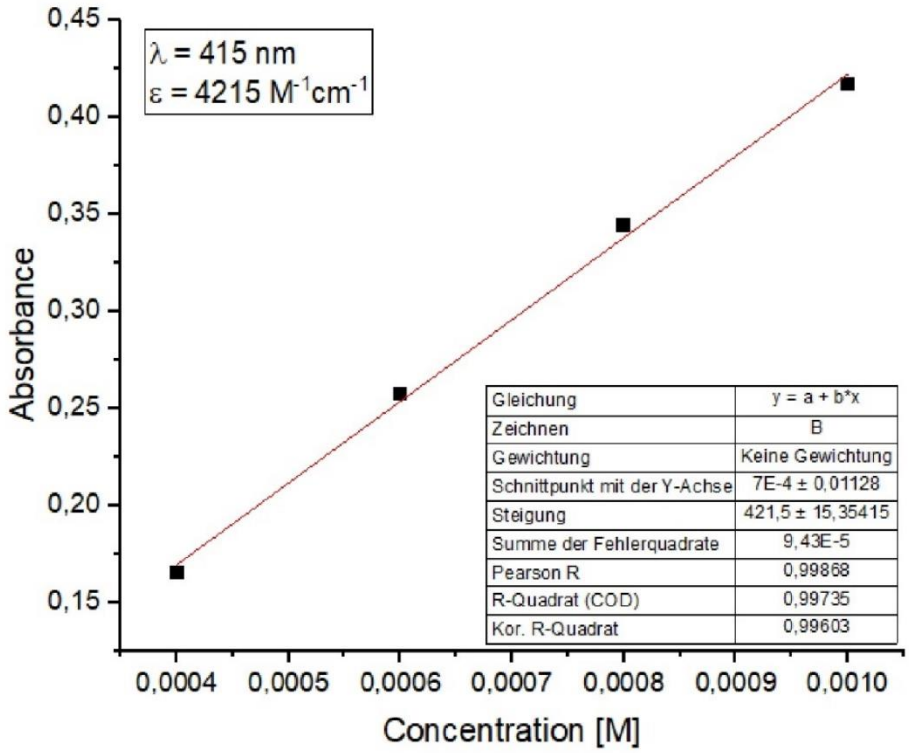

Fig S24. Determination of ε (4215 $M^{-1}cm^{-1}$) by linear regression of absorptions (λ = 415 nm) of diboratabutadiene hafnocene complex **3b** against concentration.

2.5 Methyleneborane NHC adduct **4** and borane NHC adduct **6**

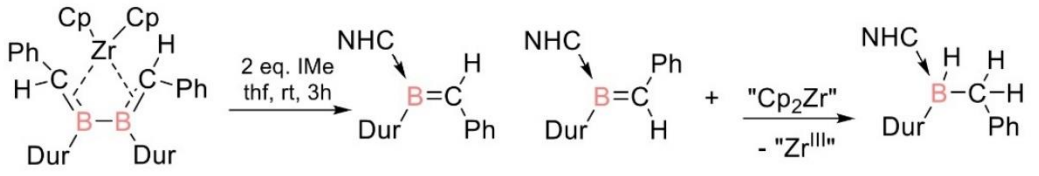

3a | *Z*-**4** | *E*-**4** | **5** | **6**

687.70 g/mol | 330.28 g/mol | 330.28 g/mol | 332.28 g/mol

At ambient temperature 400 mg diboratabutadiene complex **3a** (0.6 mmol, 1.0 equiv) and 150 mg (1.2 mmol, 2.0 equiv) tetramethyl NHC are suspended in 10 of thf. The red solution changes colour to dark red. After stirring for 3 hours the solvent is removed. After addition of a 5:1 solvent mixture of hexane:thf the suspension is filtered, the process was repeated 3 times with each 20 ml of solvent mixture. The filtrate was concentrated under reduced pressure. The saturated solution was stored at −25 °C to give methylene borane *Z*-**4** as colorless crystals in three fractions (70 mg, 35%). The resulting filtrate was dried and redissolved in hexane. The hexane solution was stored at −25 °C to give NHC borane adduct **6** as colorless crystals (25 mg, 13%).

For *Z*-**4**:

^{1}H NMR (400 MHz, C_6D_6, 300K): δ = 7.62-7.60 (m, Ph-H, 2H), 7.27-7.23 (m, Ph-H, 2H), 7.05 (s, Dur-H, 1H), 6.95-6.91 (m, Ph-H, 1H), 5.68 (s, B=CH, 1H), 3.02 (s, NHC-N-CH_3, 6H), 2.52, 2.32 (each s, Dur-CH_3, 6H), 1.13 (s, NHC-CH_3, 6H) ppm.

^{11}B NMR (128.38 MHz, C_6D_6, 300 K): δ = 26.3 (br s) ppm.

^{13}C{^{1}H} NMR (100.61 MHz, C_6D_6, 300 K): δ = 150.4 (s, Ar-C), 136.6, 132.9, 130.1, 126.9, 123.6, 120.4, (each s, Ar-C), 120.0 (br s, B=C), 32.7 (s, NHC-N-CH_3, 6H), 20.7, 19.8 (each s, Dur-CH_3), 7.9 (s, NHC-CH_3) ppm.

Elemental analysis: calc. for $C_{24}H_{31}BN_2$: C, 80.4%; H, 8.7%, N, 7.8% Found: C, 79.9%; H, 8.2%, N, 6.8%.

Melting point: 228 – 230 °C (slight decomposition)

For *E*-**4**:

^{1}H NMR (400 MHz, C_6D_6, 300K): δ = 7.62-7.60 (m, Ph-H, 2H), 7.27-7.23 (m, Ph-H, 2H), 7.05 (s, Dur-H, 1H), 6.95-6.91 (m, Ph-H, 1H), 5.41 (s, B=CH, 1H), 2.97 (s, NHC-N-CH_3, 6H), 2.54, 2.33 (each s, Dur-CH_3, 6H), 1.14 (s, NHC-CH_3, 6H) ppm.

^{11}B NMR (128.38 MHz, C_6D_6, 300 K): δ = 26 (br s) ppm.

^{13}C{ 1H} NMR (100.61 MHz, C_6D_6, 300 K): δ = 150.8 (s, Ar-C), 137.6, 132.5, 129.8, 127.6, 126.4, 124.3 124.0, (each s, Ar-C), 119.9 (br s, B=C), 32.0 (s, NHC-N-CH_3, 6H), 21.1, 20.5 (each s, Dur-CH_3), 8.1 (s, NHC-CH_3) ppm.

For **6**:

^{1}H NMR (400 MHz, C_6D_6, 300K): δ = 7.37-7.35 (m, Ph-H, 2H), 7.26-7.22 (m, Ph-H, 2H), 7.11-7.07 (m, Ph-H, 1H), 7.01 (s, Dur-H, 2H), 3.89-3.29 (q, $^{1}J_{B-H}$ = 85 Hz, BH, 1H), 2.86 (s, NHC-N-CH_3, 6H), 2.86, 2.68 (each m, Ph-CH_2, 1H), 2.37, 2.32 (each s, Dur-CH_3, 6H), 1.10 (s, NHC-CH_3, 6H) ppm.

^{11}B NMR (128.38 MHz, C_6D_6, 300 K): δ = −16.5 (d, $^{1}J_{B-H}$ = 85 Hz) ppm.

^{13}C{ 1H} NMR (100.61 MHz, C_6D_6, 300 K): δ = 150.9 (s, Ar-C), 138.1, 132.2, 129.6, 129.2, 123.0, 122.7 (each s, Ar-C), 31.7 (s, NHC-N-CH_3, 6H), 21.8, 19.0 (each s, Dur-CH_3), 7.9 (s, NHC-CH_3) ppm.

HRMS (ESI): m/z calc. for $C_{24}H_{43}BN_2$: 359.2664 $[M-H]^+$ Found: 359.2655

Melting point: 153 – 155°C (slight decomposition)

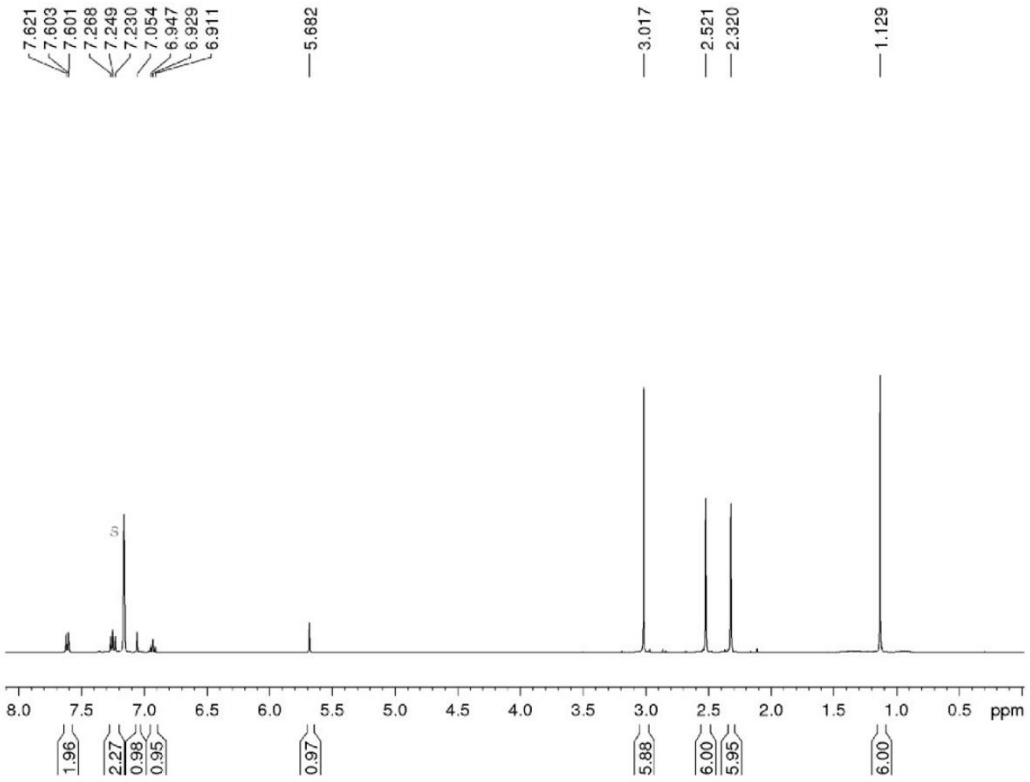

Fig S25. ^{1}H-NMR spectrum (400.1 MHz) of methyleneborane-NHC adduct *Z*-**4** in C_6D_6 (=s).

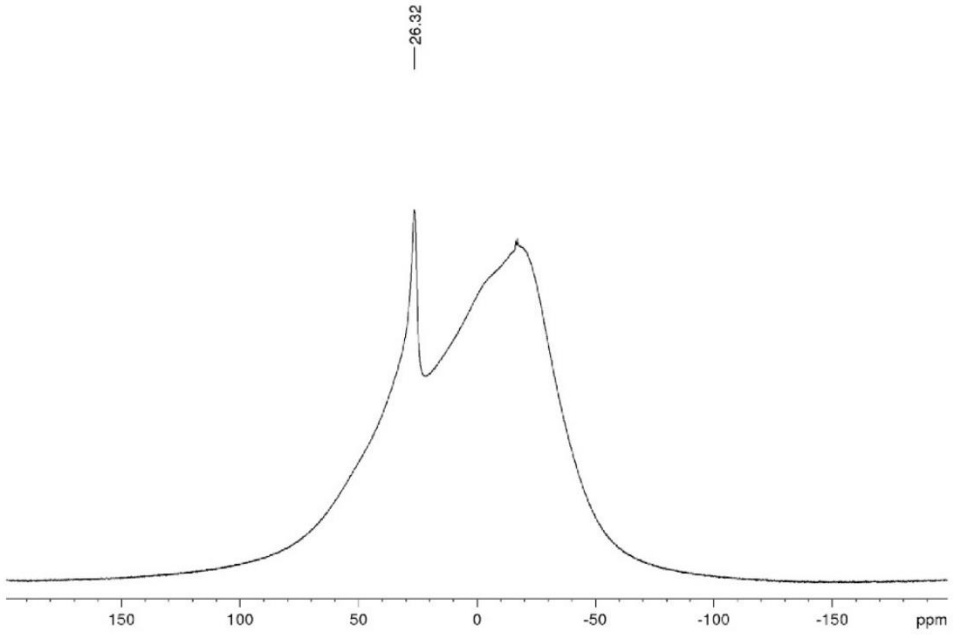

Fig S26. ^{11}B-NMR spectrum (128.4 MHz) of methyleneborane NHC adduct **4** (glass peak from 50 to −50 ppm) and slight contamination with **6** at −16.5 ppm.

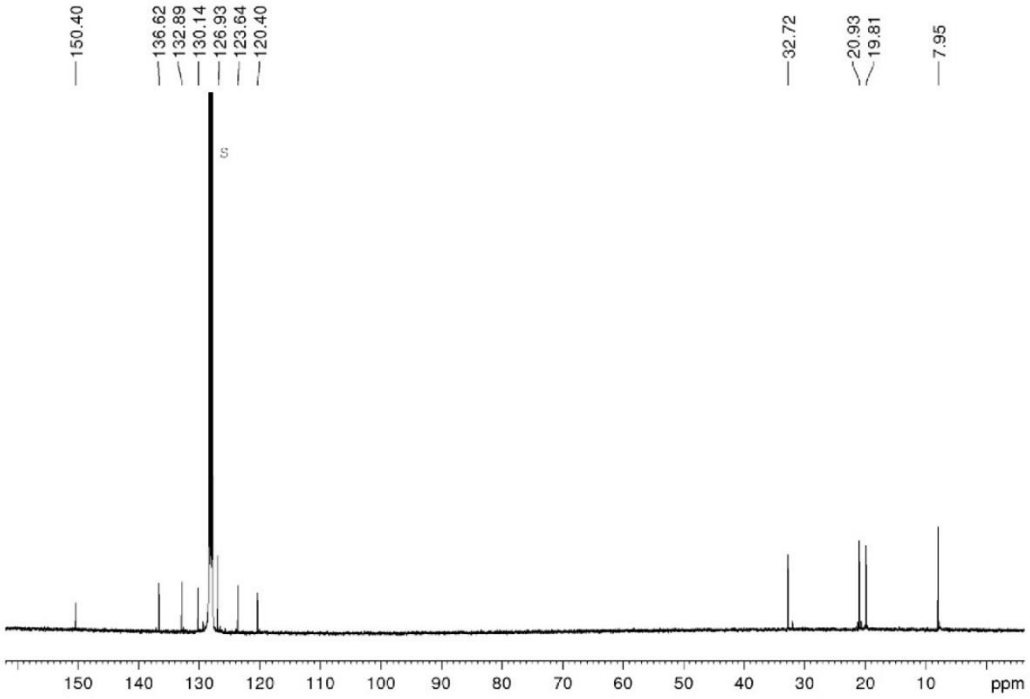

Fig S27. ^{13}C-NMR spectrum (100.61 MHz) of methyleneborane NHC adduct *Z*-**4** in C_6D_6 (=s).

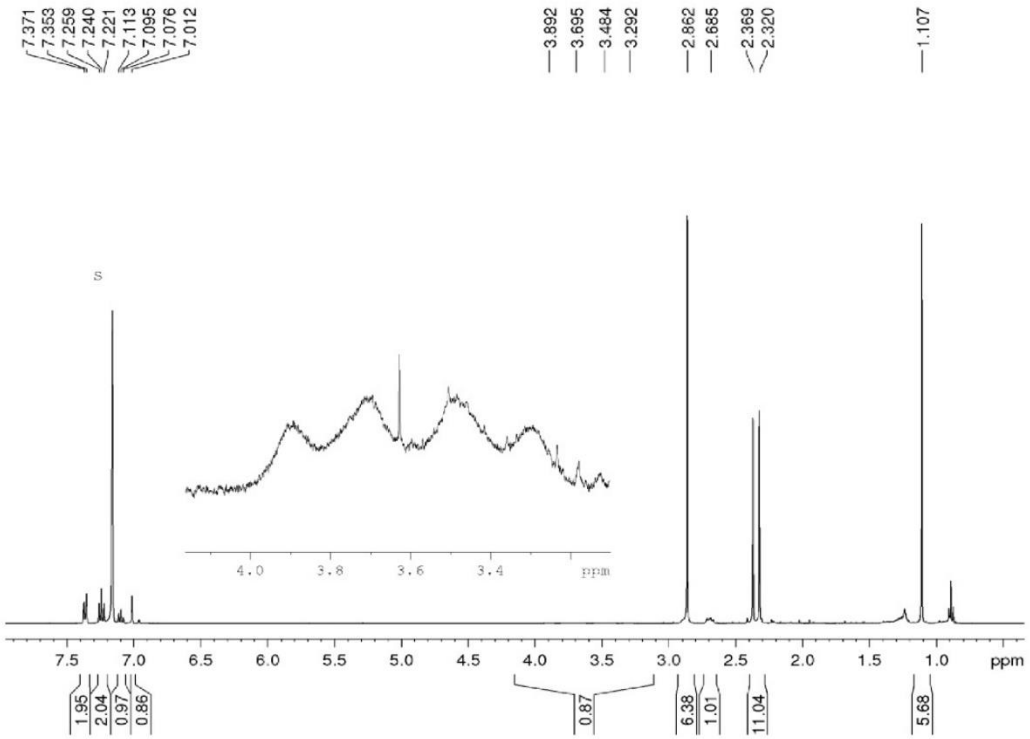

Fig S28. ^{1}H-NMR spectrum (400.1 MHz) of borane/NHC adduct **6** in C_6D_6 (=s).

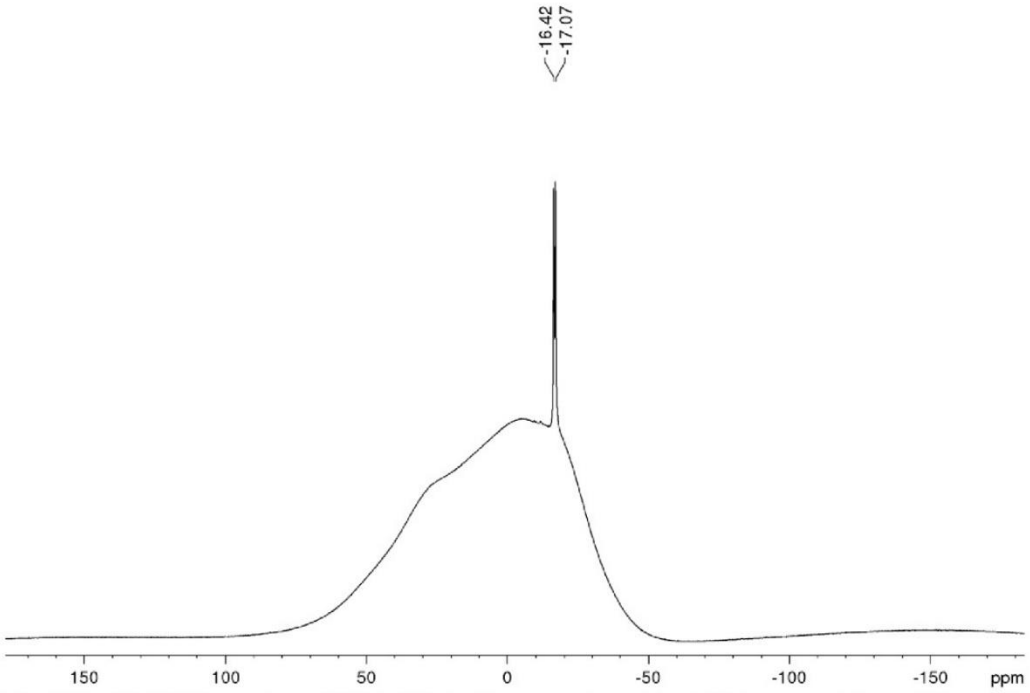

Fig S29. ^{11}B-NMR spectrum (128.4 MHz) of borane nhc adduct **6** (glass peak from 50 to −50 ppm).

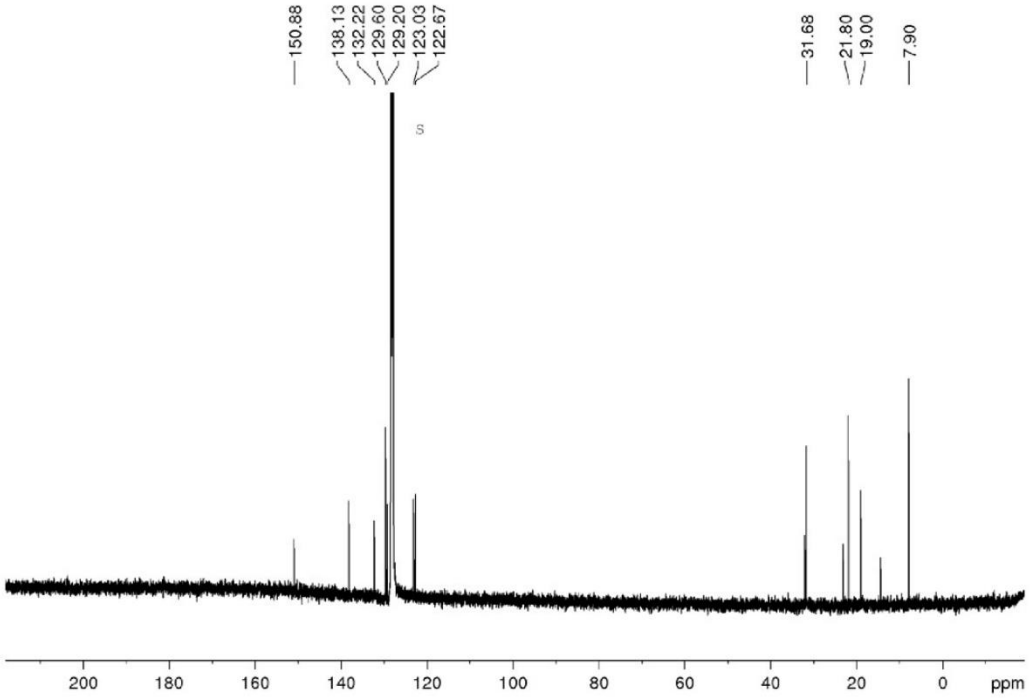

Fig S30. ^{13}C-NMR spectrum (100.61 MHz) of of borane/NHC adduct **6** in C_6D_6 (=s).

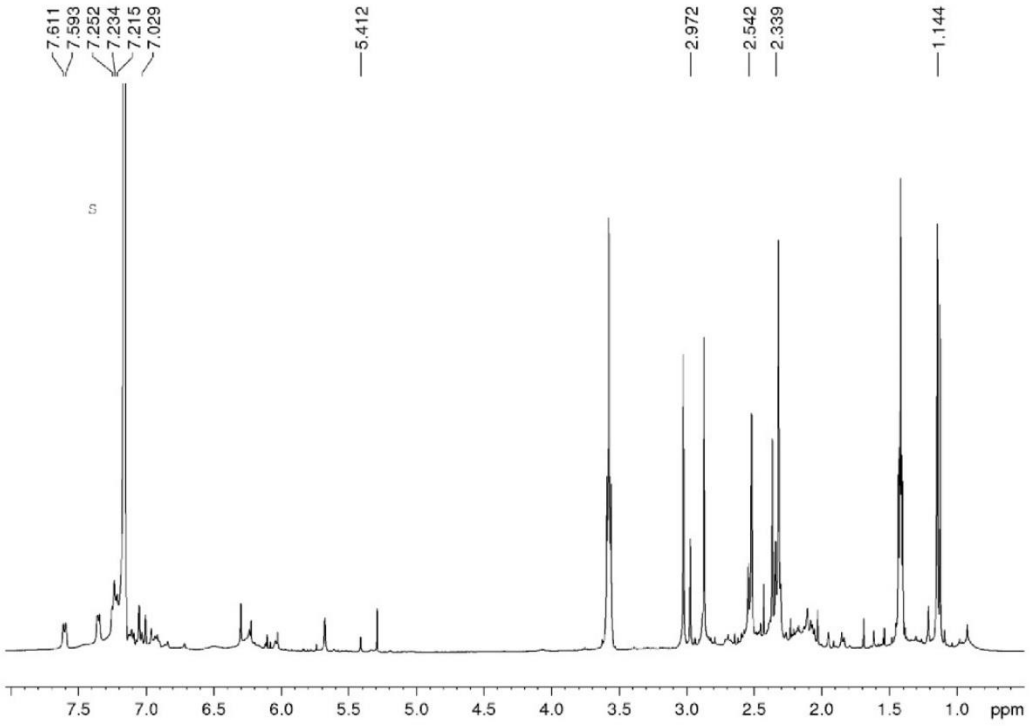

Fig S31. ^{1}H-NMR spectrum (400.1 MHz) of crude reaction mixture in C_6D_6 (=s) with *E*-**4** signals marked.

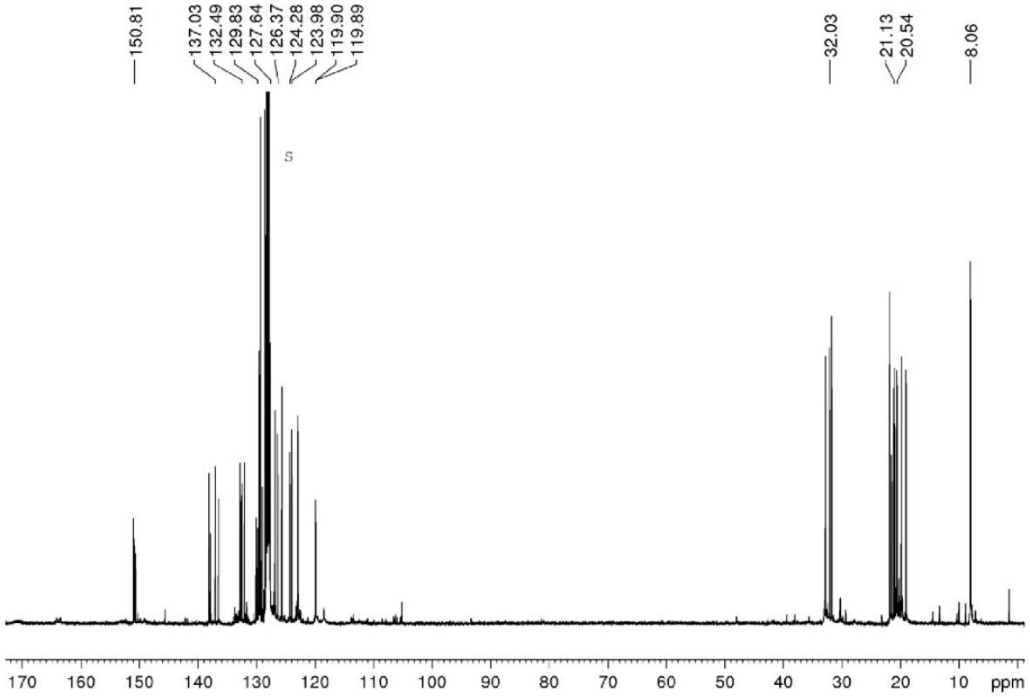

Fig S32. ^{13}C-NMR spectrum (100.61 MHz) of crude reaction mixture in C_6D_6 (=s) with *E*-**4** signals marked and traces of toluene.

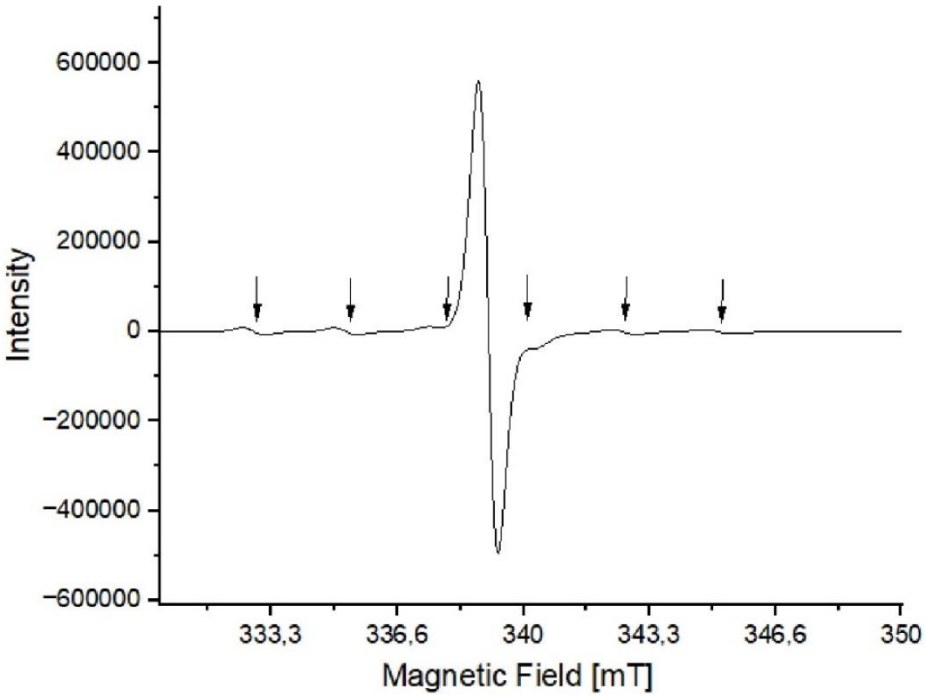

Fig S33. EPR spectrum (400.1 MHz) of paramagnetic Zr^{III} species.

3. Details on crystallographic studies

The data set was collected using a Bruker D8 Venture (**2** - **4**) or Rigaku Synergy-S (**1**, **5** - **6**) diffractometer with a microfocus sealed tube and a Photon II detector. Monochromated MoKα radiation (λ = 0.71073 Å) was used. Data were collected at temperatures given below and corrected for absorption effects using the multi-scan method. The structure was solved by direct methods using SHELXT[62] and was refined by full matrix least squares calculations on F^2 (SHELXL2018)[63] in the graphical user interface Shelxle[64].

Acknowledgment: Instrumentation and technical assistance for this work were provided by the Service Center X-ray Diffraction, with financial support from Saarland University and German Science Foundation (project number INST 256/506-1 (D8 Venture) and 256/582-1 (Synergy-S)).

3.1 Molecular structure of dibenzyldiborane(4) **1** in the solid state

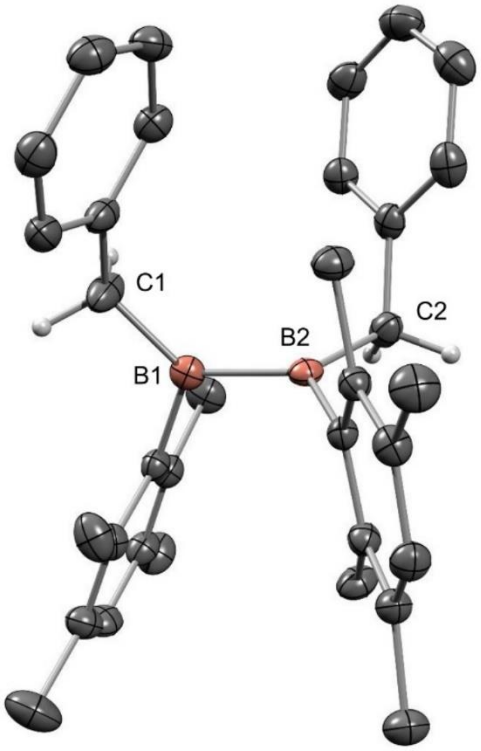

Refinement: All non H-atoms were located in the electron density maps and refined anisotropically. C-bound H atoms were placed in positions of optimized geometry and treated as riding atoms. Their isotropic displacement parameters were coupled to the corresponding carrier atoms by a factor of 1.2 (CH, CH2) or 1.5 (CH3).

Table S1. Crystal data and structure refinement for 5756_a.

Identification code	5756_a

CCDC number	2443028	
Empirical formula	C34 H40 B2	
Formula weight	470.28	
Temperature	130(2) K	
Wavelength	0.71073 Å	
Crystal system	Monoclinic	
Space group	$P2_1/c$	
Unit cell dimensions	a = 21.5454(8) Å	α = 90°.
	b = 7.6685(2) Å	β = 109.952(4)°.
	c = 17.6777(5) Å	γ = 90°.
Volume	2745.42(16) $Å^3$	
Z	4	
Density (calculated)	1.138 Mg/m^3	
Absorption coefficient	0.063 mm^{-1}	
F(000)	1016	
Crystal size	0.220 x 0.200 x 0.080 mm^3	
Theta range for data collection	2.310 to 27.101°.	
Index ranges	-26<=h<=27, -9<=k<=9, -22<=l<=20	
Reflections collected	25295	
Independent reflections	6054 [R(int) = 0.0284]	
Completeness to theta = 25.242°	100.0 %	
Absorption correction	Semi-empirical from equivalents	
Max. and min. transmission	1.0000 and 0.9536	
Refinement method	Full-matrix least-squares on F^2	
Data / restraints / parameters	6054 / 0 / 333	
Goodness-of-fit on F2	1.029	
Final R indices [I>2sigma(I)]	R1 = 0.0411, wR2 = 0.1067	
R indices (all data)	R1 = 0.0533, wR2 = 0.1157	
Extinction coefficient	n/a	
Largest diff. peak and hole	0.271 and -0.183 $e.Å^{-3}$	

3.2 Molecular structure of diboratabutadiene **2** in the solid state

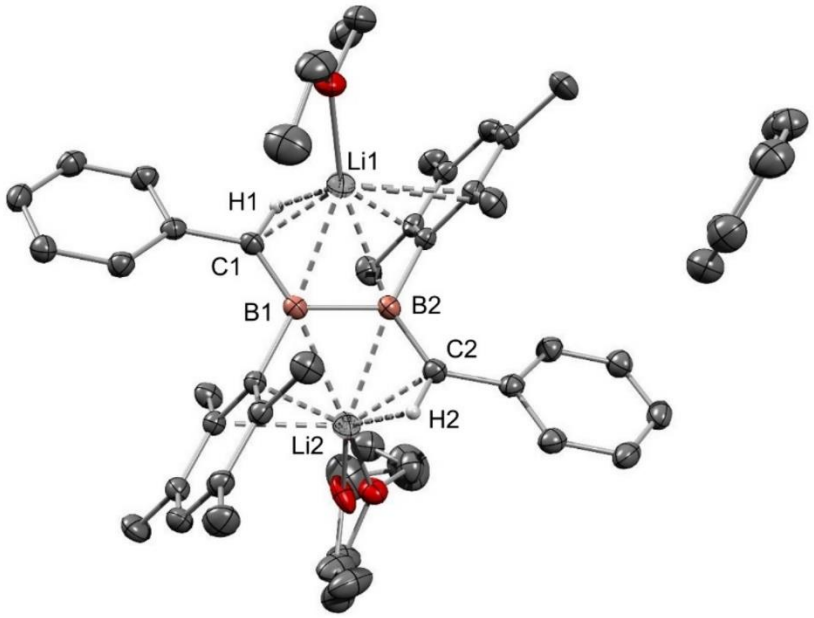

Refinement: All non H-atoms were located on the electron density maps and refined anisotropically. C-bound H atoms were placed in positions of optimized geometry and treated as riding atoms. Their isotropic displacement parameters were coupled to the corresponding carrier atoms by a factor of 1.2 (CH, CH2) or 1.5 (CH3). The methylene hydrogen atoms H1 and H2 were located on the electron density maps with a factor of 1.2 used for the isotropic displacement parameters.

Disorder: The Et_2O molecule coordinated to Li2 is disordered across two positions. The occupancy factor refined to 87 % for the major component.

Table S2. Crystal data and structure refinement for sh4723_a.

Identification code	sh4723_a	
CCDC Number	2443035	
Empirical formula	C49 H66 B2 Li2 O2	
Formula weight	722.51	
Temperature	133(2) K	
Wavelength	0.71073 Å	
Crystal system	Triclinic	
Space group	P-1	
Unit cell dimensions	a = 11.2820(4) Å	α = 111.2380(10)°.
	b = 14.2102(5) Å	β = 91.8820(10)°.
	c = 15.3201(5) Å	γ = 104.8920(10)°.

Volume	2190.68(13) $Å^3$
Z	2
Density (calculated)	1.095 Mg/m^3
Absorption coefficient	0.063 mm^{-1}
F(000)	784
Crystal size	0.285 x 0.223 x 0.182 mm^3
Theta range for data collection	1.886 to 27.896°.
Index ranges	-14<=h<=14, -18<=k<=18, -20<=l<=20
Reflections collected	59852
Independent reflections	10479 [R(int) = 0.0366]
Completeness to theta = 25.242°	99.9 %
Absorption correction	Semi-empirical from equivalents
Max. and min. transmission	0.7456 and 0.6824
Refinement method	Full-matrix least-squares on F^2
Data / restraints / parameters	10479 / 102 / 563
Goodness-of-fit on F2	1.025
Final R indices [I>2sigma(I)]	R1 = 0.0499, wR2 = 0.1376
R indices (all data)	R1 = 0.0632, wR2 = 0.1495
Extinction coefficient	n/a
Largest diff. peak and hole	0.542 and -0.306 $e.Å^{-3}$

3.3 Molecular structure of diboratabutadiene zirconocene complex **3a** in the solid state

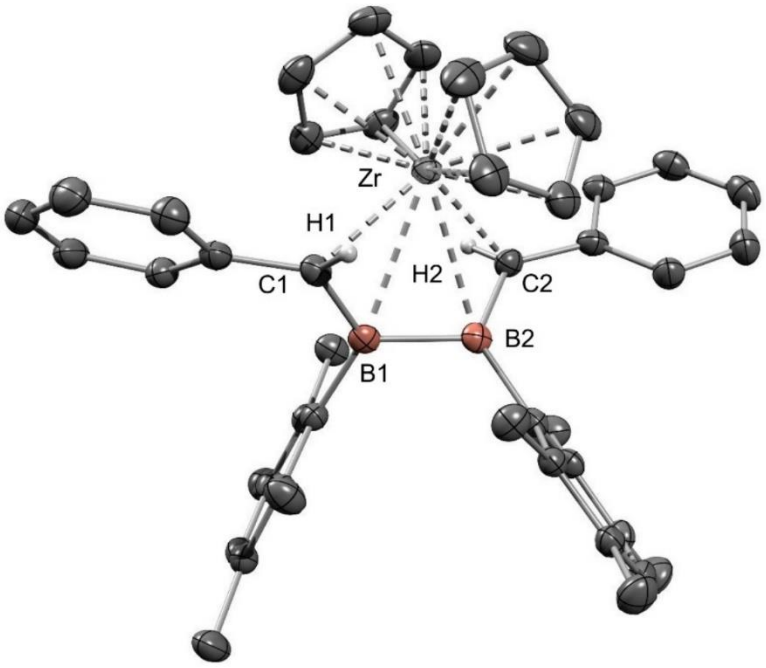

Refinement: All non H-atoms were located in the electron density maps and refined anisotropically. C-bound H atoms were placed in positions of optimized geometry and treated as riding atoms. Their isotropic displacement parameters were coupled to the corresponding carrier atoms by a factor of 1.2 (CH,) or 1.5 (CH3). C-bound H atom H1 and H2 was located on the electron density maps. Their isotropic displacement parameters were coupled to the corresponding carrier atoms by a factor of 1.2.

Table S3. Crystal data and structure refinement for sh5180_a.

Identification code	sh5180_a	
CCDC number	2443036	
Empirical formula	C44 H48 B2 Zr	
Formula weight	689.66	
Temperature	143(2) K	
Wavelength	0.71073 Å	
Crystal system	Monoclinic	
Space group	$P2_1/c$	
Unit cell dimensions	a = 12.6436(5) Å	α = 90°.
	b = 16.7458(7) Å	β = 91.065(2)°.
	c = 16.6832(7) Å	γ = 90°.
Volume	3531.7(3) Å^3	

Z	4
Density (calculated)	1.297 Mg/m^3
Absorption coefficient	0.342 mm^{-1}
F(000)	1448
Crystal size	0.200 x 0.100 x 0.060 mm^3
Theta range for data collection	2.018 to 27.928°.
Index ranges	-16<=h<=16, -22<=k<=22, -20<=l<=21
Reflections collected	56013
Independent reflections	8427 [R(int) = 0.0500]
Completeness to theta = 25.242°	99.9 %
Absorption correction	Semi-empirical from equivalents
Max. and min. transmission	0.7456 and 0.7085
Refinement method	Full-matrix least-squares on F^2
Data / restraints / parameters	8427 / 0 / 438
Goodness-of-fit on F2	1.059
Final R indices [I>2sigma(I)]	R1 = 0.0375, wR2 = 0.0753
R indices (all data)	R1 = 0.0514, wR2 = 0.0819
Extinction coefficient	n/a
Largest diff. peak and hole	0.333 and -0.567 $e.Å^{-3}$

3.4 Molecular structure of diboratabutadiene hafnocene complex **3b** in the solid state

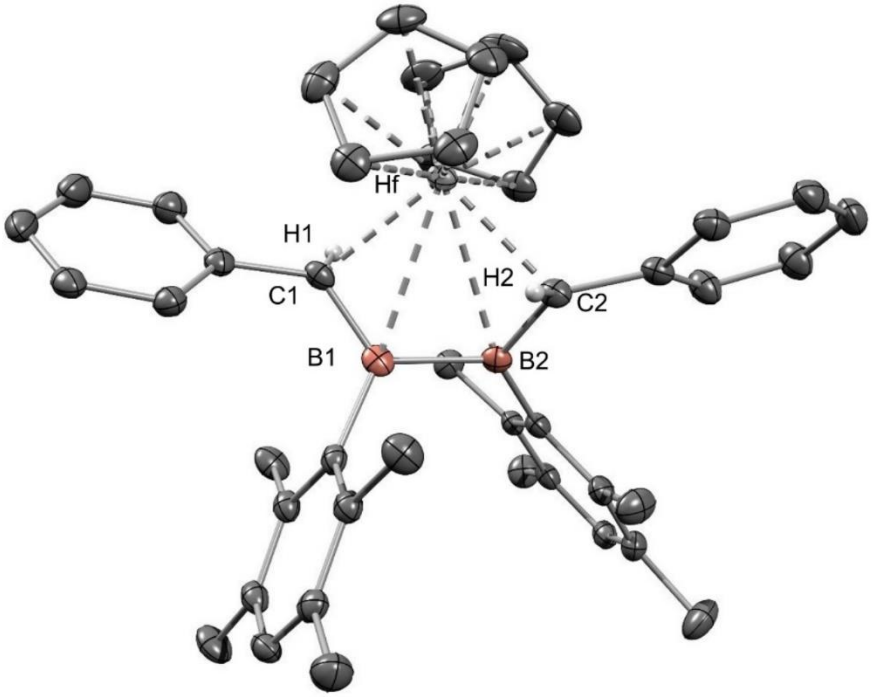

Refinement: All non H-atoms were located in the electron density maps and refined anisotropically. C-bound H atoms were placed in positions of optimized geometry and treated as riding atoms. Their isotropic displacement parameters were coupled to the corresponding carrier atoms by a factor of 1.2 (CH,) or 1.5 (CH3). The C1 and C2 bonded H-atoms were located in the electron density maps. Their positional parameters were refined using isotropic displacement parameters were set at 1.2 times the Ueq value of their parent atoms

Table S4. Crystal data and structure refinement for sh5568_a.

Identification code	sh5568_a	
CCDC number	2443038	
Empirical formula	C44 H48 B2 Hf	
Formula weight	776.93	
Temperature	130(2) K	
Wavelength	0.71073 Å	
Crystal system	Monoclinic	
Space group	$P2_1/c$	
Unit cell dimensions	a = 12.6404(4) Å	α= 90°.
	b = 16.7719(6) Å	β= 90.7550(10)°.
	c = 16.6054(5) Å	γ = 90°.
Volume	3520.1(2) $Å^3$	

Z	4
Density (calculated)	1.466 Mg/m^3
Absorption coefficient	2.994 mm^{-1}
F(000)	1576
Crystal size	0.300 x 0.180 x 0.080 mm^3
Theta range for data collection	2.018 to 27.877°.
Index ranges	-16<=h<=16, -22<=k<=22, -21<=l<=21
Reflections collected	78941
Independent reflections	8388 [R(int) = 0.0495]
Completeness to theta = 25.242°	100.0 %
Absorption correction	Semi-empirical from equivalents
Max. and min. transmission	0.7458 and 0.5688
Refinement method	Full-matrix least-squares on F^2
Data / restraints / parameters	8388 / 0 / 438
Goodness-of-fit on F^2	1.058
Final R indices [I>2sigma(I)]	R1 = 0.0158, wR2 = 0.0386
R indices (all data)	R1 = 0.0225, wR2 = 0.0400
Extinction coefficient	n/a
Largest diff. peak and hole	0.354 and -0.648 $e.Å^{-3}$

3.5 Molecular structure of methyleneborane *Z*-**4** in the solid state

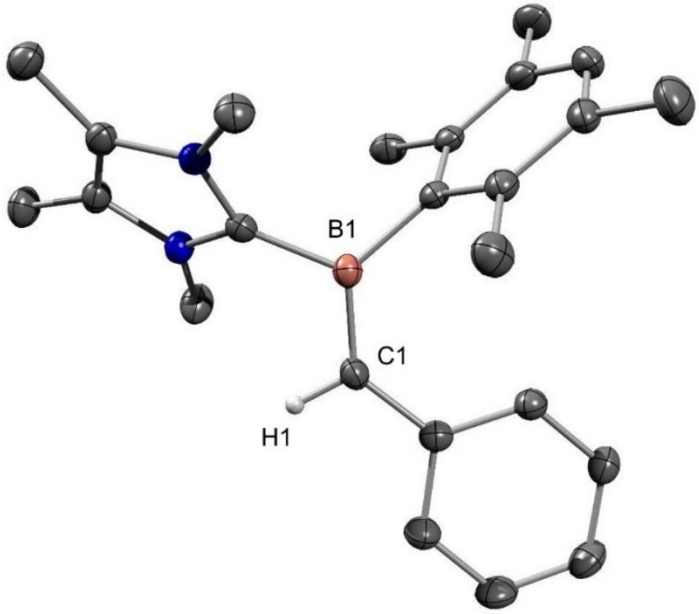

Refinement: All non H-atoms were located in the electron density maps and refined anisotropically. C-bound H atoms were placed in positions of optimized geometry and treated as riding atoms. Their isotropic displacement parameters were coupled to the corresponding carrier atoms by a factor of 1.2 (CH) or 1.5 (CH3).

Table S5. Crystal data and structure refinement for sh5744_a.

Identification code	sh5744_a	
CCDC number	2443039	
Empirical formula	C24 H31 B N2	
Formula weight	358.32	
Temperature	130(2) K	
Wavelength	0.71073 Å	
Crystal system	Monoclinic	
Space group	$P2_1/n$	
Unit cell dimensions	a = 10.8363(4) Å	α = 90°.
	b = 11.1238(3) Å	β = 103.550(4)°.
	c = 18.1882(6) Å	γ = 90°.
Volume	2131.40(13) Å^3	
Z	4	
Density (calculated)	1.117 Mg/m^3	
Absorption coefficient	0.064 mm^{-1}	
F(000)	776	
Crystal size	0.220 x 0.200 x 0.060 mm^3	

Theta range for data collection	2.304 to 27.121°.
Index ranges	-13<=h<=13, -14<=k<=13, -23<=l<=23
Reflections collected	20183
Independent reflections	4698 [R(int) = 0.0300]
Completeness to theta = 25.242°	99.9 %
Absorption correction	Semi-empirical from equivalents
Max. and min. transmission	1.0000 and 0.7795
Refinement method	Full-matrix least-squares on F^2
Data / restraints / parameters	4698 / 0 / 252
Goodness-of-fit on F2	1.056
Final R indices [I>2sigma(I)]	R1 = 0.0381, wR2 = 0.0980
R indices (all data)	R1 = 0.0459, wR2 = 0.1026
Extinction coefficient	n/a
Largest diff. peak and hole	0.263 and -0.177 e.$Å^{-3}$

3.6 Molecular structure of benzyl borane **6** in the solid state

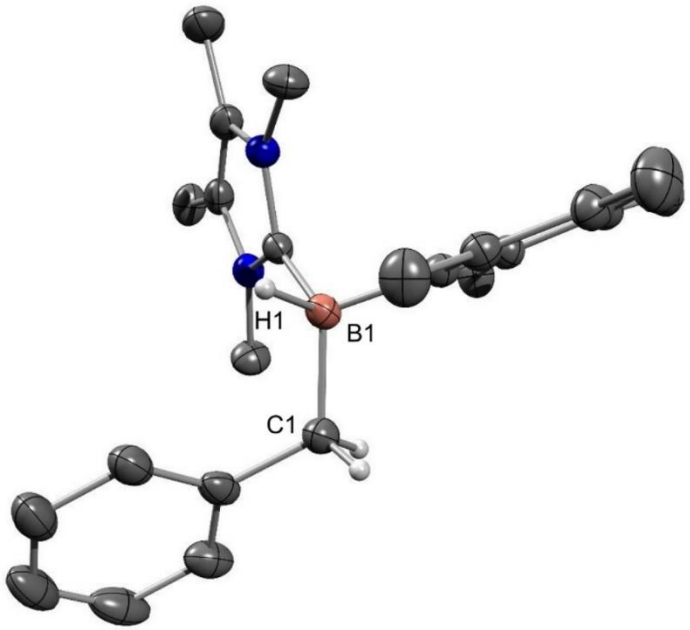

Refinement: All non H-atoms were located in the electron density maps and refined anisotropically. C-bound H atoms were placed in positions of optimized geometry and treated as riding atoms. Their isotropic displacement parameters were coupled to the corresponding carrier atoms by a factor of 1.2 (CH, CH2) or 1.5 (CH3). The B(1) bonded H1 atom was located in the electron density maps and its positional parameters were refined using isotropic displacement parameters which were set at 1.2 times the Ueq value of the boron atom.

Table S6. Crystal data and structure refinement for sh5820_a.

Identification code	sh5820_a	
CCDC number	2443043	
Empirical formula	C24 H33 B N2	
Formula weight	360.33	
Temperature	130(2) K	
Wavelength	0.71073 Å	
Crystal system	Monoclinic	
Space group	P21/c	
Unit cell dimensions	a = 10.2572(2) Å	α = 90°.
	b = 12.5465(3) Å	β = 97.321(2)°.
	c = 16.7754(4) Å	γ = 90°.
Volume	2141.26(8) Å^3	
Z	4	
Density (calculated)	1.118 Mg/m^3	
Absorption coefficient	0.064 mm^{-1}	

F(000)	784
Crystal size	0.300 x 0.240 x 0.080 mm^3
Theta range for data collection	2.448 to 27.898°.
Index ranges	-13<=h<=13, -16<=k<=16, -21<=l<=22
Reflections collected	37832
Independent reflections	5134 [R(int) = 0.0315]
Completeness to theta = 25.242°	99.9 %
Absorption correction	Semi-empirical from equivalents
Max. and min. transmission	1.0000 and 0.8196
Refinement method	Full-matrix least-squares on F^2
Data / restraints / parameters	5134 / 0 / 255
Goodness-of-fit on F2	1.065
Final R indices [I>2sigma(I)]	R1 = 0.0428, wR2 = 0.1187
R indices (all data)	R1 = 0.0507, wR2 = 0.1236
Extinction coefficient	n/a
Largest diff. peak and hole	0.282 and -0.191 e.$Å^{-3}$

4. Computational details

Computations were carried out with the Gaussian 16 program package.[65] Structural optimizations and frequency analyses were performed at the BP86/def2SVP level of theory[66-71] including the dispersion correction by Grimme.[72] The energies given are without thermal free energy correction. Single point calculations were run with the the Gaussian 16 program package at the B3LYP/def2TZVPP level of theory.[66-71] Pictures of Kohn-Sham orbitals were displayed with ChemCraft.[73]

4.1 Coordinates of optimized structures

Coordinates of diboratabutadiene 2_{opt}:

NImag = 0

−1849.5917158 Hartree

5	-0.469778000	0.767120000	-0.003189000
5	0.483338000	-0.693160000	-0.181028000
3	-1.812526000	-0.892461000	-0.884931000
3	1.774680000	0.985205000	0.746213000
6	-1.840857000	0.686985000	0.575712000
6	0.231556000	2.162503000	-0.379419000
6	1.877551000	-0.604735000	-0.701139000
6	-0.215914000	-2.091435000	0.187638000
1	-2.157967000	-0.288844000	1.014077000
6	-0.587735000	-3.002166000	-0.854788000
6	-0.214179000	-2.717844000	-2.296611000
8	-3.538161000	-1.227949000	-1.639698000
1	2.206245000	0.381411000	-1.110466000
6	0.615471000	3.070174000	0.661905000
8	3.307893000	1.112527000	1.873346000
6	-2.870169000	1.698504000	0.781123000
6	0.594742000	2.478144000	-1.725070000
6	2.937169000	-1.593430000	-0.857228000
6	-0.561536000	-2.421316000	1.534677000
6	-1.262292000	-4.216148000	-0.552879000
1	0.170185000	-1.685348000	-2.417092000
1	-1.060491000	-2.884061000	-2.996704000
1	0.611234000	-3.386728000	-2.624888000
6	-4.356581000	-0.050402000	-1.839653000

6	-4.247520000	-2.367470000	-1.115087000
6	1.326601000	4.262479000	0.360762000
6	0.238846000	2.796377000	2.105697000
6	4.540632000	1.265910000	1.139760000
6	3.387727000	0.236789000	3.014809000
6	-2.827559000	2.989209000	0.174924000
6	-4.009735000	1.416161000	1.592403000
6	1.305513000	3.667457000	-2.024836000
6	0.189209000	1.568419000	-2.861043000
6	4.161744000	-1.239738000	-1.499241000
6	2.845123000	-2.929645000	-0.364828000
6	-1.251531000	-3.622937000	1.833708000
6	-0.157676000	-1.513117000	2.672805000
6	-1.588443000	-4.497709000	0.784031000
6	-1.592707000	-5.209508000	-1.642141000
1	-4.656213000	0.374711000	-0.855747000
1	-5.277865000	-0.363676000	-2.383353000
6	-3.566934000	0.969880000	-2.637451000
1	-3.616025000	-3.244176000	-1.360362000
1	-5.206868000	-2.468492000	-1.673029000
6	-4.483074000	-2.293785000	0.389183000
6	1.656748000	4.536838000	-0.975892000
6	1.720694000	5.226973000	1.453907000
1	1.073906000	3.003111000	2.806715000
1	-0.114551000	1.754397000	2.242983000
1	-0.615036000	3.438425000	2.414395000
1	5.351802000	1.508123000	1.865731000
1	4.799336000	0.308231000	0.634588000
6	4.367951000	2.381347000	0.122871000
1	4.206274000	0.603271000	3.678370000
1	2.430136000	0.390166000	3.555304000
6	3.576104000	-1.232201000	2.656065000
1	-1.972130000	3.244155000	-0.467251000
6	-3.852431000	3.923512000	0.369984000
6	-5.035168000	2.352038000	1.786567000

1	-4.069671000	0.430249000	2.083961000
6	1.679784000	4.005631000	-3.448763000
1	-0.277385000	0.645404000	-2.469642000
1	1.057531000	1.261847000	-3.482061000
1	-0.535285000	2.065115000	-3.543136000
1	4.263982000	-0.217760000	-1.903660000
6	5.221408000	-2.147245000	-1.635472000
6	3.903484000	-3.836052000	-0.503128000
1	1.923277000	-3.244290000	0.144797000
6	-1.618640000	-3.968935000	3.257403000
1	0.314777000	-0.593559000	2.279686000
1	0.560113000	-2.014528000	3.358254000
1	-1.027385000	-1.200409000	3.288939000
1	-2.115380000	-5.438071000	1.020099000
1	-2.125920000	-6.091997000	-1.236253000
1	-0.673896000	-5.571386000	-2.152284000
1	-2.227859000	-4.765214000	-2.439881000
1	-2.668035000	1.294999000	-2.075598000
1	-4.187653000	1.871908000	-2.806471000
1	-3.256269000	0.559239000	-3.620019000
1	-5.078774000	-1.403044000	0.673236000
1	-3.517881000	-2.266633000	0.935693000
1	-5.030389000	-3.197327000	0.727958000
1	2.208715000	5.462911000	-1.211454000
1	0.836716000	5.590420000	2.020694000
1	2.247036000	6.110600000	1.041463000
1	2.392755000	4.749422000	2.200806000
1	4.120876000	3.342601000	0.614237000
1	3.558528000	2.158412000	-0.604539000
1	5.303787000	2.508723000	-0.457358000
1	4.541197000	-1.424330000	2.146582000
1	2.770809000	-1.582217000	1.981367000
1	3.554087000	-1.846131000	3.579943000
1	-3.783915000	4.909334000	-0.119174000
6	-4.968230000	3.617583000	1.174344000

1	-5.896767000	2.092959000	2.423939000
1	0.783054000	4.087787000	-4.100641000
1	2.320147000	3.218592000	-3.903217000
1	2.229929000	4.965754000	-3.506272000
1	6.149357000	-1.830437000	-2.139796000
6	5.104492000	-3.457717000	-1.135540000
1	3.793173000	-4.858266000	-0.104608000
1	-0.720700000	-4.032881000	3.909514000
1	-2.149416000	-4.939836000	3.315162000
1	-2.275058000	-3.194697000	3.711254000
1	-5.772859000	4.354963000	1.321194000
1	5.934722000	-4.173837000	-1.238346000

Coordinates of diboratabutadiene zirconium complex $3a_{opt}$:

NImag = 0

−1801.4810900 Hartree

40	-2.246344000	-0.000763000	-0.000142000
5	0.178111000	-0.884557000	-0.019539000
5	0.177533000	0.884576000	0.019576000
6	-0.835422000	-1.766690000	-0.714652000
1	-1.241242000	-1.392646000	-1.677050000
6	1.558187000	-1.333075000	0.644464000
6	1.903721000	-1.079179000	2.003398000
6	3.236774000	-1.252310000	2.453561000
6	4.221564000	-1.620773000	1.523602000
6	3.912219000	-1.896200000	0.181966000
6	2.566416000	-1.800167000	-0.255160000
6	2.272457000	-2.185706000	-1.685407000
1	1.206363000	-2.063350000	-1.938934000
1	2.869900000	-1.578041000	-2.396343000
1	2.543221000	-3.248576000	-1.865901000
6	5.007694000	-2.277981000	-0.783501000
1	4.832132000	-3.273616000	-1.244956000
1	5.069474000	-1.548421000	-1.620527000

6	3.610770000	-1.013623000	3.897923000
1	3.023322000	-1.653710000	4.590995000
1	3.419319000	0.037901000	4.208613000
6	0.861986000	-0.639329000	3.000675000
1	1.240166000	0.142827000	3.688890000
1	-0.020351000	-0.230434000	2.482691000
1	0.516678000	-1.483926000	3.638575000
6	1.557337000	1.334031000	-0.644438000
6	1.902916000	1.080423000	-2.003429000
6	3.235831000	1.254265000	-2.453663000
6	4.220497000	1.623225000	-1.523747000
1	5.267597000	1.713862000	-1.859995000
6	3.911083000	1.898462000	-0.182098000
6	2.565343000	1.801678000	0.255101000
6	2.271262000	2.187095000	1.685354000
1	2.541629000	3.250064000	1.865844000
1	1.205217000	2.064354000	1.938887000
1	2.868955000	1.579666000	2.396285000
6	5.006383000	2.280824000	0.783331000
1	5.068572000	1.551303000	1.620360000
1	5.993982000	2.307741000	0.281831000
1	4.830308000	3.276367000	1.244793000
6	3.609915000	1.015797000	-3.898045000
1	4.683768000	1.225023000	-4.073288000
1	3.419065000	-0.035850000	-4.208705000
1	3.022107000	1.655537000	-4.591121000
6	0.861296000	0.640261000	-3.000679000
1	-0.020665000	0.230577000	-2.482689000
1	0.515266000	1.484910000	-3.638121000
1	1.239830000	-0.141359000	-3.689300000
6	-0.836530000	1.766133000	0.714545000
1	-1.242235000	1.391693000	1.676853000
6	-1.001704000	3.221922000	0.606258000
6	-0.365648000	3.980968000	-0.410439000
1	0.321147000	3.471579000	-1.103033000

6	-0.582304000	5.361709000	-0.525543000
1	-0.073348000	5.924668000	-1.324511000
6	-1.436908000	6.031321000	0.369240000
1	-1.605751000	7.115272000	0.274497000
6	-2.070574000	5.298039000	1.389370000
1	-2.738239000	5.808045000	2.102457000
6	-1.855051000	3.917280000	1.503743000
1	-2.361204000	3.349237000	2.302851000
6	-2.611072000	0.227814000	-2.551313000
1	-2.017101000	-0.363233000	-3.259199000
6	-3.846424000	-0.178116000	-1.955564000
6	-4.323297000	0.922246000	-1.171049000
6	-3.350643000	1.953127000	-1.210142000
1	-3.389306000	2.913289000	-0.680323000
6	-2.290115000	1.524325000	-2.070855000
1	-1.401943000	2.117704000	-2.312759000
6	-2.288768000	-1.524964000	2.071451000
1	-1.400081000	-2.117351000	2.313869000
6	-2.611196000	-0.228578000	2.551262000
1	-2.017965000	0.363387000	3.259005000
6	-0.999577000	-3.222601000	-0.606204000
6	-0.363229000	-3.981047000	0.410757000
6	-1.852221000	-3.918703000	-1.503777000
6	-0.578928000	-5.361925000	0.526018000
6	-2.066791000	-5.299600000	-1.389252000
6	-1.432843000	-6.032282000	-0.368868000
1	0.323029000	-3.471075000	1.103453000
1	-2.358623000	-3.351145000	-2.303071000
1	-0.069762000	-5.924396000	1.325194000
1	-2.733937000	-5.810176000	-2.102413000
1	-1.600930000	-7.116337000	-0.274000000
1	5.995322000	-2.304372000	-0.282031000
1	5.268733000	-1.710866000	1.859783000
1	4.684741000	-1.222249000	4.073147000
1	-5.268217000	0.961085000	-0.617670000

1	-4.369181000	-1.126845000	-2.132480000
6	-3.348653000	-1.955270000	1.210716000
6	-3.846788000	0.175823000	1.955020000
6	-4.322346000	-0.925409000	1.170899000
1	-3.386270000	-2.915730000	0.681367000
1	-5.267084000	-0.965488000	0.617298000
1	-4.370585000	1.124078000	2.131394000

Coordinates of diboratabutadiene hafnocene complex $3b_{opt}$:

NImag = 0

−1802.4473226 Hartree

72	2.061638000	-0.000516000	-0.000238000
6	0.655508000	1.756853000	-0.708609000
6	0.654322000	-1.756677000	0.708785000
6	2.436261000	0.232194000	2.548195000
6	2.117832000	1.532540000	2.076264000
6	3.177556000	1.963497000	1.215914000
6	4.148513000	0.931175000	1.169102000
6	3.670892000	-0.173312000	1.947603000
6	3.670331000	0.170489000	-1.948671000
6	4.147566000	-0.934099000	-1.170077000
6	3.175892000	-1.965768000	-1.216130000
6	2.116063000	-1.534352000	-2.076126000
6	2.435141000	-0.234355000	-2.548583000
5	-0.368457000	0.882509000	-0.015823000
5	-0.369148000	-0.881879000	0.015709000
1	1.047099000	1.379110000	-1.676682000
6	0.821678000	3.214645000	-0.611098000
1	1.045642000	-1.379028000	1.676939000
6	0.819604000	-3.214597000	0.611574000
1	1.844211000	-0.360288000	3.256510000
1	1.229830000	2.124884000	2.321231000
1	3.216312000	2.925453000	0.689316000
1	5.090999000	0.970374000	0.611543000

1	4.194248000	-1.122226000	2.121881000
1	4.194270000	1.118987000	-2.123481000
1	5.090288000	-0.973752000	-0.612947000
1	3.214225000	-2.927581000	-0.689240000
1	1.227557000	-2.126186000	-2.320499000
1	1.843139000	0.358332000	-3.256766000
6	-1.745040000	1.339331000	0.649209000
6	-1.745974000	-1.338075000	-0.649197000
6	0.190478000	3.979302000	0.403829000
6	1.671334000	3.903743000	-1.516283000
6	1.668915000	-3.903996000	1.516858000
6	0.187884000	-3.979123000	-0.403127000
6	-2.753001000	1.804158000	-0.251462000
6	-2.089881000	1.090947000	2.009095000
6	-2.754079000	-1.802560000	0.251491000
6	-2.090754000	-1.089607000	-2.009087000
1	-0.493763000	3.474106000	1.102011000
6	0.409030000	5.360482000	0.510674000
6	1.888498000	5.285073000	-1.410605000
1	2.173263000	3.331095000	-2.314766000
1	2.171243000	-3.331468000	2.315170000
6	1.885277000	-5.285473000	1.411468000
6	0.405638000	-5.360452000	-0.509692000
1	-0.496154000	-3.473700000	-1.101346000
6	-4.098291000	1.904836000	0.186334000
6	-2.459062000	2.180808000	-1.684261000
6	-3.422303000	1.267492000	2.459672000
6	-1.047329000	0.652529000	3.006345000
6	-4.099392000	-1.902909000	-0.186314000
6	-2.460252000	-2.179192000	1.684322000
6	-3.423220000	-1.265817000	-2.459667000
6	-1.048099000	-0.651409000	-3.006326000
1	-0.095854000	5.928310000	1.308760000
6	1.260235000	6.024306000	-0.391597000
1	2.553312000	5.790571000	-2.129517000

1	2.549843000	-5.791198000	2.130450000
6	1.256527000	-6.024569000	0.392658000
1	-0.099642000	-5.928163000	-1.307612000
6	-4.407080000	1.635259000	1.529281000
6	-5.193669000	2.284782000	-0.780018000
1	-1.393334000	2.055916000	-1.937844000
1	-2.728634000	3.242808000	-1.871464000
1	-3.057304000	1.569110000	-2.391106000
6	-3.795815000	1.033139000	3.904899000
1	-0.697576000	1.498687000	3.639702000
1	-0.167219000	0.238220000	2.488195000
1	-1.426072000	-0.125697000	3.698748000
6	-4.408097000	-1.633327000	-1.529279000
6	-5.194871000	-2.282534000	0.780049000
1	-3.058394000	-1.567337000	2.391115000
1	-1.394510000	-2.054461000	1.937928000
1	-2.730021000	-3.241128000	1.871584000
6	-3.796651000	-1.031359000	-3.904898000
1	-0.167885000	-0.237369000	-2.488134000
1	-1.426649000	0.126973000	-3.698659000
1	-0.698590000	-1.497610000	-3.639757000
1	1.430490000	7.108600000	-0.303502000
1	1.426161000	-7.108978000	0.304786000
1	-5.453747000	1.728895000	1.866064000
1	-5.257995000	1.551606000	-1.613673000
1	-5.016068000	3.277885000	-1.246169000
1	-6.180817000	2.315913000	-0.277864000
1	-3.606548000	-0.018130000	4.217818000
1	-4.869224000	1.244490000	4.080344000
1	-3.206572000	1.673554000	4.596143000
1	-5.454781000	-1.726730000	-1.866072000
1	-5.017541000	-3.275684000	1.246207000
1	-6.182030000	-2.313397000	0.277900000
1	-5.258990000	-1.549340000	1.613701000
1	-4.870088000	-1.242530000	-4.080391000

1	-3.207487000	-1.671839000	-4.596146000
1	-3.607204000	0.019893000	-4.217765000

4.2 TD-DFT calculations

Excitation energies and oscillator strengths of diboratabutadiene 2_{opt} in diethylether:

171: HOMO, 172: LUMO

Excited State 1: Singlet-A 2.8530 eV 434.58 nm f=1.1357 <S**2>=0.000

171 -> 172 0.69463

This state for optimization and/or second-order correction.

Total Energy, E(CIS/TDA) = -1851.31648941

Copying the excited state density for this state as the 1-particle RhoCI density.

Excited State 2: Singlet-A 3.3703 eV 367.88 nm f=0.0054 <S**2>=0.000

171 -> 173 0.69517

Excited State 3: Singlet-A 3.4318 eV 361.28 nm f=0.0149 <S**2>=0.000

170 -> 172 -0.12848

171 -> 174 0.68056

Excited State 4: Singlet-A 3.4919 eV 355.06 nm f=0.0200 <S**2>=0.000

170 -> 172 0.44440

171 -> 175 -0.41668

171 -> 176 0.30806

Excited State 5: Singlet-A 3.5134 eV 352.89 nm f=0.0908 <S**2>=0.000

169 -> 172 0.16164

170 -> 172 0.31422

171 -> 174 0.14120

171 -> 175 0.53017

171 -> 176 0.23448

Excited State 6: Singlet-A 3.5866 eV 345.68 nm f=0.0009 <S**2>=0.000

169 -> 172 0.11921
170 -> 172 -0.36138
171 -> 176 0.55050
171 -> 180 0.15741

Excited State 7: Singlet-A 3.6384 eV 340.76 nm f=0.1335 <S**2>=0.000
169 -> 172 0.66499
171 -> 175 -0.16242
171 -> 176 -0.12948

Excited State 8: Singlet-A 3.7333 eV 332.10 nm f=0.0062 <S**2>=0.000
171 -> 177 0.68110

Excited State 9: Singlet-A 3.7498 eV 330.65 nm f=0.0675 <S**2>=0.000
171 -> 178 0.67901

Excited State 10: Singlet-A 4.0048 eV 309.59 nm f=0.0005 <S**2>=0.000
171 -> 179 0.69080
171 -> 180 0.12142

Excited State 11: Singlet-A 4.1325 eV 300.02 nm f=0.0029 <S**2>=0.000
170 -> 173 0.66714
171 -> 180 -0.14401

Excited State 12: Singlet-A 4.1719 eV 297.19 nm f=0.0017 <S**2>=0.000
168 -> 172 -0.21138
170 -> 173 -0.14507
170 -> 174 0.48425
170 -> 175 -0.18316
171 -> 180 -0.37477

Excited State 13: Singlet-A 4.2046 eV 294.88 nm f=0.0013 <S**2>=0.000
168 -> 172 -0.17965
170 -> 174 0.39681
170 -> 175 0.21879
171 -> 180 0.42962
171 -> 181 -0.14948

Excited State 14: Singlet-A 4.2296 eV 293.14 nm f=0.0116 <S**2>=0.000
171 -> 181 0.68323

Excited State 15: Singlet-A 4.2346 eV 292.79 nm f=0.0029 <S**2>=0.000
168 -> 172 0.62400
169 -> 174 -0.10366
170 -> 174 0.27539

Excited State 16: Singlet-A 4.2761 eV 289.95 nm f=0.0006 <S**2>=0.000
167 -> 172 0.62363
169 -> 173 0.14468
170 -> 175 -0.22554

Excited State 17: Singlet-A 4.3023 eV 288.18 nm f=0.0209 <S**2>=0.000
167 -> 172 0.25790
170 -> 175 0.51573
170 -> 176 -0.28737
171 -> 180 -0.17356

Excited State 18: Singlet-A 4.3308 eV 286.28 nm f=0.0310 <S**2>=0.000
169 -> 176 -0.10459
170 -> 175 0.22320
170 -> 176 0.60587
171 -> 180 -0.11720

Excited State 19: Singlet-A 4.4791 eV 276.80 nm f=0.0004 <S**2>=0.000

171 -> 182 0.69201

Excited State 20: Singlet-A 4.5061 eV 275.15 nm f=0.0017 <S**2>=0.000

164 -> 172 0.17512

165 -> 172 -0.13664

166 -> 172 -0.12484

170 -> 177 0.51059

170 -> 178 0.37503

171 -> 178 0.12857

Excitation energies and oscillator strengths of diboratabutadiene zirconium complex $3a_{opt}$ in toluene:

167: HOMO, 168: LUMO

Excited State 1: Singlet-A 2.7994 eV 442.90 nm f=0.0943 <S**2>=0.000

166 -> 168 -0.25204

167 -> 169 0.64274

167 -> 170 0.11388

This state for optimization and/or second-order correction.

Total Energy, E(CIS/TDA) = -1802.96177518

Copying the excited state density for this state as the 1-particle RhoCI density.

Excited State 2: Singlet-A 2.8742 eV 431.37 nm f=0.0836 <S**2>=0.000

166 -> 169 0.21847

167 -> 168 0.65351

Excited State 3: Singlet-A 2.9644 eV 418.24 nm f=0.0703 <S**2>=0.000

166 -> 168 0.65068

167 -> 169 0.24051

Excited State 4: Singlet-A 3.1615 eV 392.17 nm f=0.0208 <S**2>=0.000

166 -> 169 0.64806

167 -> 168 -0.21460

Excited State 5: Singlet-A 3.4329 eV 361.16 nm f=0.0061 <S**2>=0.000

165 -> 168 0.69186

Excited State 6: Singlet-A 3.4381 eV 360.62 nm f=0.0044 <S**2>=0.000

163 -> 169 0.26082

164 -> 168 0.20933

165 -> 169 0.61700

Excited State 7: Singlet-A 3.4972 eV 354.53 nm f=0.0097 <S**2>=0.000
164 -> 168 0.66871
165 -> 169 -0.18838

Excited State 8: Singlet-A 3.5218 eV 352.05 nm f=0.0042 <S**2>=0.000
163 -> 168 -0.32228
164 -> 169 0.61643

Excited State 9: Singlet-A 3.5505 eV 349.21 nm f=0.0005 <S**2>=0.000
163 -> 169 0.64581
165 -> 169 -0.27918

Excited State 10: Singlet-A 3.5580 eV 348.47 nm f=0.0245 <S**2>=0.000
163 -> 168 0.61741
164 -> 169 0.32404

Excited State 11: Singlet-A 3.6218 eV 342.33 nm f=0.0006 <S**2>=0.000
162 -> 169 0.67118
164 -> 169 0.11049
167 -> 170 -0.14102

Excited State 12: Singlet-A 3.6564 eV 339.09 nm f=0.1724 <S**2>=0.000
162 -> 168 0.68365

Excited State 13: Singlet-A 3.8045 eV 325.89 nm f=0.4206 <S**2>=0.000
162 -> 169 0.13560
167 -> 169 -0.12817
167 -> 170 0.66194

Excited State 14: Singlet-A 4.0539 eV 305.84 nm f=0.0272 <S**2>=0.000
166 -> 170 0.62844

167 -> 171 0.26052

Excited State 15: Singlet-A 4.1040 eV 302.10 nm f=0.0323 <S**2>=0.000
159 -> 168 -0.10719
161 -> 168 0.67803

Excited State 16: Singlet-A 4.1979 eV 295.35 nm f=0.0019 <S**2>=0.000
159 -> 169 -0.17135
161 -> 169 0.24625
166 -> 170 -0.11792
167 -> 171 0.43780
167 -> 173 0.27353
167 -> 175 0.30064

Excited State 17: Singlet-A 4.2872 eV 289.20 nm f=0.0603 <S**2>=0.000
160 -> 169 0.31109
166 -> 171 -0.23042
166 -> 173 -0.19826
167 -> 172 0.52694

Excited State 18: Singlet-A 4.3144 eV 287.37 nm f=0.0638 <S**2>=0.000
157 -> 169 -0.10921
159 -> 169 0.18809
161 -> 169 0.54695
166 -> 170 0.11772
166 -> 172 0.11328
167 -> 171 -0.12268
167 -> 173 -0.23880
167 -> 175 0.14030

Excited State 19: Singlet-A 4.3160 eV 287.27 nm f=0.0137 <S**2>=0.000

156 -> 168 -0.10259
161 -> 169 -0.14609
166 -> 170 0.14908
167 -> 171 -0.34908
167 -> 173 0.30983
167 -> 175 0.40910

Excited State 20: Singlet-A 4.3868 eV 282.63 nm f=0.0100 <S**2>=0.000
157 -> 168 -0.29750
158 -> 169 0.11741
159 -> 168 0.29176
160 -> 169 -0.13464
166 -> 171 0.13600
166 -> 175 -0.11549
167 -> 172 0.12969
167 -> 174 0.44487
167 -> 177 0.12207

Excitation energies and oscillator strengths of diboratabutadiene hafnocene complex 3b$_{opt}$ in toluene:

167: HOMO, 168: LUMO

Excited State 1: Singlet-A 2.9743 eV 416.85 nm f=0.1750 <S**2>=0.000

166 -> 169 0.19368

167 -> 168 0.66370

167 -> 170 -0.10023

This state for optimization and/or second-order correction.

Total Energy, E(CIS/TDA) = -1803.91385042

Copying the excited state density for this state as the 1-particle RhoCI density.

Excited State 2: Singlet-A 3.0719 eV 403.61 nm f=0.0840 <S**2>=0.000

166 -> 168 -0.29940

167 -> 169 0.62507

Excited State 3: Singlet-A 3.1493 eV 393.69 nm f=0.0523 <S**2>=0.000

166 -> 169 0.67102

167 -> 168 -0.18721

Excited State 4: Singlet-A 3.3026 eV 375.41 nm f=0.0545 <S**2>=0.000

166 -> 168 0.61789

167 -> 169 0.29576

Excited State 5: Singlet-A 3.4977 eV 354.48 nm f=0.0040 <S**2>=0.000

163 -> 168 0.26861

165 -> 168 0.63948

Excited State 6: Singlet-A 3.5835 eV 345.98 nm f=0.0118 <S**2>=0.000

162 -> 168 0.16995

164 -> 168 0.13018

165 -> 169 0.66371

Excited State 7: Singlet-A 3.5867 eV 345.68 nm f=0.0009 <S**2>=0.000

162 -> 168 -0.17485
163 -> 169 -0.11162
164 -> 168 0.66907

Excited State 8: Singlet-A 3.6070 eV 343.73 nm f=0.0013 <S**2>=0.000
163 -> 168 0.64961
165 -> 168 -0.26474

Excited State 9: Singlet-A 3.6561 eV 339.12 nm f=0.0103 <S**2>=0.000
164 -> 169 0.69015
165 -> 168 -0.10825

Excited State 10: Singlet-A 3.6799 eV 336.92 nm f=0.0140 <S**2>=0.000
162 -> 168 0.64476
164 -> 168 0.15713
165 -> 169 -0.20365

Excited State 11: Singlet-A 3.7154 eV 333.70 nm f=0.0283 <S**2>=0.000
163 -> 169 0.68921

Excited State 12: Singlet-A 3.7951 eV 326.69 nm f=0.1659 <S**2>=0.000
162 -> 169 0.68601

Excited State 13: Singlet-A 3.9665 eV 312.58 nm f=0.3275 <S**2>=0.000
167 -> 168 0.10654
167 -> 170 0.68003

Excited State 14: Singlet-A 4.1748 eV 296.98 nm f=0.0355 <S**2>=0.000
161 -> 168 0.10384
166 -> 170 0.62092
167 -> 171 -0.27816

Excited State 15: Singlet-A 4.2653 eV 290.68 nm f=0.0223 <S**2>=0.000

161 -> 169 0.68275

Excited State 16: Singlet-A 4.2990 eV 288.40 nm f=0.0000 <S**2>=0.000
159 -> 168 0.22870
161 -> 168 0.25996
166 -> 170 0.20429
166 -> 172 -0.16617
167 -> 171 0.51012
167 -> 173 -0.15097

Excited State 17: Singlet-A 4.3391 eV 285.74 nm f=0.0888 <S**2>=0.000
160 -> 168 0.32030
166 -> 171 -0.29817
166 -> 173 0.17341
167 -> 172 0.49376

Excited State 18: Singlet-A 4.3799 eV 283.08 nm f=0.0860 <S**2>=0.000
159 -> 168 -0.14508
161 -> 168 0.59468
166 -> 170 -0.14113
166 -> 172 0.10535
167 -> 173 0.23943

Excited State 19: Singlet-A 4.4544 eV 278.34 nm f=0.0030 <S**2>=0.000
157 -> 168 -0.13813
159 -> 168 -0.24808
161 -> 168 -0.16453
166 -> 170 0.14138
166 -> 172 0.27251
167 -> 171 0.33284
167 -> 173 0.36292
167 -> 175 0.11736

Excited State 20: Singlet-A 4.5032 eV 275.32 nm f=0.1458 <S**2>=0.000

158 -> 168 0.13236

160 -> 168 0.11007

166 -> 171 0.58741

166 -> 173 0.15606

167 -> 172 0.25045

4.3 Molecular orbitals

Selected frontier orbitals of diboratabutadiene complex $3a_{opt}$:

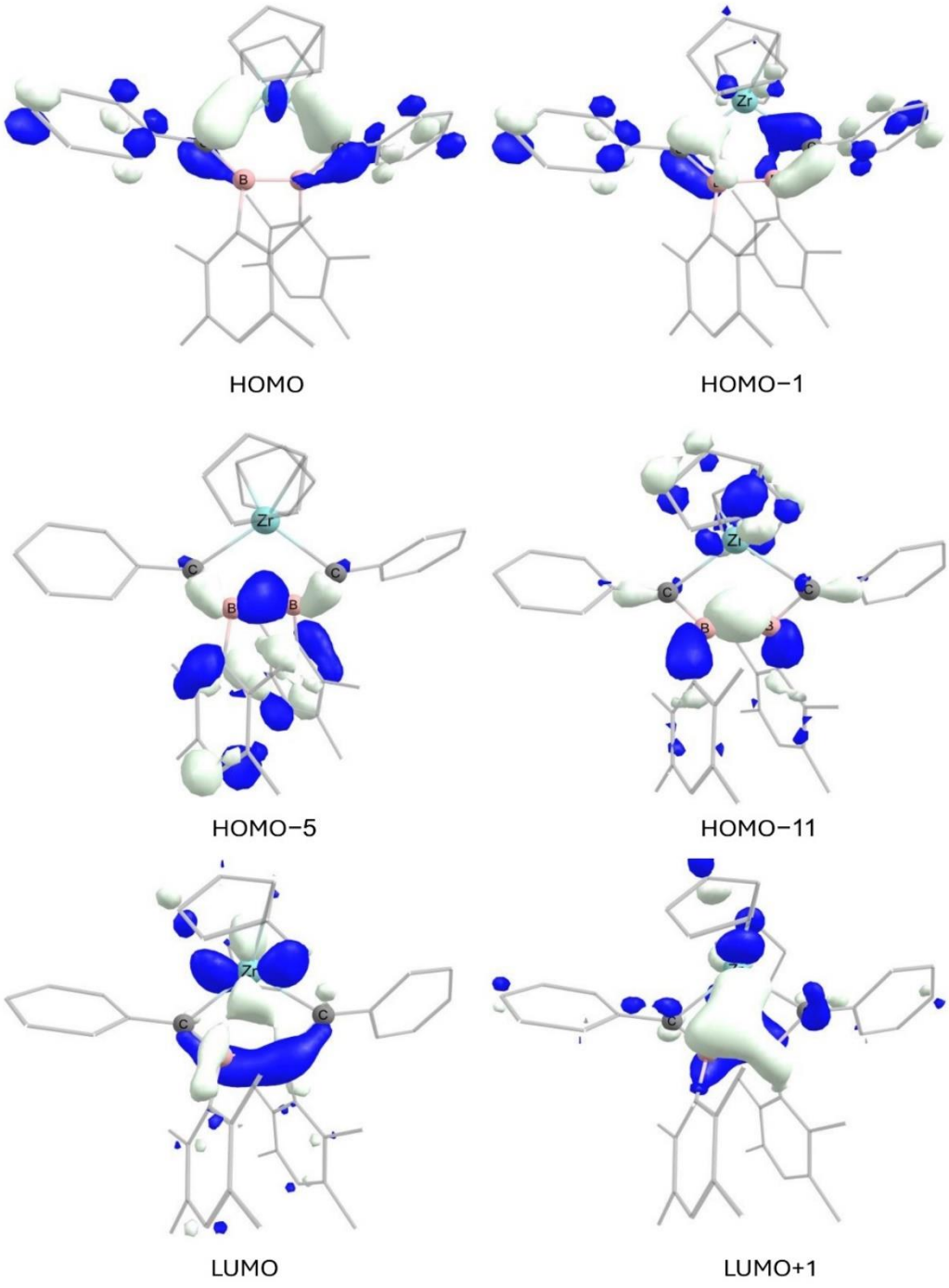

Selected frontier orbitals of diboratabutadiene hafnocene complex $3b_{opt}$:

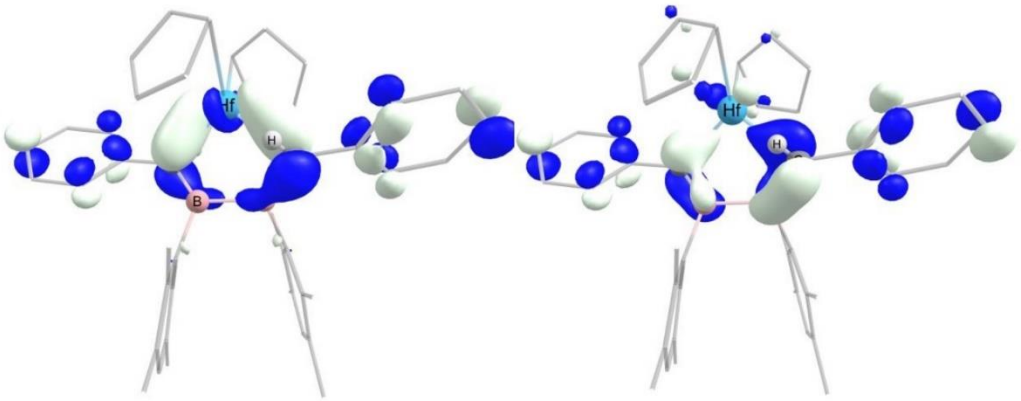

HOMO

HOMO−1

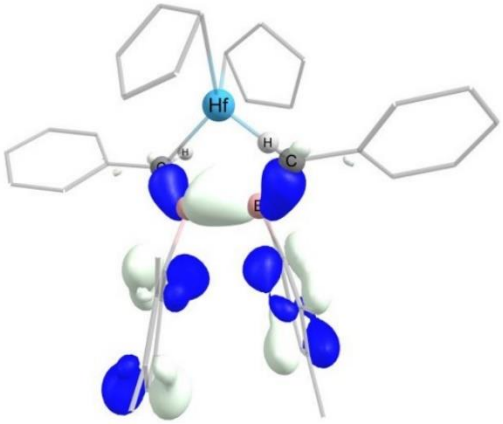

HOMO−5

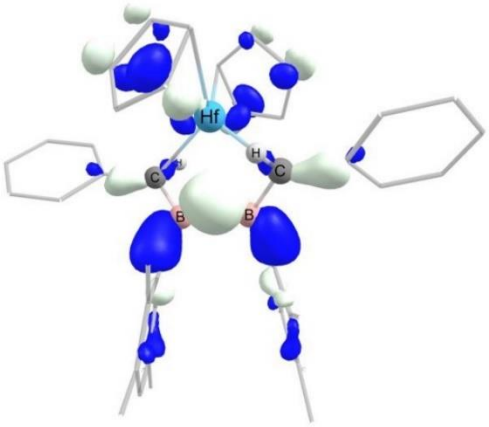

HOMO−11

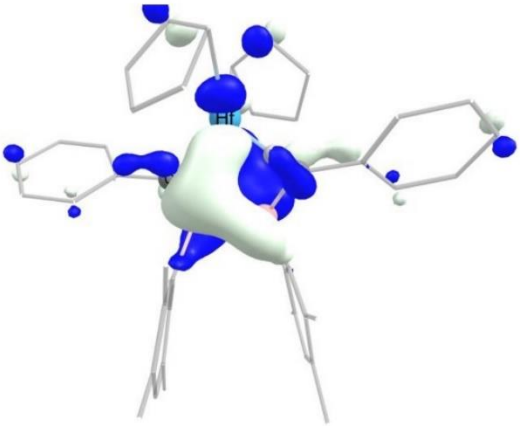

LUMO

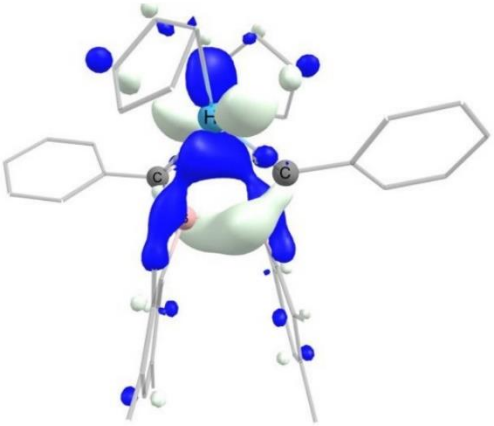

LUMO+1

References

[61] G. R. Fulmer, A. J. M. Miller, N. H. Sherden, H. E. Gottlieb, A. Nudelman, B. M. Stoltz, J. E. Bercaw, K. I. Goldberg, *Organometallics* **2010**, *29*, 2176 – 2179.

[62] G. M. Sheldrick, *Acta Cryst.* **2015**, *A71*, 3 − 8.

[63] G. M. Sheldrick, *Acta Cryst.* **2015**, *C71*, 3 − 8.

[64] C. B. Hübschle, G. M. Sheldrick, B. Dittrich, *J. Appl. Crystallogr.* **2011**, *44,* 28 − 28 .

[65] Gaussian 09, Revision A.02, M. J. Frisch, G. W. Trucks, H. B. Schlegel, G. E. Scuseria, M. A. Robb, J. R. Cheeseman, G. Scalmani, V. Barone, G. A. Petersson, H. Nakatsuji, X. Li, M. Caricato, A. Marenich, J. Bloino, B. G. Janesko, R. Gomperts, B. Mennucci, H. P. Hratchian, J. V. Ortiz, A. F. Izmaylov, J. L. Sonnenberg, D. Williams-Young, F. Ding, F. Lipparini, F. Egidi, J. Goings, B. Peng, A. Petrone, T. Henderson, D. Ranasinghe, V. G. Zakrzewski, J. Gao, N. Rega, G. Zheng, W. Liang, M. Hada, M. Ehara, K. Toyota, R. Fukuda, J. Hasegawa, Ishida, M. T. Nakajima, Y. Honda, O. Kitao, H. Nakai, T. Vreven, K. Throssell, J. A. Montgomery Jr, J. E. Peralta, F. Ogliaro, M. Bearpark, J. J. Heyd, E. Brothers, K. N. Kudin, V. N. Staroverov, T. Keith, R. Kobayashi, J. Normand, K. Raghavachari, A. Rendell, J. C. Burant, S. S. Iyengar, J. Tomasi, M. Cossi, J. M. Millam, M. Klene, C. Adamo, R. Cammi, J. W. Ochterski, R. L. Martin, K. Morokuma, O. Farkas, J. B. Foresman, D. J. Fox, Gaussian, Inc., Wallingford CT, **2016**.

[66] J. P. Perdew, *Phys. Rev. B* **1986**, *33*, 8822 – 8824.

[67] A. D. Becke, *Phys. Rev. A* **1988**, *38*, 3098 – 3100.

[68] A. Schäfer, H. Horn, R. Ahlrichs, *J. Chem. Phys.* **1992**, *97*, 2571 – 2577.

[69] A. Schäfer, C. Huber, R. Ahlrichs, *J. Chem. Phys.* **1994**, *100*, 5829 – 5835.

[70] F. Weigend, R. Ahlrichs, *Phys. Chem. Chem. Phys.* **2005**, *7*, 3297 – 3305.

[71] F. Weigend, *Phys. Chem. Chem. Phys.* **2006**, *8*, 1057 – 1065.

[72] S. Grimme, J. Antony, S. Ehrlich, H. Krieg, *J. Chem. Phys.* **2010**, *132*, 154104.

[73] Chemcraft - graphical software for visualization of quantum chemistry computations. https://www.chemcraftprog.com

6 Literature

[1] a) V. E. Viola, G. J. Mathews, *Sci. Am.* **1987**, *256*, 38 – 45; b) D. K. Duncan, F. Primas, L. M. Rebull, A. M. Boesgaard, C. P. Deliyannis, L. M. Hobbs, J. R. King, S. G. Ryan, *Astrophys. J.* **1997**, *488*, 338 – 349.

[2] A. A. Yaroshevsky, *Geochem. Int.* **2006***, 44,* 48 – 55.

[3] W. G. Woods, Environ. Health Perspect. **1994**, *102*, 5 – 11.

[4] J. L. Gay-Lussac, L. J. Thenard, *Ann. Chim.* **1808**, *68*, 169 – 174.

[5] H. Davy, *Phil. Trans. R. Soc. Lond.* **1808**, *98*, 333 – 370.

[6] H. Moissan, *Ann. Chim. Phys.* **1895**, *6*, 296 – 320.

[7] G. Liu, X. Meng, H. Zhang, G. Zhao, H. Pang, T. Wang, P. Li, T. Kako, J. Ye, *Angew. Chem. Int. Ed.* **2017**, *56*, 5570 – 5574; b) X. Xie, M. F. Haddow, S. M. Mansell, N. C. Norman, C. A. Russell, *Chem. Commun.* **2011**, *47*, 3748 – 3750.

[8] R. A. Smith, *J. Non-Cryst. Solids* **1986**, *84*, 421 – 432.

[9] M. Hubert, A. J. Faber, *Phys. Chem. Glasses: Eur. J. Glass Sci. Technol. B* **2014**, *55*, 136 – 158.

[10] K. K. Shen in *Polymer Green Flame Retardants* (Eds.: C. D. Papaspyrides, P. Kiliaris) Elsevir, **2014**, *pp.* 367 – 388.

[11] J. Hong, S. Mutalik, P. P. Pescarmona, L. Protesescu, *Chem. Mater.* **2024**, *36*, 2147 – 2164.

[12] M. M. Balakrishnnarajan, P. D. Pancharatan, R. Hoffmann, *New J. Chem.* **2007**, *31*, 473 – 485.

[13] M. Hooper, *Tenside Surfactants Deterg.* **1996**, *33*, 366 – 373.

[14] a) F. Degryse, *Boron* **2017**, *2*, 111 – 122; b) P. H. Brown, N. Bellaloui, M. A. Wimmer, E. S. Bassil, J. Ruiz, H. Hu, H. Pfeffer, F. Dannel, V. Römheld, *Plant Biol.* **2002**, *4*, 205 – 223.

[15] I. B. Sivaev, *Molecules* **2023**, *28*, 6287.

[16] A. Suzuki, *Angew. Chem. Int. Ed.* **2011**, *50*, 6722 – 6737.

[17] H. C. Brown, *H. C. Brown, Nobel Lecture*, **1979**.

[18] L. Xu, G. Wang, S. Zhang, H. Wang, L. Wang, L. Liu, J. Jiao, P. Li, *Tetrahedron* **2017**, *73*, 7123 – 7157.

[19] D. O. Zharkov, A. V Yudinka, T. Riesebeck, P. S. Loshchenova, E. A. Mostovich, G. L. Dianov, *Am. J. Cancer Res.* **2021**, *11*, 4668 – 4682.

[20] a) R. J. Grams, W. L. Santos, I. R. Scorei, A. Abad-Garcia, C. A. Rosenblum, A. Bita, H. Cerecetto, C. Vinas, M. A. Soriano-Ursua, *Chem. Rev.* **2024**, *124*, 2441 – 2511; b) S. Song, P. Gao, L. Sun, D. Kang, J. Kongsted, V. Poongavanam, P. Zhang, X. Liu, *Acta Pharm. Sin. B* **2021**, *11*, 3035 – 3059; c) P. Stockmann, M. Gozzi, R. Kuhnert, M. B. Sarosi, E. Hey-Hawkins, *Chem. Soc. Rev.* **2019**, *48*, 3497 – 3512; d) J. P. M. Antonio, R. Russo, C. P. Carvalho, P. M. S. D. Cal, P. M. P. Gois, *Chem. Soc. Rev.* **2019**, *13*, 3513 – 3536.

[21] a) M. J. D. Bosdet, W. E. Piers, *Can. J. Chem.* **2009**, *87*, 8 – 29; b) C. R. McConell, S.-Y. Liu, *Chem. Soc. Rev.* **2019**, *48*, 3436 – 3453; c) M. M. Lorenzo-García, D. Bonifazi, *Chimia (Aarau).* **2017**, *71*, 550 – 557; d) K. Sethia, I. Roy, *Handbook of Boron Nanostructures,* Pan Stanford Publishing, Danvers, **2016**, pp. 101 – 121.

[22] S. Yamaguchi, K. Tamao, *Chem. Lett.* **2005**, *34*, 2 – 7.

[23] Z. Huang, S. Wang, R. D. Dewhurst, N. V. Ignat'ev, M. Finze, H. Braunschweig, *Angew. Chem. Int. Ed.* **2020**, *59*, 8800 – 8816.

[24] M.-A. Legare, C. Pranckevicius, H. Braunschweig, *Chem. Rev.* **2019**, *119*, 8231 – 8261.

[25] B. J. Graham, R. T. Raines, *J. Org. Chem.* **2024**, *89*, 2069 – 2089.

[26] Y. Su, R. Kinjo, *Chem. Soc. Rev.* **2019**, *13*, 3613 – 3659.

[27] W. Siebert, *Adv. Organomet. Chem.* **1980**, *18*, 301 – 340.

[28] P. Laszlo, *Angew. Chem. Int. Ed.* **2000**, 39, 2071 – 2072.

[29] a) L. Pauling, The Nature of the Chemical Bond, Cornell UniversityPress, Ithaca, **1945**, p. 259; b) L. Pauling, *J. Am. Chem. Soc.* **1931**, *53*, 3225 – 3237; c) S. H. Bauer, *J. Am. Chem. Soc.* **1937**, *59*, 1096 – 1103; d) S. H. Bauer, *Chem. Rev.* **1942**, *31*, 46 – 75.

[30] H. C. Longuet-Higgins, R. P. Bell, *J. Chem. Soc.* **1943**, 250 - 255.

[31] a) W. N. Lipscomb, *Science.* **1977**, *196*, 1047 – 1055; b) W. N. Lipscomb, *Angew. Chem.* **1977**, *89*, 685 – 696.

[32] a) M. Arrowsmith, H. Braunschweig, T. E. Stennett, *Angew. Chem. Int. Ed.* **2016**, *56*, 96 – 115. b) H. Braunschweig, R. D. Dewhurst, S. Mozo, *ChemCatChem* **2015**, *7*, 1630 – 1638; c) P. D. Pancharatna, S. H. Dar, U. D. Chowdhury, M. M. Balakrishnarajan, *J. Phys. Chem. A* **2022**, *116*, 3219 – 3228; d) E. Osorio, J. K. Olson, W. Tiznado, A. I. Boldyrev, *Chem. Eur. J.* **2012**, *18*, 9677 – 9681; e) H.

Braunschweig, R. D. Dewhurst, **2013**, *52*, 3574 – 3583.

[33] a) E. C. Neeve, S. J. Geier, I. A. I. Mkhalid, S. A. Westcott, T. B. Marder, *Chem. Rev.* **2016**, *116*, 9091 – 9161; b) J. Hartwig, *Chem. Soc. Rev.* **2011**, *40*, 1992 – 2002; c) I. A. I. Mkhalid, J. H. Barnard, T. B. Marder, J. M. Murphy, J. F. Hartwig, *Chem. Rev.* **2010**, *110*, 890 – 931.

[34] a) B. Su, R. Kinjo, *Synthesis* **2017**, *49*, 2985 – 3034; b) B. J. Wang, M. P. Groziak, *Adv. Heterocycl. Chem.* **2016**, *118*, 47 – 90.

[35] A. Escande, M. J. Ingleson, *Chem. Commun.* **2015**, *51*, 6257 – 6274.

[36] K. Messner, B. Vuong, G. K. Tranmer, *Pharmaceuticals* **2022**, *15*, 264.

[37] R. N. Grimes, *Chem. Rev.* **1992**, *92*, 251 – 268.

[38] M. Arrowsmith, H. Braunschweig, T. E. Stennett, *Angew. Chem. Int. Ed.* **2017**, *56*, 96 – 115.

[39] A. Stock, A. Brandt, H. Fischer, *Ber. Dtsch. Chem. Ges.* **1925**, *58*, 643 – 657.

[40] R. J. Brotherton, A. L. McCloskey, L. L. Petterson, H. Steinberg, *J. Am. Chem. Soc* **1960**, *82*, 6242 – 6245.

[41] H. Braunschweig, R. D. Dewhurst, *Angew. Chem. Int. Ed.* **2013**, *52*, 3574 – 3583.

[42] H. Nöth, W. Meister, *Z. Naturforsch. B* **1962**, *17*, 714 – 718.

[43] H. Nöth, H. Schick, W. Meister, *J. Organomet. Chem.* **1964**, *1*, 401 – 410.

[44] A. Moezzi, M. M. Olmstead, P. P. Power, *J. Chem. Soc. Dalton Trans.* **1992**, 2429 – 2434.

[45] H. Nöth, M. Wagner, *Chem. Ber.* **1991**, *124*, 1963 – 1972.

[46] W. Biffar, H. Nöth, H. Pommerening, *Angew. Chem. Int. Ed. Engl.* **1980**, *19*, 56 – 57.

[47] J. Knizek, I. Krossing, H. Nöth, W. Ponikwar, *Eur. J. Inorg. Chem.* **1998**, 505 – 509.

[48] H. Braunschweig, M. Gross, K. Hammond, M. Friedrich, M. Kraft, A. Oechsner, K. Radacki, S. Stellwag, *Chem. Eur. J.* **2008**, *14*, 8972 – 8979.

[49] H. Braunschweig, T. Kupfer, J. Mies, A. Oechsner, *Eur. J. Inorg. Chem.* **2009**, 2844 – 2850.

[50] H. Braunschweig, A. Damme, *Acta Crystallogr. E66* **2010**, o3367.

[51] S. R. Wang, M. Arrowsmith, J. Böhnke, H. Braunschweig, T. Dellermann, R. D. Dewhurst, H. Kelch, I. Krummenacher, J. D. Mattock, J. H. Müssig, T. Thiess, A. Vargas, J. Zhang, *Angew. Chem. Int. Ed.* **2017**, *56*, 8009 – 8013.

[52] G. Knörzer, H. Seyffer, H. Pritzkow, W. Siebert, *Z. Naturforsch. B* **1990**, *45*, 985 – 988.

[53] H. Braunschweig, M. Gross, K. Hammond, M. Friedrich, M. Kraft, A. Oechsner, K. Radacki, S. Stellwag, *Chem. Eur. J.* **2008**, *14*, 8972 – 8979.

[54] H. Hommer, H. Nöth, J. Knizek, W. Ponikwar, H. Schwenk-Kircher, *Eur. J. Inorg. Chem.* **1998**, *2*, 1519 – 1527.

[55] H. Klusik, A. Berndt, *Angew. Chem. Int. Ed. Engl.* **1981**, *20*, 870 – 871.

[56] A. Moezzi, M. M. Olmstead, P. P. Power, *J. Am. Chem. Soc.* **1992**, *114*, 2715 – 2717.

[57] W. J. Grigsby, P. P. Power, *Chem. Commun.* **1996**, 2235 – 2236.

[58] H. Nöth, J. Knizek, W. Ponikwar, *Eur. J. Inorg. Chem.* **1999**, 1931 – 1937.

[59] a) T. Kaese, T. Trageser, H. Budy, M. Bolte, H.-W. Lerner, M. Wagner, *Chem. Sci.* **2018**, *9*, 3881 – 3891; b) S. Akiyama, K. Yamada, M. Yamashita, *Angew. Chem. Int. Ed.* **2019**, *58*, 11806 – 11810.

[60] J. Messelsberger, M. Kumar, S. J. Goodner, D. Munz, *Org. Chem. Front.* **2021**, *8*, 6663 – 6669.

[61] Y. Wang, B. Quillan, P. Wie, C. S. Wannere, Y. Xie, R. B. King, H. F. Schaefer, P. v. R. Schleyer, G. H. Robinson, *J. Am Chem. Soc.* **2007**, *129*, 12412 – 12413.

[62] H. Braunschweig, R. D. Dewhurst, K. Hammond, J. Mies, K. Radacki, A. Vargas, *Science* **2012**, *336*, 1420 – 1422.

[63] a) L. C. Ducati, N. Takagi, G. Frenking, *J. Phys. Chem. A* **2009**, *113*, 11693 – 11698; b) A. Papakondylis, E. Miliordos, A. Mavridis, *J. Phys. Chem. A* **2004**, *108*, 4335 – 4340; c) M. P. Mitoraj, A. Michalak, *Inorg. Chem.* **2011**, *50*, 2168 - 2174; d) N. Holzmann, A. Stasch, C. Jones, G. Frenking, *Chem. Eur. J.* **2011**, *17*, 13517 – 13525.

[64] a) S.-D. Li, H.-J. Zhai, L.-S. Wang, *J. Am. Chem. Soc.* **2008**, *130*, 2573 – 2579; b) M. Zhou, N. Tsumori, Z. Li, K. Fan, L. Andrews, Q. Xu, *J. Am. Chem. Soc.* **2002**, *124*, 12936 – 12937.

[65] a) R. J. Wright, M. Brynda, P. P. Power, *Angew. Chem. Int. Ed.* **2006,** *45*, 5953 – 5956; b) J. Su, X.-W. Li, R. C. Crittendon, G. H. Robinson, *J. Am. Chem. Soc.* **1997**, *119*, 5471 – 5472.

[66] R. C. Fischer, P. P. Power, *Chem. Rev.* **2010**, *110*, 3877 – 3923

[67] a) J. Böhnke, H. Braunschweig, W. C. Ewing, C. Hörl, T. Kramer, I.

Krummenacher, J. Mies, A. Vargas, *Angew. Chem. Int. Ed.* **2014**, *53*, 9082 – 9085; b) J. Böhnke, H. Braunschweig, T. Dellermann, W. C. Ewing, K. Hammond, O. C. Jimenez-Halla, T. Kramer, J. Mies, *Angew. Chem. Int. Ed.* **2015**, *54*, 13801 – 13805.

[68] a) L. Englert, U. Schmidt, M. Dömling, M. Passargus, T. E. Stennett, A. Hermann, M. Arrowsmith, M. Härterich, J. Müssig, A. Phillipps, D. Prieschl, A. Rempel, F. Rohm, K. Radacki, F. Schorr, T. Thiess, J. O. C. Jimenez-Halla, Holger Braunschweig, *Chem. Sci.* **2021**, *12*, 9506 – 9515; b) M. Arrowsmith, J. Böhnke, H. Braunschweig, M. A. Celik, C. Claes, W. C. Ewing, I. Krummenacher, K. Lubitz, C. Schneider, *Angew. Chem. Int. Ed.* **2016**, *55*, 11271 – 11275.

[69] J. T. Goettel, H. Braunschweig, *Coord. Chem. Rev.* **2019**, *380*, 184 – 200.

[70] H. Braunschweig, A. Damme, R. D. Dewhurst, A. Vargas, *Nature Chem.* **2013**, *5*, 115 – 121.

[71] G. Zweifel, H. Arzoumanian, *J. Am. Chem. Soc.* **1967**, *89*, 291 – 295.

[72] H. Klusik, A. Berndt, *Angew. Chem. Int. Ed. Engl.* **1983**, *22*, 877 – 877.

[73] A. Berndt, *Angew. Chem. Int. Ed. Engl.* **1993**, *32*, 985 – 1009.

[74] a) R. Hunold, J. Allwohn, G. Baum, W. Massa, A. Berndt, *Angew. Chem. Int. Ed. Engl.* **1988**, *27*, 961 – 963; b) J. Allwohn, M. Pilz, R. Hunold, W. Massa, A. Berndt, *Angew. Chem. Int. Ed. Engl.* **1990**, *29*, 1032 – 1033.

[75] M. Michel, S. Kar, L. Endres, R. D. Dewhurst, B. Engels, H. Braunschweig, *Nat. Synth.* **2025**.

[76] a) R. J. Maza, J. J. Carbo, E. Fernandez, *Adv. Synth. Catal.* **2021**, *363*, 2274 – 2289; b) J. Möbus, G. Kehr, C. G. Daniliuc, R. Fröhlich, G. Erker, *Dalton Trans.* **2014**, *43*, 632 – 638.

[77] A. B. Cuenca, E. Fernandez, *Chem. Soc. Rev.* **2021**, *1*, 72 – 86.

[78] a) C. Chen, *Nat. Rev. Chem.* **2018**, *2*, 6 – 14; b) S. Mecking, *Angew. Chem. Int. Ed.* **2001**, *40*, 534 – 540; c) H. H. Brintzinger, D. Fischer, R. Mülhaupt, B. Rieger, R. M. Waymouth, *Angew. Chem. Int. Ed. Engl.* **1995**, *34*, 1143 – 1170; d) M. Stürzel, S. Mihan, R. Mülhaupt, *Chem. Rev.* **2016**, *116*, 1398 – 1433.

[79] a) M. J. S. Dewar, *Bull. Soc. Chim. Fr.* **1951**, *48*, 112 – 135; b) J. Chatt, L. A. Duncanson, *J. Chem. Soc.* **1953**, 2939 – 2947; c) J. Chatt, L. A. Duncanson, L. M. Venanzi, *J. Chem. Soc.* **1955**, 4456 – 4460.

[80] M. Eaton, Y. Zhang, S.-Y. Liu, *Chem. Soc. Rev.* **2024**, *53*, 1915 – 1935.

[81] a) A. M. Canfield, D. Rodina, S. M. Paradine, *Angew. Chem. Int. Ed.* **2024**, *63*, e202401550; b) S. K.-H. Thiele, D. R. Wilson, *J. Macromol. Sci. Part C Polym. Rev.* **2003**, *43*, 581 – 628; c) G. Ricci, G. Leone, *Polyolefins J.* **2014**, *1*, 43 – 60.

[82] M. Pilz, J. Allwohn, P. Willershausen, W. Massa, A. Berndt, *Angew. Chem. Int. Ed. Engl.* **1990**, *29*, 1030 – 1032.

[83] R. Littger, H. Nöth, M. Thomann, M. Wagner, *Angew. Chem. Int. Ed. Engl.* **1993**, *32*, 295 – 297.

[84] D. Scheschkewitz, A. Ghaffari, P. Amseis, M. Unverzagt, G. Subramanian, M. Hofmann, P. v. R. Schleyer, H. F. Schäfer III, G. Geiseler, W. Massa, A. Berndt, *Angew. Chem. Int. Ed.* **2000**, *39*, 1272 – 1275.

[85] D. Scheschkewitz, M. Hofmann, A. Ghaffari, P. Amseis, C. Präsang, W. Mesbah, G. Geiseler, W. Massa, A. Berndt, *J. Organomet. Chem.* **2002**, *646*, 262 – 270.

[86] C. Präsang, P. Amseis, D. Scheschkewitz, G. Geiseler, W. Massa, M. Hofmann, A. Berndt, *Angew. Chem. Int. Ed.* **2006**, *45*, 6745 – 6747.

[87] a) G. Gabbert, W. Weinmann, H. Pritzkow, W. Siebert, *Angew. Chem. Int. Ed. Engl.* **1992**, *31*, 1603 – 1605; b) C. Chen, C. G. Daniliuc, G. Kehr, G. Erker, *J. Am. Chem. Soc.* **2021**, *143*, 21312 – 21320; c) H. Braunschweig, Q. Ye, K. Radacki, A. Damme, *Angew. Chem. Int. Ed.* **2012**, *51*, 7839 – 7842; d) A. Hermann, F. Fantuzzi, M. Arrowsmith, T. Zorn, I. Krummenacher, B. Ritschel, K. Radacki, B. Engels, H. Braunschweig, *Angew. Chem. Int. Ed.* **2020**, *59*, 15717 – 15725; e) R. A. Thornton, B. M. Lindley, *Organometallics* **2023**, *42*, 1454 – 1458.

[88] G. E. Herberich, C. Ganter, L. Wesemann, *Chem. Ber.* **1990**, *123*, 49 – 51.

[89] C. Präsang, Y. Sahin, M. Hoffmann, G. Geiseler, W. Massa, A. Berndt, *Eur. J. Inorg. Chem.* **2004**, 3063 – 3073.

[90] A. Okorn, A. Jayaraman, L. Englert, M. Arrowsmith, T. Swoboda, J. Weigelt, C. Brunecker, M. Hess, A. Lamprecht, C. Lenczyk, M. Rang, H. Braunschweig, *Chem. Sci.* **2022**, *13*, 7566 – 7574.

[91] J. Teichmann, H. Stock, H. Pritzkow, W. Siebert, *Eur. J. Inorg. Chem.* **1998**, 459 – 463.

[92] C. Präsang, M. Hofmann, G. Geiseler, W. Massa, A. Berndt, *Angew. Chem. Int. Ed.* **2002**, *41*, 1526 – 1529.

[93] C. Präsang, Y. Sahin, M. Hofmann, G. Geiseler, W. Massa, A. Berndt, *Eur. J.*

Inorg. Chem. **2008**, 5046 – 5055.

[94] a) Y. Sahin, Ö. S. Aslantürk, T. Celik, R. Sevincek, M. Aygün, K. Metin, E. Firinci, H. Özgener, *Bioorg. Chem.* **2021**, *117*, 105443; b) Y. Sahin, E. P. Coban, M. Aygün, R. Sevincek, H. Özgener, H. H. Biyik, K. Metin, B. Gürbüz, *J. Mol. Struct.* **2023**, *1277*, 13489; c) Y. Sahin, E. P. Coban, R. Sevincek, H. H. Biyik, H. Özgener, M. Aygün, *Bioorg. Chem.* **2021**, *106*, 104494.

[95] Y. Mu, Y. Dai, D. A. Ruiz, L. L. Leo, L.-P. Xu, C.-H. Tung, L. Kong, *Angew. Chem. Int. Ed.* **2024**, *63*, e202405905.

[96] J. Seufert, E. Welz, I. Krummenacher, V. Paprocki, J. Böhnke, S. Hagspiel, R. D. Dewhurst, R. Tacke, B. Engels, H. Braunschweig, *Angew. Chem. Int. Ed.* **2018**, *57*, 10752 – 10755.

[97] K. E. Krahulic, G. D. Enright, M. Parvez, R. Roesler, *J. Am. Chem. Soc.* **2005**, *127*, 4142 – 4143.

[98] P. Bissinger, H. Braunschweig, M. A. Celik, C. Claes, R. D. Dewhurst, S. Endres, H. Kelch, T. Kramer, I. Krummenacher, C. Schneider, *Chem. Commun.* **2015**, *51*, 15917 – 15920.

[99] a) L. Zhu, Z. Feng, R. Kinjo, *J. Am.Chem. Soc.* **2024**, *146*, 20945 – 20950; b) L. Zhu, R. Kinjo, *Angew. Chem. Int. Ed.* **2022**, *61*, e202207631; c) D. Prieschl, G. Belanger-Chabot, X. Guo, M. Dietz, M. Müller, I. Krummenacher, Z. Lin, H. Braunschweig, *J. Am. Chem. Soc.* **2020**, *142*, 1065 – 1076; d) B. Riegel, H.-D. Hausen, W. Schwarz, G. Heckmann, H. Binder, E. Fluck, A. Dransfeld, P. v. R. Schleyer, *Z. Allg. Anorg. Chem.* **1996**, *622*, 1462 – 1470.

[100] R. N. Grimes, *Acc. Chem. Res.* **1978**, *11*, 420 – 427.

[101] a) D. Bromm, U. Seebold, M. Noltemeyer, A. Meller, *Chem. Ber.* **1991**, *124*, 2645 - 2649; b) A. Meller, D. Bromm, W. Maringgele, A. Heine, D. Stalke, G. M. Sheldrick, *Chem. Ber.* **1990**, *123*, 293 – 294; c) W. Maringgele, A. Heine, M. Noltemeyer, A. Meller, *J. Organomet. Chem.* **1994**, *468*, 25 – 35.

[102] a) X. Wang, M. Sabat, R. N. Grimes, *J. Am. Chem. Soc.* **1994**, *116*, 2687 – 2688; b) J. R. Pipal, R. N. Grimes, *Organometallics* **1993**, *12*, 4452 – 4458; c) X. Wang, M. Sabat, R. N. Grimes, *J. Am. Chem. Soc.* **1995**, *117*, 12227 – 12234.

[103] D. Scheschkewitz, P. Amseis, G. Geiseler, W. Massa, M. Hofmann, A. Berndt, *Eur. J. Inorg. Chem.* **2005**, 4078 – 4085.

[104] a) E. Firinci, R. Sevincek, B. Bursali, H. Özgener, O. Burgaz, C. Sen, M. Aygün,

Y. Sahin, *Inorg. Chim. Acta* **2019**, *496*, 119038; b) X. Xie, M. F. Haddow, S. M. Mansell, N. C. Norman, C. A. Russell, *Chem. Commun.* **2011**, *47*, 3748 – 3750; c) B. Riegel, G. Heckmann, H.-D. Hausen, W. Schwarz, H. Binder, E. Fluck, St. Grundei, H. Nöth, M. Schmidt, M. L. McKee, A. Dransfeld, P. v. R. Schleyer, *Z. Allg. Anorg. Chem.* **1995**, *621*, 1111 – 1122.

[105] E. Beck, D. Bröllos, I. Krummenacher, T. Kupfer, M. Dietz, T. Wellnitz, C. Mihm, H. Braunschweig, *Nat. Commun*. **2025**, *5304*.

[106] R. Littger, N. Metzler, H. Nöth, M. Wagner, *Chem. Ber.* **1994**, *127*, 1901 – 1908.

[107] H. T. W. Shere, M. S. Hill, M. F. Mahon, *Polyhedron* **2023**, *244*, 116588.

[108] H. Nöth, H. Fußstetter, H. Pommerening, T. Taeger, *Chem. Ber.* **1980**, *113*, 342 – 357.

[109] J. T. Patton, S. G. Feng, K. A. Abboud, *Organometallics* **2001**, *20*, 3399 – 3405.

[110] H. Hosoya, T. Akiyama, K. Mashima, H. Tsurugi, *Dalton Trans.* **2023**, *52*, 13154 – 13160.

[111] H. Nöth, W. Rattay, *J. Organomet. Chem.* **1986**, *308*, 131 – 152

[112] A. Krämer, J.-K. Uhm, S. E. Garner, H. Pritzkow, W. Siebert, *Z. Naturforsch*. B **1990**, 1019 – 1021.

[113] S. M. van der Kerk, P. H. M. Budzelaar, A. van der Kerk-van Hoof, G. J. M. van der Kerk, P. v. R. Schleyer, *Angew. Chem. Int. Ed. Engl.* **1983**, *22*, 48.

[114] M. Hildenbrand, H. Pritzkow, U. Zenneck, W. Siebert, *Angew. Chem.* **1984**, *96*, 371 – 372

[115] M. Hildenbrand, H. Pritzkow, W. Siebert, *Angew. Chem. Int. Ed. Engl.* **1985**, *24*, 759 – 760.

[116] a) D. E. Kaufmann, W. Schacht, *Pure Appl. Chem.* **1991**, *63*, 383 – 386; b) D. E. Kaufmann, R. Boese, A. Scheer, *Chem. Ber.* **1994**, *127*, 2349 – 2351.

[117] T. Brückner, M. Arrowsmith, M. Heß, K. Hammond, M. Müller, H. Braunschweig, *Chem. Commun.* **2019**, *55*, 6700 – 6703.

[118] A. Gärtner, L. Meier, M. Arrowsmith, M. Dietz, I. Krummenacher, R. Bertermann, F. Fantuzzi, H. Braunschweig, *J. Am. Chem. Soc.* **2022**, *144*, 21363 – 21370.

[119] A. Häfner, L. Endres, M. Arrowsmith, C. Mimh, S. Fuchs, S. Nees, K. Radacki, I. Krummenacher, R. Bertermann, F. Fantuzzi, H. Braunschweig, *Inorg. Chem. Front.* **2025**, Advance Article.

[120] T. Thiess, M. Ernst, T. Kupfer, H. Braunschweig, *Chem. Eur. J.* **2020**, *26*, 2967

– 2972.

[121] . Maringgele, A. Heine, M. Noltemeyer, A. Meller, *J. Organomet. Chem.* **1994**, *468*, 25 – 35.

[122] T. Habereder, H. Nöth, M. Wagner, *Eur. J. Inorg. Chem.* **2001**, 1665 – 1669.

[123] B. Thiele, P. Paetzold, U. Englert, *Chem. Ber.* **1992**, *125*, 2681 – 2686.

[124] H.-J. Himmel, *Angew. Chem. Int. Ed.* **2019**, *58*, 11600 – 11617.

[125] C.-J. Maier, H. Pritzkow, W. Siebert, *Angew. Chem. Int. Ed. Engl.* **1999**, *38*, 1666 – 1668.

[126] E. Beck, I. Krummenacher, T. Kupfer, M. Dietz, M. Michel, K. Hammond, H. Braunschweig, *Chem* **2025**, *11*, 102338.

[127] J. Wang, Q. Ye, *Chem. Eur. J.* **2024**, *30*, e202303695.

[128] a) H. Braunschweig, Q. Ye, K. Radacki, *Chem. Commun.* **2009**, 6979 – 6981; b) H. Braunschweig, Q. Ye, K. Radacki, P. Brenner, G. Frenking, S. De, *Inorg. Chem.* **2011**, *50*, 62 – 71; c) H. Braunschweig, Q. Ye, K. Radacki, T. Kupfer, *Dalton Trans.* **2011**, *40*, 3666 – 3670; d) H. Braunschweig, A. Damme, R. D. Dewhurst, S. Ghosh, T. Kramer, B. Pfaffinger, K. Radacki, A. Vargas, *J. Am. Chem. Soc.* **2013**, *135*, 1903 – 1911; e) H. Braunschweig, R. D. Dewhurst, K. Radacki, C. W. Tate, A. Vargas, *Angew. Chem. Int. Ed.* **2014**, *53*, 6263 – 6266; f) H. Braunschweig, P. Brenner, R. D. Dewhurst, I. Krummenacher, B. Pfaffinger, A. Vargas, *Nat. Commun.* **2012**, *872*, 1 - 6.

[129] a) C. A. Coulson, W. E. Moffitt, *J. Chem. Phys.* **1947**, *15*, 151; b) C. A. Coulson, W. E. Moffitt, *Philos. Mag.* **1949**, *40*, 1 – 35; c) K. B. Wiberg, *Acc. Chem. Res.* **1996**, *29*, 229 – 234.

[130] a) R. Hoffmann, R. W. Alder, C. F. Wilcox Jr., *J. Am. Chem.Soc.* **1970**, *92*, 4992 – 4993; b) R. Hoffmann, *Pure Appl. Chem.* **1971**, *28*, 181 – 194.

[131] E. D. Jemmis, G. Subramanian, G. N. Srinivas, *J. Am. Chem. Soc.* **1992**, *114*, 7939 – 7941.

[132] Y. Wang, X. Zhang, J. Han, Q. Li, R. Wei, D. A. Ruiz, L. L. Liu, C.-H. Tung, L. Kong, *Angew. Chem. Int. Ed.* **2022**, *61*, e202117053.

[133] A. Hübner, T. Kaese, M. Diefenbach, B. Endeward, M. Bolte, H.-W. Lerner, M. C. Holthausen, M. Wagner, *J. Am. Chem. Soc.* **2015**, *137*, 3705 – 3714.

[134] H. Klusik, C. Pues, A. Berndt, *Z. Naturforsch.* B **1984**, *39*, 1042 – 1045.

[135] R. Wehrmann, H. Meyer, A. Berndt, *Angew. Chem.* Int. Ed. Engl. **1985**, *24*, 788

– 790.

[136] H. Meyer, G. Schmidt-Lukas, G. Baum, W. Massa, A. Berndt, *Z. Naturforsch.* B **1988**, *43*, 801 – 806.

[137] P. Willershausen, G. Schmidt-Lukas, C. Kybart, J. Allwohn, W. Massa, M. L. McKee, P. v. R. Schleyer, A. Berndt, *Angew. Chem. Int. Ed.* **1992**, *31*, 1384 – 1386.

[138] D. Steiner, C. Balzereit, H.J. Winkler, N. Stamatis, M. Hofmann, P. v. R. Schleyer, W. Massa, A. Berndt, *Angew. Chem. Int. Ed.* **1994**, *33*, 2303 – 2306.

[139] M. Menzel, D. Steiner, H. J. Winkler, D. Schweikart, S. Mehle, S. Fau, G. Frenking, W. Massa, A. Berndt, *Angew. Chem. Int. Ed.* **1995**, *34*, 327 – 329.

[140] A. Kekulé, *Bull. Soc. Chim. Fr.* **1865**, *3*, 98 – 110.

[141] a) E. Hückel, *Z. Phys.* **1931**, *70*, 204 – 286; b) E. Hückel, *Z. Phys.* **1931**, *72*, 310 – 337; c) E. Hückel, *Z. Phys.* **1932**, *76*, 628 – 648; d) L. Pauling, *J. Am. Chem. Soc.* **1926**, *48*, 1132 – 1143; e) L. Pauling, G. W. Wheland, *J. Chem. Phys.* **1933**, *1*, 362 – 374.

[142] K. Komatsu, T. Kitagawa, *Chem. Rev.* **2003**, *103*, 1371 – 1428.

[143] M. Unverzagt, PhD thesis, Marburg University, **1997**.

[144] D. Steiner, H. J. Winkler, C. Balzereit,T. Happel, W. Massa, A. Berndt, M. Hofmann, G. Subramanian, P. v. R. Schleyer, *Angew. Chem. Int. Ed. Engl.* **1996**, *35*, 1990 – 1992.

[145] Y. Sahin, A. Ziegler, T. Happel, H. Meyer, M. J. Bayer, H. Pritzkow, W. Massa, M. Hofmann, P. v. R. Schleyer, W. Siebert, A. Berndt, *J. Organomet. Chem.* **2003**, *680*, 244 – 256.

[146] W. Lößlein, H. Pritzkow, P. v. R. Schleyer, L. R. Schmitz, W. Siebert, *Eur. J. Inorg. Chem.* **2001**, 1949 – 1956.

[147] T. Kupfer, H. Braunschweig, K. Radacki, *Angew. Chem. Int. Ed.* **2015**, *54*, 15084 – 15088.

[148] S. Morisako, R. Shang, Y. Yamamoto, H. Matsui, M. Nakano, *Angew. Chem. Int. Ed.* **2017**, *56*, 15234 – 15240.

[149] Z. Feng, R. Kinjo, *Chem* **2025**, *11*, 102255.

[150] C. Xu, F. Cao, X. Chen, M. Chen, Z. Mo, *J. Am. Chem. Soc.* **2025**, *147*, 1207 – 1213.

[151] M. Müller, P. Paetzold, *Coord. Chem. Rev.* **1998**, *176*, 135 – 155.

[152] P. Paetzold, B. Rednez-Stormanns, R. Boese, *Chem. Ber.* **1991**, *124*, 2435 – 2441

[153] T. E. Stennet, A. Jayaraman, T. Brückner, L. Schneider, H. Braunschweig, *Chem. Sci.* **2020**, *11*, 1335 – 1341.

[154] P. Paetzold, L. Geret-Baumgarten, R. Boese, *Angew. Chem. Int. Ed. Engl.* **1992**, *31*, 1040 – 1042

[155] a) H. Braunschweig, P. Constantinidis, T. Dellermann, W. C. Ewing, I. Fischer, M. Hess, F. R. Knight, A. Rempel, C: Schneider, S. Ullrich, A. Vargas, J. D. Woollins, *Angew. Chem. Int. Ed.* **2016**, *55*, 5606 – 5609; b) A. Stoy, M. Arrowsmith, M. Eyßlein, T. Dellermann, J. Mies, K. Radacki, T. Kupfer, H. Braunschweig, *Inorg. Chem.* **2021**, *60*, 12625 – 12633; c) S. R. Wang, M. Arrowsmith, J. Böhnke, H. Braunschweig, T. Dellermann, R. D. Dewhurst, H. Kelch, I. Krummenacher, J. D. Mattock, J. H. Müssig, T. Thiess, A. Vargas, J. Zhang, *Angew. Chem. Int. Ed.* **2017**, *56*, 8009 – 8013.

[156] H. Braunschweig, A. Damme, R. D. Dewhurst, T. Kramer, T. Kupfer, K. Radacki, E. Siedler, A. Trumpp, K. Wagner, C. Werner, *J. Am. Chem. Soc.* **2013**, *135*, 8702 – 8707.